The Thesis Committee for Nathan D. Williams

Certifies that this is the approved version of the following thesis:

A Predictive Exploration Model for MVT Pb-Zn Mineralization in Central Texas: Insights from the Southeast Missouri Lead District

APPROVED BY

SUPERVISING COMMITTEE:

James Richard Kyle, Supervisor

Brent A. Elliott

Robert G. Loucks

A Predictive Exploration Model for MVT Pb-Zn Mineralization in Central Texas: Insights from the Southeast Missouri Lead District

by

Nathan D. Williams, B.S.

Thesis

Presented to the Faculty of the Graduate School of

The University of Texas at Austin

in Partial Fulfillment

of the Requirements

for the Degree of

Master of Science in Geological Sciences

The University of Texas at Austin

May 2017

Dedication

For my wife, Meghan

Acknowledgements

Abstract

A Predictive Exploration Model for MVT Pb-Zn Mineralization in Central Texas: Insights from the Southeast Missouri Lead District

Nathan D. Williams, M.S. Geo Sci

The University of Texas at Austin, 2017

Supervisor: James Richard Kyle

Minor Pb-Zn occurrences on the flanks of the Llano Uplift in Central Texas have many geologic similarities to the world-class Mississippi Valley Type (MVT) deposits of Southeast Missouri. In both areas, metallic sulfides are hosted in dolomitized Cambrian carbonates, commonly in areas where local basement highs forced depositional pinch-outs of the basal sandstones. In Southeast Missouri, mineralization has been attributed to basinal fluid migration associated with late Paleozoic Ouachita deformation and appears to be spatially related to regional faults that may have served as fluid conduits. In Central Texas, there is also evidence that mineralization is associated with basinal fluids tied to Ouachita deformation and abundant regional faults serve as plausible fluid pathways. Moreover, Southeast Missouri and Central Texas are distinctly rich in Pb, an atypical characteristic for MVT deposits that are usually Zn dominant. These similarities suggest that an understanding of spatial associations between sites of known mineralization and regional geology, geochemistry, and geophysics in Southeast Missouri will be a useful guide in future exploration efforts in Central Texas.

The weights-of-evidence approach is used to evaluate regional geology, geochemistry, and geophysical datasets and produce posterior probability maps for MVT deposits in Southeast Missouri. Host rock characteristics, stream sediment geochemistry, and proximity to basement highs are some of the most useful data for predicting these deposits. Model parameters derived from Southeast Missouri are applied to the Llano Uplift region of Central Texas. Although available data sets for Central Texas are less detailed than Southeast Missouri, the Central Texas models generally agree with areas known to contain MVT mineralization. A higher resolution basement structure map for Central Texas would be useful for more detailed analysis. Central Texas model results are compared with semi-quantitative geochemical data from insoluble residues from wells throughout the Llano region and indicate that the model may be useful in explaining the measured Pb concentrations in these wells. Several new permissive areas to the south and southwest of the Precambrian core of the Llano Uplift are identified that may warrant additional follow up investigation. This work illustrates the potential utility of mineral potential modeling to prioritize areas for exploration for undiscovered MVT mineralization in Central Texas.

Table of Contents

List of Tables

List of Figures

xiii

xiv

Chapter 1: Introduction

The Mississippi Valley Type (MVT) deposits of Southeast Missouri are some of the largest and highest grade Pb-Zn deposits in the world, with an estimated 17 million tons of lead produced since French explorers began mining in the area in the early 18th Century (Snyder and Gerdemann, 1968; Missouri DNR; Seeger, 2008). There are notable geologic similarities between the giant MVT ore deposits of Southeast Missouri and several minor lead and zinc occurrences in Paleozoic sedimentary rocks surrounding the Llano Uplift in Central Texas (Comstock, 1890; Baker, 1933; Barnes, 1956; Allie, 1981). The similarities between the two regions and presence of minor near-surface Pb-Zn occurrences suggest that the geologic conditions in Texas may be favorable for more economically viable but as yet undiscovered mineralization.

Comstock (1890), in one of the earliest descriptions of lead mineralization in Central Texas, wrote:

> *It is very probable that systematic exploration in this region may result in the discovery of large and valuable deposits of galena, for the rocks, the mode of occurrence, and the geologic age of the ore beds correspond generally with the conditions existing in Missouri, Illinois, and Wisconsin, where lead has been successfully produced.*

In spite of this early optimism, intermittent exploration in Central Texas in the 20th century failed to produce economic deposits of even a fraction of the size of those in Missouri. Recorded lead production in Central Texas in the 20th Century was limited to 29 tons of concentrate from a mine on Silver Creek in 1930 (Baker, 1935). If large, undiscovered Pb-Zn orebodies exist in Central Texas, a thorough understanding of the spatial relationships and predictive quality of factors associated with MVT mineralization

in Southeast Missouri may be useful in exploring for them. In essence, mineral potential studies such as this one are the practical application of a descriptive, conceptual deposit model to the exploration of undiscovered ore deposits.

PURPOSE

This project tests the question: "Can an effective mineral potential map showing the areas most likely to contain undiscovered MVT mineralization in Central Texas be developed with data-driven model parameters derived from the geologically similar Southeast Missouri MVT districts?" The lack of known MVT deposits in Central Texas that could be used to train a data-driven model would traditionally necessitate a knowledge-driven approach that is by definition more subjective than data-driven models (Bonham-Carter, 1994). This work is a case study in applying out-of-sample inference as described by Harris et al. (2003) to a geologically similar study area significantly outside of the area in which model parameters are estimated.

Harris et al. (2003) employ this method of training a mineral potential model in a well-explored area and applying the model parameters to unexplored portions of their study areas, although in their study, the model parameters are applied in the same general geographic region from which they were derived. Fabbri and Chung (2008) noted that in general, the relationships between evidential layers and mineralization are typically confined to the study area from which are determined. As a result, a major challenge of this study is how to best derive evidence layers so that the calculated weights are transferable from the training area. This necessitates limiting the use of data where the magnitude of values considered is dependent on the location and manipulating these layers to reduce this location-based dependence.

The effectiveness of these models is evaluated by traditional statistical methods of model evaluation as well as by examining physical evidence for MVT fluid migration. As noted by Nykänen and Ojala (2007), this final step of physically evaluating prospectivity models with field evidence is not typically a component of published mineral potential studies. This study generally follows these steps:

1. Generate a series of mineral potential models for the Southeast Missouri MVT District

2. Statistically evaluate the Missouri models using blind tests

3. Apply model parameters (weights) from the best performing models to Central Texas

4. Evaluate the ability of the Central Texas models to predict known near-surface MVT occurrences

5. Compare model results to physical evidence of MVT mineralization to assess model effectiveness

LOCATION AND GEOLOGIC SETTING

The three primary subdistricts of the Southeast Missouri Lead District form an inverted "U" shape in the Paleozoic units around the exposed Precambrian crystalline rocks of the Ozark Uplift in the St. Francois Mountains approximately 120 km (75 mi) south-southwest of St. Louis, Missouri (Figures 1.1 and 1.2). These subdistricts include the Old Lead Belt to the north of the St. Francois Mountains, Fredericktown-Mine La Motte to the east, and the Viburnum Trend, also known as The New Lead Belt, to the west (Seeger, 2008). The extent of the Southeast Missouri study area is the Rolla 1×2 degree quadrangle which includes these MVT subdistricts and was the extent of the USGS Conterminous United States Mineral Assessment Program (CUSMAP) study (Pratt et al., 1981; Pratt et

3
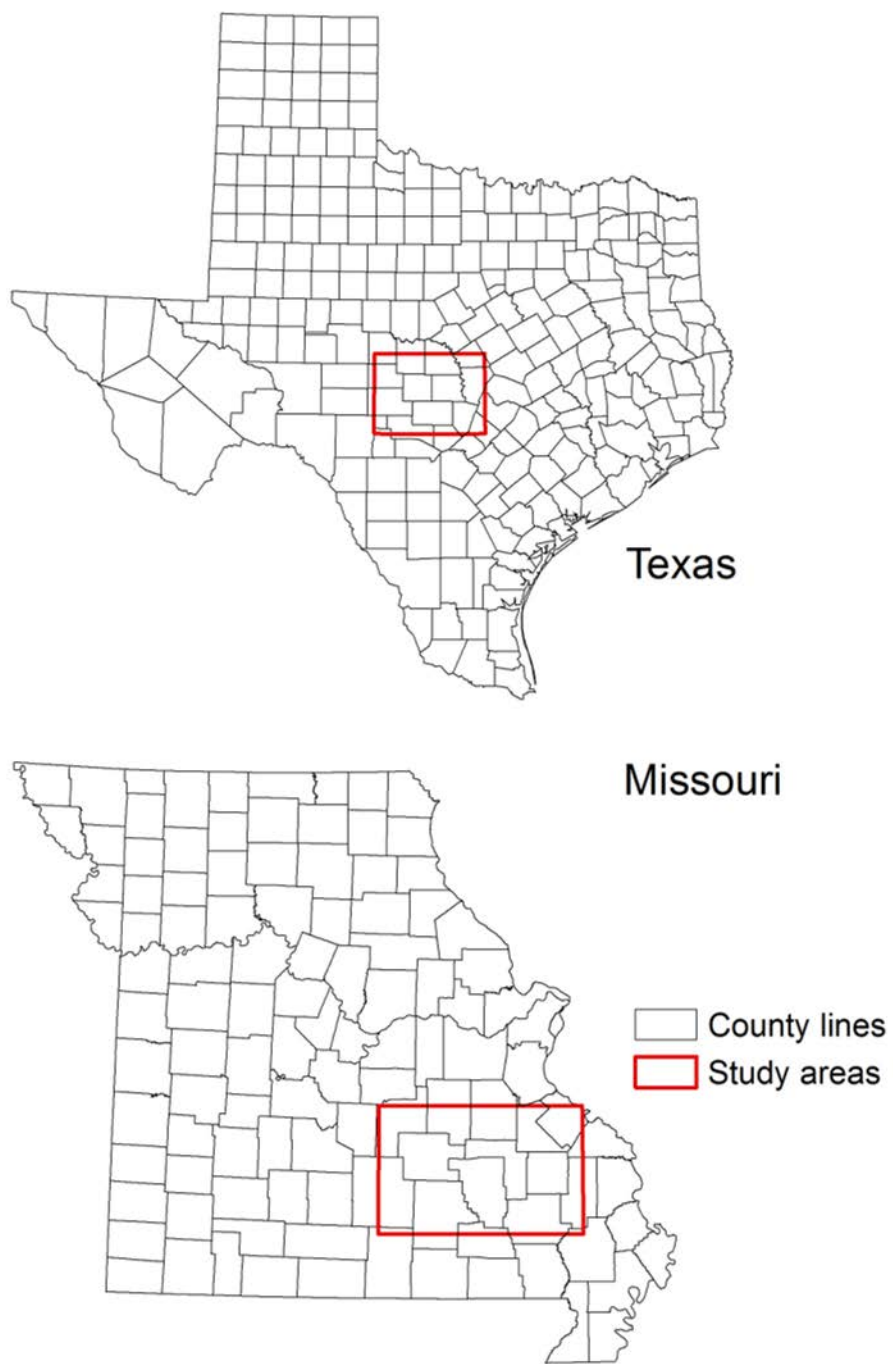
Figure 1.1: Central Texas and Southeast Missouri study area locations.
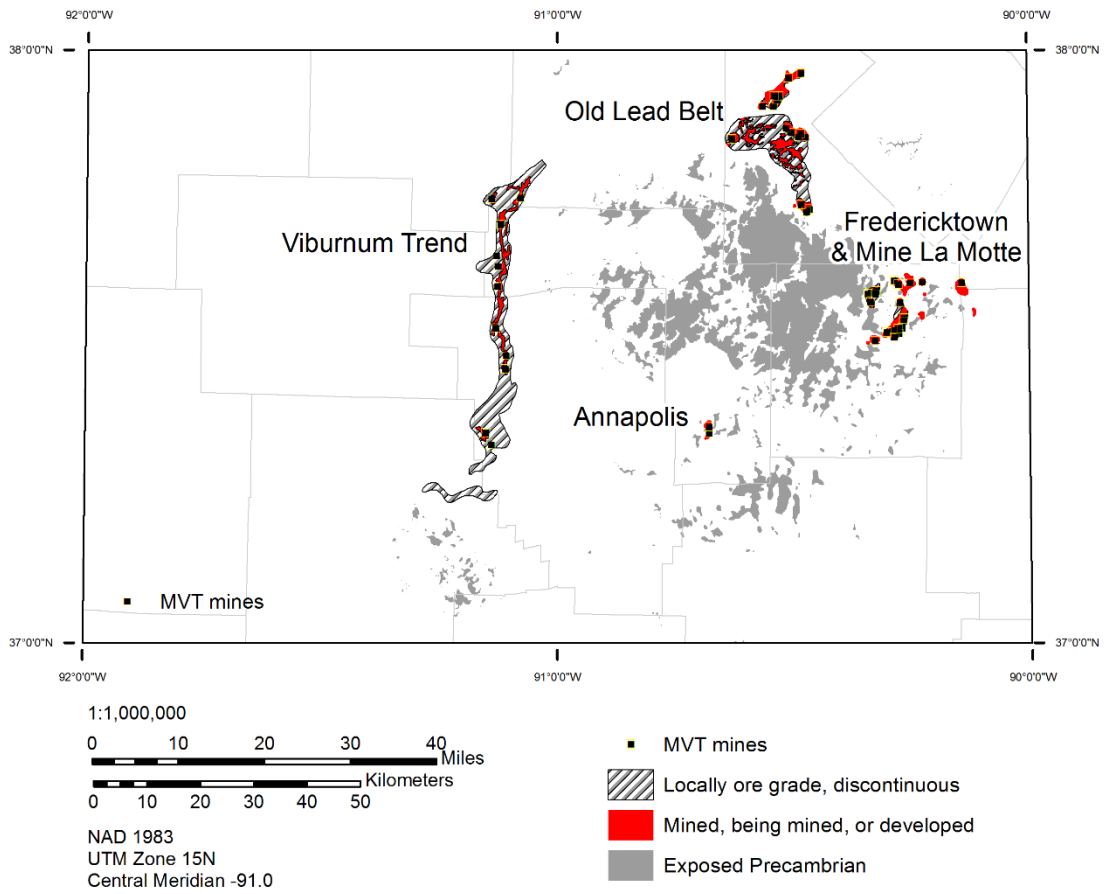
Figure 1.2: Primary subdistricts of the Southeast Missouri Lead District. Mining data compiled by Geza Kisvarsanyi and Mary H. Miller in Pratt et al. (1981).

al., 1986) from which much of the map data for this analysis was derived. Neither of these studies includes the minor Indian Creek subdistrict 5 km (3 miles) north of the study area in north central Washington County.

In Central Texas, the center of the exposed crystalline Precambrian core of the Llano Uplift is located approximately 120 km (75 mi) northwest of Austin, Texas (Figure 1.1). Five near-surface MVT occurrences in Paleozoic sedimentary rocks are located on the east and south sides of the exposed Precambrian core of the uplift (Figure 1.3). The most well-known of these occurrences, and the only to produce lead commercially, is the Silver Creek Mine located on the northeast side of Lake Buchannan in Burnet County (Baker, 1935). Other prospect areas in the Llano region include Slaughter Gap and Hog Thief Bend (Scott Klett area, Barnes, 1956) in Burnet County, and Iron Rock Creek in Blanco County. Additional sulfide occurrences have been reported in the Riley Mountains in Llano County and in the Kuykendall Ranch (Cherokee Creek) area in Lampassas County (Smith et al., 1981). Similar to the Southeast Missouri study area, the Central Texas area of interest is two degrees in east-west extent, but is 1.25 degrees in north-south extent encompassing all of the Llano 1×2 degree quadrangle and the southern quarter of the Brownwood quadrangle.

Geologic setting

Both the Llano and Ozark Uplifts are positioned at the margins of the stable interior craton of North America. In both of these uplift events, erosional processes have created an irregular topography and exposed the Proterozoic crystalline bedrock cores. (Barnes and Bell, 1977). During the Cambrian, this irregular topography was a primary control on the deposition of overlying carbonate and siliciclastic strata that now form roughly ring-shaped patterns on the flanks of the exposed basement rocks (Figure 1.4). Beginning in the
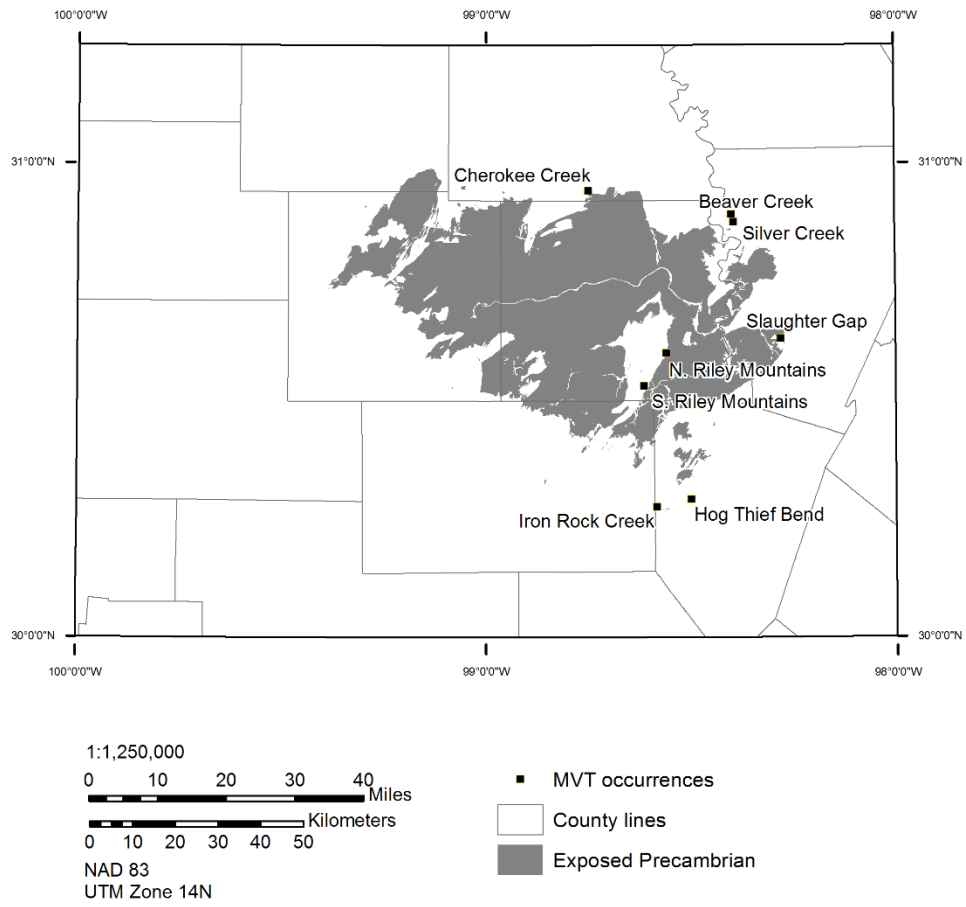
Figure 1.3: MVT occurrences in the Llano region of Central Texas.

Central Texas
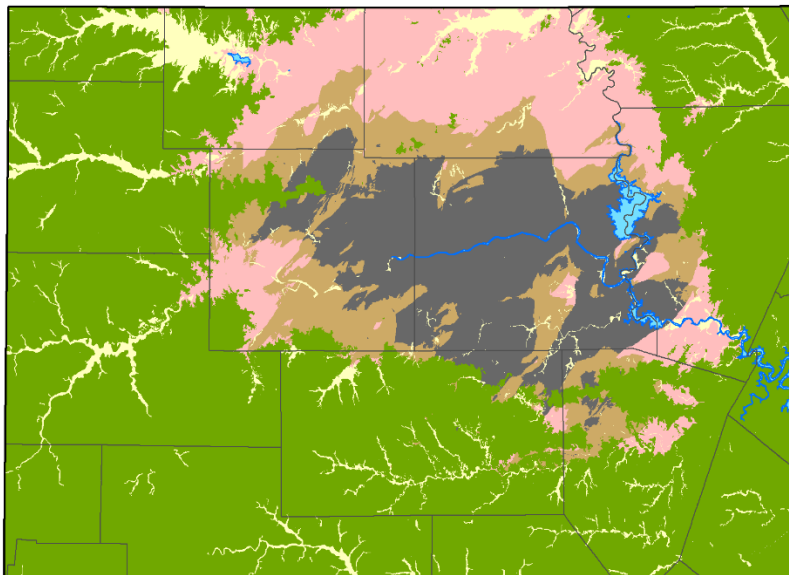
0 10 20 30 40
Miles
Kilometers
0 10 20 30 40 50

1:1,500,000
NAD 1983
Texas UTM Zone 14N
Missouri UTM Zone 15N

Southeast Missouri
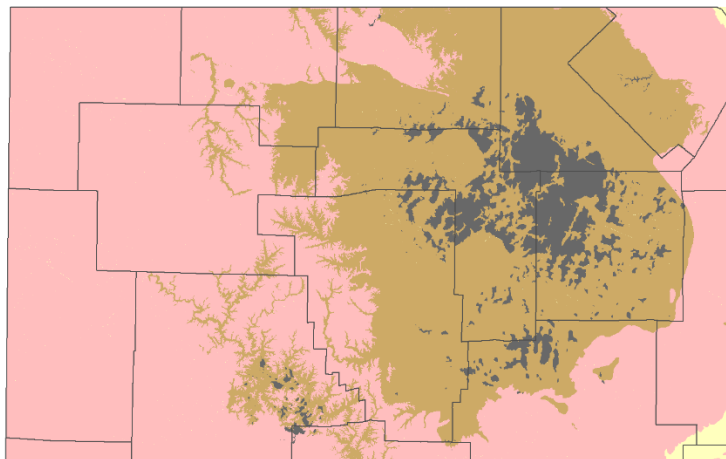
- County lines
- Water
- Quaternary
- Cretaceous
- Undiff Paleozoic
- Cambrian
- Precambrian

Figure 1.4: Simplified geologic maps of the Central Texas and Southeast Missouri study areas at the same scale.

Pennsylvanian and continuing into the Permian, both the Southeast Missouri and Central Texas regions underwent deformation during the Ouachita Orogeny as the African and North American plates collided during the assembly of Pangea (Blakey, 2003). This deformation is thought to be responsible for the widespread normal faulting and structural complexity in the Llano Uplift (Barnes, 1956). Ouachita deformation is considered a likely mechanism of MVT fluid migration responsible for the Pb-Zn mineralization in both Central Texas (McBride et al., 2002; Young and Jackson, 1981) and Southeast Missouri (Horrall et al., 1996; Leach and Rowan, 1986). This timing of mineralization agrees with dates determined from paleomagnetic studies of minerals associated with the MVT minerals (Farr and Gose, 1991; Wisniowiecki et al., 1983; Wu and Beales, 1981; Symons et al., 1998). MVT mineralization is largely concentrated in the carbonate units overlying the basal sandstones in both regions (Figure 1.5).

Central Texas stratigraphy

The crystalline basement exposed at the surface in the center of the Llano Uplift covers an area of approximately 3200 km2 (1250 mi2) and consists of metamorphic rocks ranging in age from 1.36 to 1.24 Ga that have been intruded by ~1.1 Ga granites (Mosher et al., 2008). Following the granite intrusions, nearly 500 million years of uplift and erosion removed an estimated 8 to 10 km (5 to 6 mi) of cover (Kyle and McBride, 2012; Krause, 1996) and produced an irregular surface with up to 240 m (800 ft) of local relief (Barnes, 1956; Barnes and Bell, 1977). Deposition of the Moore Hollow Group consisting of the Riley and Wilberns Formations began with sea-level transgression from the southeast in the Late Middle Cambrian.

The three members of the Riley Formation are the basal Hickory Sandstone, the Cap Mountain Limestone, and the Lion Mountain Sandstone. The Hickory Sandstone is
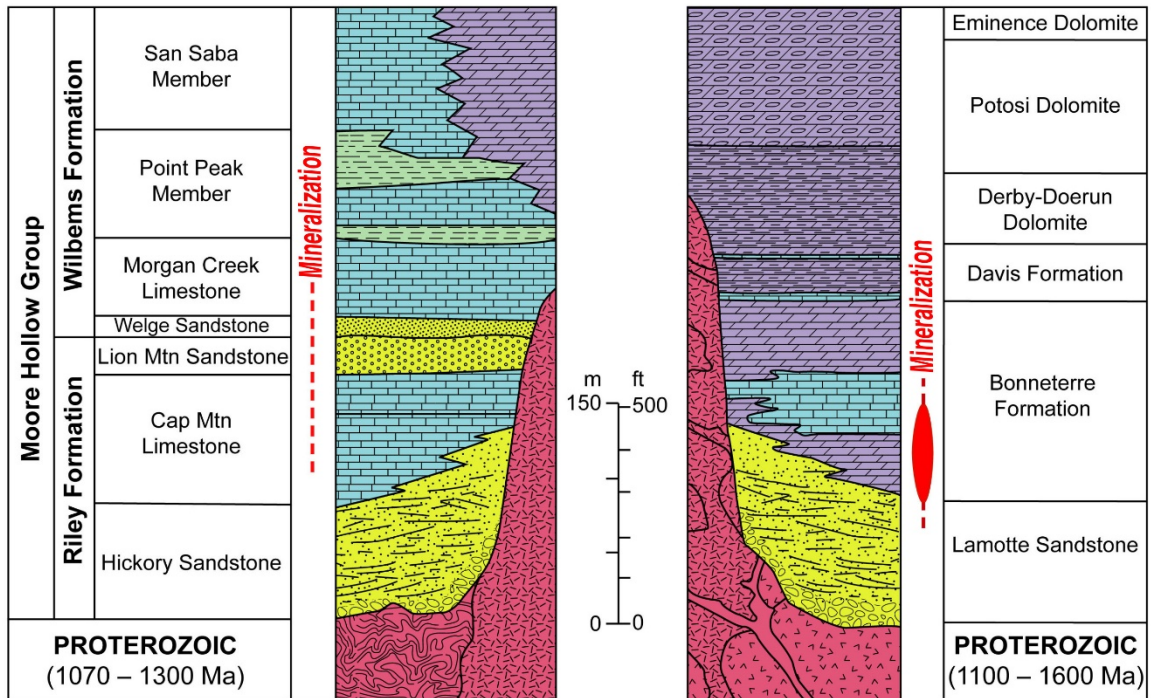
Figure 1.5: Generalized stratigraphy of the Llano region of Central Texas and the Ozark Uplift area of Southeast Missouri showing mineralized zones. From Kyle (2010).

predominantly a marine sandstone that ranges in composition from arkose to quartz arenite (McBride et al., 2002). It was deposited unconformably on the Precambrian surface from which it was derived and is commonly a conglomerate close to this boundary. The Hickory ranges in thickness from 85-145 m (275-475 ft) with a gradational contact into the overlying Cap Mountain Limestone (Barnes and Bell, 1977), which is the main host of Pb mineralization in most near-surface occurrences in Central Texas. The Cap Mountain in surface exposures ranges in thickness from 50-150 m (175-500 ft) with a thickness of nearly 200 m (650 ft) from a well in Kerr County south of the Llano Uplift reported by Barnes and Bell (1977). Although compositionally varied, the carbonate portion of the Cap Mountain consists mainly of limestone with minor dolostone. Similar to its lower contact, the upper contact between the Cap Mountain Limestone and Lion Mountain Sandstone is gradational and generally poorly defined. The Lion Mountain Member is a thin, 9 to 21 m (30 to 70 ft) thick, glauconitic quartz sandstone that has a sharp upper contact with the Welge Sandstone Member of the Wilberns Formation.

The Wilberns Formation consists of the Welge Sandstone, Morgan Creek Limestone, Point Peak, and San Saba Members. The Welge Sandstone is mainly a marine quartz sandstone with varying amounts of glauconite, especially in the eastern portion of the Llano Uplift area (Barnes and Bell, 1977). It ranges in thickness from 3 to 9 m (10 to 30 ft). The upper boundary between the Welge Sandstone and Morgan Creek Limestone is gradational. The Morgan Creek Limestone is an oolitic and glauconitic, coarse granular limestone with thicknesses of between 35 and 44 m (115 to 145 ft). It is overlain by the nonresistant, calcareous siltstones of the Point Peak Member with an average thickness of about 45 m (150 ft) in the Llano region. The Wilberns Formation is capped by the San Saba Member, which is compositionally variable but consists mainly of limestone and

dolostone. The San Saba Member ranges in thickness from about 85 to 137 m (275 to 450 ft).

Southeast Missouri stratigraphy

The structural crest of the Ozark Uplift is exposed at the surface in the St. Francois Mountains of Southeast Missouri (Bickford and Mose, 1975). These rocks cover an area of approximately 1,000 km2 (385 mi2) and consist of a variety of dominantly volcanic and plutonic rocks ranging in age from 1.53 to 1.41 Ga. As in the Llano area of Central Texas, uplift and extensive erosion of these rocks produced irregular topography with up to 300 m (1000 ft) of local relief onto which Late Cambrian sediments were deposited (Thacker and Anderson, 1977).

The basal Lamotte Sandstone immediately overlying the Precambrian rocks is the only siliciclastic unit in the study area as the bulk of the overlying stratigraphy is made up of carbonate rocks (Thacker and Anderson, 1977). Like the Hickory Sandstone in Central Texas, the Lamotte is a quartz sandstone of marine origin. The thickness of the Lamotte is variable because of the irregularities of the Precambrian surface on which it was deposited with a maximum thickness of about 135 m (450 ft) (Snyder and Gerdemann, 1968). The upper contact of the Lamotte with the Bonneterre Formation is gradational.

The Bonneterre Formation conformably overlies the Lamotte and is the primary host of MVT mineralization in Southeast Missouri. In the Southeast Missouri mining districts, the Bonneterre is mostly dolostone, although it is generally limestone elsewhere (Snyder and Gerdemann, 1968). The general thickness of the Bonneterre in the study area is between 120 and 150 m (400 and 500 ft), although it is much thicker in parts of Missouri farther to the southeast. The upper contact of the Bonneterre with the Davis Formation is unconformable (Thacker and Anderson, 1977).

12

The Davis Formation, the lower member of the Elvins Group, consists of interbedded shale, limestone, and siltstone (Thacker and Anderson, 1977) averaging about 50 m (175 ft) thick (Snyder and Gerdemann, 1968). This formation is locally an important trap for mineralizing fluids (Kisvarsanyi, 1977). The contact with the overlying Derby-Doe Run Dolomite Member of the Elvins Group is placed at the shift from characteristically green shales of the Davis Formation to brown shales of the Derby-Doe Run.

The Derby-Doe Run Dolomite, the upper member of the Elvins Group, consists of argillaceous dolomite with brown shale partings common in the lower portions (Thacker and Anderson, 1977). The Derby-Doe Run contact with the overlying Potosi Dolomite is likely gradational. The total thickness of the formation is approximately 35 m (115 ft) (Tarr, 1936).

The Potosi Dolomite is a massive and vuggy dolomite (Thacker and Anderson, 1977) with a maximum thickness of about 120 m (400 ft) (Tarr, 1936). The contact between the Potosi and the overlying Eminence Dolomite is gradational (Thacker and Anderson, 1977).

The Eminence Dolomite is the uppermost Cambrian unit in Missouri, consisting of massive, vuggy, and coarsely crystalline dolomite with abundant chert (Thacker and Anderson, 1977). It is unconformably overlain by the Lower Ordovician Gunter Sandstone Member of the Gasconade Formation. The maximum thickness of the Eminence Dolomite is 60 m (200 ft) (Tarr, 1936).

THE MVT DEPOSIT MODEL

MVT deposits, so named for their abundance in and near the Mississippi Valley in the central United States, are a major source of Pb and Zn. The ore mineralogy of these deposits is characteristically simple and consists primarily of sphalerite (ZnS) and galena

13

(PbS) with varying amounts of Fe sulfides. They are formed by the precipitation of metals from relatively low temperature (<150° C) fluids with compositions similar to modern oilfield brines. These fluids formed by the evaporation of seawater and are soured from sedimentary basins near the deposits. Although several methods of fluid transport have been proposed, a popular mechanism is by gravity-driven flow during tectonic uplift (Leach and Rowan, 1986). They are typically hosted in carbonate rocks, primarily dolostones and less commonly in limestones, and rarely in sandstone (e.g., Indian Creek in Southeast Missouri) (Gutierrez, 1987). These deposits are typically stratabound which is probably related to bedding parallel permeability pathways of various origins in the host rock.

It is necessary to distinguish between spatial and nonspatial characteristics of MVT deposits for the purposes of mineral potential mapping. For this study, spatial characteristics are defined as those that can be (and commonly are) mapped, although there is some ambiguity in this definition. For example, "they occur close to faults" is a spatial characteristic of these deposits while "they are epigenetic" is a nonspatial characteristic. While nonspatial characteristics are useful for categorizing known ore deposits and may be used to select a unified set of training points for a prospectivity model, the lack of a spatial component makes them unsuitable for predicting the spatial distribution of unknown deposits. Table 1.1 shows some characteristics of MVT deposits from the USGS MVT Deposit Model (Leach et al., 2010) grouped into spatial and nonspatial categories.

Central Texas MVT occurrences

Known occurrences of MVT mineralization in Central Texas are confined to Paleozoic strata below the basal Morgan Creek Limestone member of the Wilberns Formation with most occurring in the Cap Mountain Limestone Member of the Cambrian

Spatial	Nonspatial
No genetic relationship to igneous activity	Epigenetic
Hosted in dolostone or limestone	Dominant ore minerals are sphalerite and galena
Occur at the flanks of basins or foreland thrust belts	Ore fluids were brines formed from the evaporation of seawater
Occur in clusters forming large districts	Deposition temperatures range from 75 C to 150 C
Deposition controlled by faults, dissolution collapse breccias, and lithology transitions	Sulfides range from coarse to fine and from massive to disseminated
Some deposits associated with subsurface topographic highs	Sulfides occur as carbonate replacements and open-space fill
	Dolomitization, dissolution, and brecciation are common alteration products

Table 1.1:   Select spatial and nonspatial characteristics of MVT deposits. Data from the USGS MVT Deposit Model (Leach et al., 2010).

Riley Formation (Figure 1.5) (Barnes, 1956). The most studied MVT base metal occurrences in the vicinity of the Llano Uplift in Central Texas are the Silver Creek and Beaver Creek areas located on the northeast side of Lake Buchannan in Burnet County, Slaughter Gap and Hog Thief Bend (Scott Klett area, Barnes, 1956) in Burnet County, and Iron Rock Creek in Blanco and Gillespie Counties.

The Silver Creek Mine and Beaver Creek prospect are associated with granite knobs (Barnes, 1956). Barnes noted that mineralization in mine workings at Silver Creek are in the Welge Sandstone and Morgan Creek Limestone Members of the Wilberns Formation although drill logs from the Eagle-Picher company drilled on the property in 1925 indicate Pb in the Lion Mountain Sandstone and Cap Mountain Limestone Members of the Riley Formation as well. Barnes reports Pb concentrations of up to 5.47% in insoluble residue from samples collected at Silver Creek. The mineralization at Silver Creek is associated with collapse structures where limestone dissolution created breccia zones (Smith et al., 1981), but no collapse structures are present at the nearby Beaver Creek prospect. Mineralization at Beaver Creek appears to be stratigraphically lower than at Silver Creek with galena in the Cap Mountain Limestone near the overlying Lion Mountain Sandstone.

The Slaughter Gap prospect is also in the Cap Mountain Limestone and associated with a granite knob (Barnes, 1956). Barnes (1956) described about 90 m (300 ft) of sparse galena mineralization, but noted that this small amount does little to encourage additional prospecting. Lead was present in two boreholes drilled by the Eagle-Picher Company immediately east of the Slaughter Gap prospect although Barnes (1956) did not report additional details for these bore holes. Barnes (1956) reported up to 0.52% Pb in insoluble residue from a sample collected at the waste dump at Slaughter Gap.

16

The Hog Thief Bend area, described by Barnes (1956) as the Scott Klett area, consists of several pits in the Cap Mountain Limestone surrounding an exposed granite knob. Samples analyzed by Barnes contain up to 1.47% Pb in insoluble residue. Barnes noted that the Pb and Zn concentrations are not suggestive of an economically significant deposit, but postulated that additional and more substantial mineralization may exist stratigraphically lower in the Cap Mountain Limestone near the contact with the underlying Hickory Sandstone.

Galena at Iron Rock Creek is also in the Cap Mountain Limestone near a series of granite outcrops (Barnes, 1956). Barnes also noted that there is little Pb or Zn present at the surface, but suggested that there may be significant mineralization in the subsurface in the vicinity of the contact between the Cap Mountain Limestone and Hickory Sandstone adjacent to the granite hills.

Southeast Missouri MVT deposits

The Southeast Missouri Lead District is comprised of the Old Lead Belt, Fredericktown Mine Lamotte, and Viburnum Trend subdistricts (Seeger, 2008; Snyder and Gerdemann, 1968). Lead has been produced from Southeast Missouri nearly continuously since it was first discovered by French miners near Fredericktown in 1720 (Tarr, 1936). Mineralization is mainly hosted in the Bonneterre Formation although there are a few significant occurrences in stratigraphically higher and lower formations (Figure 1.5). Early mining efforts were concentrated on the east and north flanks of the St. Francois Mountains, where surface exposures of the Bonneterre Formation facilitated exploration and permitted relatively shallow mining. As the Pb resources in these areas became increasingly depleted toward the middle of the 20th century, exploration by the St. Joseph Lead Company resulted in the discovery of the Indian Creek subdistrict in 1948 (Wharton,

1975) and the Viburnum Trend, or New Lead Belt, to the west of the St. Francois Mountains in 1955 (Missouri DNR, Missouri Lead Mining History by County). As is the case in the Old Lead Belt, mineralization at Indian Creek and along the Viburnum Trend is primarily hosted in the Bonneterre Formation, although the Bonneterre Formation is covered by younger units and most mining is at greater depths as a result. The Viburnum Trend has been the source of all Pb production from the Southeast Missouri District since 1972 (Ohle, 1990).

As in Central Texas, there is a noted relationship between mineralization in the Southeast Missouri district and Precambrian knobs that resulted in depositional pinchouts of the basal Lamotte Sandstone. Throughout the district, mineralization is associated with digitate algal reef strata where detrital carbonate sediments have been trapped by organic structures. Faults are also known to have been major controls on mineralization with evidence for faulting occurring before, during, and after mineralization (Snyder and Gerdemann, 1968).

A comparison of MVT mineralization in Central Texas and Missouri compiled by Allie (1981) is shown in Table 1.2.

PREVIOUS WORK

Geology of MVT deposits and occurrences in Southeast Missouri and Central Texas

The USGS MVT deposit model (Leach et al., 2010) notes that the MVT deposit type was formally recognized in the late 1930s (Bastin, 1939). In the foreword of this collection, Bastin (1939) described the "amazingly voluminous literature" that had already been accumulated over the previous 50 years. There is an immense amount of information related to virtually all aspects of MVT mineralization in Southeast Missouri. Some general descriptions of the geology and mineralization of the Southeast Missouri district include

	Southeast Missouri	Central Texas
Host rock	Major deposits occur in shallow-water carbonates of Upper Cambrian Bonneterre Formation. Principal productions from certain stratigraphic horizons, although stratabound ore extends through entire Upper Cambrian-Lower Ordovician sequence. Unconformities, both basement and intrastratal, influences depositional and diagenetic facies.	Best known occurrences found in shallow subtidal carbonates of Upper Cambrian Cap Mountain. Stratabound sulfides concentrated in middle and basal Cap Mountain although sulfides are found throughout Riley Formation rocks. Pre-upper Cambrian basement unconformity influences depositional and diagenetic facies.
Diagenetic modification	Most ore deposits are confined to areas of regional dolostone development within the Bonneterre. Karstification is an important process in the development of some deposits.	All major prospect areas except Slaughter Gap found in dolomitized portions of the Cap Mountain. Few discernible karstification features present although Silver Creek prospect contains a mineralized collapse structure.
Regional mineralization controls	Deposits occur on margins of Pre-Cambrian Ozark Dome. Well-developed faulting peripheral to Ozark Dome may be important in ground preparation of some ore zones. Ore zones located near Precambrian topographic highs where the basal Upper Cambrian sequence is absent. Deposits located near facies boundaries of sedimentary or diagenetic origin.	Prospect areas located along margins of Precambrian Llano Uplift. Faulting present along periphery of Llano Uplift may be important in preparation of mineralized zones. Sulfide occurrences localized near Precambrian topographic highs where the basal Upper Cambrian sequence is absent. Deposits located near facies boundaries of sedimentary or diagenetic origin.
Local mineralization controls	Sedimentary structures: reefs, bars, slump breccias, and local facies changes important in ore localization. Sedimentary facies changes: ore occurs near pinchouts of Lamotte clastics against Precambrian basement. Diagenetic structures: solution collapse breccias and zones of secondary porosity often important ore hosts.	Sedimentary structures: lenses of fossiliferous or allochemical debris, laminations, layers important in sulfide localization. Sedimentary facies changes: sulfides occur near pinchout of Hickory clastics against PC basement. Diagenetic structures: solution collapse structure hosts sulfides at Silver Creek; secondary porosity zones well-developed in host rocks at Iron Rock Creek and Hog Thief Bend.
Ore mineralogy	Principal ore and gangue minerals are galena, sphalerite, pyrite, marcasite, chalcopyrite, dolomite, and calcite. A lead-dominant district with a Pb:Zn ratio of about 7:1. Minerals deposited in a complex overlapping sequence beginning with early iron sulfides followed by galena and sphalerite respectively.	Common minerals include pyrite and marcasite with dolomite; galena and sphalerite occur in minor amounts. Lead is considerably more common than Zn in all deposits. Minerals deposited in a complex sequence beginning with iron sulfides followed by galena and sphalerite.
Ore character	Coarse crystals of ore and gangue minerals filling open space of vugs, fractures, and breccia bodies most common textures. Disseminated "replacement" ore is associated with cavity-filling in some districts. Deposits relatively low-grade: 4-6% Pb, 1-2% Zn with appreciable amounts of Cu, Ag, Co, and Ni.	Open-space filling of sulfides in vugs, along fractures, and in breccia zones. Disseminated sulfides developed by removal of carbonate grains, are common in some mineral zones. Prospects uneconomic; highest assays from Silver Creek where 1-5 wt. % Pb was found in the collapse structure.

Table 1.2: A comparison of Southeast Missouri and Central Texas MVT mineralization. From Allie (1981).

Tarr (1936), Ohle and Brown (1954), and Snyder and Gerdemann (1968). An entire issue of Economic Geology (1977, v. 72, no. 3) covers topics related to the Viburnum Trend. A partial list of the numerous general reviews of the MVT deposit type include Anderson and Macqueen (1982), Sangster (1996), Leach et al. (2005), and the USGS MVT deposit model (Leach et al., 2010) as well as a Society of Economic Geologists Special Publication on carbonate hosted Pb-Zn deposits (1996, Special Publication No. 4).

There is substantially less published information available for even the four best known and studied Central Texas MVT occurrences at Silver Creek-Beaver Creek, Slaughter Gap, Hog Thief Bend, and Iron Rock Creek. Early descriptions of mineralization at these and other Central Texas locations by Comstock (1890, 1891), Paige (1911), and Baker (1933, 1935) noted the apparent similarities with mineralization in Southeast Missouri. Barnes (1956) described the character of mine workings and mineralization at Silver and Beaver Creeks and included descriptions from boreholes drilled in the 1920s. Allie (1981) detailed the stratigraphy and diagenetic history of the host rocks and origin of MVT mineralization at Iron Rock Creek. Allie's work was based largely on the examination of core from 30 boreholes drilled by Lehmann and Associates of Minnesota in the mid to late 1970s, which appears to be the last significant commercial exploration activity for base metal deposits in Central Texas. Smith et al. (1981) described regional zonation patterns of elements associated with MVT mineralization with a focus on the Hog Thief Bend area also using cores drilled by Lehmann and Associates. Farr and Gose (1991) report a Permian age of mineralization in breccias at Silver Creek from paleomagnetic data.

Barnes and Bell (1977) compiled a comprehensive report on the Paleozoic stratigraphy of the Moore Hollow Group in the Llano region of Central Texas with additional significant contributions to facies interpretations of the Riley Formation by

Krause (1996). McBride et al. (2002) described the character of the Hickory Sandstone in detail and noted a lack of evidence for widespread hot-fluid migration through the unit.

Prospectivity mapping of mineral deposits

Although there are prospectivity studies for essentially all mineral deposit types, those listed below represent an incomplete list compiled to illustrate the variety of deposit types and prospectivity modeling techniques that have been applied to them. Volcanogenic massive sulfide (VMS) prospectivity in Sweden was modeled by Carranza and Sadeghi (2010) using evidential belief functions and by Stensgaard et al. (2006) in west Greenland. Lindsay et al. (2014) evaluated porphyry Cu deposits in Arizona using weights-of-evidence and fuzzy logic, and Daneshfar (1998) modeled Cu-Au and Cu-Mo porphyry potential in southern British Columbia using fuzzy logic. Nykänen et al. (2008) used fuzzy logic to model Iron Oxide Cu-Au mineral potential in Finland. Feltrin (2008) attempted to integrate weights-of-evidence and a knowledge-driven approach (a weighted overlay method) to identify likely areas of Pb-Zn SEDEX mineralization in Australia. Harris et al. (2003) compared the effectiveness of weights-of-evidence, probabilistic neural networks (PNN), logistic regression, and discriminant analysis in predicting Carlin type Au in Nevada and intrusion-related Cu in Mexico and Nevada. Some additional work is presented in a 2010 special issue of Ore Geology Reviews (v. 38, no.3) devoted to mineral potential studies.

MVT specific prospectivity studies include an evaluation of MVT potential on the Leonard Shelf in the Canning Basin in Australia using fuzzy logic (D'Ercole et al., 2000). Daneshfar et al. (2006) used both weights-of-evidence and logistic regression to map MVT potential on Northern Baffin Island in northeastern Canada. Lindsay et al. (2016) used fuzzy logic to model mineral potential for a variety of deposit types including MVT in the Kimberley region of northwestern Australia.

The USGS conducted at least two assessments of MVT potential of the Rolla quadrangle between 1975 and 1982 as part of the CUSMAP program (Pratt, 1981; Pratt et al., 1986). The first of these assessments (Pratt et al., 1981) consisted of a manual synthesis of a variety of map data to identify areas likely to contain different types of mineral resources. Undiscovered MVT deposits were deemed the most likely type to exist in the Rolla quadrangle. The second assessment in 1982 (Pratt et al., 1986) used the same data and followed the same general approach as the first and had similar findings, but the data were manipulated digitally using a computer.

Chapter 2: Methods

Mineral potential, or prospectivity mapping, is a process of integrating and analyzing geospatial evidence to determine exploration targets for undiscovered mineral deposits within a permissive region (Carranza, 2009). The basic process involves combining various pieces of map evidence associated with a particular deposit type. The more overlap of evidence, the greater the potential for a deposit existing. This is conceptually similar to the traditional method of using a light table to physically stack various geologic, geophysical, and geochemical maps to identify overlapping relationships between these evidence layers and known mineralization. The advancement of computers capable of efficiently manipulating spatial data as part of a Geographic Information System (GIS) has enabled these types of spatial data to be visualized and quantified in more powerful ways and has facilitated the development of a variety of mineral potential mapping techniques.

As discussed in Carranza (2009), predictive modeling techniques may be categorized as either mechanistic or empirical. Mechanistic, or theoretical, modeling involves using mathematical equations to describe processes related to the phenomena being studied. Bonham-Carter (1994) suggested that mechanistic modeling to predict mineral deposits is impractical because of the complexity of factors that govern deposit formation. The work described here focuses instead on empirical modeling, which seeks to quantify the relationship between an outcome and the predictor variables that govern the outcome; the outcome is the presence of a mineral deposit and the predictor variables are spatial evidence layers associated with known deposits. Empirical modeling can be further categorized as either knowledge-driven or data-driven.

KNOWLEDGE-DRIVEN MODELS

In the context of minerals exploration, there are two required inputs for knowledge-driven, or qualitative models: geospatial evidence maps related to the deposits being sought and an "expert" to assign weights to the evidence maps (Figure 2.1). The assignment of weights to the evidence maps is based on the subjective judgement and experience of the expert. The efficiency of prospectivity maps generated using these methods is a reflection of both the quality of the expert judgement and the quality of the evidence maps. The major advantages of the knowledge-driven approach are that it is relatively simple to conceptualize and execute and does not require known deposits in the model area to train the model. This latter benefit makes it an especially appropriate technique in greenfield exploration environments where a lack of known deposits to train a model prevents a data-driven approach. The weighted overlay and fuzzy algebra methods are qualitative empirical (knowledge-driven) methods commonly applied to mineral potential mapping.

DATA-DRIVEN MODELS

The data-driven, or quantitative, empirical modeling approach also requires various geospatial evidence maps of the area of interest, but relies on known deposits in the model area rather than the judgement of an expert to determine the model parameters, or weights (Figure 2.2). These deposits function as training points for the model and the weights assigned to the evidence maps are determined quantitatively from the spatial relationships between the evidence and known deposits. A critical assumption is that the most likely areas to contain undiscovered mineralization are similar to those that contain known deposits. Although this method does not rely on the judgement of an expert to identify the relative importance the evidence maps, it requires a sufficient number of known deposits in the study area to train the model, which usually limits the application of data-driven
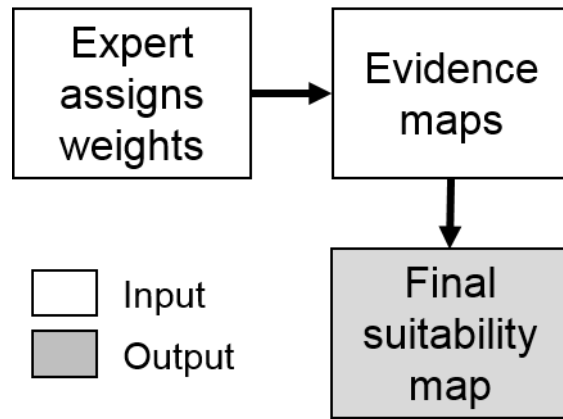
Figure 2.1:   Flow chart of the knowledge-driven approach to mineral potential modeling.
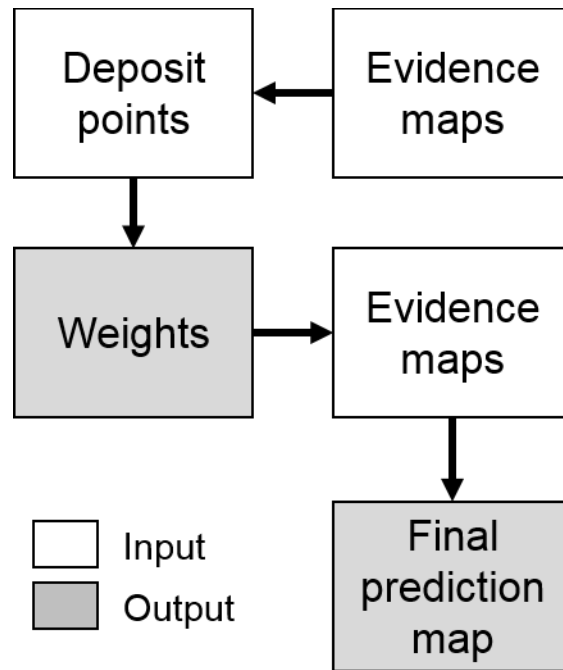
Figure 2.2: Flow chart of the data-driven approach to mineral potential modeling.

methods in greenfield exploration settings. This study is primarily concerned with the data-driven weights-of-evidence and the related fuzzy weights techniques.

WEIGHTS-OF-EVIDENCE

The weights-of-evidence method is one of many data-driven empirical modeling techniques. Agterberg and Cheng (2002) noted that the method was initially developed for and applied to medical diagnosis, but has since been successfully applied to a variety of geoscience problems and commonly to mineral potential mapping. Mathematically, the weights-of-evidence method is the log-linear form of Bayes rule, from which the posterior probability of a mineral deposit occurring is estimated from the spatial association between known deposits and different conditionally-independent evidence maps (Bonham-Carter, 1994).

Southeast Missouri is an ideal location to apply and evaluate data-driven prospectivity method like weights-of-evidence because it is a mature mining district with a relative abundance of data related to MVT mineralization available and a sufficient number of known deposits to train and test prospectivity models. Substantially fewer data are available for Central Texas – only a handful of MVT occurrences and no deposits representing large orebodies. Because of this, a mineral potential analysis for Central Texas would normally be restricted to qualitative, knowledge-driven methods. However, this work attempts to take advantage of the geologic similarities between Central Texas and Southeast Missouri and use model parameters quantitatively derived from Southeast Missouri in an estimation of mineralization potential in Central Texas.

Weights-of-evidence is used in this study for two primary reasons. First, like all data-driven approaches, it is by definition more objective than knowledge-driven methods because it does not rely on the potentially variable opinion or experience of an expert to

assign weights to the input layers. Secondly, The weights-of-evidence method has been demonstrated to have superior performance compared to other data-driven techniques like artificial neural networks or evidential belief functions when the input evidence maps are incomplete or missing information (Harris et al., 2003; Ford et. al., 2015). In the Central Texas study area in particular, several of the evidence maps are known to be incomplete because of the relatively limited modern exploration efforts and to the complication of postmineralization Cretaceous cover that hampers the collection of structural and other information in the underlying Paleozoic formations.

Several authors have suggested that a limitation of the weights-of-evidence method as it is traditionally used is that it requires the input evidence maps to be in binary form that correspond to presence or absence of a particular feature (Harris et al., 2003; Cheng and Agterberg, 1999). Continuous data, like proximity to geologic features or gravity and magnetic data, must be parsed into discrete intervals, or classes, and only a single class (typically the class with the highest contrast value) is incorporated in the final potential map. This results in a loss of potentially useful data from the classes that are excluded (Cheng and Agterberg, 1999; Singer and Kouda, 1999). Agterberg and Bonham-Carter (2005) argued that this discretization of a pattern to binary form is actually a positive facet of the weights-of-evidence method because it helps reduce the effects of regional variability in the data.

Conceptually, this reduction in regional variability by simplification (converting evidence to binary form) is similar to how a descriptive deposit-model works. For example, some MVT deposits are hosted by dolostones and some by limestones. The statement "most MVT deposits are hosted by carbonates" is accurate for both situations, although some specificity is lost when the general term "carbonates" is used rather than dolostone or limestone. In the same way, multivariate modeling techniques such as logistic regression

28

and artificial neural networks may be able to more fully capture the complexity between continuous-type evidence maps and deposits than bivariate techniques like weights-of-evidence in a given area (Carranza, 2009). However, as an objective of this study is to apply model parameters derived in Southeast Missouri to Central Texas, the reduction and simplification of continuous evidence maps to binary form as necessitated by the weights-of-evidence method may actually increase the portability of the model parameters from one area to another. Harris et al. (2003) used the term "out-of-sample inference" to describe the application of model parameters from one area to another and noted that this concept is commonly applied to exploration, although their application seems to be in the same general area that was used to train their model.

Bonham-Carter (1994, chapter 9) discussed the steps involved in applying the weights-of-evidence method. These are paraphrased below:

1. Collect evidence maps that may be of use in predicting a particular mineral deposit based on a conceptual deposit model.
2. Calculate weights and use these to reclassify each evidence map to binary form in a way that maximizes the spatial association between the evidence and training points.
3. Check for conditional independence (CI) and delete maps that cause CI violations.
4. Combine binary weight maps and prior odds to generate posterior probability maps.

A fifth additional step not described by Bonham-Carter (1994), but that comprised a significant portion of this work, is the evaluation of the model performance or model validation.

Although there are a variety of open-source and commercial GIS plug-ins available to carry out weights-of-evidence analyses, this study was conducted using only the built-in functionality of ArcGIS 10.3 and the Spatial Analyst and 3D Analyst extensions (ESRI, 2014). Weights were calculated in an external spreadsheet program, then added to the evidence layers using the raster calculator. The raster calculator was also the means of integrating the weighted evidence layers to produce the posterior probability maps. This "manual" process is more time consuming than using purpose-built software, but allowed more control in fine-tuning interval classes for which weights were calculated.

Collect evidence maps and initial data processing

A conceptual geologic model that summarizes the characteristics of the deposit type of interest should be the foundation of any prospectivity analysis because it facilitates the selection of useful evidence maps. These evidence maps show the distribution of spatial factors known or suspected to be associated with the deposit type being sought. In a data-driven evaluation, the deposit model is also the means of selecting training points for the mineral potential model. From a practical standpoint, the conceptual model helps prevent wasted effort in collecting data that is unlikely to be related to mineralization and facilitates the selection of suitable training points when multiple deposit types occur in the study area. Most of the data used for this study are publicly available in digital format, with the exception of the CUSMAP data layers for the Southeast Missouri district and some geophysical surveys for Central Texas that were scanned and digitized from analog hard-copy maps. A more thorough discussion of the evidence layers considered in this study and the geologic justification for their selection is presented in the following chapter.

Data related to mineral deposits must generally be manipulated until they are in a useable form for mineral potential studies. Some common manipulation includes creating

proximity classes, or buffer zones, around point, line, or polygon features; interpolating point data into continuous surfaces; and creating derivative layers from primary data (such as slope from elevation and geochemical anomaly maps from stream sediment geochemistry) (Figure 2.3).

Although not a requirement for the weights-of-evidence method, all data for this study are evaluated in raster format because of the relative ease of implementation within a GIS. Hengl (2006, Table 1) noted that the raster resolution, or cell size, should be a function of the map scale where the coarsest legible resolution should be less than or equal to the scale number multiplied by 0.0025 and the finest legible resolution should be greater than or equal to the scale number multiplied by 0.0001. Because much of the Southeast Missouri map data was digitized from the CUSMAP assessment maps at 1:250,000 scale (scale number of 250,000), this corresponds to a suitable resolution between 25 and 625 m (80 to 2050 ft). A 100 m (330 ft) cell size is used in this study because it simplifies area calculations. The closest two point locations for the Southeast Missouri MVT deposits considered in this study are 620 m (2030 ft) apart, thus a cell size of 100 m (330 ft) guarantees that no two deposits will occupy either the same or neighboring cells.

Calculate weights

The weights-of-evidence method uses the log-linear form of Bayes Rule to update a prior probability of a deposit using conditional probabilities from the association of evidence layers and known deposits (Bonham-Carter, 1994). The likelihood of a deposit occurring in a given area increases when different pieces of evidence associated with mineralization are also present in the area.

31
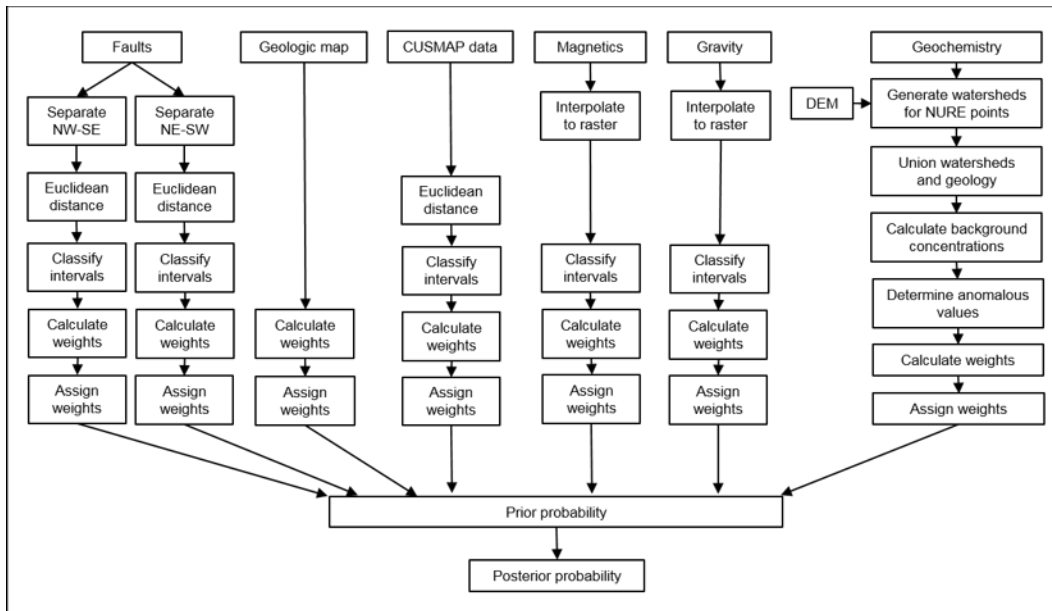
Figure 2.3: Summary of geoprocessing operations in the weights-of-evidence method.

If a given area is divided into small and equal sized unit cells large enough to only contain one mineral deposit, the prior probability of a deposit in any unit cell, $P\{D\}$, is given by the equation:

$$P\{D\} = N\{D\} / N\{T\}$$

where $N\{D\}$ is the number of deposit cells and $N\{T\}$ is the total number of cells in the deposit area (Bonham-Carter, 1994).

The probability of a given cell containing a deposit is higher when evidential features positively associated with mineralization are also present at that cell location. Because of this, the prior probability can be updated to a posterior probability using weights that represent the degree of spatial association between known deposits and evidence layers. These concepts are illustrated in Figures 2.4 and 2.5.

The calculation of weights is based on the fact that there are only four possible spatial relationships given a group of deposits and a binary map pattern representing the presence or absence of some evidence (Figure 2.6). The probabilities at each of these four situations are used to derive the positive and negative weights-of-evidence, W^+ and W^-, respectively. The first situation (case A) occurs at unit cells that contain both a known deposit and the binary evidence layer in consideration. The second situation (case B) occurs at unit cells where a deposit is present but the map pattern is absent. The third situation (case C) occurs at unit cells where the map pattern is present without a deposit, and the final situation (case D) occurs at unit cells where both the map pattern and a deposit are absent. The probability for each of the situations is calculated using the equations in Figure 2.7 with sample calculations shown in Figure 2.8.

For case A, the probability of the binary pattern being present given the presence of a deposit, $P\{B|D\}$, is given by the equation:

$$P\{B|D\} = P\{B{\cap}D\} / P\{D\}$$
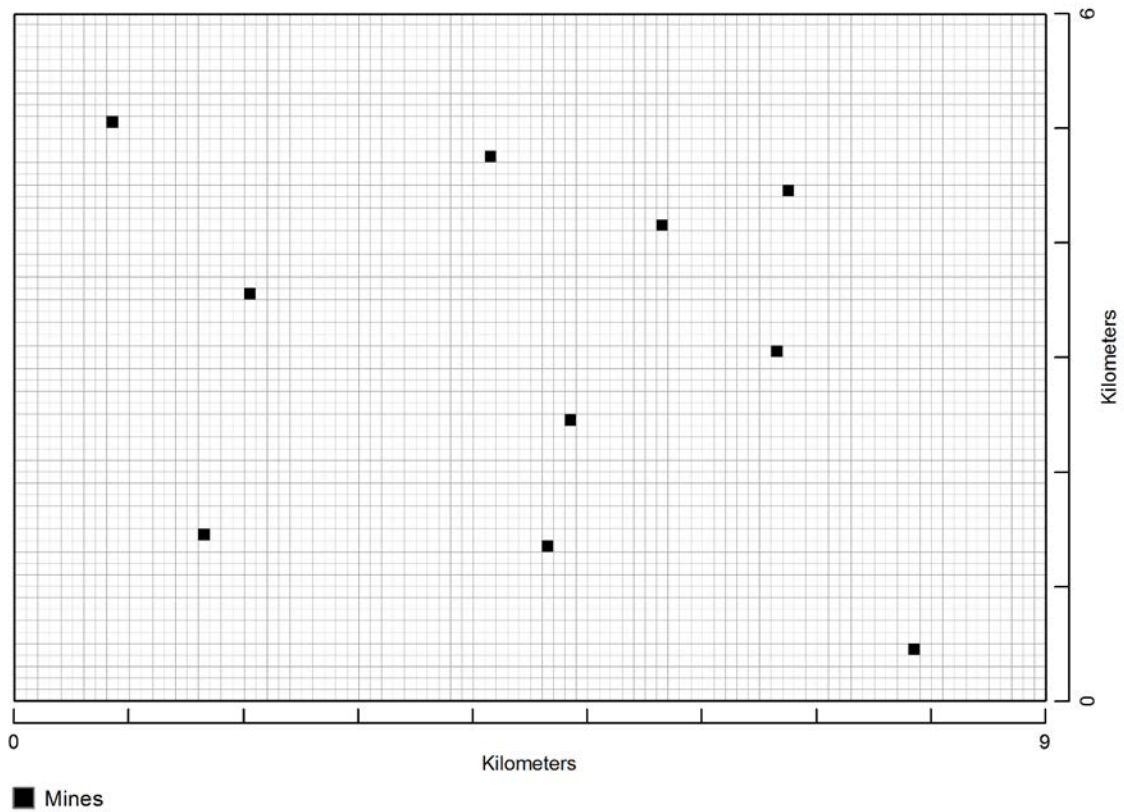
Figure 2.4: Schematic illustration of the prior probability of a mineral deposit in a study area. The prior probability of a deposit existing is equal to the total number of deposits (N(D)) divided by the total number of unit cells (N(T)) in the study area. In this example, a unit cell is 100 x 100 m, N(T) = 5400 and N(D) = 10. Thus, the prior probability of a deposit (P(D)) = 0.001852.
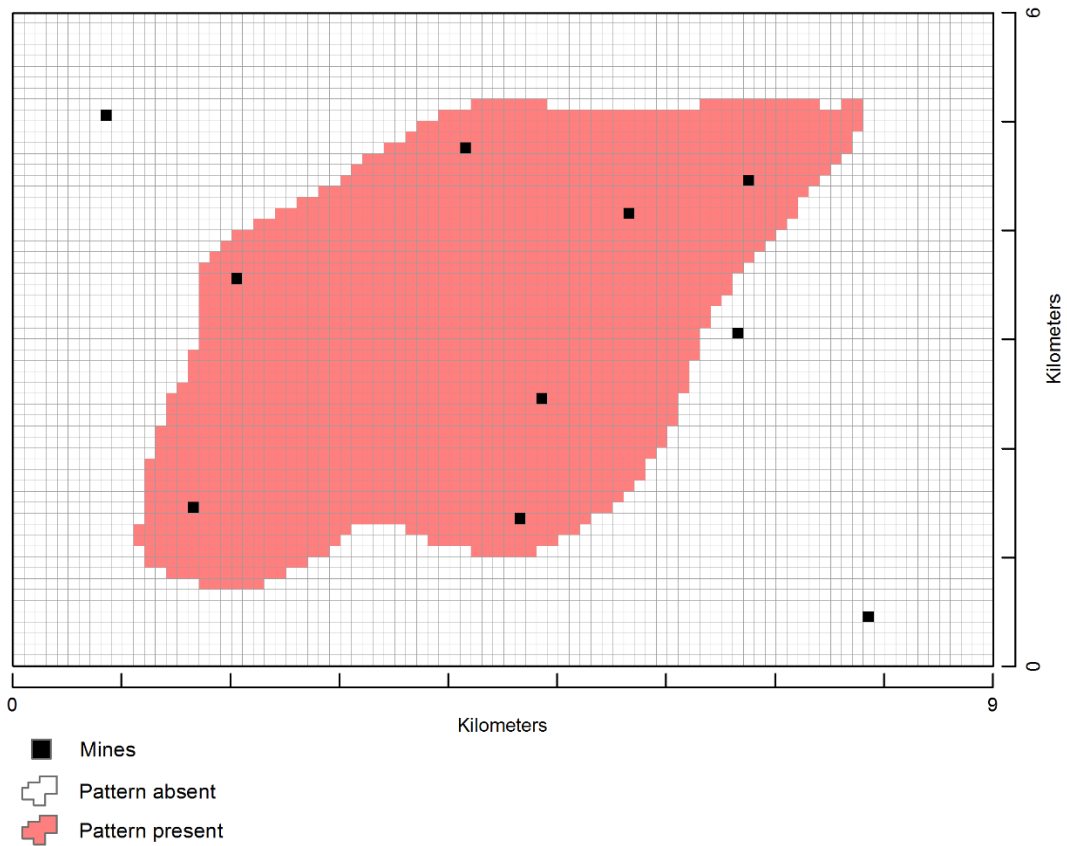
Figure 2.5: Schematic illustration of the probability of a deposit given a binary map pattern. The probability of a deposit occurring in a particular cell given the presence of a binary evidence pattern (P(D|B)) is equal to the number of cells containing both a deposit and the binary pattern (N(B∩D)) divided by the total number of binary pattern cells. In this example, 7 of 10 deposits occur on the binary pattern and there are a total of 1890 pattern cells. Thus P(D|B) = 0.003704, which is twice as high as the probability when the binary pattern is not considered.
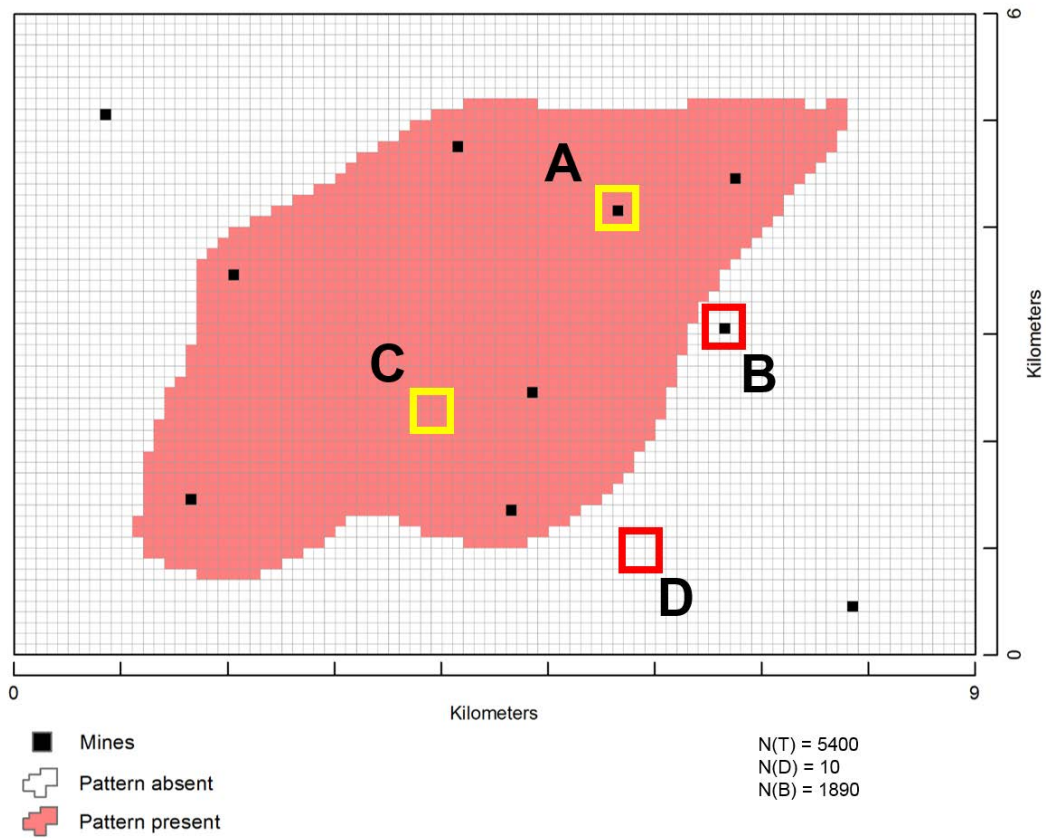
Figure 2.6: Illustration of the four possible relationships between deposits and a binary map pattern. Situation A occurs at every cell that contains both a deposit and the binary pattern. Situation B occurs in cells that contain deposits with no pattern. Situation C occurs in cells that contain the binary pattern and no deposits, and situation D occurs in cells that do not contain either deposits or the binary pattern.

	Pattern present	**Pattern absent**
Deposit present	**A** $P\{B|D\} = \dfrac{P\{B \cap D\}}{P\{D\}}$	**B** $P\{\widehat{B}|D\} = \dfrac{P\{\widehat{B} \cap D\}}{P\{D\}}$
Deposit absent	**C** $P\{B|\widehat{D}\} = \dfrac{P\{B \cap \widehat{D}\}}{P\{\widehat{D}\}}$	**D** $P\{\widehat{B}|\widehat{D}\} = \dfrac{P\{\widehat{B} \cap \widehat{D}\}}{P\{\widehat{D}\}}$

Figure 2.7: Probabilities equations for each unique situation given deposits and a binary pattern. Equations from Bonham-Carter (1994).

	Pattern present	**Pattern absent**
Deposit present	**A** $$P\{B|D\} = \frac{7}{10} = 0.7$$	**B** $$P\{\widehat{B}|D\} = \frac{(10-7)}{10} = 0.3$$
Deposit absent	**C** $$P\{B|\widehat{D}\} = \frac{1890 - 7}{5400 - 10} = 0.3494$$	**D** $$P\{\widehat{B}|\widehat{D}\} = \frac{(5400-1890-10+7)}{(5400 - 10)}$$ $$= 0.6506$$

Figure 2.8: Sample probability calculations. Values are derived from previous figures.

where P{B∩D} is the number of cells occupied by both the pattern and deposit and P{D} is the total number of deposits (Bonham-Carter, 1994). In the example study area shown in Figure 2.6, there are a total of ten deposits, and seven of these ten occur in cells that also contain the binary pattern, therefore the probability for situation A is 0.7.

For case B, the probability of the pattern being absent given the presence of a deposit, $P\{\hat{B}|D\}$, is given by the equation:

$$P\{\hat{B}|D\} = P\{\hat{B}\cap D\} / P\{D\}$$

where $P\{\hat{B}\cap D\}$ is the number of cells that contain a deposit and no pattern and P{D} is the total number of deposits (Bonham-Carter, 1994). Using the example study area, the probability for case B is 0.3. The probabilities for situations A and B add up to one.

For case C, the probability of the pattern being present given the absence of a deposit, $P\{B|\hat{D}\}$ is given by the equation:

$$P\{B|\hat{D}\} = P\{B\cap\hat{D}\} / P\{\hat{D}\}$$

where $P\{B\cap\hat{D}\}$ is the number of cells containing the pattern without a deposit and $P\{\hat{D}\}$ is the total number of cells in the study area minus the number of deposits (Bonham-Carter, 1994). In the example, the probability for situation C is 0.3494.

For case D, the probability of the pattern being absent given the absence of a deposit, $P\{\hat{B}|\hat{D}\}$, is given by the equation:

$$P\{\hat{B}|\hat{D}\} = P\{\hat{B}\cap\hat{D}\} / P\{\hat{D}\}$$

where $P\{\hat{B}\cap\hat{D}\}$ is the number of cells that contain neither a deposit nor the pattern and $P\{\hat{D}\}$ is the total number of cells in the study area minus the number of deposits (Bonham-Carter, 1994). As is true for cases A and B, the sum of probabilities C and D will always equal one.

Assuming that there is a positive spatial association between the map pattern and the deposits, the probability of case A will be larger than 0.5 with larger numbers corresponding to stronger associations. Because A plus B will equal one, if case A is larger than 0.5, case B must be less than 0.5, and the probability of case B will decrease as the probability of A increases. Similarly, case C will have a probability less than 0.5 and case D will have a probability greater than 0.5.

From these four probabilities, the Sufficiency and Necessity Ratios are calculated (Bonham-Carter, 1994). The Sufficiency Ratio, LS, is given by the equation:

$$LS = P\{B|D\} / P\{B|\widehat{D}\}$$

which is probability A divided by probability C (Figure 2.9).

The Necessity Ratio, LN, is given by the equation:

$$LN = P\{\widehat{B}|D\} / P\{\widehat{B}|\widehat{D}\}$$

which is probability B divided by probability D (Figure 2.10). When there is a positive spatial association between the binary map pattern and the known deposits, the Sufficiency Ratio has a value greater than one and the Necessity Ratio has a value less than one. The positive weight, W^+, is equal to the natural logarithm of the Sufficiency Ratio:

$$W^+ = Log_e (LS)$$

and the negative weight, W^-, is equal to the natural logarithm of the Necessity Ratio:

$$W^- = Log_e (LN).$$

The positive weight is a measure of the strength of association between the presence of evidence and the presence of deposits, and the negative weight is a measure of strength of association between the absence of evidence and absence of deposits. The difference between the weights is termed the contrast, C, and is equal to W^+ minus W^-:

$$C = W^+ - W^-.$$

A

$$P\{B|D\} = \frac{P\{B \cap D\}}{P\{D\}}$$

C

$$P\{B|\widehat{D}\} = \frac{P\{B \cap \widehat{D}\}}{P\{\widehat{D}\}}$$

Sufficiency ratio (LS)

$$= \frac{P\{B|D\}}{P\{B|\widehat{D}\}} = 2.0034$$

W⁺

$$= \log_e LS = 0.6948$$
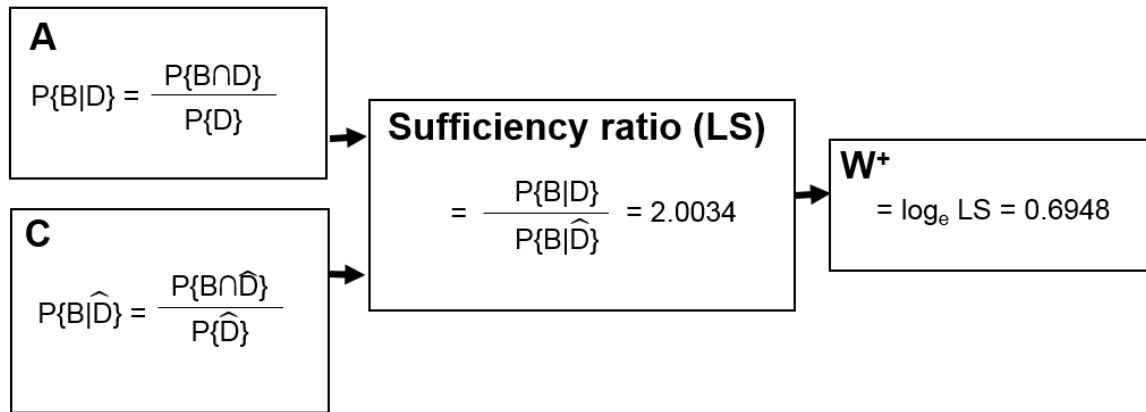
Figure 2.9: Sufficiency ratio calculations. The sufficiency ratio (LS) is the ratio of probability situations A and C, and the positive weight is the natural logarithm of the sufficiency ratio. The values shown above are from the example used in previous figures.

B

$$P\{\widehat{B}|D\} = \frac{P\{\widehat{B} \cap D\}}{P\{D\}}$$

D

$$P\{\widehat{B}|\widehat{D}\} = \frac{P\{\widehat{B} \cap \widehat{D}\}}{P\{\widehat{D}\}}$$

Necessity ratio (LN)

$$= \frac{P\{\widehat{B}|D\}}{P\{\widehat{B}|\widehat{D}\}} = 0.4611$$

W⁻

$$= \log_e LN = -0.7741$$
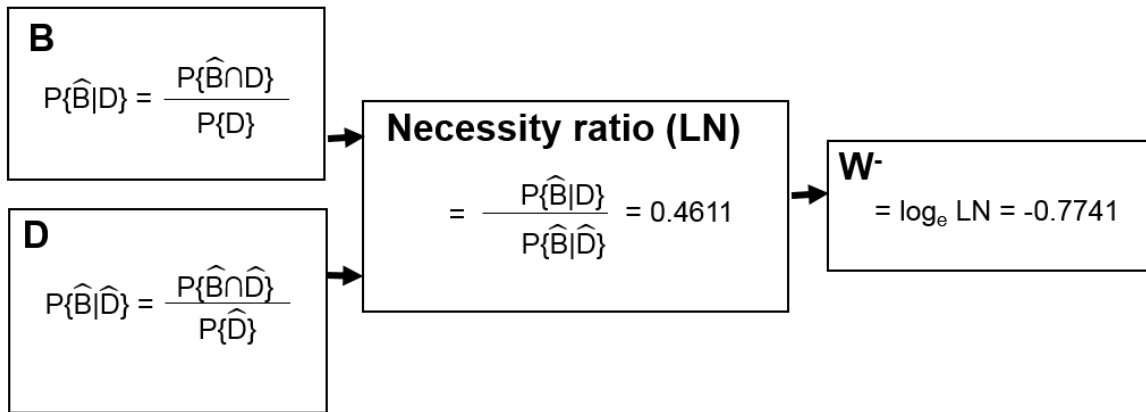
Figure 2.10: Necessity ratio calculations. The necessity ratio (LN) is the ratio of situations B and D, and the negative weight is the natural logarithm of the necessity ratio. The values shown above are from the example used in previous figures. The contrast for this example is 1.4689.

The studentized contrast is the contrast divided by its standard deviation ($C/\sigma C$). Both the contrast and studentized contrast values can be useful in selecting the best binary evidence from a particular theme to be incorporated in the posterior probability map, but this study makes more extensive use of the studentized contrast as a means of evaluating evidence.

Combine weights maps

After weights have been calculated for each binary interval of each evidence map, the interval with the highest studentized contrast value is identified. This is the interval with the strongest spatial association with known deposits. The positive weight (W^+) for that interval is assigned to every unit cell where the factor is present, and the negative weight (W^-) is assigned to unit cells where the factor is absent (Figure 2.11).

Bayes Rule states that the conditional probability of a deposit occurring at each unit cell (in logit form), given a group of binary evidence maps, is equal to the prior logit at the cell plus the sum of all positive and negative weights for each evidence map at that cell location. The prior logit is equal to the natural logarithm of the prior odds (O), $O = 1 / (1-P)$ where P is the prior probability. The binary evidence maps are added to this prior logit to produce the posterior odds map. The posterior logit map can then be converted into a probability map, P, using the equation:

$$P = e^x / (1+e^x)$$

where x is the posterior logit value at each cell in the map area.

The resulting map consists of areas of unique conditions that share the same posterior probability of a mineral deposit. These unique conditions are areas that share the same overlapping evidence. The number of possible unique conditions for a given model is dependent on the number of input maps, where $UC = 2^n$, and n is the number of binary

43
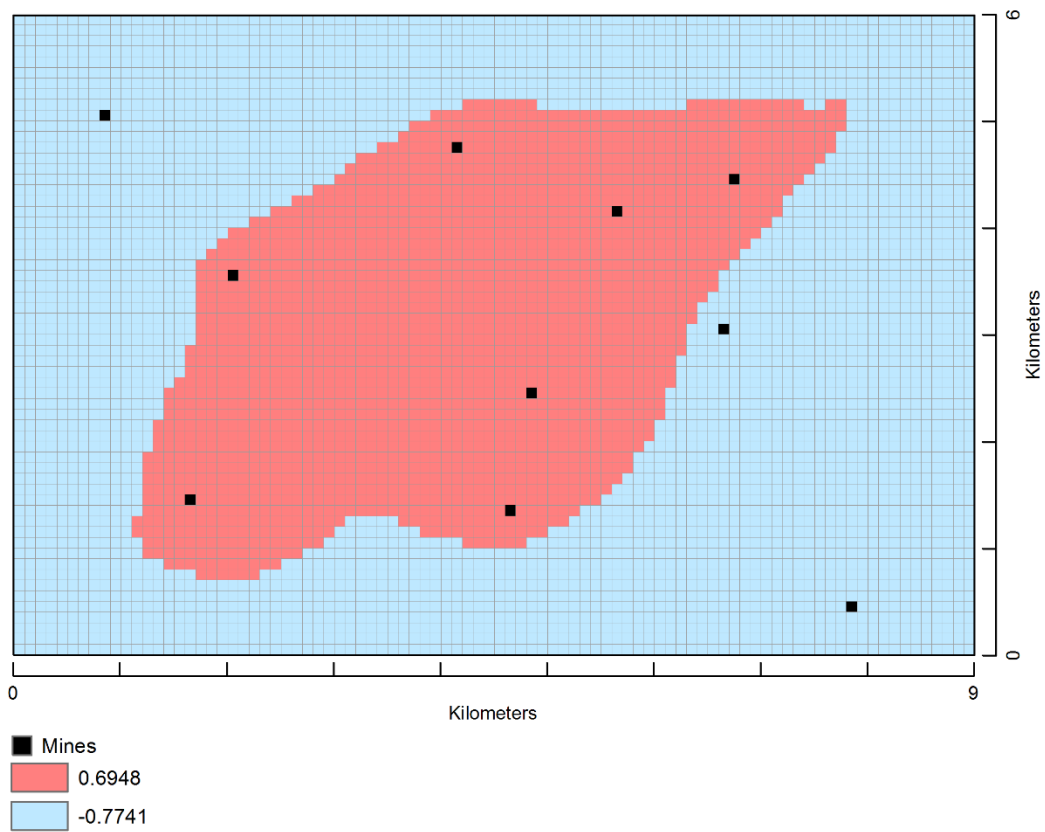
Figure 2.11: Assignment of positive and negative weights to binary evidence. The positive weight (W+) is assigned to cells where the pattern is present and the negative weight (W-) is assigned to all other cells. Areas with "no data" are assigned a value of 0.

weights maps incorporated in the model (Bonham-Carter, 1994). If data is missing from a particular evidence map, this area is assigned a weight of zero. This ensures areas with no data have no impact on the final posterior probability map, but also makes the evidence map ternary (W^+, W^-, and no data) and therefore increases the number of unique conditions. This ability to effectively handle missing evidence in the input maps is a noted advantage of the weights-of-evidence method over other mineral potential approaches.

Fuzzy weights

As mentioned above, there is some debate as to whether the classification of continuous data to binary form for use in the weights-of-evidence method is a positive or negative aspect of the method. Whether or not the discretization is positive or negative, the fuzzy weights method was developed as a means of more efficiently incorporating continuous data into a model. In this study, models produced using fuzzy inputs rather than binary inputs tended to have slightly higher efficiency scores than those produced using only binary variables.

In the fuzzy weights method as described by Cheng and Agterberg (1999), a fuzzy membership function is fit to the contrast values for a multiclass evidence map (Figures 2.12-2.14). The maximum W^+ is then applied to the highest contrast, with scaled weights assigned to other interval classes based on their contrast values.

Evaluate model performance

Because the ultimate objective of a mineral potential model is to highlight target areas likely to contain undiscovered deposits, the evaluation of models should consider how well a particular model does works. This study evaluates model performance conventionally using blind testing and associated prediction rate curves to determine model efficiency scores. Conditional independence (CI) of evidence layers in a model is also
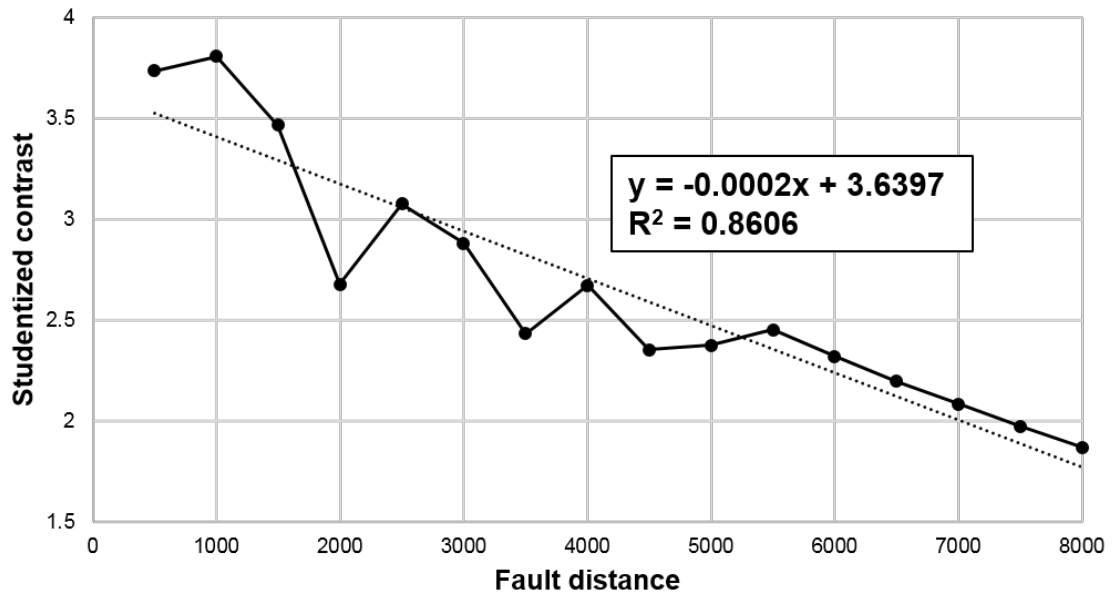
Figure 2.12: Studentized contrasts vs. fault proximity classes. Note the approximately linear relationship.
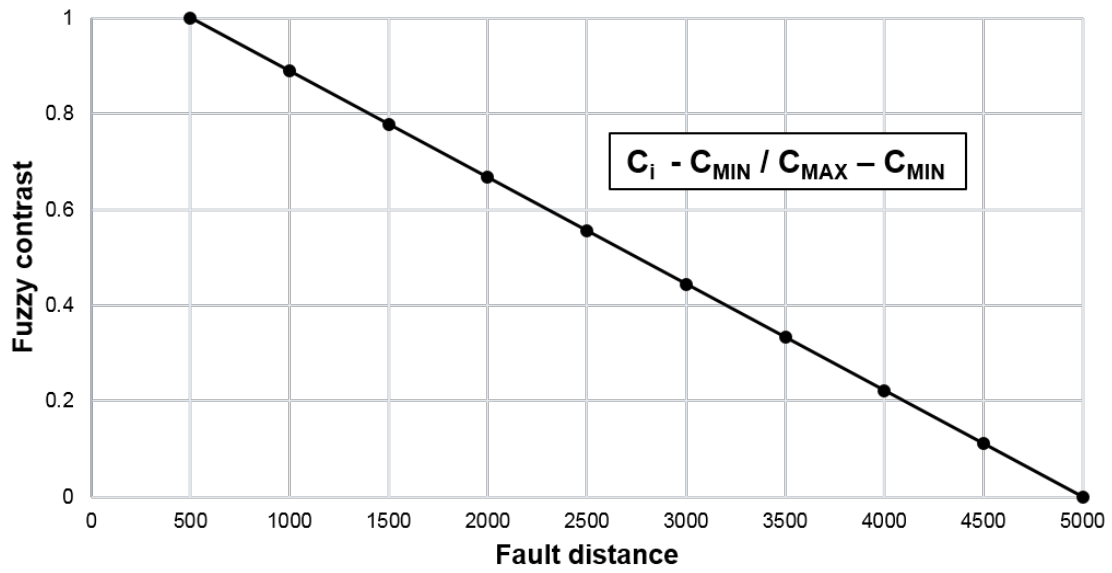
Figure 2.13: Fuzzified contrast vs. fault proximity class. Fuzzy values range from 1 to 0.

The chart shows:
- Y-axis: **Fuzzy weight** with values 1.5, 1, 0.5, 0, -0.5, -1, -1.5
- X-axis: **Fault distance** with values 0, 1000, 2000, 3000, 4000, 5000, 6000
- Equation box: $((W^+_{MAX} - W^-_{MIN}) * \text{Fuzzy } C_i) + W^-_{MIN}$
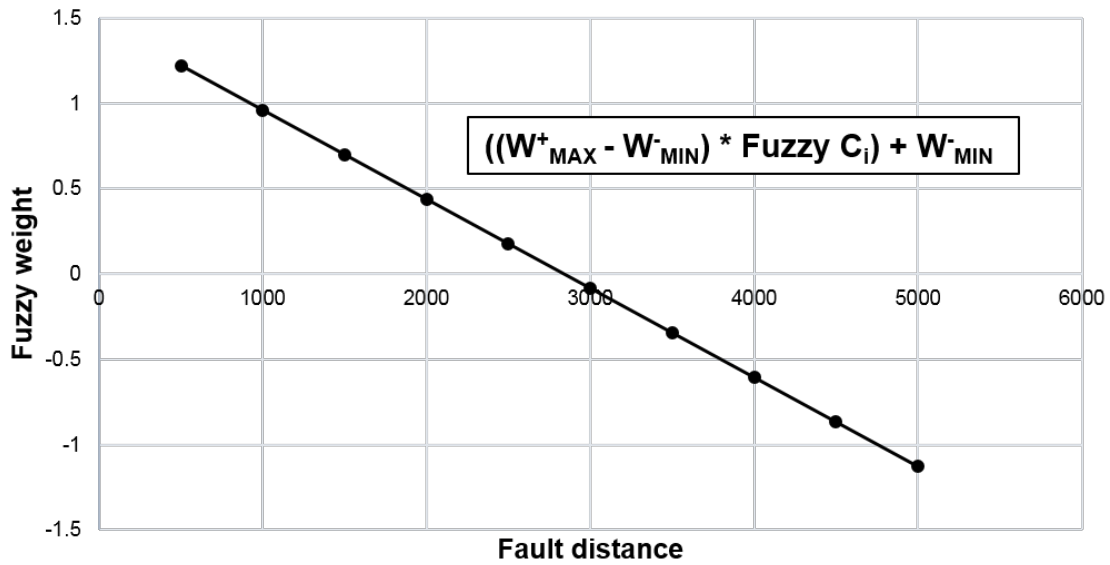
Figure 2.14: Fuzzy weight vs. fault proximity class. Weights are assigned to each proximity class based on the fuzzified contrast value. The maximum positive weight is assigned to the fuzzy contrast value of 1 corresponding to the 500 m proximity class and the minimum negative weight is assigned to the fuzzy contrast value of 0 corresponding to the 5000 m proximity class.

considered. Additionally, Central Texas models are evaluated using historic, semiquantitative geochemistry measurements from insoluble residues derived from core and cuttings from wells within the study area.

Blind testing

Blind testing is carried out by dividing the known deposits in a study area into a training and a validation, or testing, set. The weights for each evidence layer are calculated using only the deposits in the training set. As a result, the model is "blind" to the deposits in the validation set, which allows the model to be evaluated based on how well it "predicts" the location of these deposits (Fabbri and Chung, 2008).

Efficiency of classification

A prediction rate curve (PRC) can be used to show how well a particular model "predicts" the training deposit points used to generate the model (Chung and Fabbri, 2003). This curve is created by ordering the unique conditions from highest to lowest posterior probability, then plotting the cumulative number of deposits predicted by the cumulative area occupied by the unique conditions. The area under this curve can be calculated to determine an efficiency score (Raines, 2006). A model that predicts many deposits in a small amount of the overall area will have a steep initial slope on the PRC and result in an efficiency score close to one, or 100%. When the association between the model and validation deposits is random as would be the case for a poorly performing model, the PRC will be a line with a slope of one and an efficiency score of 50%.

Nonpredicted deposits

Deposits that fall within these areas of lower posterior probability are poorly classified. They represent either deposits that are dissimilar to the other training points or suggest that the evidence themes considered in the model are insufficient to effectively

predict deposit locations. As model performance improves, the number of poorly classified deposits is reduced (Schmitt, 2010).

Conditional independence

Conditional independence (CI) is a required assumption in weights-of-evidence modeling (Bonham-Carter, 1994). CI means that evidence maps used to generate the predictive model are predictive of the deposits of interest, but not of other evidence. For example, the assumption of CI necessitates that only one of the several geochemical anomaly maps generated for this study be used in a predictive model. If the presence of a geochemical anomaly is the result of MVT mineralization, then Pb anomalies should occur in the same catchment basins as Zn anomalies. Therefore, using both Pb and Zn anomalies as evidence in the predictive model would result in inflated posterior probabilities in the areas where both occur (Bonham-Carter, 1994; Agterberg and Cheng, 2002). These issues can sometimes be resolved by combining the input maps, for example by using the Boolean "OR" operator to create a map that shows areas that contain either Pb or Zn anomalies.

Conditional independence is evaluated by the CI ratio, which is equal to the number of actual deposits divided by the number of predicted deposits (Schmitt, 2010). Because the probability of a deposit occurring in a given area is equal to the number of deposit cells divided by the total number of cells, the number of predicted deposits for each unique condition can be calculated by multiplying the posterior probability of the unique condition by its area. This number is summed for the entire map resulting in the total number of predicted deposits. Bonham-Carter (1994) suggested that a violation of CI of more than 15% (CI ratio values lower than 0.85) should be considered significant, but allows that in practice, there are always more predicted than actual deposits.

Chapter 3: Data

Most geospatial data used for this study are publicly available. The singular exception to this is a series of aeromagnetic maps that have been processed to show areas of Precambrian basement highs for a portion of the Central Texas study area. These data were donated to the University of Texas in the spring of 2016 by Ernest K. Lehmann & Associates of Minneapolis. The data presented as maps were collected as a part of wider exploration efforts for Pb mineralization in Central Texas in the 1970s and early 1980s.

Much of the data for the Southeast Missouri analysis were digitized from maps published in the USGS CUSMAP assessments of the Rolla quadrangle (Pratt et al., 1981). As part of these studies, the authors identified and evaluated the map distribution of diagnostic and permissive criteria associated with known MVT deposits using a descriptive model (Pratt et al., 1986). The authors defined diagnostic criteria as those that are associated with nearly all known deposits and are thought to be required for a deposit to exist and permissive criteria as those that are thought to be important to some deposits, but are not required for a deposit to exist. Although the authors published evidence maps showing the distribution of these features, they note that these maps are "highly generalized." In addition, portions of the Rolla quadrangle are lacking sufficient data for some of the criteria resulting in incomplete maps.

In addition to these CUSMAP evidence layers, basement structure, surficial geology, gravity, magnetics, and geochemistry data were also evaluated. These are especially important pieces of information because there are similar quality datasets available for both Southeast Missouri and Central Texas. Many of these maps were processed to make a variety of derivative maps in an effort to increase contrast values and to reduce location dependence and increase portability of the data.

As discussed in the previous chapter, the C/σC value is used as the benchmark for evaluating classes within the evidence maps. Evidence classes with high C/σC values tend to predict a large number of deposits in a small amount of the map area (Table 3.1). Weights and contrast values for each proximity class in the evidence layers are included in Appendix A.

SOUTHEAST MISSOURI MVT MINES

The location of 49 MVT mines that were used as training and testing points for the SEMO models were digitized from a map compiled by Kisvarsanyi and Miller published in the first CUSMAP assessment of the Rolla quadrangle (Pratt et al., 1981). These points represent the shaft locations for mines in each of the three main subdistricts described earlier as well as Annapolis area mines to the south of the St. Francois Mountains. A total of 25 mines were randomly selected as training points and the remaining 24 were used as testing points to validate the models (Figure 3.1).

MVT CONSIDERATIONS

Data were selected for this study based on assumed usefulness in predicting MVT deposits and have been categorized into one of five MVT ore considerations (Table 3.2). These considerations are modified after ore controls from the USGS MVT deposit model (Leach et al., 2010): faults and fractures, dissolution collapse breccias, lithological/facies transitions, basement structures, and presence of MVT/trace element mineralization. The first three considerations are identified as the most important ore controls in the USGS deposit model and are interpreted to be controls related to permeability pathways for the mineralizing fluids. Basement topography is noted to be locally significant in both Southeast Missouri and in Central Texas. The last consideration, MVT/trace element mineralization, is not an MVT control, but there are geochemical signatures associated with

52

Data used to satisfy consideration	Best Class	C	σC	C/σC	σC/C	% Area	% Deposits
Proximity to algal reef rocks	1500 m	2.71	0.40	6.78	0.15	6%	48%
Host rock unit	Elvins Grp and Bonneterre Fm	2.34	0.40	5.81	0.17	7%	44%
Bouguer gravity anomaly	-15 - -10 mGal	2.30	0.41	5.63	0.18	6%	40%
Stream sediment geochemistry	Pb OR Zn OR Cu	2.67	0.47	5.62	0.18	5%	44%
Proximity to basement highs	500 m	1.92	0.41	4.70	0.21	9%	40%
Anomalous base metal concentrations in Bonneterre	Present	1.76	0.40	4.38	0.23	14%	48%
Proximity to NWSE faults	500 m	1.81	0.43	4.21	0.24	7%	32%
Proximity to all faults	1000 m	1.52	0.40	3.81	0.26	19%	52%
Proximity to limestone dolostone interface	14500 m	1.89	0.50	3.78	0.26	38%	80%
Proximity to Lamotte pinchouts	2500 m	1.32	0.40	3.30	0.30	22%	52%
Percent magnetic response	35 - 35%	1.29	0.41	3.17	0.32	15%	40%
Magnetic slope	6.8 - 37.5%	2.13	0.74	2.89	0.35	58%	92%
Magnetic response	300 - 400 nT	1.30	0.55	2.38	0.42	5%	16%
Proximity to brown rock/white rock interface	4000 m	2.18	1.10	1.99	0.50	36%	83%
Proximity to magnetic hills	2000 m	0.70	0.43	1.62	0.62	51%	68%
Bouguer gravity slope	0.5 - 11%	0.54	0.41	1.32	0.76	47%	60%
Proximity to NESW faults	7000 m	0.44	0.40	1.10	0.91	45%	56%
Proximity to tin granite plutons in basement	0 m	0.48	0.50	0.97	1.03	13%	20%

Table 3.1:   Summary of contrasts for the best performing Southeast Missouri evidence classes.
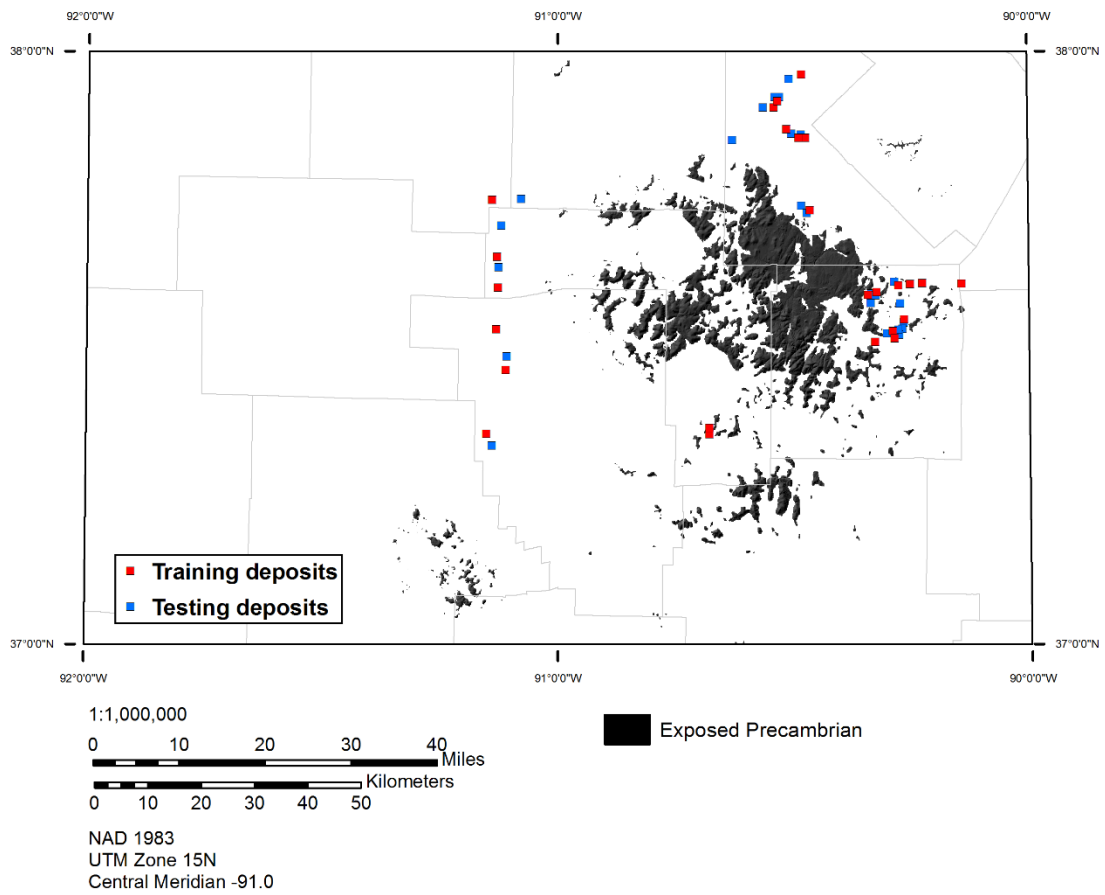
Figure 3.1:   Training and testing (validation) deposit locations in Southeast Missouri. Data digitized from a map compiled by Geza Kisvarsanyi and Mary Miller in Pratt et al., 1981.

MVT ore controls	Data used to evaluate mineralization controls
Faults and fractures	Proximity to faults
Dissolution collapse breccias	Proximity to faults
Lithological/facies transitions	Host rock lithology Proximity to algal reef rocks* Proximity to brown rock-white rock interface* Proximity to Limestone-dolostone Interface* Proximity to Lamotte pinchouts*
Basement structures	Bouguer gravity anomaly Magnetic response Proximity to basement highs Proximity to tin granite plutons in basement*
Presence of MVT/trace element mineralization	Stream sediment geochemistry Anomalous base metal concentrations in Bonneterre*

Table 3.2:   MVT mineralization controls and associated data used to model prospectivity in Southeast Missouri. An asterisk indicates CUSMAP data only applicable to Southeast Missouri.

these deposits that can be useful in exploration. The following discussion is organized by these considerations.

Faults and fractures

Many of the earliest investigations of MVT deposits in Southeast Missouri and Central Texas noted the spatial relationship between mineralization and faults (e.g., Tarr, 1936; Ohle and Brown, 1954; Comstock, 1891). Leach et al. (2010) noted that in most MVT districts, faults themselves are not mineralized, but mineralization is concentrated in dilatency zones adjacent to faults. Numerous authors note the relationship between mineralization in Southeast Missouri and northwest-southeast oriented faulting (i.e., the Ste. Genevieve, Simms Mountain, Cedar Creek, and Palmer faults) (Tarr, 1936; Ohle and Brown, 1954; Thacker and Anderson, 1977) although there are also northeast-southwest oriented faults (the Ashbank system) (Snyder and Gerdemann, 1968). Snyder and Gerdemann (1968) discussed evidence for faulting occurring in the Southeast Missouri district pre-, syn-, and postmineralization based on the relationships between the faults and ore.

In addition to the previous authors, Pratt et al. (1981) considered proximity to faults a diagnostic criterion in the CUSMAP assessment of the Rolla quadrangle. The Southeast Missouri fault data considered in this study was digitized from these CUSMAP maps (Figure 3.2). Weights and contrasts for the proximity to all faults as well as the proximity to only faults oriented NW-SE (90-180°) and NE-SW (0-90°) were calculated in 500 m (1,600 ft) intervals (Figure 3.3). The highest C/σC value for these three evaluations is 4.21 for the 500 m (1,600 ft) buffer zone around NW-SE oriented faults. This buffer corridor occupies 7.2% of the map area and contains 32% of the training deposits. When all faults are considered regardless of their orientation, the highest C/σC value drops to 3.81 for the
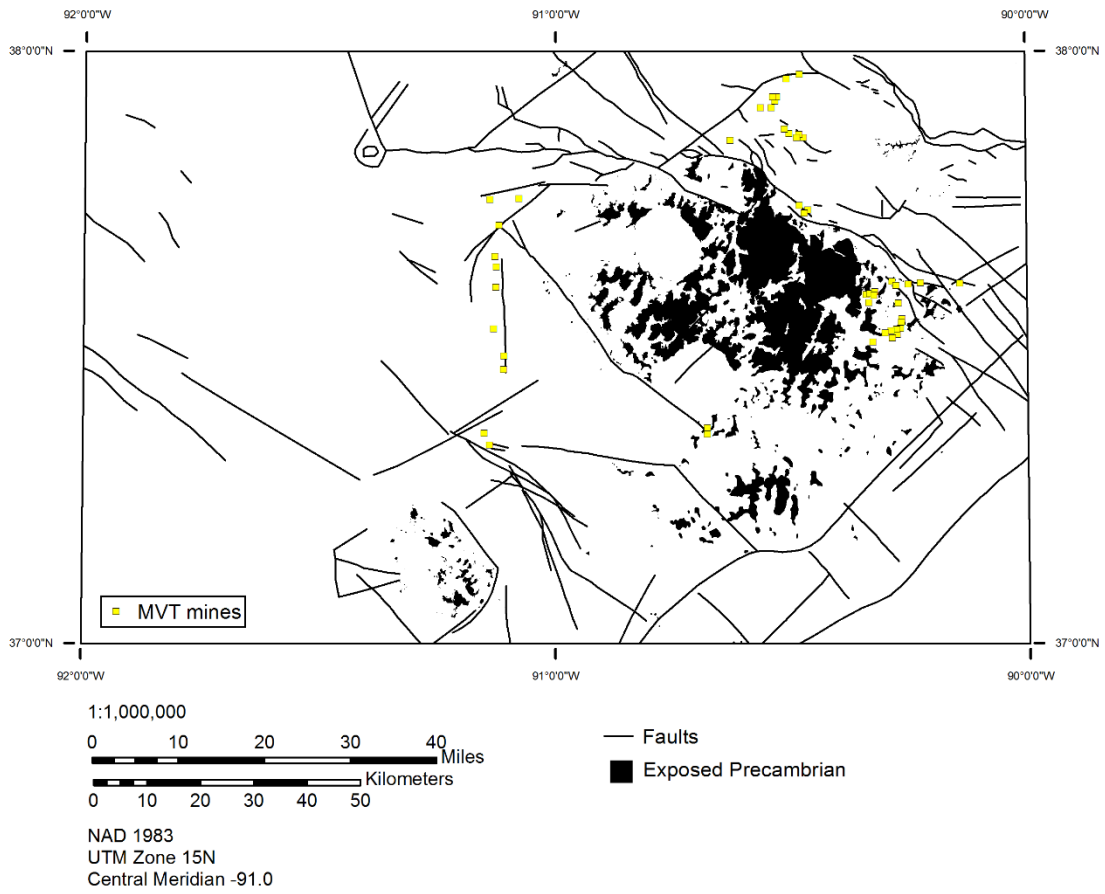
Figure 3.2:   Southeast Missouri faults. Digitized from CUSMAP diagnostic criteria map
(Prat et al., 1981).
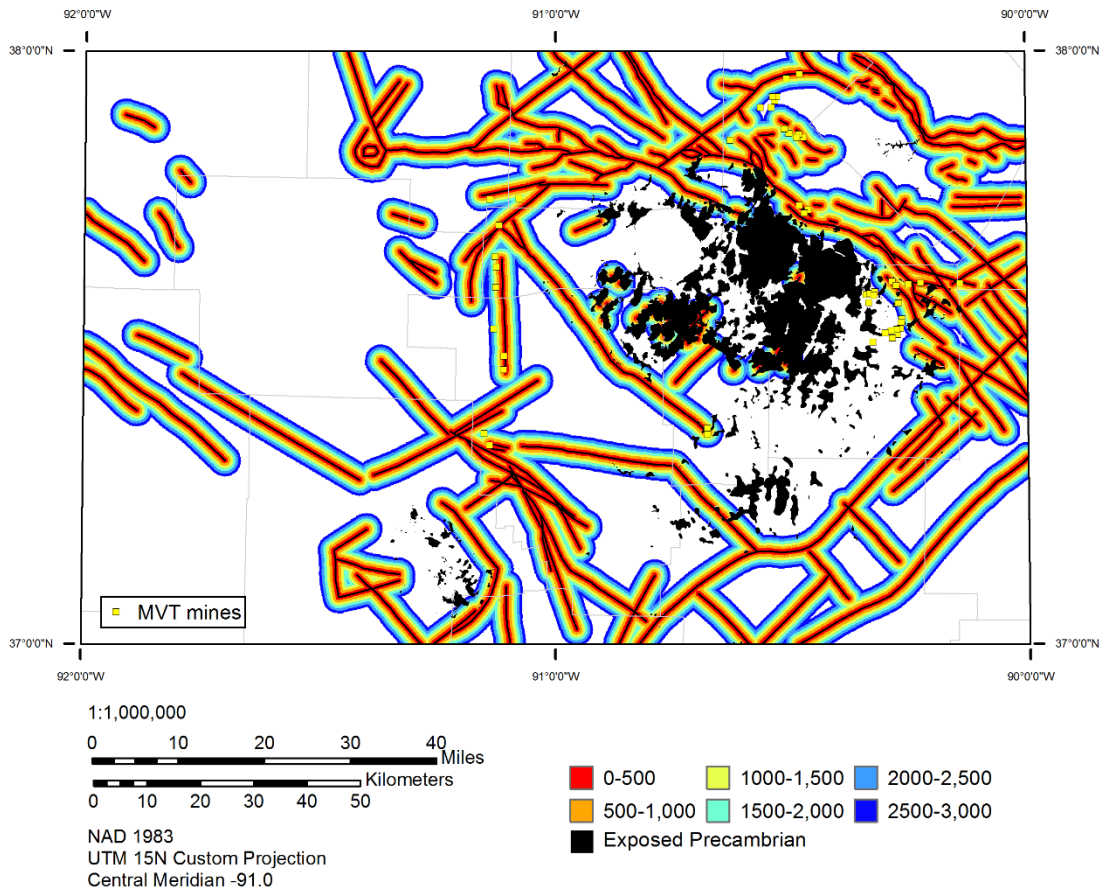
Figure 3.3:   Southeast Missouri fault proximity classes. Although only distances from 0-3000 m are shown here for clarity, distances up to 8500 m were evaluated.

1000 m (3300 ft) buffer corridor which covers 19.1% of the study area but contains 52% of the training deposits (Figure 3.4).

There are several sources of fault data available for Central Texas that vary in scale and completeness of coverage. Initially, fault data from the Geologic Database of Texas (GDbT) digital database at 1:250,000 was incorporated in the Texas models (Figure 3.5). However, examining the distribution of faults contained in this GDbT data and the Southeast Missouri faults showed that there was a much higher fault density in the Central Texas data. Additionally, fault information in Central Texas is complicated by the presence of Cretaceous strata that cover the older Paleozoic sedimentary units of interest and that cover the older faults. This is especially apparent in the GDbT fault data as the trace of most faults in Paleozoic units end where overlain by Cretaceous units.

As a result of the difference in fault density in Southeast Missouri and Central Texas, as well as the issue with Cretaceous cover, fault data from the Tectonic Map of Texas (Ewing et al., 1990) was ultimately used in the Texas models (Figure 3.6). The smaller scale of this map compared to the GDbT fault data means that only relatively large faults are included in the map, which reduces the fault density in the study area to an amount that appears to be more compatible with the Southeast Missouri area. Additionally, this map contains more faults in the portion of the map area covered by Cretaceous rocks. Even so, it is likely that there are additional faults buried by Cretaceous cover. To account for this, areas of the map with Cretaceous rocks and no faults were given a weight of 0, which minimizes the effects of a lack of data in the final models.

Dissolution collapse breccias

The presence of dissolution collapse breccias is noted as an important control on ore mineralization in the Viburnum Trend, although these features are nonexistent or were
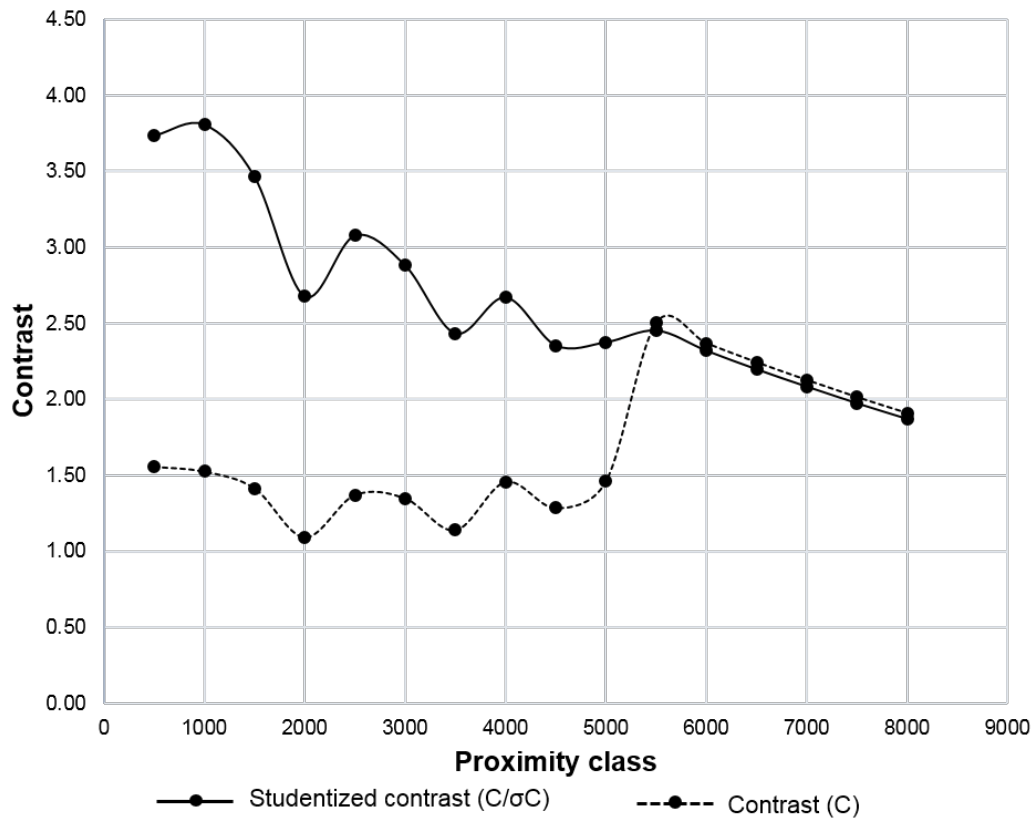
Figure 3.4:   Southeast Missouri fault proximity classes vs. contrast values. Note the approximately linear negative trend between studentized contrast and proximity class distance. Evidence maps with linear contrast trends are suitable for fuzzification.
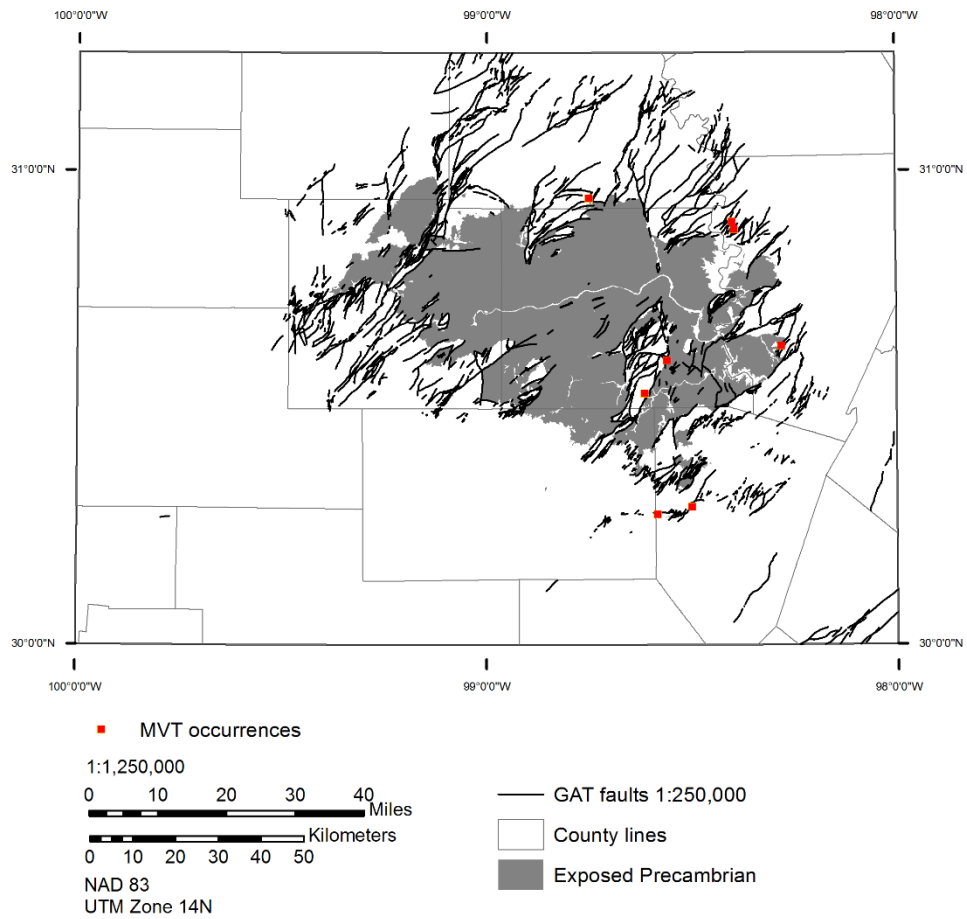
Figure 3.5:   Central Texas fault data from the Llano and Brownwood sheets of the
Geologic Atlas of Texas (vector files from the Geologic Database of Texas).
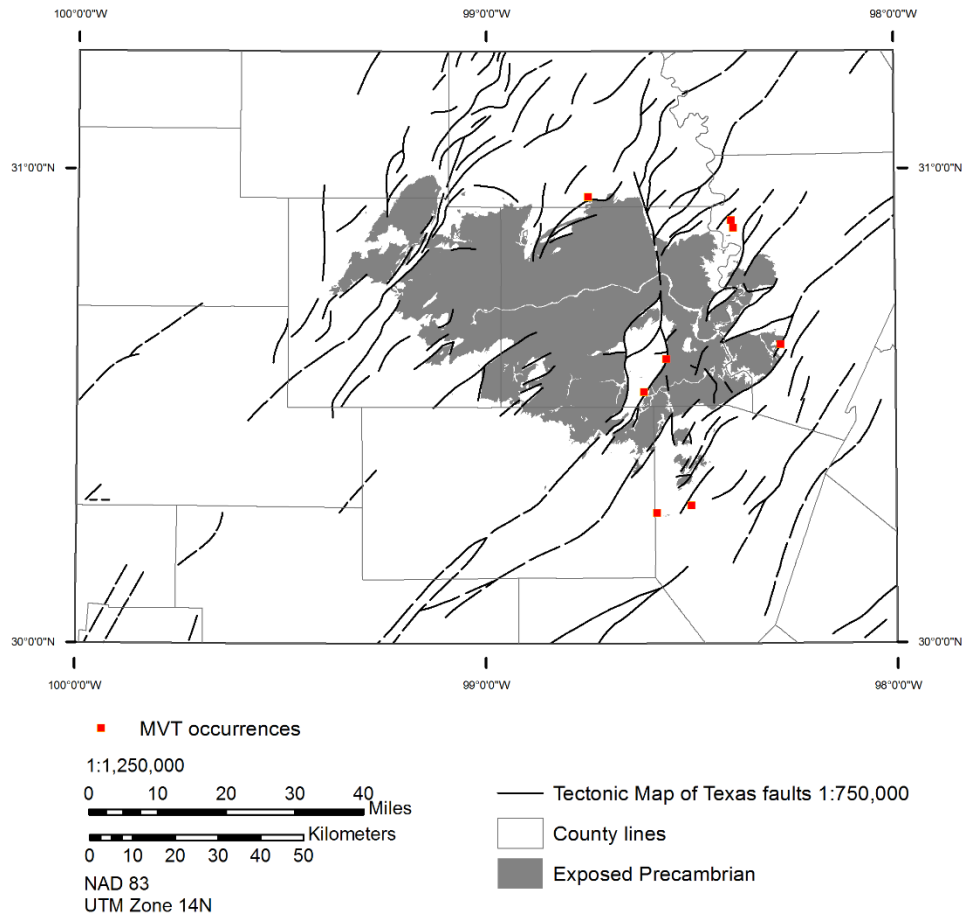
Figure 3.6:   Central Texas fault data from the Tectonic Map of Texas (Ewing et al., 1990).

not recognized in the Old Lead Belt (Ohle, 1990). Barnes (1956) noted the relationship between mineralization and a collapse structure at the Silver Creek occurrence in Central Texas. Unfortunately, the presence of dissolution collapse breccias tends to be highly variable, discontinuous, and difficult to map at a useable scale for a regional mineral potential assessment. The CUSMAP authors did not incorporate dissolution collapse breccias in their evaluation of the Rolla quadrangle. This study assumes that dissolution collapse breccias are most likely to occur near faults related to higher potential for acid surface water interaction and dissolution of carbonate rocks.

Lithologic and facies transitions

The CUSMAP assessment of the Rolla quadrangle incorporated four recognition criteria that can be grouped into the lithological and facies transitions consideration and at least two others that are related to lithology but that are not discussed here. The first three of these criteria, proximity to the limestone-dolostone interface, proximity to the white rock-brown rock interface, and near algal reef facies rocks were considered diagnostic criteria. The fourth criteria, near pinchouts of the Lamotte Sandstone was considered to be a permissive criteria. Although the CUSMAP maps were the source of input data for this study, numerous other authors noted these relationships prior to the CUSMAP assessment.

Near the limestone-dolostone interface

In Southeast Missouri, most MVT deposits are hosted in dolostones and tend to be close to the limestone-dolostone interface (Pratt et al., 1981). The proximity to the limestone-dolostone evidence map was generated from the digitized CUSMAP layer (Figure 3.7) by creating 500 m (1,600 ft) buffers from the limestone-dolostone interface line into the dolostone (Figure 3.8). Counterintuitively, the C/σC values for these buffer intervals generally increase with increasing distance from the interface line (Figure 3.9).

63
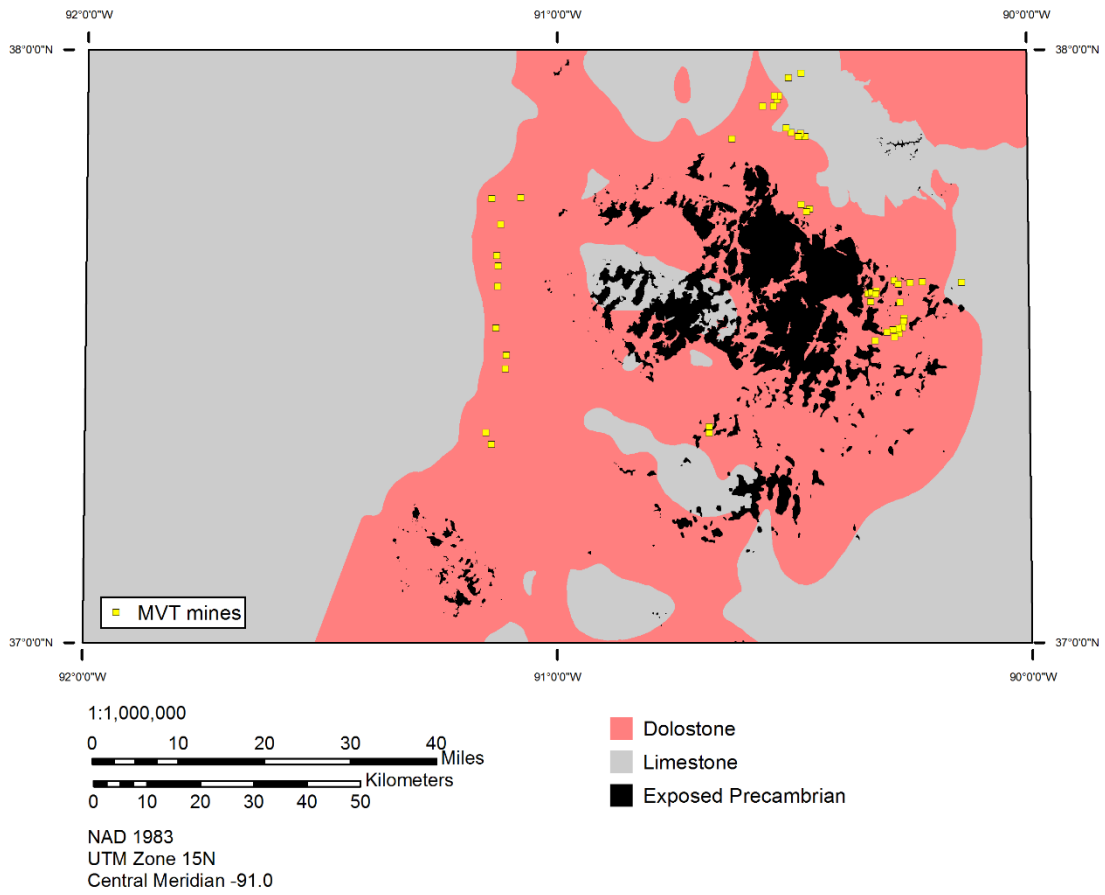
Figure 3.7: Limestone-dolostone interface in Southeast Missouri. Digitized from CUSMAP diagnostic criteria (Pratt et al., 1981).
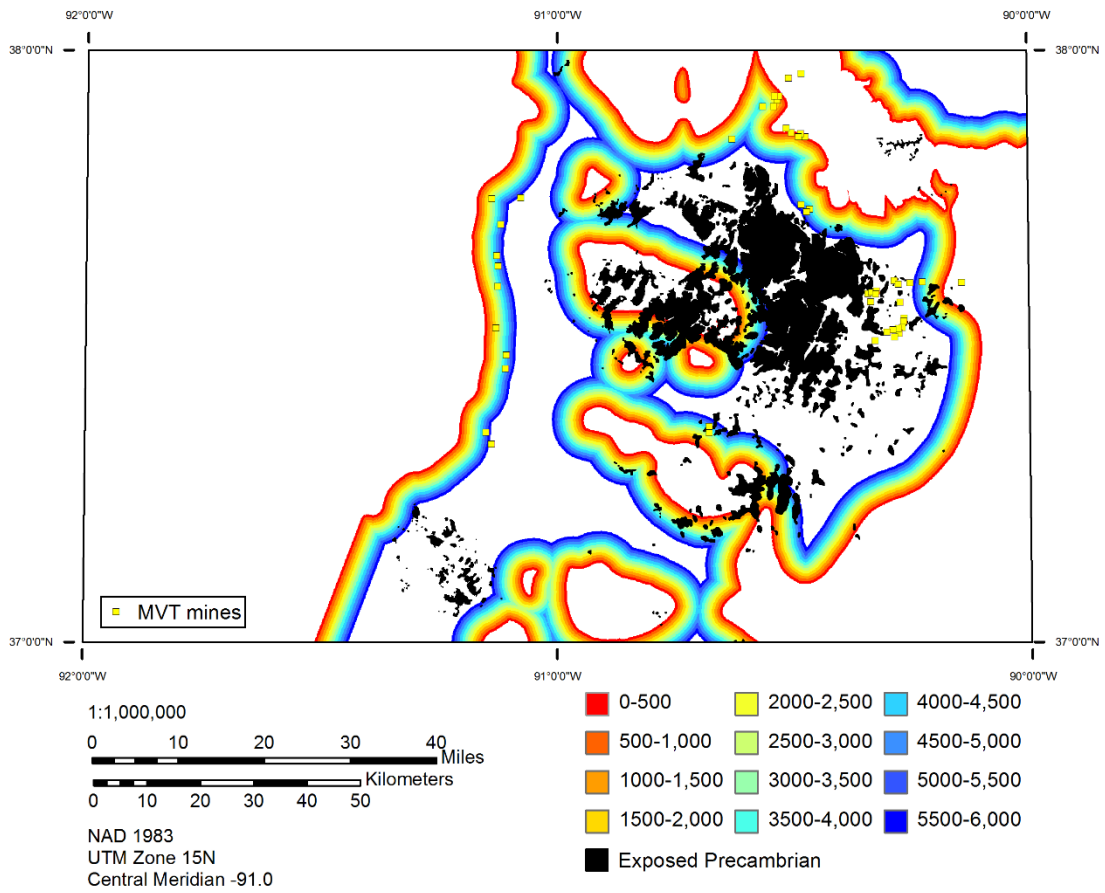
Figure 3.8: Select Southeast Missouri limestone-dolostone interface proximity classes. Although only intervals from 0-6000 m are shown here, distances of up to 15,000 m were evaluated.
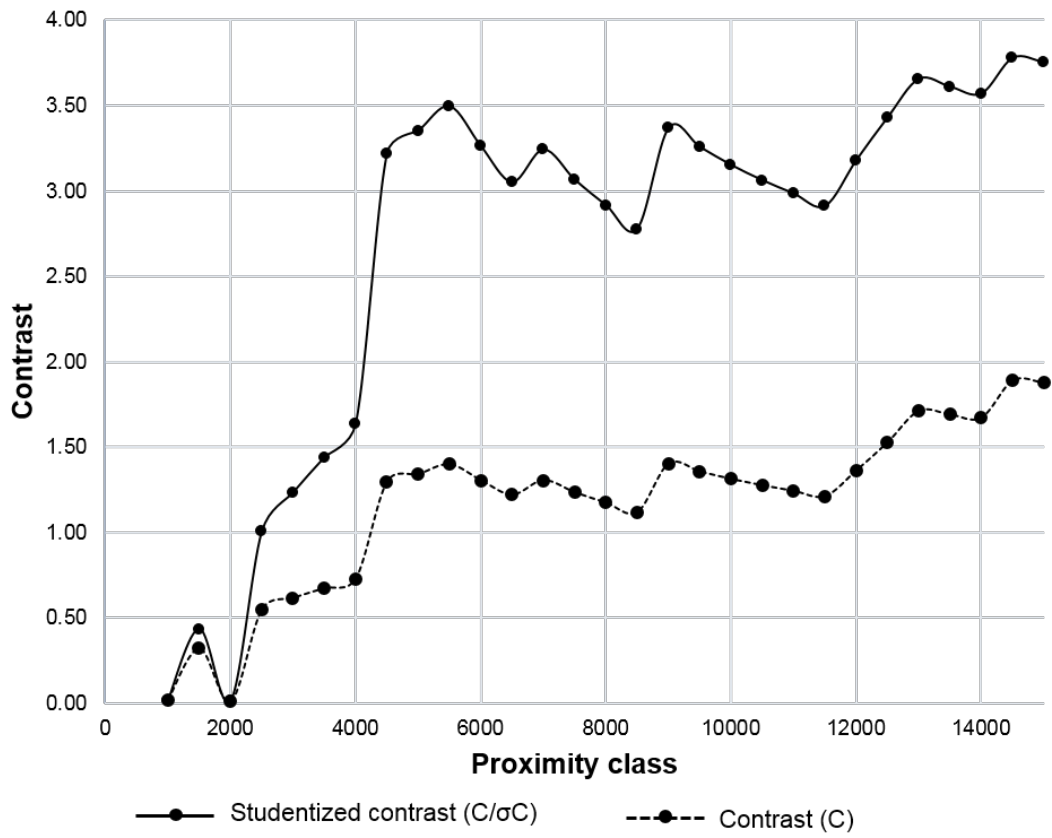
Figure 3.9:   Limestone-dolostone interface contrast vs. proximity class.

The deposits along the Viburnum Trend and in the Old Lead Belt north of the exposed Precambrian as well as the Annapolis Mines to the south tend to have a stronger relationship to this interface line that those in the Fredericktown and Mine La Motte area to the east. However, 10 of the 25 training deposits (40%) occur in the Fredericktown and Mine La Motte area. The maximum $C/\sigma C$ value is 3.78 for the 14,500 m (47, 500 ft) buffer class which occupies 37.7% of the map area and contains 80% of the training deposits.

Near the white rock-brown rock interface

Most Southeast Missouri MVT deposits are hosted in "brown rock," or finely crystalline brown dolostones, close to the interface with "white rock," or coarse, recrystallized white dolostones (Pratt et al., 1981). Ohle (1990) noted that much more of the brown rock is ore-bearing in the Viburnum Trend than in the Old Lead Belt. The CUSMAP data showing this interface only exists for the Viburnum Trend area (Figure 3.10). Because the original data is a line representing this interface, a cutoff buffer had to be determined beyond which would be considered "no data" for the purposes of the weights calculations. A 10,000 m (33,000 ft) buffer distance was selected as this cutoff, although none of the six training deposits located along the Viburnum Trend occur beyond the 6,000 m (20,000 ft) buffer zone (Figure 3.11). The highest $C/\sigma C$ value is 1.99 for the 4,000 m (13,000 ft) buffer zone which occupies 36% of the pattern area and contains five of the six (83.3%) deposits along the Viburnum Trend (Figure 3.12).

Near algal reef rocks

Pratt et al. (1981) noted that most Southeast Missouri MVT deposits occur within or near algal reef facies rocks and considered this a diagnostic criterion in their evaluation. Specifically, mineralization is strongly concentrated near the black shale-bearing contact zone between organic algal structures and clastic carbonate sediments (Snyder and
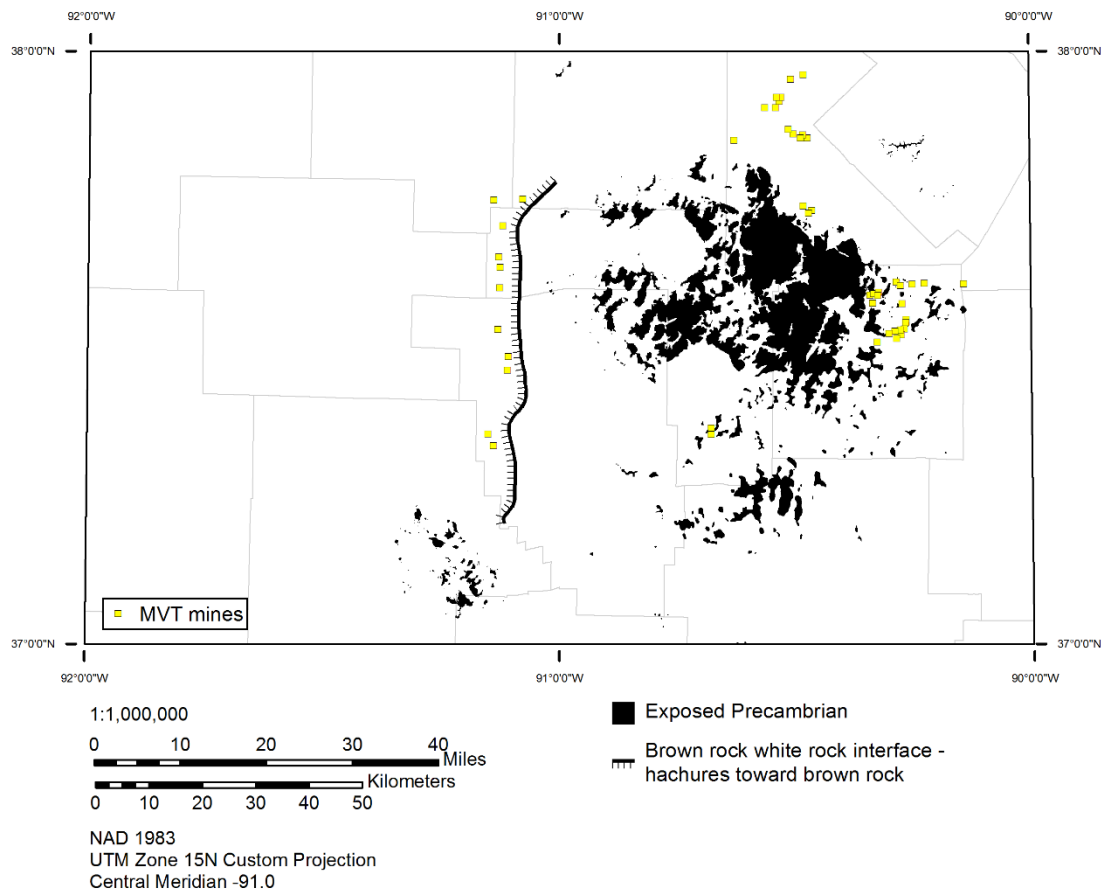
Figure 3.10: Southeast Missouri brown rock-white rock interface. Digitized from CUSMAP diagnostic criteria (Pratt et al., 1981).
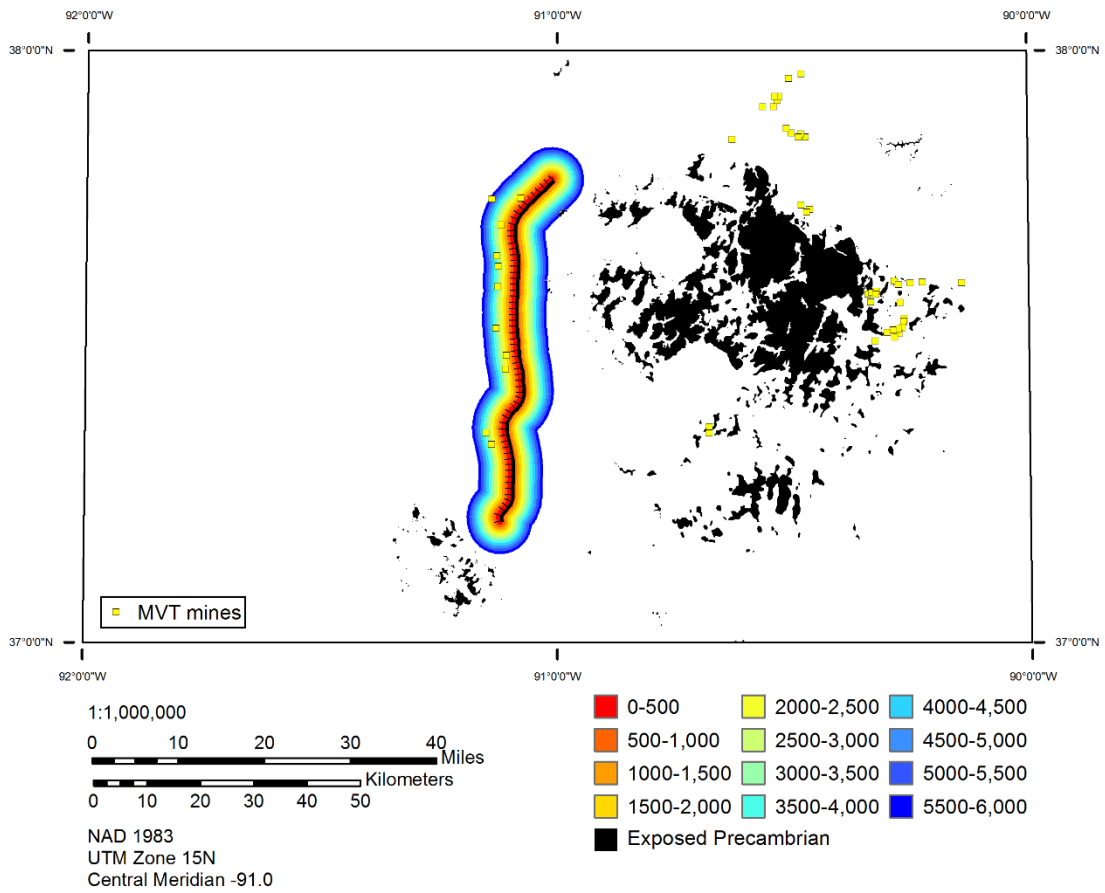
Figure 3.11: Select 500 m white rock-brown rock proximity classes. Only distances to 6,000 m are shown here although distances up to 10,000 m were evaluated. Distances beyond 10,000 m were considered to have no data.
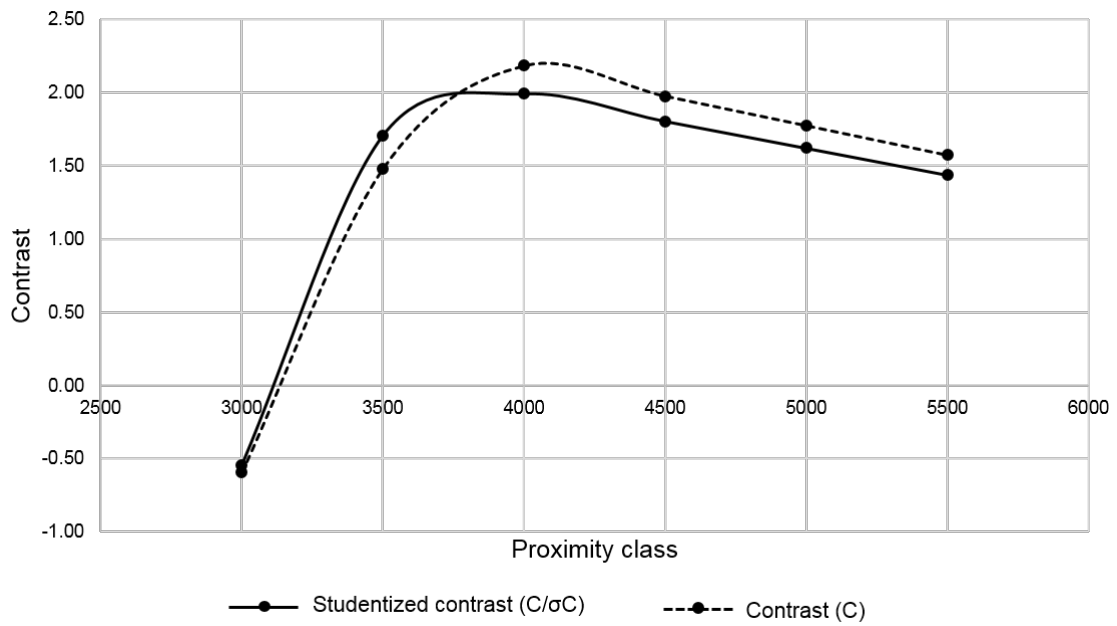
Figure 3.12: Brown rock-white rock contrasts vs. proximity class. No deposits occur closer than 2,500 m and all six training deposits along the Viburnum Trend are within 6,000 m of the interface line.

Gerdemann, 1968). The CUSMAP polygon data showing the reef-rock distribution (Figure 3.13) was buffered, and weight and contrast values were calculated for the 500 m (1,600 ft) buffer corridors (Figure 3.14). The highest C/σC value is 6.78 and is associated with the 1,500 m (4,900 ft) buffer zone that occupies 5.8% of the study area and contains 48% of the training deposits (Figure 3.15). This evidence layer is the best performing predictor of MVT deposits in Southeast Missouri.

Near pinchouts of the Lamotte Sandstone

Snyder and Gerdemann (1968) described "pinchout-type" ore bodies as one of the major ore forms in the Southeast Missouri district. These ore zones occur where Precambrian hills had enough relief to result in depositional pinchouts of the Lamotte Sandstone. The result is that mineralizing fluids were forced out of the favorable Lamotte Sandstone aquifer where lateral permeability was reduced in these pinchout zones and into the overlying Bonneterre Formation carbonates (Kisvarsanyi, 1977). Fluid pressure was not high enough to force the brines through the overlying Davis Shale, effectively trapping them in the Bonneterre Formation. The CUSMAP authors considered proximity to pinchouts of the Lamotte Sandstone to be a permissive rather than diagnostic criteria in their assessment of the Rolla quadrangle (Pratt et al., 1981).

The CUSMAP polygon data showing the pinchout locations of the Lamotte (Figure 3.16) was digitized and buffered into 500 m (1,600 ft) corridors (Figure 3.17). The highest C/σC value is 3.30 for the 2,500 m (8,200) buffer corridor (Figure 3.18). Four training deposits (16%) occur in the 14.5% of the study area where the Lamotte is mapped as entirely pinched out and five training deposits (20%) occur at distances greater than 15,000 m (49,000 ft) from these pinchouts.
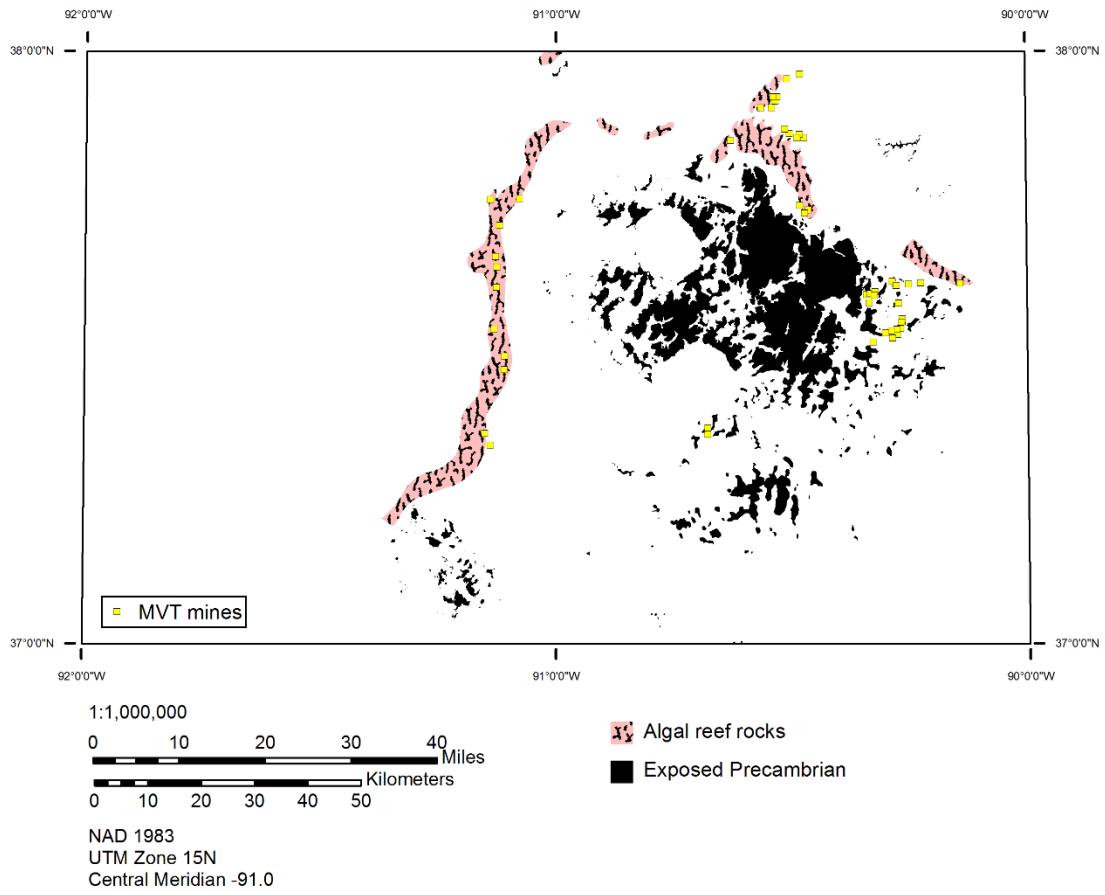
Figure 3.13: Algal reef rocks in Southeast Missouri. Digitized from CUSMAP diagnostic criteria (Pratt et al., 1981).
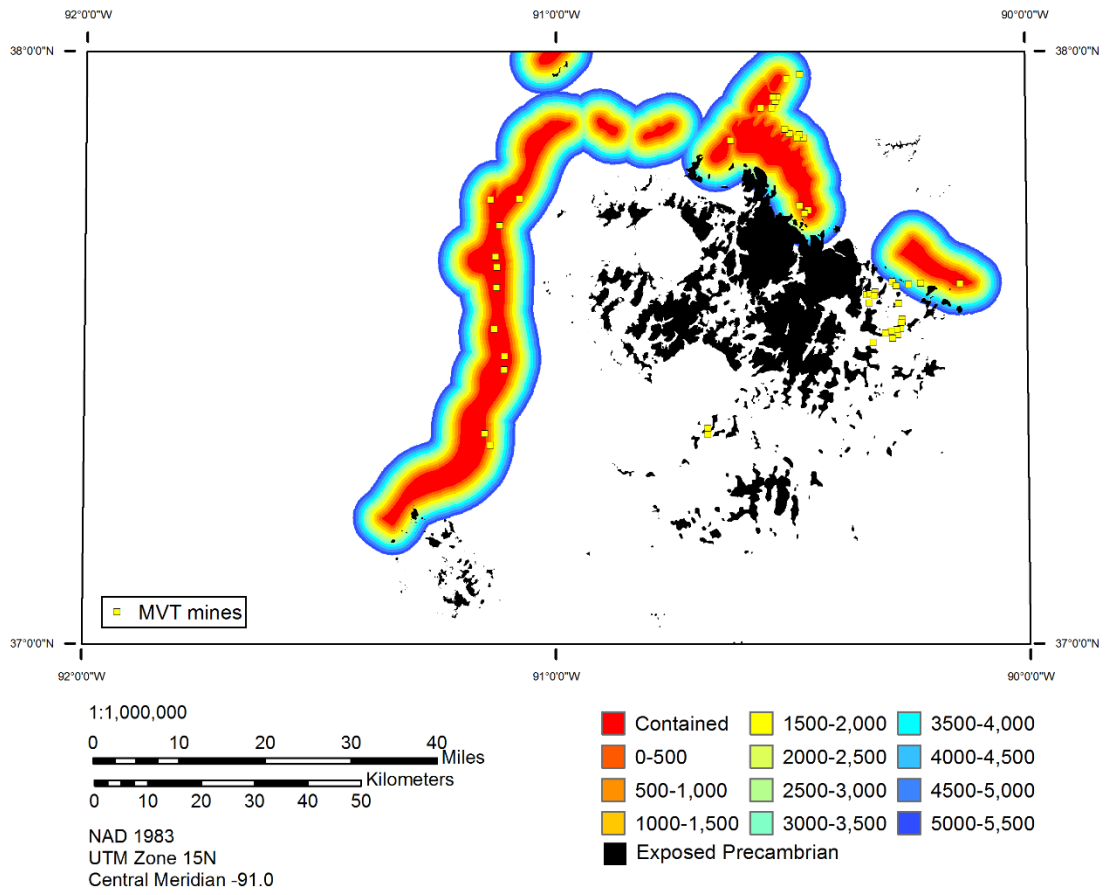
Figure 3.14: Select 500 m algal reef proximity classes for Southeast Missouri. Only distances to 5,500 m are shown here for clarity, although distances up to 15,000 m were evaluated.
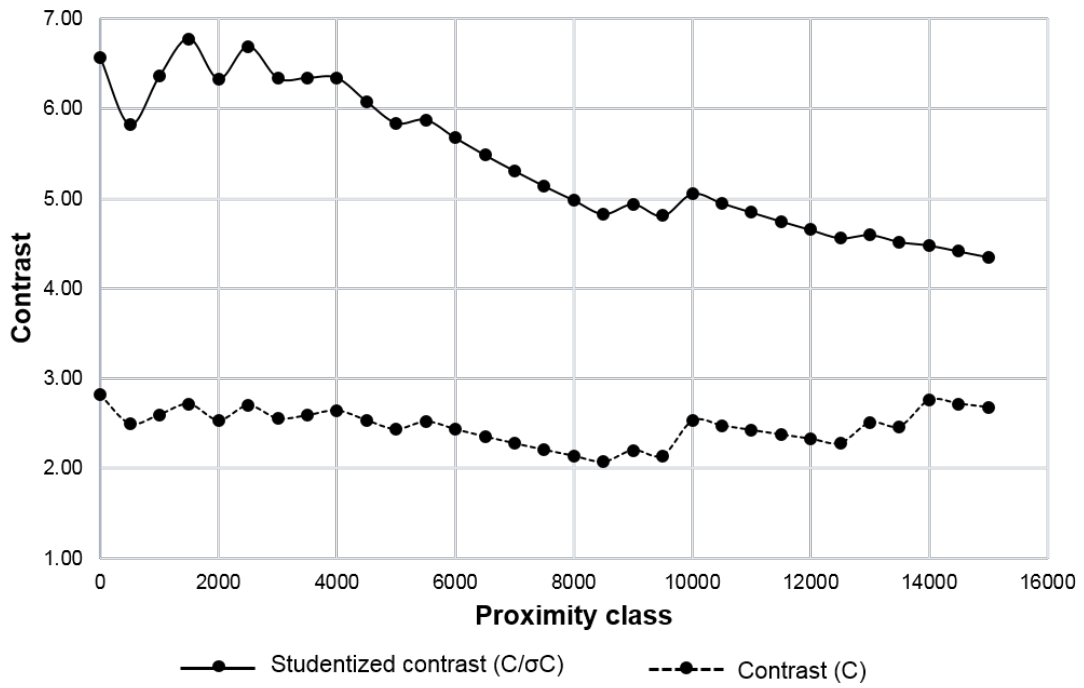
Figure 3.15: Algal reef contrasts vs. proximity class.
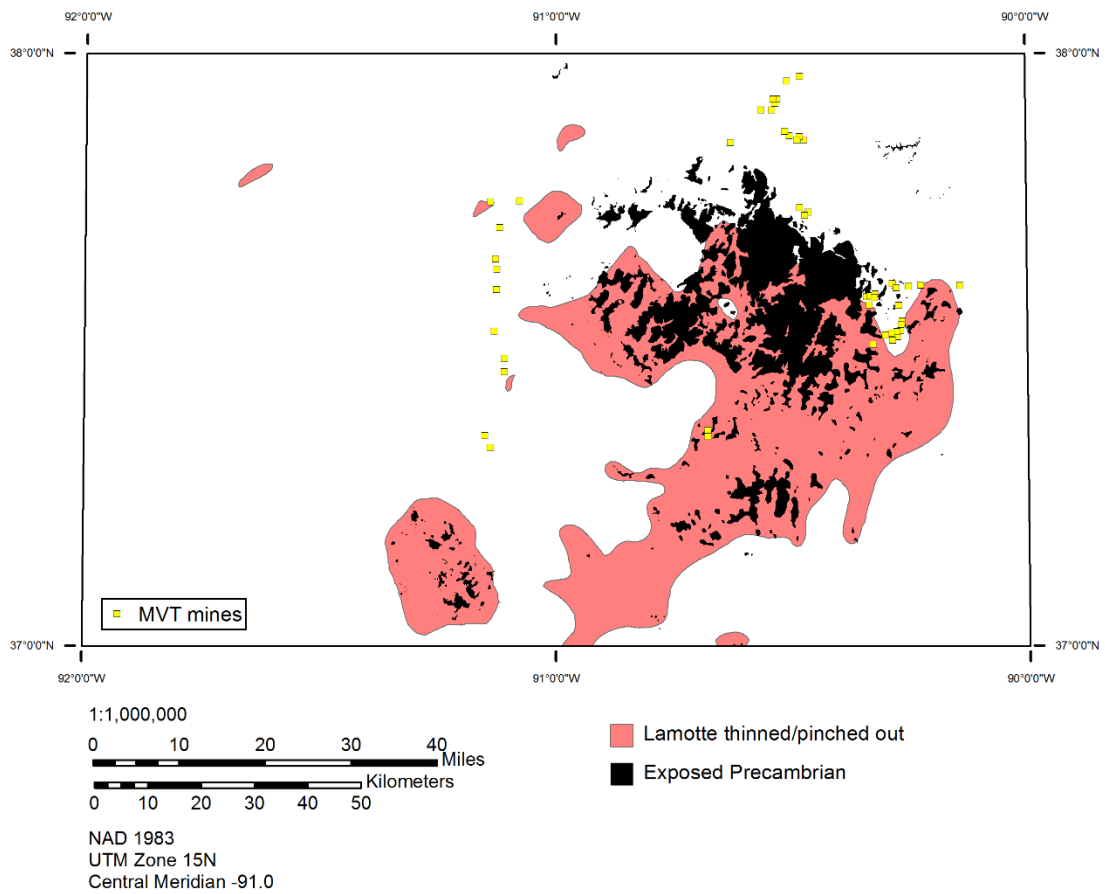
Figure 3.16: Pinch-outs or thinning in the Lamotte Sandstone in Southeast Missouri.
Digitized from CUSMAP permissive criteria (Pratt et al., 1981).
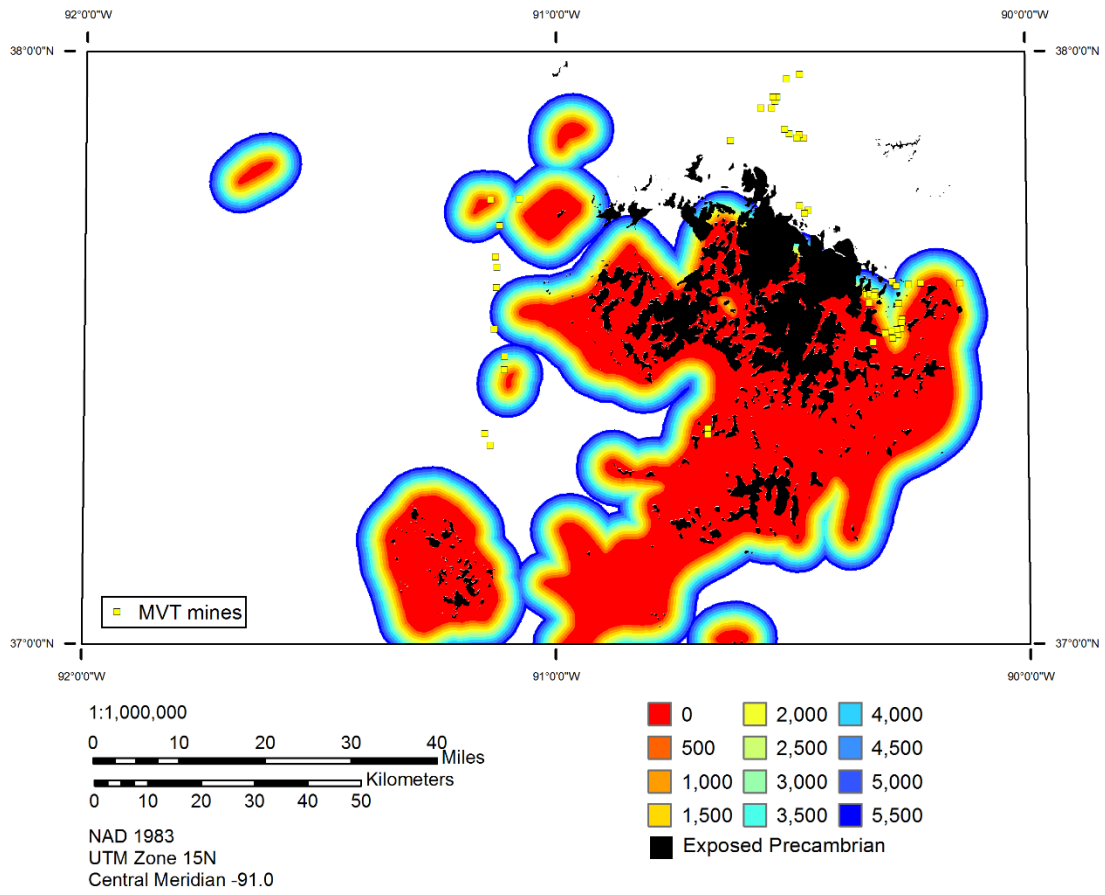
Figure 3.17: Select 500 m Lamotte Sandstone pinchout proximity classes. Only the 0-5,500 m classes are shown for clarity although distances up to 12,000 m were evaluated.
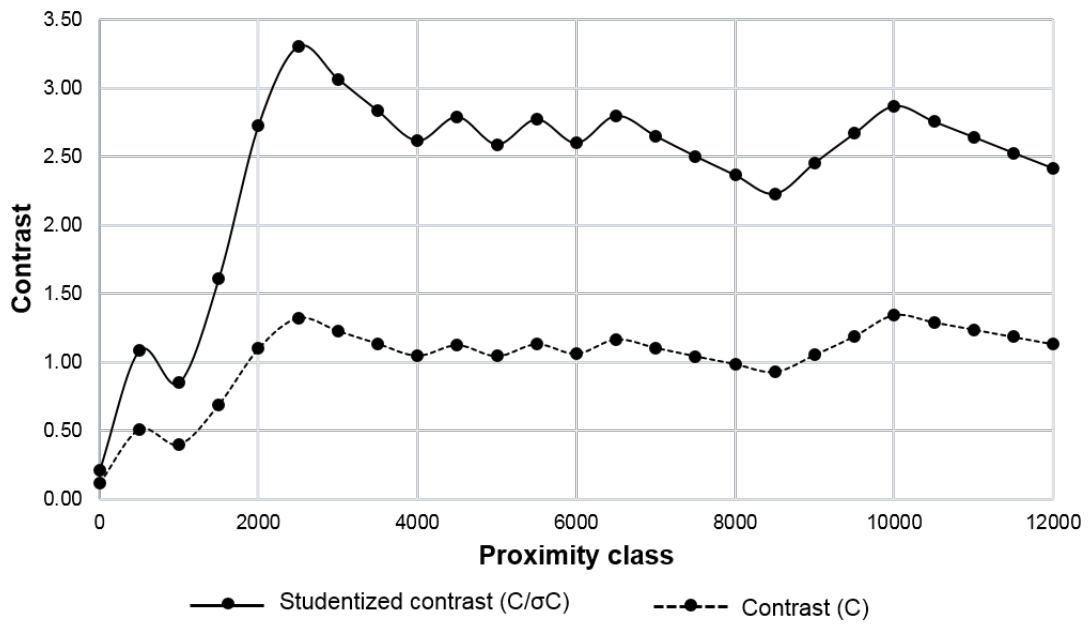
Figure 3.18: Lamotte Sandstone contrasts vs. proximity class.

Surface geology

Geologic maps are a common source of data for many mineral prospectivity studies not only because mineral deposits are obviously related to geology, but also because geologic maps tend to be some of the more complete forms of information in many areas where minerals exploration is occurring. A visual examination of a geologic map of Southeast Missouri shows an obvious relationship between surficial exposures of the Bonneterre Formation and MVT mines, especially in the Old Lead Belt and Fredericktown and Mine La Motte areas north and east of the exposed Precambrian. This relationship is borne out in the relatively high $C/\sigma C$ value associated with this evidence discussed below. However, this relationship can be misleading. Economic mineralization in the Viburnum Trend is also almost exclusively confined to the Bonneterre Formation in spite of surficial exposures of younger units, illustrating the challenges of approaching a three-dimensional problem with two-dimensional data. To accommodate this, some models for both Southeast Missouri and Central Texas do not include surficial geology as an input (although these tended perform more poorly).

The Southeast Missouri geologic map data used for this study was compiled from 1:500,000 scale vector data for Missouri (MO Bedrock 500k, 2011) and Illinois (Kolata, 2005) (Figure 3.19). It should be noted that this regional map does not distinguish between the Bonneterre Formation and the overlying Elvins Group which contains the Davis and Derby-Doe Run Dolomite. Unsurprisingly, the Elvins Group and Bonneterre Dolomite group was the best performing evidence considered. These formations occupy 7% of the study area and contain 44% of the training deposits resulting in a $C/\sigma C$ value of 5.81.

Central Texas geology for this study was derived from the GDbT 1:250,000 vectorized maps derived from the Llano and Brownwood sheets of the Geologic Atlas of Texas (Figure 3.20).

78
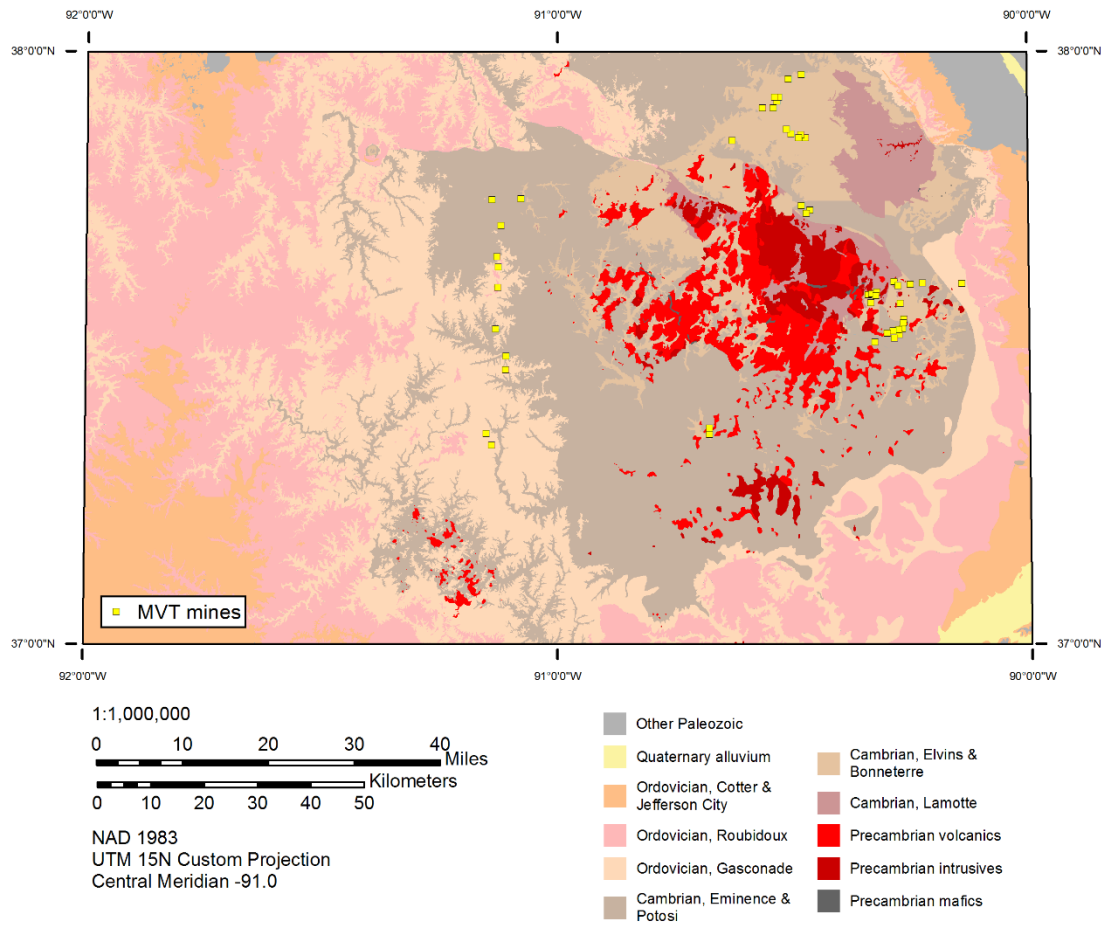
Figure 3.19: Geologic map of the Southeast Missouri study area. Data from the Missouri Department of Natural Resources.
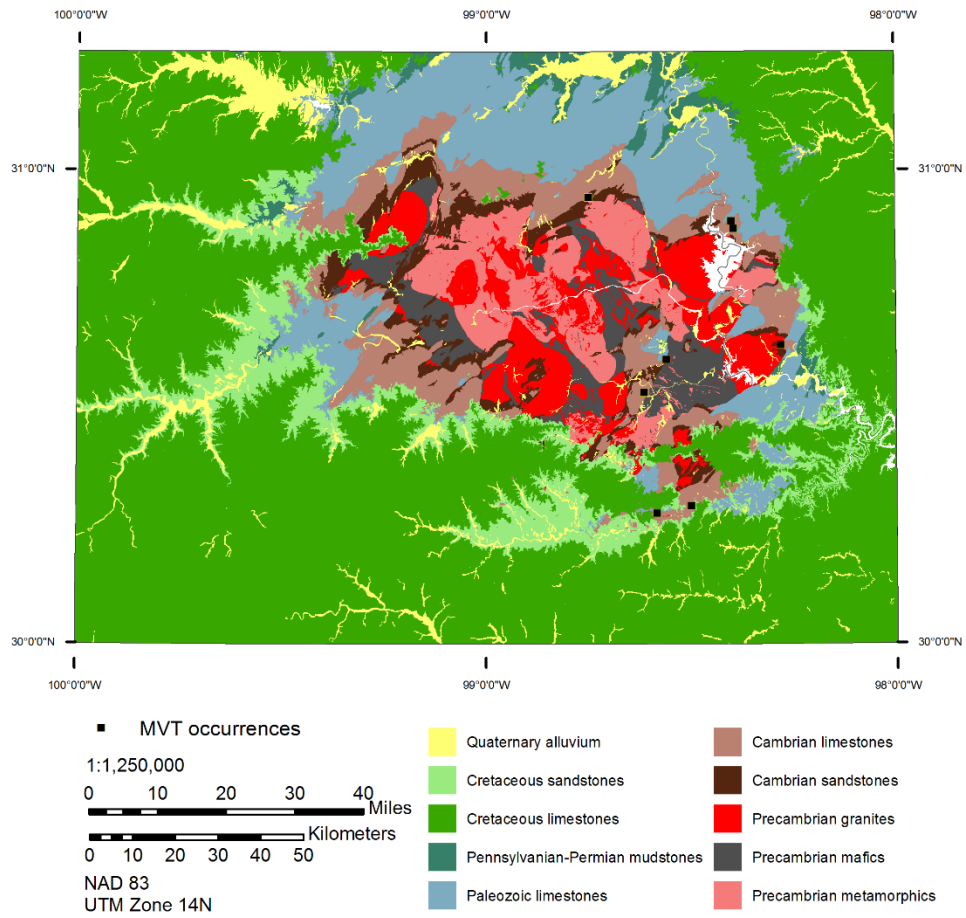
Figure 3.20: Simplified geologic map of Central Texas. Modified from the Geologic Database of Texas.

Basement structures

Basement structures, especially knobs or hills in the crystalline Precambrian basement are important controls on MVT mineralization in both Southeast Missouri (Leach et al., 2010; Pratt et al., 1986) and Central Texas (Paige, 1911; Baker, 1935; Barnes, 1956). These basement highs formed as a result of differential erosion prior to the deposition of overlying sedimentary strata. They are a major factor governing the facies, character, and thickness of overlying sedimentary rocks (Kisvarsanyi, 1977), which in turn affected the fluid paths of mineralizing solutions and ultimately the deposition of MVT ores. Krause (1996) noted a similar relationship between Precambrian basement highs and the overlying Riley Formation in Central Texas.

Rolla Quadrangle structural contour map

The basement elevation map for the Rolla Quadrangle was derived from a basement structural contour map (Kisvarsanyi, 1979). This map was produced using data from 526 wells, 70 of which penetrated the Lamotte Sandstone and the remaining 456 of which reached the Precambrian surface. The map was georeferenced, then the contours, faults, and well locations were digitized as lines and points in ArcGIS. The contours were interpolated to a continuous surface raster using the proprietary "Topo to Raster" 3D Analyst tool (ESRI, 2014). This tool generates a hydrologically correct raster surface and permits the input of "cliff" features, which serve as barriers during the interpolation and which permits the resulting raster to account for offsets in the basement surface related to faults. Elevation data from a 10 m (30 ft) resolution digital elevation model (DEM) from the National Elevation Dataset (2009) contoured to a 20 m (60 ft) interval were used as elevation values for portions of the map where Precambrian rocks are exposed at the surface (Figure 3.21).
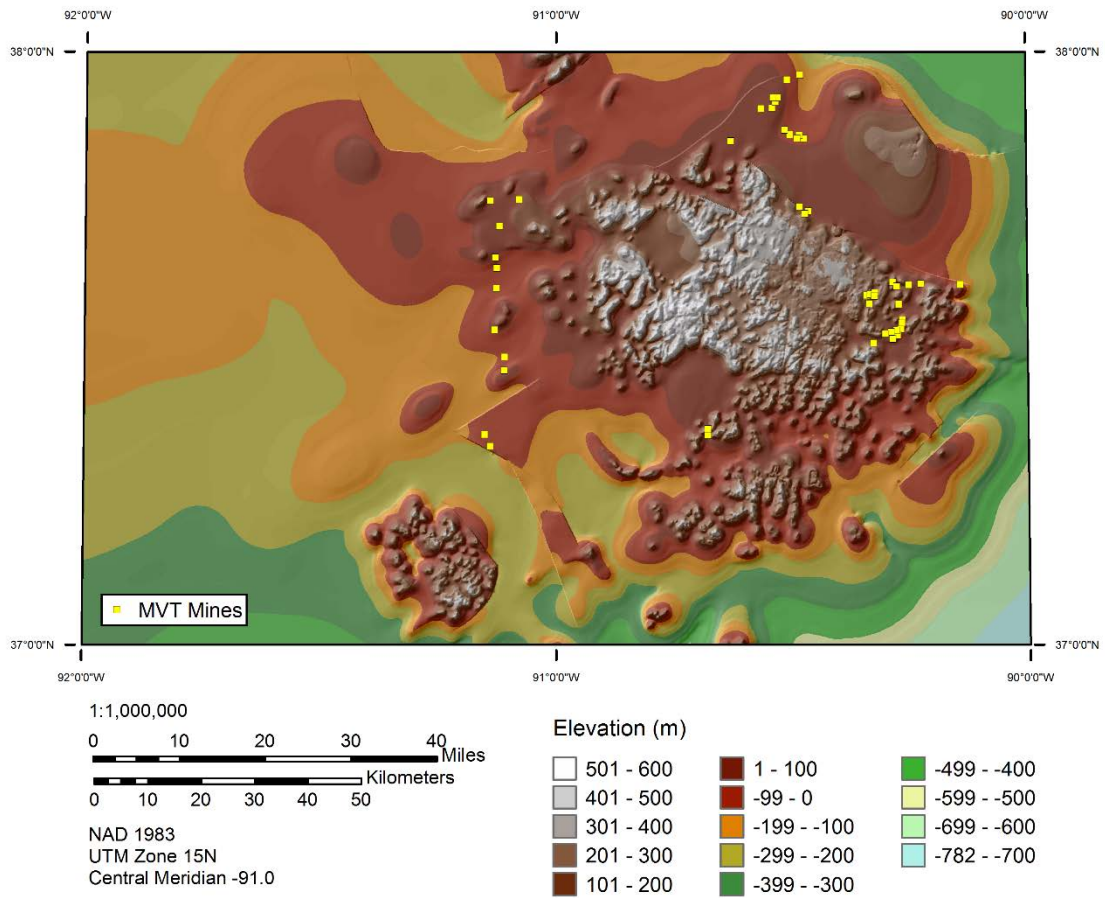
Figure 3.21: Structure map of the top of the Precambrian basement in Southeast Missouri. Created using data digitized from Kisvarsanyi (1979).

In alignment with the aim of maximizing the portability of model parameters from one area to another, the following method was used to objectively identify hills from this Precambrian elevation surface. This method remains applicable to areas where the magnitude of elevation values may be significantly different from Southeast Missouri. The hills identified using this method generally appear to line up spatially with hills identified by the CUSMAP authors (Figure 3.22), although this method produced many more hills than were considered in the CUSMAP study.

First, the basement structure raster is inverted so high points become low points and low points to high points using the equation:

$$Elev_{inv} = Elev_i - (Elev_{max} * -1)) + Elev_{min})$$

where $Elev_{inv}$ is the inverted elevation, $Elev_i$ is the elevation at a given raster cell i, $Elev_{max}$ is the maximum raster elevation, and $Elev_{min}$ is the minimum raster elevation. After the elevation raster is inverted, cells with an undefined drainage direction (sinks) are "filled" until a drainage direction is defined (Figure 3.23). Hills are identified by subtracting the nonfilled, inverted raster from the filled, inverted raster. Only hills that occupy more than nine raster cells (90,000 m^2; 970,000 ft^2) are retained which correspond to hills roughly 300×300 m (980×980 ft) in diameter.

Five-hundred meter (1,600 ft) wide proximity classes were generated around each of these basement hills (Figure 3.24). The highest C/σC value is 4.70 for the 500 m (1,600 ft) proximity class which occupies 8.9% of the map area and contains 40% of the training deposits (Figure 3.25).

Magnetics

Previous authors have noted the usefulness of geophysical data in assessments of MVT potential, especially in mapping the types and depth to basement rocks and in
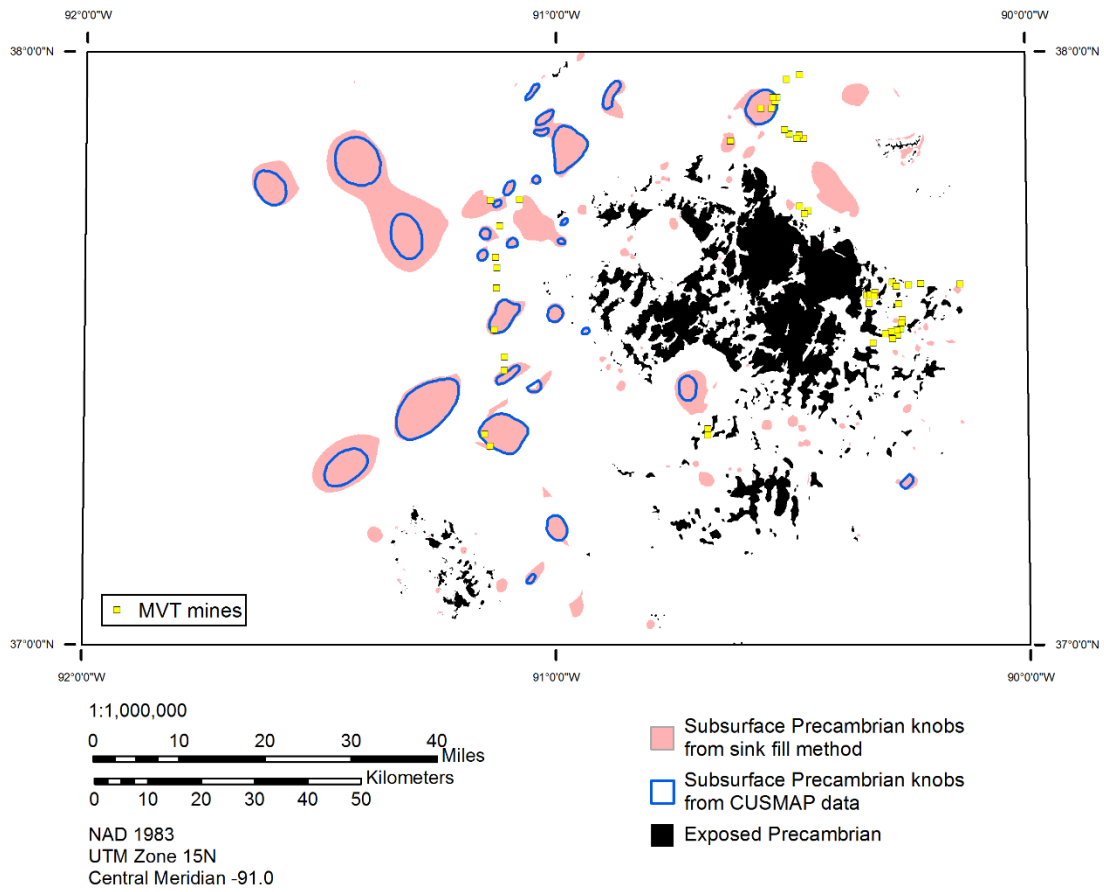
Figure 3.22: Precambrian knobs identified during the CUSMAP study (Pratt et al., 1981) and knobs derived using the sink fill method. See text for a description of the sink fill method.
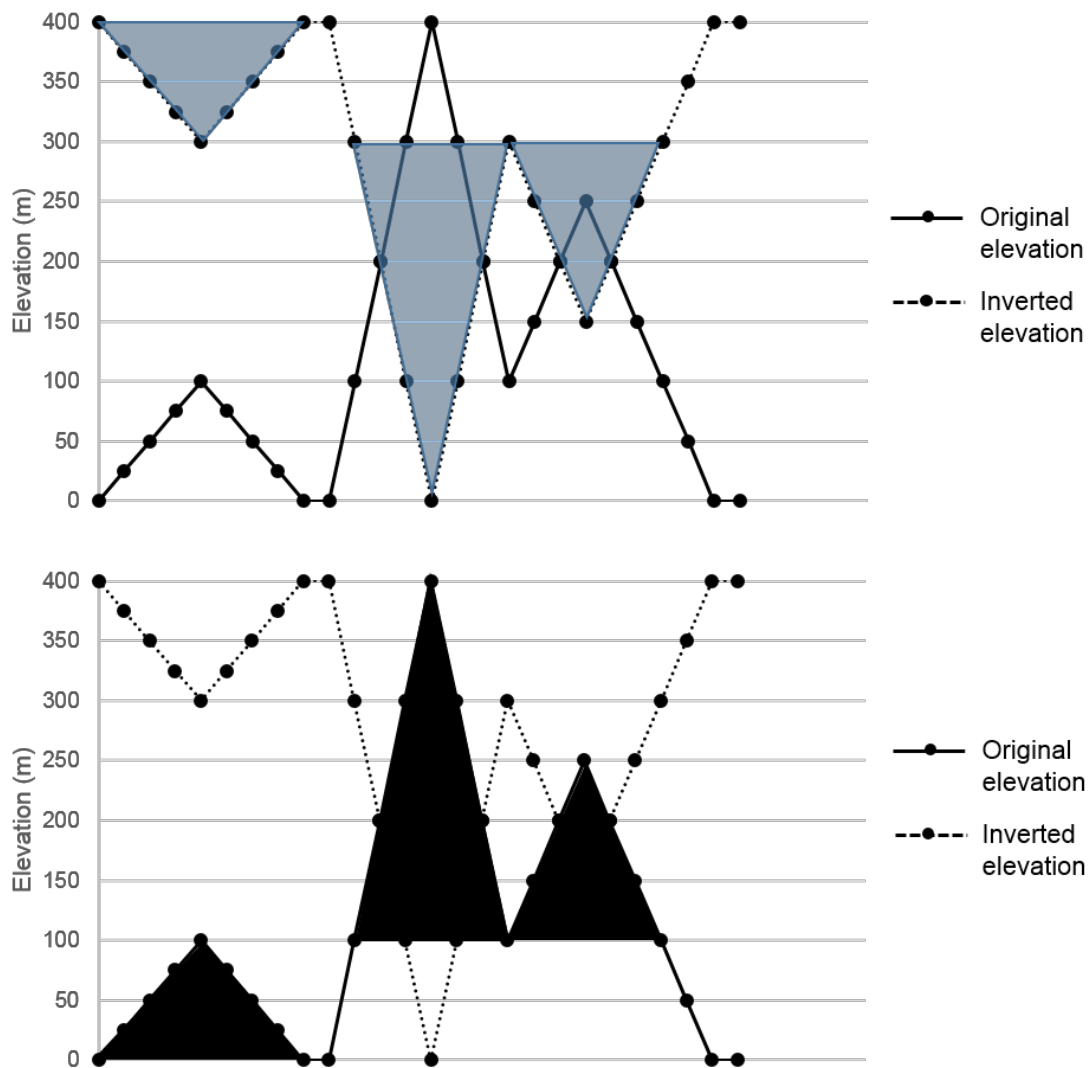
Figure 3.23: Schematic illustration of the sink fill method of identifying Precambrian knobs. The top and bottom portions represent the elevation profile for a given area. The areas in blue on the top portion are elevations that would be "filled" and the portions in black at the bottom are the knobs identified by subtracting the inverted elevation from the filled elevation.
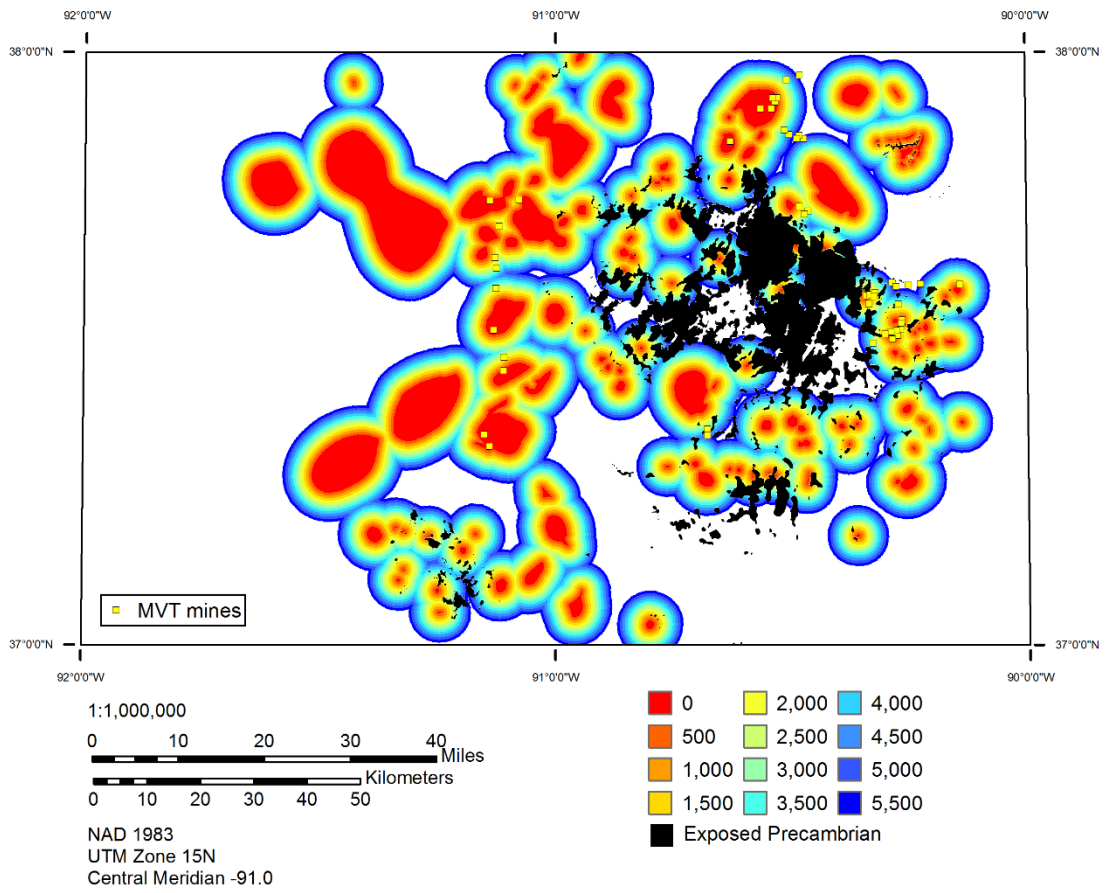
Figure 3.24: Select 500 m Precambrian knob proximity classes. All training deposits occur within 6,500 m of knob outlines, but only the 0-5,500 m classes are shown here for clarity.
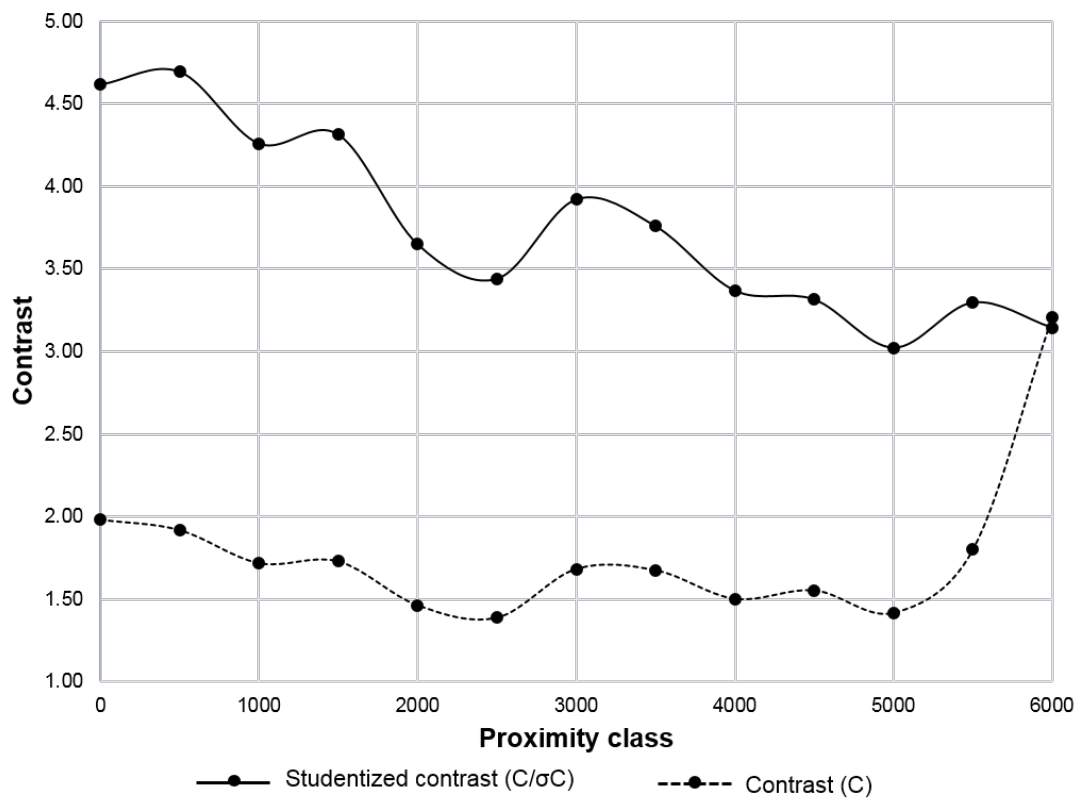
Figure 3.25: Precambrian knob contrasts vs. proximity class.

identifying subsurface faults (Leach et al., 2010). Cordell and Knepper (1987) used aeromagnetic data to identify specific basement rock types in the Southeast Missouri District and suggested a possible association between the magnetics data and ore trends. Geophysical data is commonly processed using inversion and deconvolution techniques to calculate depth to source. For example, Allingham (1976) used aeromagnetic data to calculate depth to Precambrian rocks in Southeast Missouri. Fullagar et al. (2004) and D'Ercole et al. (2000) used gravity and magnetics data to calculate the depth to the top of the limestone host rock and depth to Precambrian basement respectively as part of their studies of MVT mineralization on the Lennard Shelf in Western Australia.

Other authors (e.g., Daneshfar et al., 2006) noted a positive association between MVT mineralization and aeromagnetic data without attempting to ascribe only a single geologic reason for the relationship. Magnetics data in this study are used in this latter manner. There is a notable relationship between MVT mineralization in Southeast Missouri and the reclassified magnetic data as evidenced by the high-contrast values for some magnetics classes. This may be related to the subsurface Precambrian topography, lithology, or some other aspect of the carbonate basin geometry, but no attempt is made here to further investigate the association. It is possible that systematically processing the available magnetic data for Central Texas (as was done for the Lehmann data discussed below) to produce depth to basement maps will be a more efficient use of the information in future work.

Gridded magnetics point data (Daniels et al., 2002) with point spacing of 1000 m (3,300 ft) were re-interpolated to continuous surfaces (Figures 3.26 and 3.27) using the natural neighbor method (Stibson, 1981). This interpolation method uses Thiessen polygons to determine interpolation weights and produces a relatively smooth output without inferring trends in the data. The resulting surfaces ranges in value from -695-1767
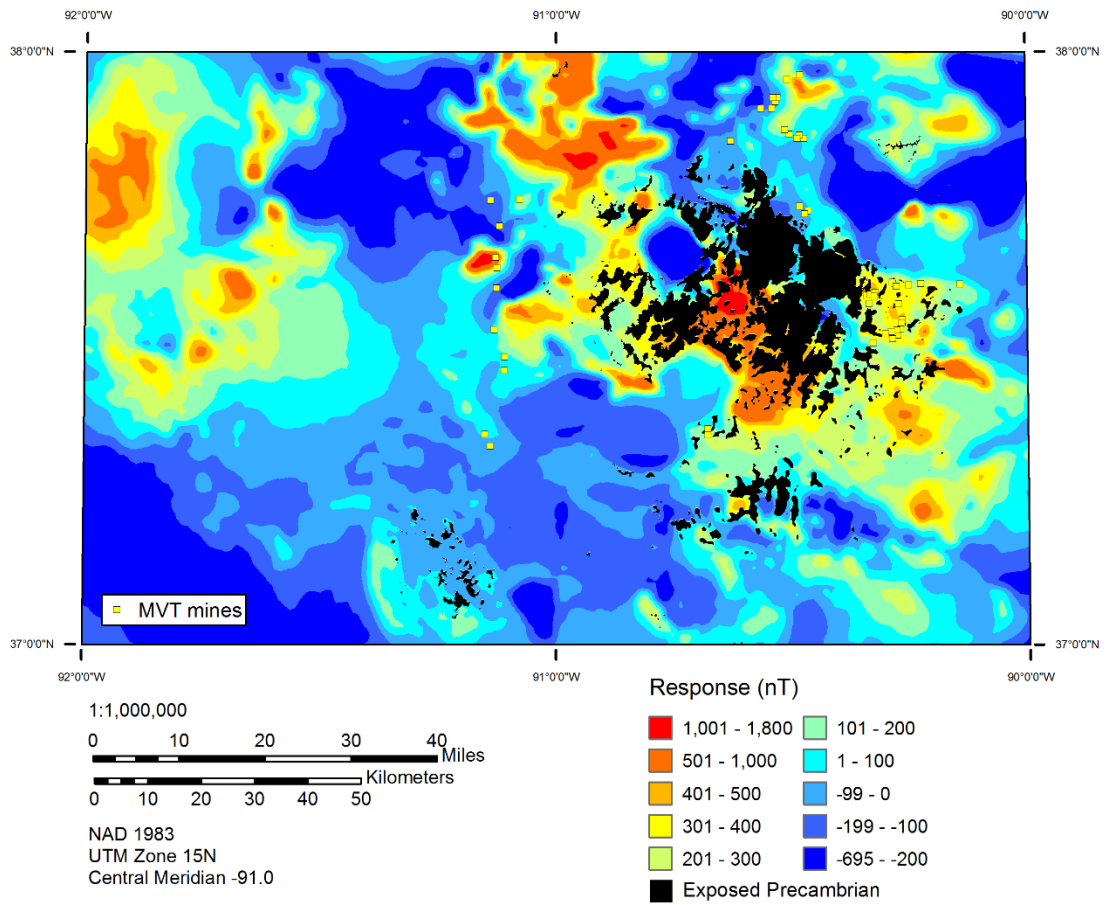
Figure 3.26: Southeast Missouri magnetic response classes generated from gridded points. Data from the Magnetic Anomaly Map of North America (Daniels et al., 2002).
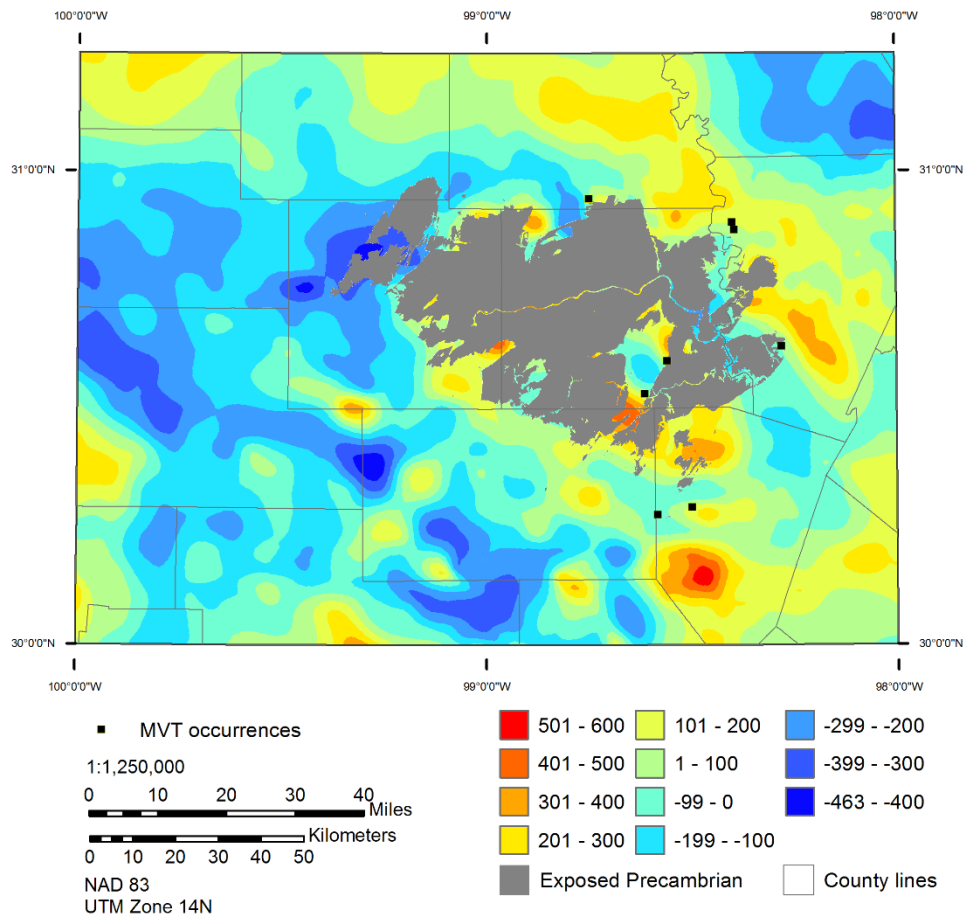
Figure 3.27: Central Texas magnetic response classes generated from gridded points. Data from the Magnetic Anomal Map of North America (Daniels et al., 2002).

nT for Southeast Missouri and from -463-1073 nT for Central Texas. These surfaces were then classified into 100 nT intervals and weights were calculated for each interval in Southeast Missouri. The contrast values are highest for intermediate magnetic intensity values in Southeast Missouri.

However, there are likely differences in the specific compositions and geometries of basement rocks that make up Highs (hills) in Central Texas compared to Southeast Missouri. These differences probably extend to the magnetic signatures associated with these rocks, which means that the Southeast Missouri magnetic interval with the highest studentized contrast value (300-400 nT) may not be the interval most strongly associated with MVT mineralization in Central Texas. An examination of the Central Texas magnetic data with the near surface MVT occurrences seems to confirm this as all eight Central Texas occurrences fall in magnetic contour values between -50 and 150 nT.

To compensate for this regional variability, a series of derivative maps were produced from the magnetics data. The first of these maps is a reclassification of the magnetic intensity values into percentages of the maximum intensity using the equation:

$$Mag_{pct} = ((Mag_i - Mag_{min}) / (Mag_{max} - Mag_{min})) * 100$$

where Mag_{pct} is the percent of magnetic intensity, Mag_i is the intensity value at a given raster cell, Mag_{max} is the maximum magnetic intensity in the raster, and Mag_{min} is the minimum magnetic intensity. This new layer was classified into 10% intervals and weights were calculated for each. This map produced the highest contrast value of any of any of the magnetics maps considered with the data range from 35-45% of maximum intensity producing a $C/\sigma C$ value of 3.17. This interval occupies 15.5% of the map area and contains 40% of the training deposits.

In addition, maps were created representing the slope of the original magnetic surface both in nT/m and as a percent of the maximum slope, and a map of proximity to

"magnetic hills" where hills were determined using the method described above for Precambrian basement hills. None of these maps resulted in C/σC values as high as the percent magnetic intensity map.

Gravity

In the USGS deposit model, Leach et al. (2010) noted that detailed gravity data may be useful in directly detecting MVT deposits because of the relatively high density of the ore minerals with respect to the carbonate host. The regional gravity data available for this study lacks the resolution to directly detect this localized variation from orebodies. Instead, the regional gravity data readily available for this study was treated as a potential proxy for the basement surface with the same justification as the magnetics data.

The gravity anomaly maps were generated from gravity base station point data that are part of the North American Gravity Database described by Hildenbrand et al. (2002) and publicly available from the University of Texas El Paso Regional Geospatial Service Center. These were interpolated to continuous surfaces of the complete Bouguer anomaly values reduced to a background density of 267 (cbanom267) at each data point using the natural neighbor method for both Central Texas and Southeast Missouri (Figures 3.28 and 3.29). The gravity surfaces range in value from -67.99 to -1.03 mGal in Southeast Missouri and -85.27 to 3.30 mGal in Central Texas. These maps were then classified into 5 mGal intervals and weights were calculated for each class in Southeast Missouri. The -15 to -10 mGal contour interval is the best MVT predictor with a C/σC value of 5.63. This interval contains 40% of the training deposits in 6.3% of the map area.

As with the magnetics data, a slope map was produced for the gravity surface. This map was less effective at predicting the training deposits, with the highest C/σC value is

92
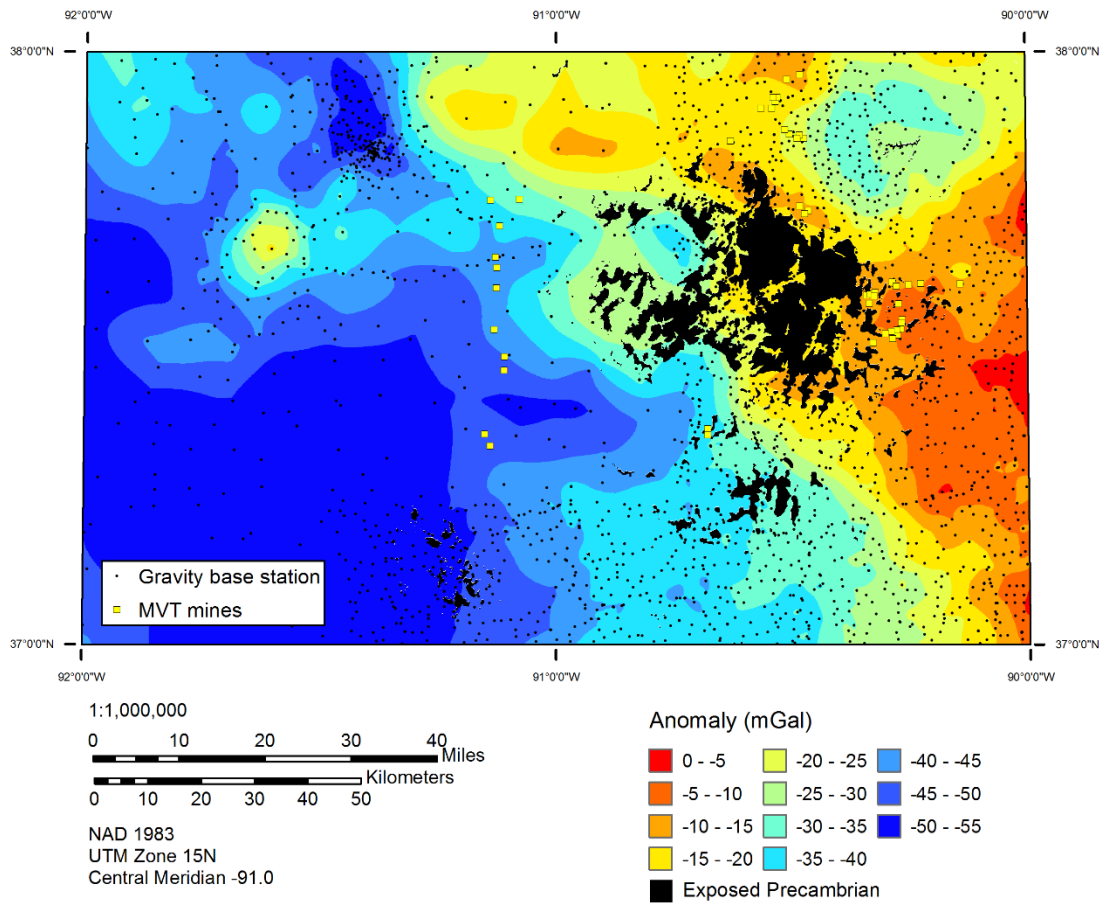
Figure 3.28: Southeast Missouri gravity anomaly classes. Base station data from the North American Gravity Database (Hildenbrand et al, 2002).
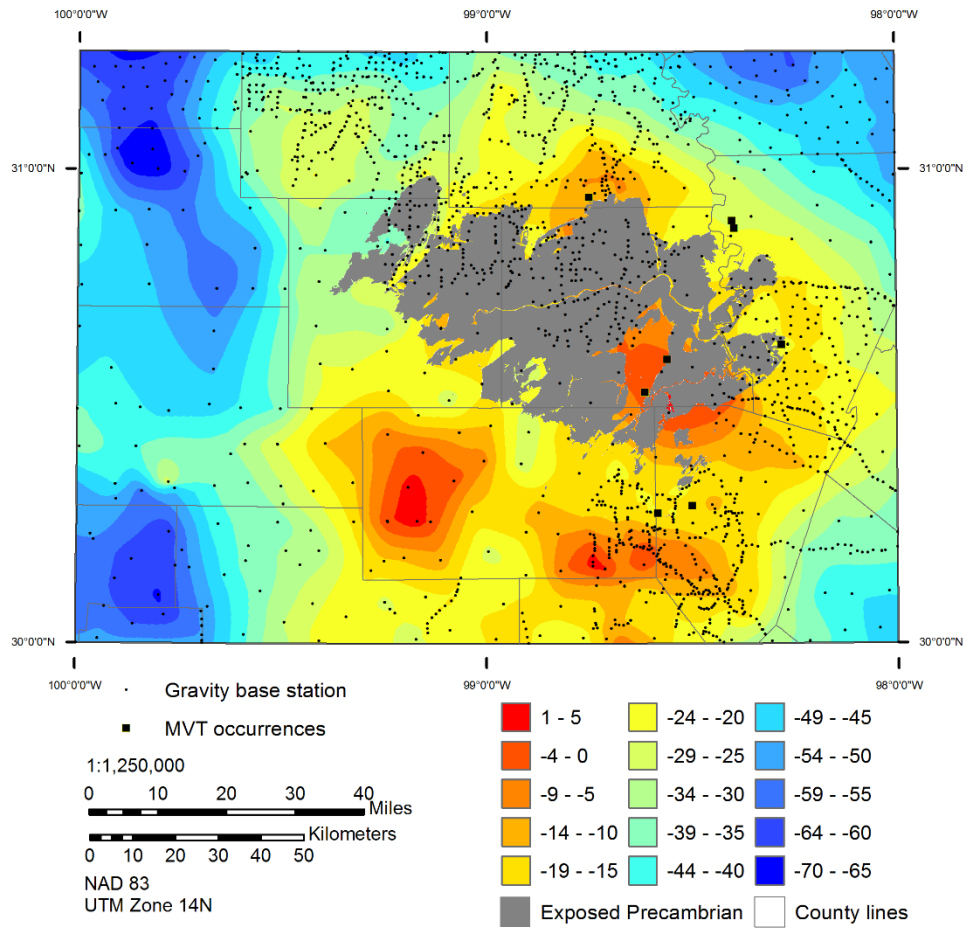
Figure 3.29: Central Texas gravity anomaly classes. Base station data from the North American Gravity Database (Hildenbrand et al., 2002).

1.32 for the 0.05-0.11 mGal/m range. This interval occupies 46.6% of the map area and contains 60% of the training deposits.

Close examination of the gravity maps shows that the continuous surfaces generated from the interpolation of base station data are relatively coarse as a result of the wide spacing of the base stations over portions of the study areas (especially the western portions). The result is that the gravity maps probably lack the necessary resolution to map variability related to irregular Precambrian topography in the subsurface. As a result, these maps were not used to generate any of the models in spite of their relatively high C/σC scores.

Proximity to tin granite plutons

In addition to presence of buried Precambrian hills, the CUSMAP authors also considered proximity to two-mica, tin granite plutons in the basement as a separate permissive criterion in their assessment of the Rolla quadrangle (Figure 3.30). This was the weakest performing of all CUSMAP criteria considered with a maximum C/σC value of 0.97 for the areas contained within the surface expression of these tin granite plutons (distance of 0 m; 0 ft) (Figures 3.31 and 3.32). These areas occupy 13.4% of the study area and contain only 20% of the deposits.

Lehmann data

The basement structure data for Central Texas covers a portion of the study area east and south of the Llano Uplift (Paterson, Grant, and Watson Limited, 1981a) (Figure 3.33). These maps are part of a collection of data recently donated to the University of Texas at Austin by North Central Mineral Ventures of Minneapolis, Minnesota. These maps were processed from contracted magnetic surveys flown in the Kerr Basin and Ouachita Trend areas and show areas where basement rocks are interpreted to be within
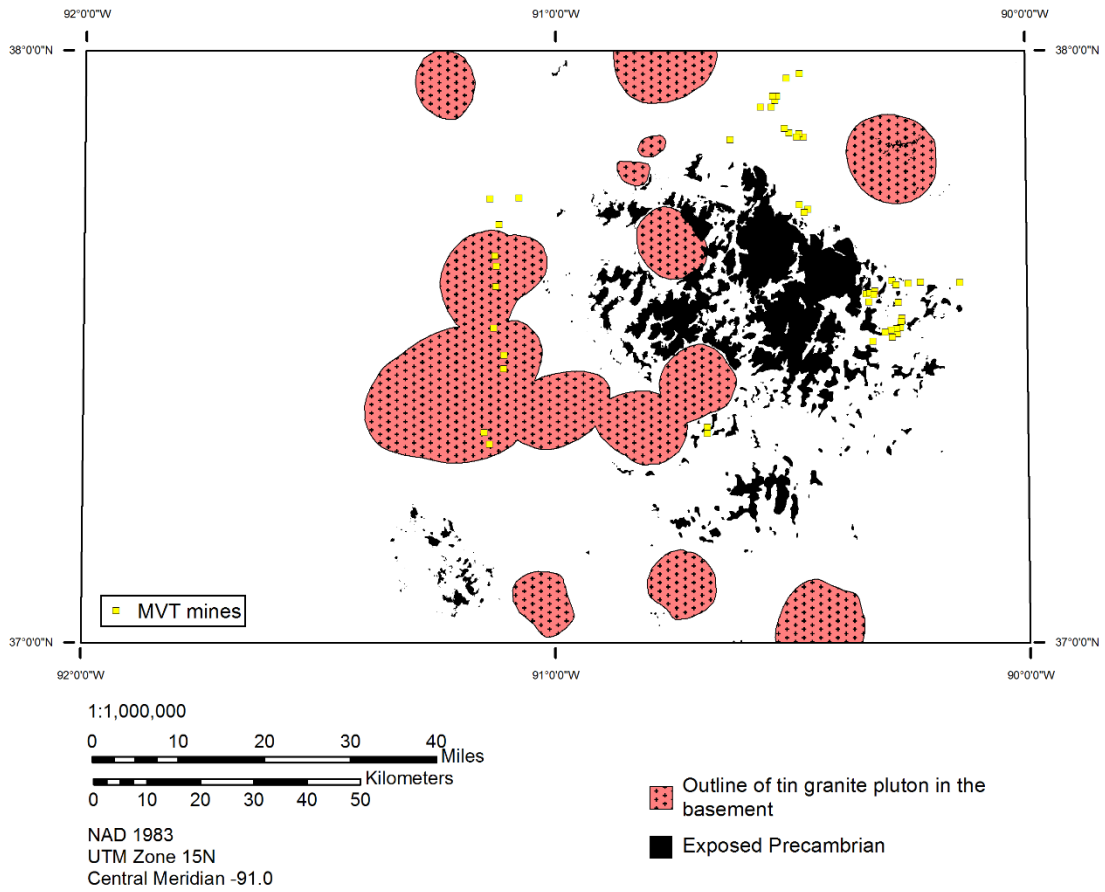
Figure 3.30: Outlines of tin granite plutons in the basement of Southeast Missouri. Digitized from CUSMAP permissive criteria (Pratt et al., 1981).
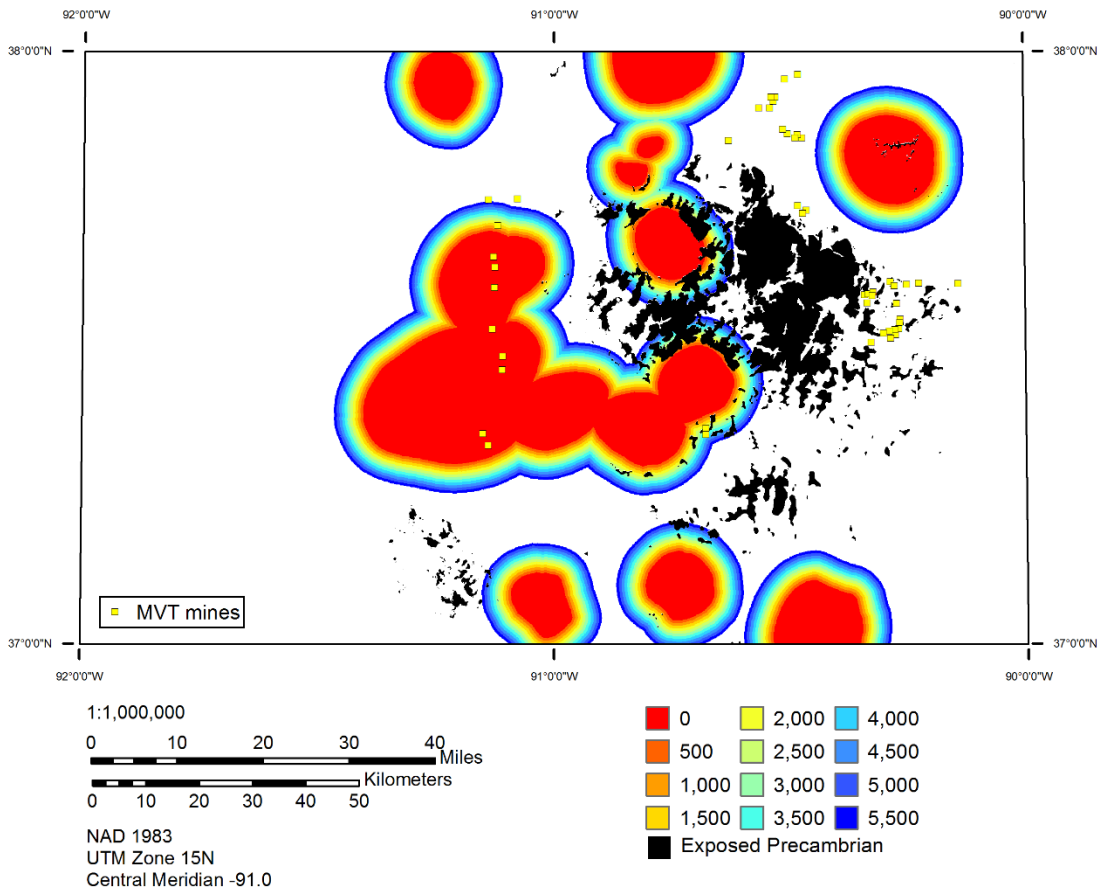
Figure 3.31: Select 500 m tin granite pluton proximity classes for Southeast Missouri. Only distances up to 5,500 m are shown here for clarity although distances up to 15,000 m were evaluated.
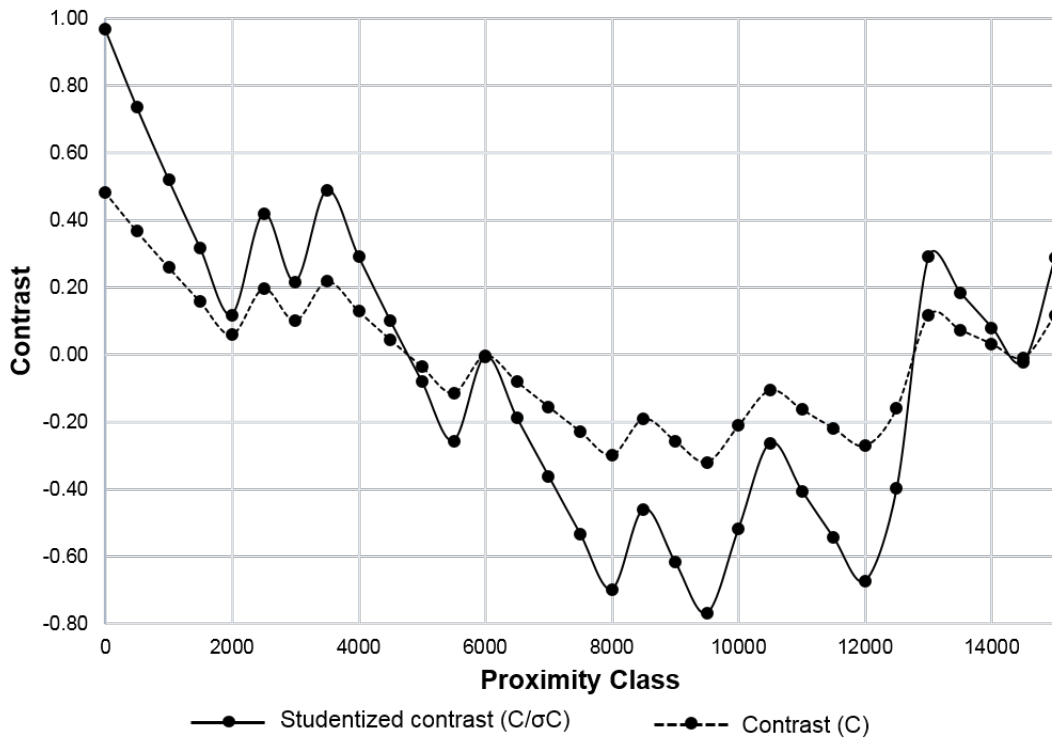
Figure 3.32: Tin granite pluton contrasts vs. proximity class.
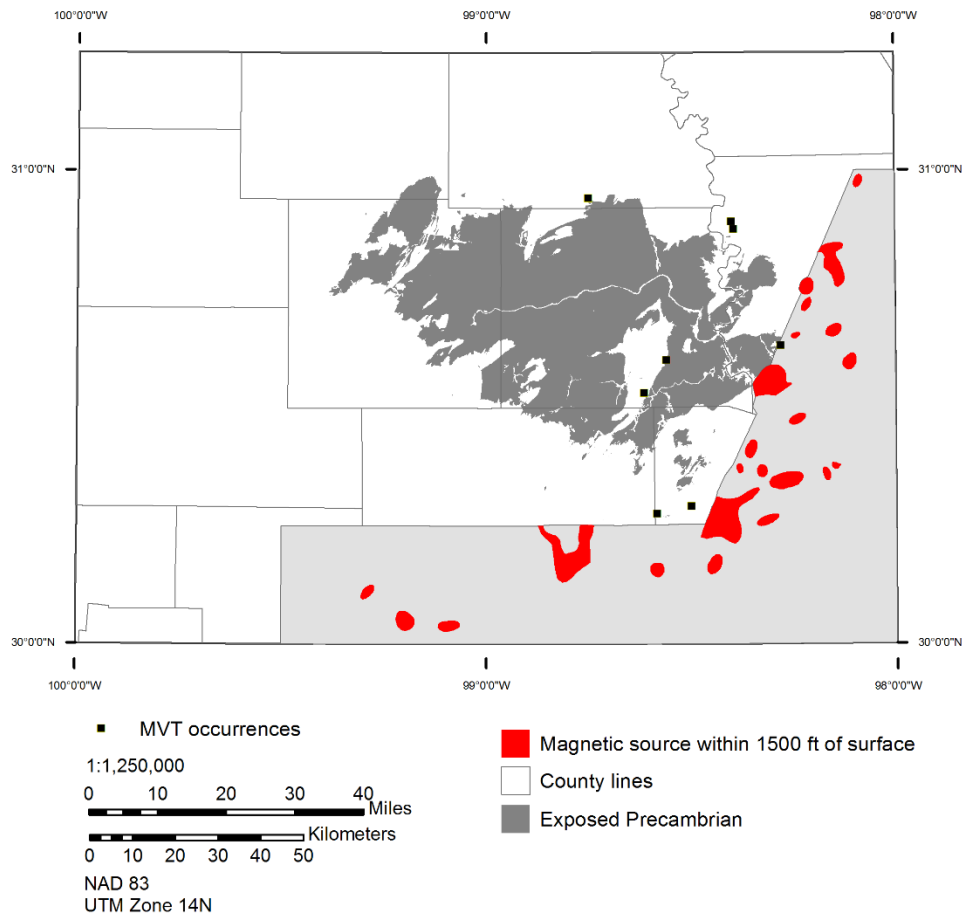
Figure 3.33: Basement highs in Central Texas interpreted from magnetics data (from
Paterson, Grant, and Watson Limited, 1981a).

approximately 460 m (1,500 ft) of the surface. These areas are assumed to represent basement highs. A related series of maps of the same area from a follow-up investigation was initially considered as a potential source of fault data for the Central Texas models (Paterson, Grant, and Watson Limited, 1981b).

Presence of MVT and trace element mineralization

Leach et al. (1995) summarized the major, minor, and trace geochemical characteristics for some major North American MVT deposits and suggested that Cd, Ag, As, and Mo may be useful pathfinder elements for mineralization in Southeast Missouri. Unfortunately, the reported values for these elements appear unreliable in the readily available stream sediment geochemistry data extensively used in this study.

Near elevated base metal concentrations in insoluble residues of the Bonneterre Formation

The CUSMAP authors considered proximity to elevated base metal concentrations (Pb) and Ag in insoluble residues of the Bonneterre Formation to be a diagnostic criterion in their assessment of MVT potential in the Rolla quadrangle (Pratt et al., 1981) (Figure 3.34). This data layer was not buffered, but evaluated in its published (binary) form that shows anomalous and nonanomalous areas as polygons. The anomalous area occupies 13.8% of the study area and contains 48% of the training deposits, resulting in a $C/\sigma C$ value of 4.38.

Stream-sediment geochemistry

The raw data used to generate geochemical anomaly maps are from the publicly available National Uranium Resource Evaluation (NURE) Hydrogeochemical and Stream Sediment Reconnaissance (HSSR) dataset (USGS, 2004). The main purpose of the NURE program was to discover additional domestic uranium resources (Smith, 2006). Although
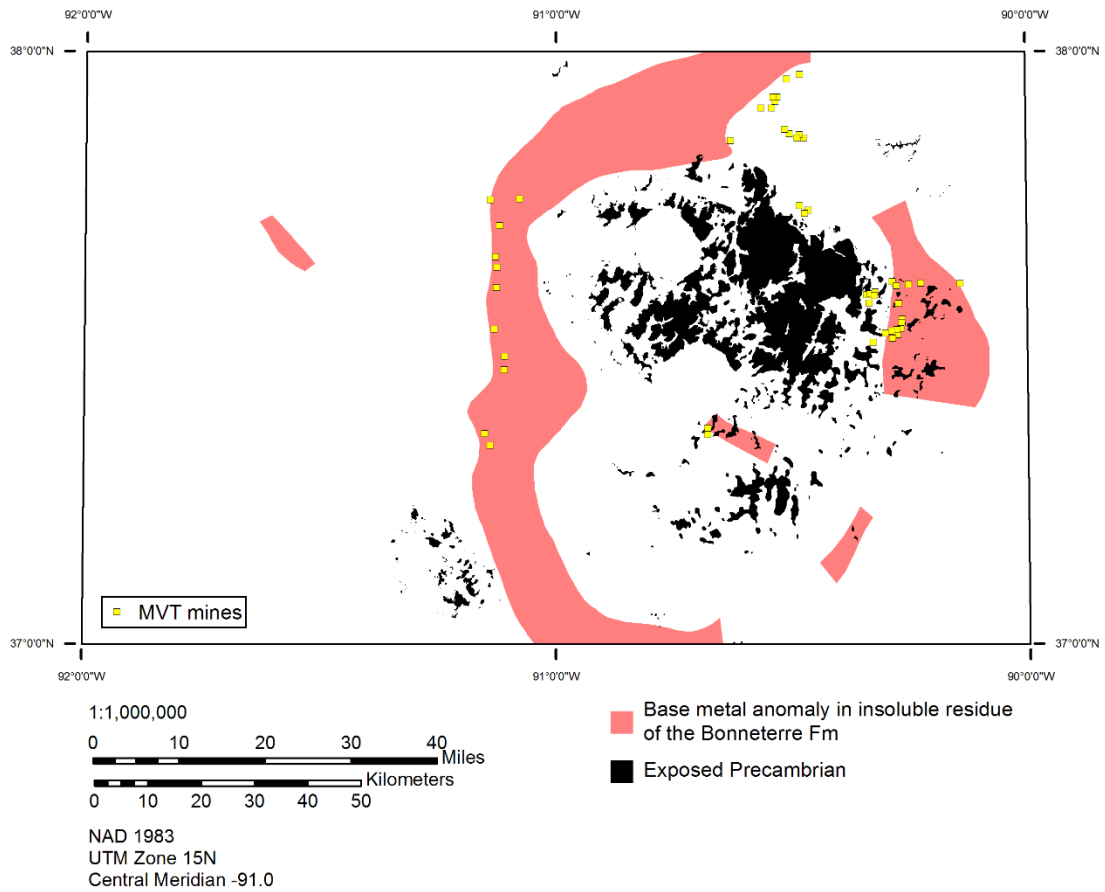
Figure 3.34: Anomalous base metal concentrations in insoluble residues of the
Bonneterre Formation in Southeast Missouri. Digitized from CUSMAP
diagnostic criteria (Pratt et al., 1981).

101

samples were originally analyzed only for uranium, later analyses tested for a variety of other elements. A major appeal of this dataset is that there is information available for a large portion of the U.S., including at least partial coverage of both the Southeast Missouri and Central Texas study areas. Unfortunately, only a portion of the Southeast Missouri Rolla quadrangle contains useable information because of inaccurate or missing data.

A typical stream-sediment sample contains a blend of materials derived from upstream sources. Most of the sediment is likely from background, nonmineralized sources, but some may be from mineralized sources (Carranza, 2009). The general process to separate anomalous from background measurements involves calculating an expected background value for each element of interest in each catchment basin in the study area, then subtracting these background values from measured values. The difference between the background and the measured concentrations for a particular element in a given catchment basin is called the uni-element residual. Residuals that are higher than a determined threshold value are considered anomalous.

The ArcGIS hydrology toolset was used to delineate the catchment basins that contribute sediment to each NURE sample location. Anomalous elemental concentrations in each of these basins were calculated following the method described by Carranza (2009). Leach et al. (1995) described geochemical pathfinders for select MVT districts in North America and indicated that Cd may be useful in Southeast Missouri. Unfortunately, the NURE data for Southeast Missouri does not include valid Cd data. The USGS deposit model describes an irregular zoning pattern of Pb, Zn, Cu, Ni, and Co in the Southeast Missouri MVT districts (Leach et al., 2010). Anomaly maps for each of these elements were derived from the NURE data for both Southeast Missouri and Central Texas. A detailed description of the GIS operations used to produce the anomaly maps is included in Appendix B, and the general approach is summarized below.

Carranza (2009) noted that the distribution of geochemical data must be approximately symmetrical before calculating weighted average background values related to lithology. However, Carranza also suggested that exploration geochemical data are almost never normally distributed. One solution to this problem is to log-transform the raw geochemical data, which tends to produce distributions closer to normal. Log-transformed and untransformed normal Q-Q plots for each of the five elements considered in this study are shown in (Figure 3.35). These plots show the actual values plotted against expected normal values. Deviations from a straight line indicate non-normal distributions.

After the data have been log-transformed, a weighted mean concentration for every element of interest is determined for each lithology (M_j) in the study area:

$$M_j = \sum_{i=1}^{n} Y_i \hat{X}_{ij} / \sum_{i=1}^{n} \hat{X}_{ij} \qquad \text{(Carranza, 2009)}$$

where Y_i are measured elemental concentrations in the stream sediment samples i, and $\hat{X}_{ij}$ is the area of each lithology in catchment basin i (Figures 3.36 and 3.37). After the mean concentrations have been calculated for each lithology (Tables 3.3 and 3.4), these values are used to calculate an expected background concentration (Y'_i) in each catchment basin (i):

$$Y'_i = \sum_{j=1}^{m} M_j \hat{X}_{ij} / \sum_{j=1}^{m} \hat{X}_{ij} \qquad \text{(Carranza, 2009)}$$

A basin is considered anomalous if the actual minus expected concentration ($Y_i - Y'_i$), or geochemical residual, in that basin is greater than a threshold value, which is usually determined from exploratory data analysis (Carranza, 2009) (Figure 3.38). A common threshold value is the upper inner fence (UIF) which is defined as:

$$UIF = UH + (1.5 \text{ x } IQR)$$

where UH is the upper hinge (the value half way between the median and maximum) and the IQR is the interquartile range. Another common threshold value is the
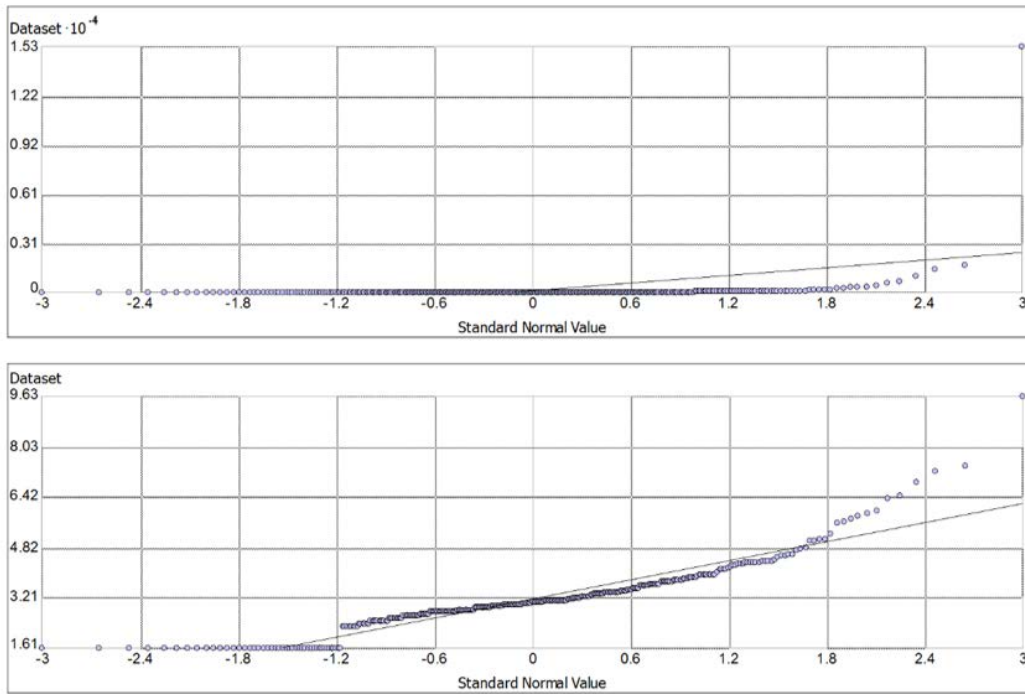
Figure 3.35: Loge-transformed (lower) and non-transformed (upper) normal QQ plots of
NURE values for Pb in Southeast Missouri.
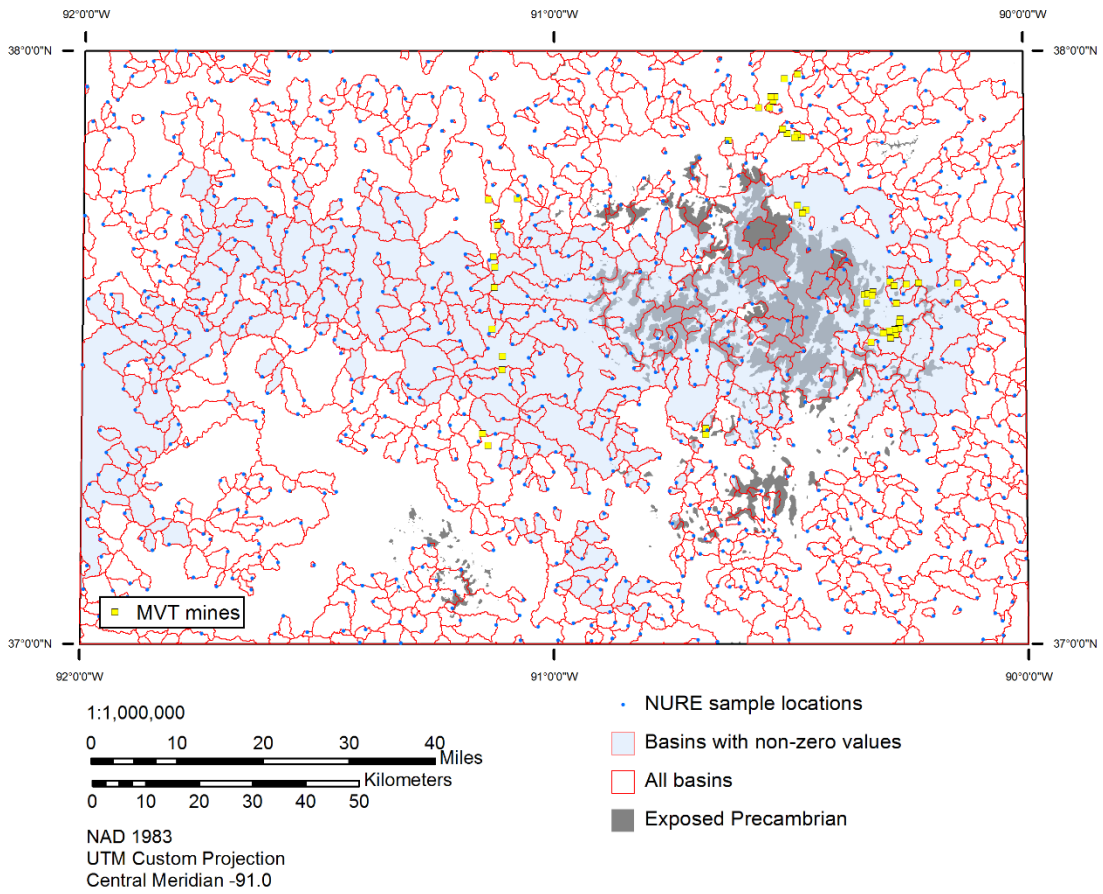
Figure 3.36: Southeast Missouri catchment basins for NURE samples. Only basins with non-zero NURE values are used for geochemical anomaly calculations.
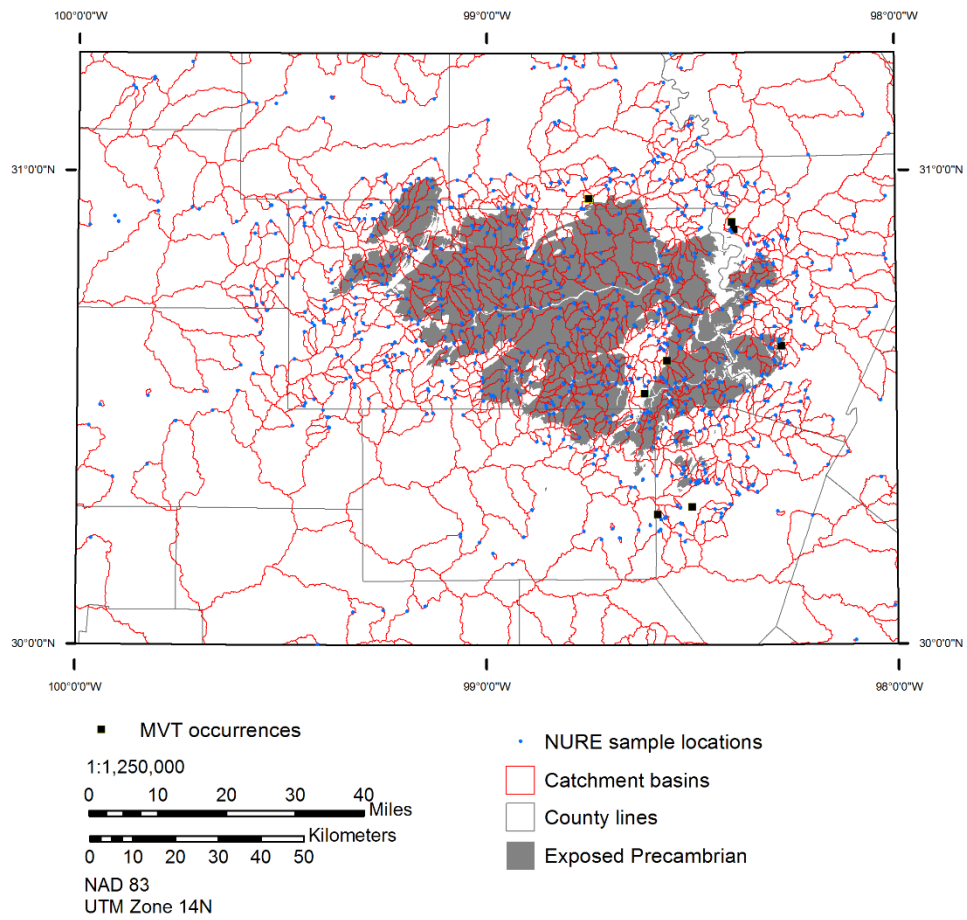
Figure 3.37: Central Texas catchment basins for NURE samples.

Unit	Avg Pb (ppm)	Avg Zn (ppm)	Avg Ba (ppm)	Avg Co (ppm)	Avg Cu (ppm)	Avg Ni (ppm)	Avg Fe (pct)
diabase dikes and sills	56	79	309	16	20	23	4.6
Elvins Group and Bonneterre Dolomite	44	48	304	12	17	15	2.6
Eminence and Potosi Dolomites	36	45	214	11	16	14	1.8
Gasconade Dolomite	17	29	192	8	12	12	1.5
Jefferson City/Cotter Dolomite	19	32	330	8	12	11	1.6
Lamotte Sandstone	44	49	310	17	19	21	3.2
Roubidoux Formation	14	21	246	6	10	9	1.3
St. Francois Moundatins Intrusive Suite	52	51	310	16	21	21	3.6
St. Francois Moundatins Volcanic Supergroup	42	53	331	12	18	15	3.2

Table 3.3:   Background geochemical values for Southeast Missouri. Calculations made using loge-transformed data, but converted to ppm/pct for display.

Units	Avg Pb (ppm)	Avg Zn (ppm)	Avg Ba (ppm)	Avg Co (ppm)	Avg Cu (ppm)	Avg Ni (ppm)
Cambrian Limestone	8	51	304	4	5	7
Cambrian Sandstone	10	48	495	5	6	9
Cretaceous Intrusive	2	100	40	2	4	4
Cretaceous Limestone	6	79	106	2	4	5
Cretaceous Sandstone	8	58	268	3	4	6
Paleozoic Limestone	8	83	164	2	8	8
Pennsylvanian-Permian Evaporite	10	100	150	2	20	10
Pennsylvanian-Permian Mudstone	9	99	161	2	17	10
Precambrian Granite	16	66	595	5	6	8
Precambrian Mafic	12	69	550	8	10	14
Precambrian Metamorphic	8	56	593	7	5	13
Quaternary Alluvium	8	94	142	2	11	8
Tertiary Sandstone	6	100	68	2	6	8

Table 3.4:   Background geochemical values for Central Texas.
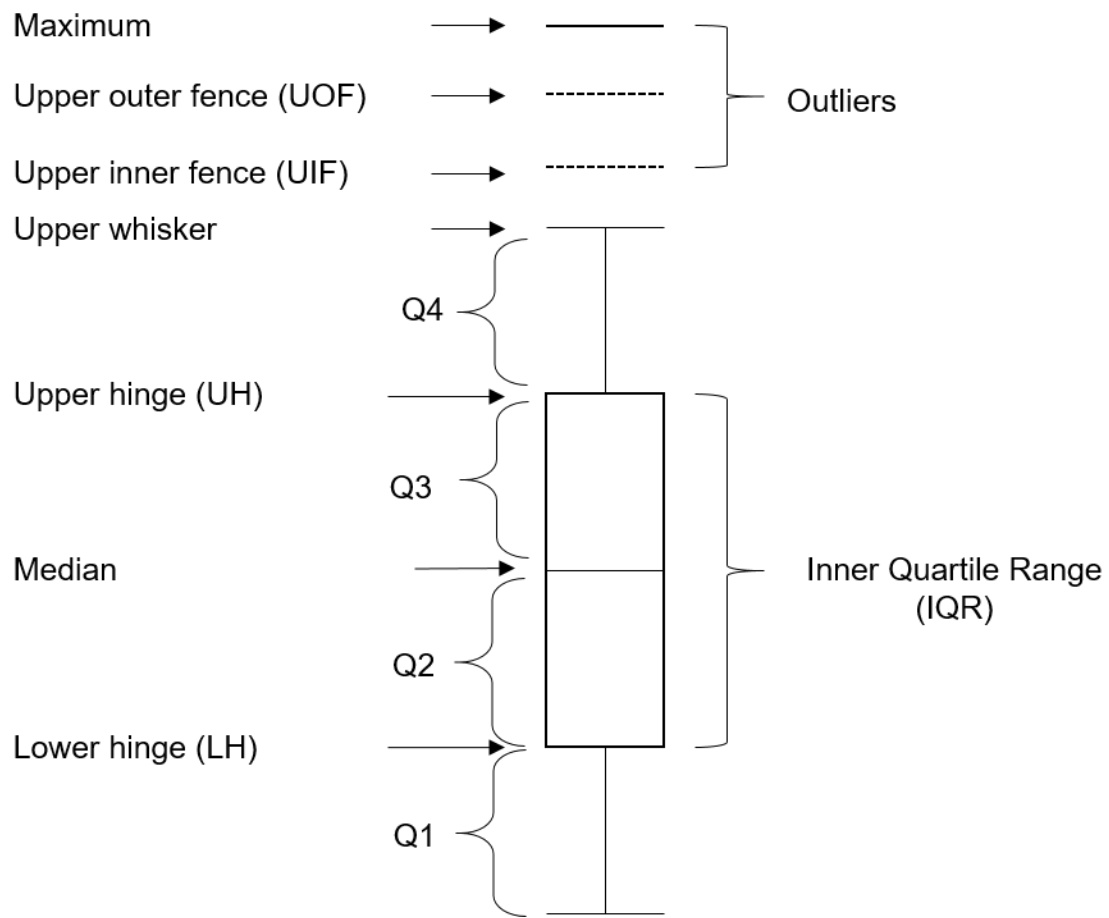
Figure 3.38: Components of a box and whisker plot for exploratory data analysis of geochemical data. Modified from Carranza (2009).

median + 2MAD, where MAD is the median of absolute deviations from the median residual value. Both threshold definitions are considered in this study.

Carranza (2009) proposed the following equation rearranged from Hawkes (1976) to account for the downstream dilution of stream sediments from an anomalous source:

$Y_aA_a = A_i(Y_i - Y'_i) + Y'_iA_a$

where $A_i(Y_i - Y'_i)$ is the area of a catchment basin i multiplied by the uni-element residual and Y'_iA_a is the background concentration multiplied by the area of the anomalous source. Moon (1999) suggested that this equation fails to account for variable terrain and the distance between the sample and anomalous source. Moon instead proposed using the "productivity rating" of Polikarpochkin (cited in Moon, 1999) by eliminating the second term (Y'_iA_a) of this equation to leave only the area and concentration terms. Moon (1999) noted the problem of variable catchment basin sizes and suggested that the productivity equation effectively accounts for this. The catchment basin sizes for both study areas are highly variable, however, a qualitative evaluation of the productivity values and noncorrected residuals in the Southeast Missouri study area shows that only the largest catchment basins are identified as anomalous using the productivity equation. For this reason, the noncorrected residuals are used in weights calculations for this study.

Weights were calculated for Pb, Zn, Cu, Ni, and Co uni-element residuals that exceeded the threshold values identified using the exploratory data analysis techniques discussed above (Table 3.5). In addition to the uni-element anomalies, the Boolean 'OR' operator was used to generate a new map for areas that contain either Pb or Zn uni-element residual outliers (defined as greater than the UIF) (Figure 3.39). This binary map had the highest $C/\sigma C$ value of 4.1 and contained 26.7% of the training deposits while occupying only 3.3% of the study area. Unlike Southeast Missouri, very few of the uni-element values in Central Texas met the threshold value defined as greater than the UIF. For this reason,

	Element	Median	UH	LH	IQR	UOF	UIF	Median + 2MAD	Number anomalous basins UIF	% Anomalous UIF	Num anomalous Med + 2MAD	% Anomalous Med + 2MAD
Southeast Missouri (n=369)	Pb	-0.12	0.26	-0.59	0.84	1.95	1.52	0.75	12	3.3%	36	9.8%
	Zn	-0.12	0.27	-0.43	0.70	2.38	1.32	0.58	6	1.6%	42	11.4%
	Ba	-0.01	0.30	-0.33	0.62	2.17	1.24	0.62	2	0.5%	23	6.2%
	Co	0.07	0.34	-0.28	0.62	2.22	1.28	0.68	2	0.5%	32	8.7%
	Cu	-0.09	0.32	-0.41	0.73	2.51	1.42	0.63	7	1.9%	54	14.6%
	Ni	-0.03	0.34	-0.37	0.71	2.47	1.41	0.68	5	1.4%	49	13.3%
	Fe	0.06	0.29	-0.24	0.53	1.87	1.08	0.61	7	1.9%	24	6.5%
Central Texas (n=1226)	Pb	0.22	0.67	-0.58	1.25	4.42	2.54	1.41	1	0.1%	28	2.3%
	Zn	0.12	0.24	-0.44	0.68	2.29	1.27	0.57	1	0.1%	54	4.4%
	Ba	0.06	0.35	-0.28	0.64	2.26	1.31	0.72	14	1.1%	98	8.0%
	Co	-0.04	0.49	-0.21	0.70	2.57	1.53	0.72	15	1.2%	156	12.7%
	Cu	-0.07	0.51	-1.02	1.54	5.13	2.82	1.26	0	0.0%	45	3.7%
	Ni	0.05	0.46	-0.40	0.86	3.03	1.74	0.91	16	1.3%	110	9.0%

Table 3.5: Geochemical threshold values for Southeast Missouri and Central Texas. Threshold values in loge form for Southeast Missouri and Central Texas. The n value is the number of basins for each area. The right portion of the table shows the number of anomalous basins defined by each threshold.
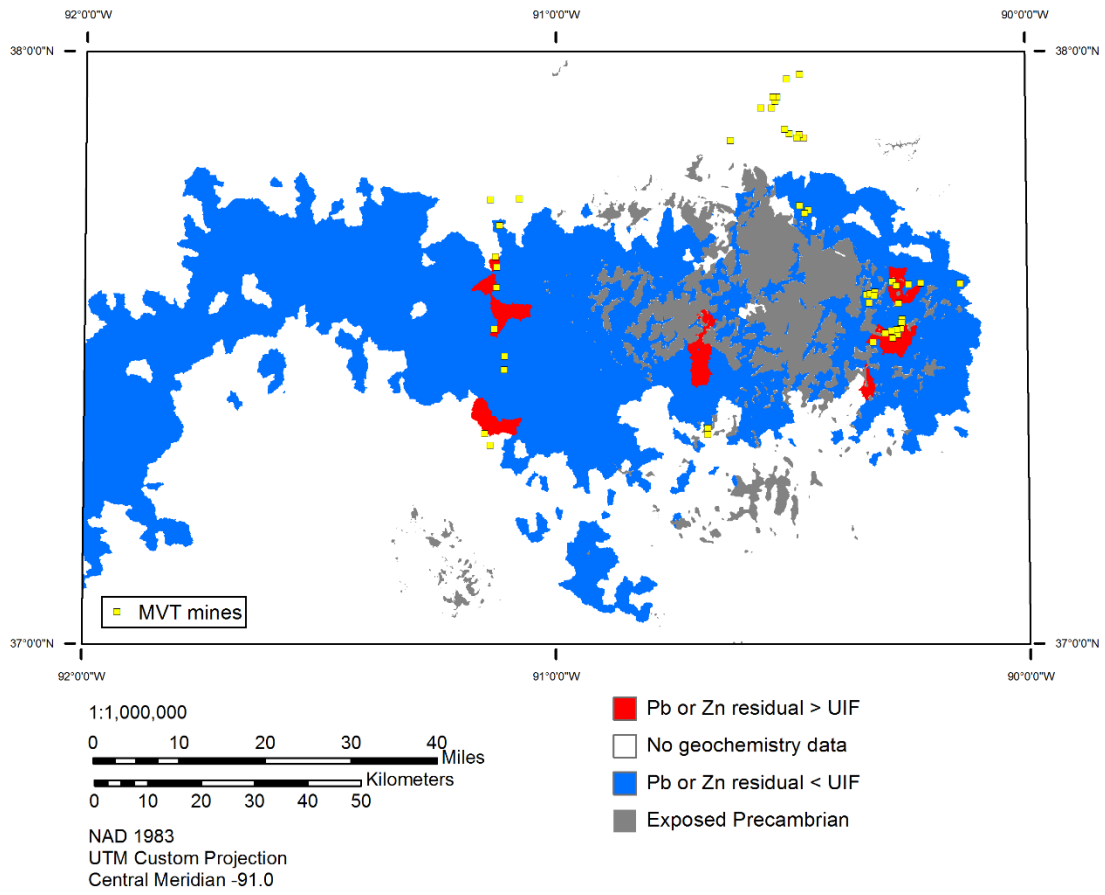
Figure 3.39: Southeast Missouri Pb or Zn geochemical residuals greater than the UIF
threshold.

the Co anomaly defined as greater than the median + 2MAD (Figures 3.40 and 3.41) was used as an alternate geochemical evidence layer. The C/σC value for this map is 2.7 and it contains 20% of the training deposits in 4.1% of the map area.

Central Texas NURE processing

There were 131 separate map units on the geologic map of Central Texas over the extent of the catchment basins for the stream sediment geochemistry data compared to 9 for the Southeast Missouri area. Prior to calculating background values for the catchment basins, the number of units needed to be reduced. Map units were grouped based on lithology and age to reduce the number of units to 13, then weighted averages were calculated for each and uni-element residuals were calculated for all catchment basins following the method described above.
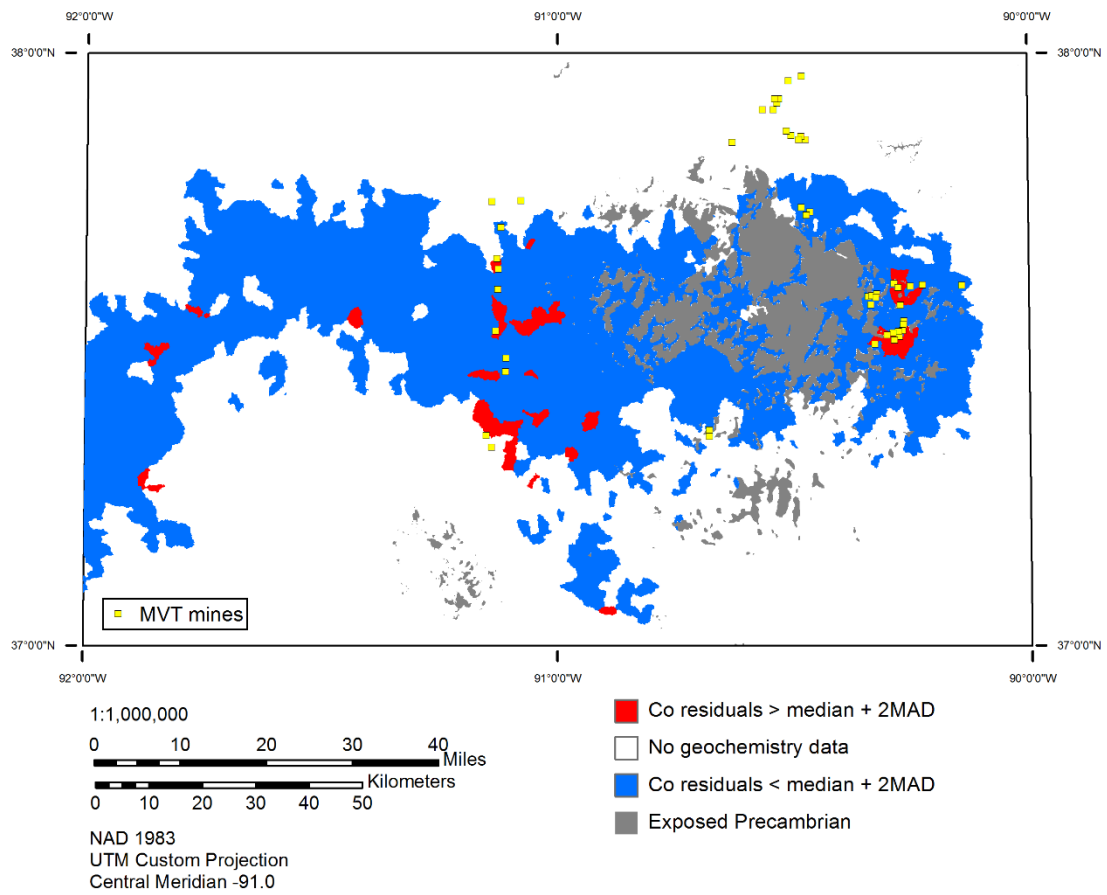
Figure 3.40: Southeast Missouri Co residuals greater than the median + 2MAD threshold. Note the similar distribution to the Pb or Zn anomaly map.
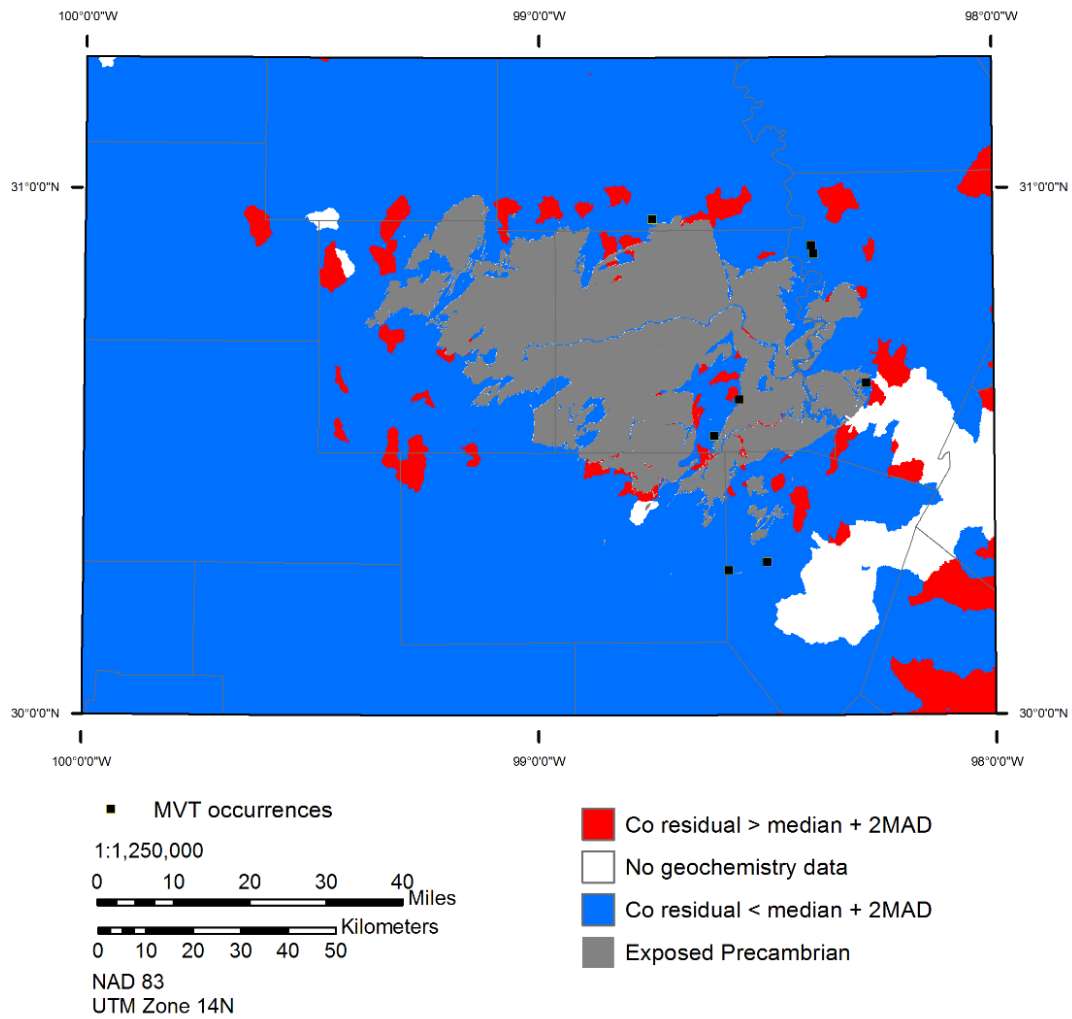
Figure 3.41: Central Texas Co residuals greater than the median + 2MAD threshold.

Chapter 4: Results

Fourteen mineral potential models were generated for Southeast Missouri and three for Central Texas using fuzzy and binary evidence layers. Each of these maps incorporates different combinations of the evidence layers discussed in the preceding chapter (Tables 4.1 and 4.2). The goal for every successive model is to increase the efficiency, decrease or eliminate the degree of conditional independence (CI) violation, and reduce or eliminate the number of nonpredicted validation deposits.

The Southeast Missouri models can be grouped in two categories. The first category consists of models that incorporate any of the available data for Southeast Missouri. These models make heavier use of the CUSMAP algal reef rock data layer that has a high $C/\sigma C$ value and is therefore a good predictor of Southeast Missouri MVT deposits. The result is that these models have higher efficiency scores and lower numbers of nonpredicted deposits although they tend to be worse violators of conditional independence.

The second category of models only incorporate Southeast Missouri data that is also available for Central Texas. In general, this second category of models uses faults, surface geology, stream-sediment geochemistry data, and either proximity to basement highs or magnetics data instead of algal reef rock proximity. Although these models tend to have slightly lower efficiency scores, they theoretically represent the best expected outcomes for Central Texas because they incorporate the same types of evidence as the Central Texas models. These models also have higher CI ratios which indicates a lower degree of CI violation.

In each category, there are models that use only binary evidence (BM designation) and models that use a combination of binary and fuzzy evidence layers (FM designation). The three evidence layers that can be either binary or fuzzy are proximity to faults,

Category	Model	Faults	Geology	Geochemistry	Basement highs	Algal reef	Magnetics
I	BM101	NWSE - 500m	Bonneterre	Pb or Zn UIF	500m	1500	
	FM101	NWSE Fuzzy	Bonneterre	Pb or Zn UIF	Fuzzy	Fuzzy	
	BM102	NWSE - 500m	Bonneterre	Co 2MAD	500m	1500	
	FM102	NWSE Fuzzy	Bonneterre	Co 2MAD	Fuzzy	Fuzzy	
	BM103	NWSE - 500m		Co 2MAD	500m	1500	
II	BM111	NWSE - 500m	Bonneterre	Pb or Zn UIF	500m		
	FM111	NWSE Fuzzy	Bonneterre	Pb or Zn UIF	Fuzzy		
	BM112	NWSE - 500m	Bonneterre	Co 2MAD	500m		
	FM112	NWSE Fuzzy	Bonneterre	Co 2MAD	Fuzzy		
	BM113	NWSE - 500m	Bonneterre	Co 2MAD			35-45%
	FM113	NWSE Fuzzy	Bonneterre	Co 2MAD			35-45%
	BM114	NWSE - 500m		Co 2MAD			35-45%
	FM114	NWSE Fuzzy		Co 2MAD			35-45%
	BM115	NWSE - 500m	Bonneterre	Co 2MAD	500m		35-45%

Table 4.1: Southeast Missouri model summary. Data considered in each Southeast Missouri model. The faults, basement highs, and algal reefs evidence maps are either binary corresponding to the proximity class with the highest C/sC value, or fuzzy. Geochemistry evidence maps are either Pb or Zn anomalies with residual values greater than the upper inner fence (UIF) or Co anomalies with residual values greater than the median + 2MAD (median of absolute deviations from the median).

Model	Faults	Geology	Geochemistry	Basement highs
TM111	Ewing Fuzzy	Paleozoic Limestone	Co 2MAD	Bsmt Fuzzy OR Mag 35-45%
TM112	Ewing Fuzzy	Cap Mountain Limestone	Co 2MAD	Bsmt Fuzzy OR Mag 35-45%
TM113	Ewing Fuzzy		Co 2MAD	Bsmt Fuzzy OR Mag 35-45%

Table 4.2: Central Texas model summary. Data considered in each Central Texas model. The basement highs data consists of the fuzzy weights for proximity to basement highs for the portion of the study area where data is available, and magnetics weights for the remainder of the study area.

proximity to basement highs, and proximity to algal reef rocks. The models that use the fuzzy classification of these data have higher efficiency scores than their binary counterparts, but are also worse violators of CI. Model performance is summarized in Tables 4.3 and 4.4.

In order to facilitate the visual comparison of models with widely varying posterior probabilities, figures of the following models are symbolized based on the percentage of map area occupied by the unique conditions. For example, the cutoff value of "1%" shows the 1% of the map with the highest posterior probabilities. The cutoff value of "15%" shows the highest posterior probabilities that occupy 15% or less of the map area. The portion of the map area symbolized in light gray for all Southeast Missouri models is the portion where the posterior probability is lower than the prior probability. For all Central Texas models, the portion of the maps shown in light gray is the map area containing the lower 80% of posterior probabilities.

CATEGORY I MODELS

Binary Model 101 (BM101) (Figures 4.1 and 4.2) incorporates weights for proximity to NW-SE oriented faults (within 500 m (1,600 ft)), presence of Elvins Group and Bonneterre Dolomite, presence of Pb or Zn stream sediment anomalies as defined by residual values greater than the upper inner fence (UIF), proximity to basement highs (within 500 m (1,600 ft)), and proximity to algal reef rocks (within 1500 m (4,900 ft)). The total model efficiency is 87.8% with four of the twenty-four validation deposits (16.7%) not occurring in an area with a higher posterior probability than the prior probability – these deposits are not predicted by the model. The total area with higher posterior probabilities occupies only 16.7% of the study area and contains 87.5% of the testing deposits.

118

Category	Model	Efficiency	CI ratio	Not predicted
I	BM101	87.82%	37.82%	12.50%
	FM101	91.92%	14.71%	12.50%
	BM102	87.31%	40.65%	16.67%
	FM102	91.76%	15.47%	16.67%
	BM103	76.41%	60.02%	20.83%
II	BM111	80.58%	81.27%	16.67%
	FM111	90.48%	60.92%	20.83%
	BM112	80.03%	83.98%	16.67%
	FM112	90.45%	61.73%	20.83%
	BM113	88.80%	77.88%	20.83%
	FM113	87.79%	60.15%	8.33%
	BM114	78.11%	93.63%	25.00%
	FM114	77.26%	81.75%	37.50%
	BM115	88.20%	76.55%	16.67%

Table 4.3:   Southeast Missouri model performance summary. Efficiency scores, CI ratios, and percentages of non-predicted deposits for each Southeast Missouri model.

Model	Efficiency
TM111	90.27%
TM112	94.50%
TM113	76.90%

Table 4.4:   Central Texas model performance summary. Efficiency scores for Central Texas models.
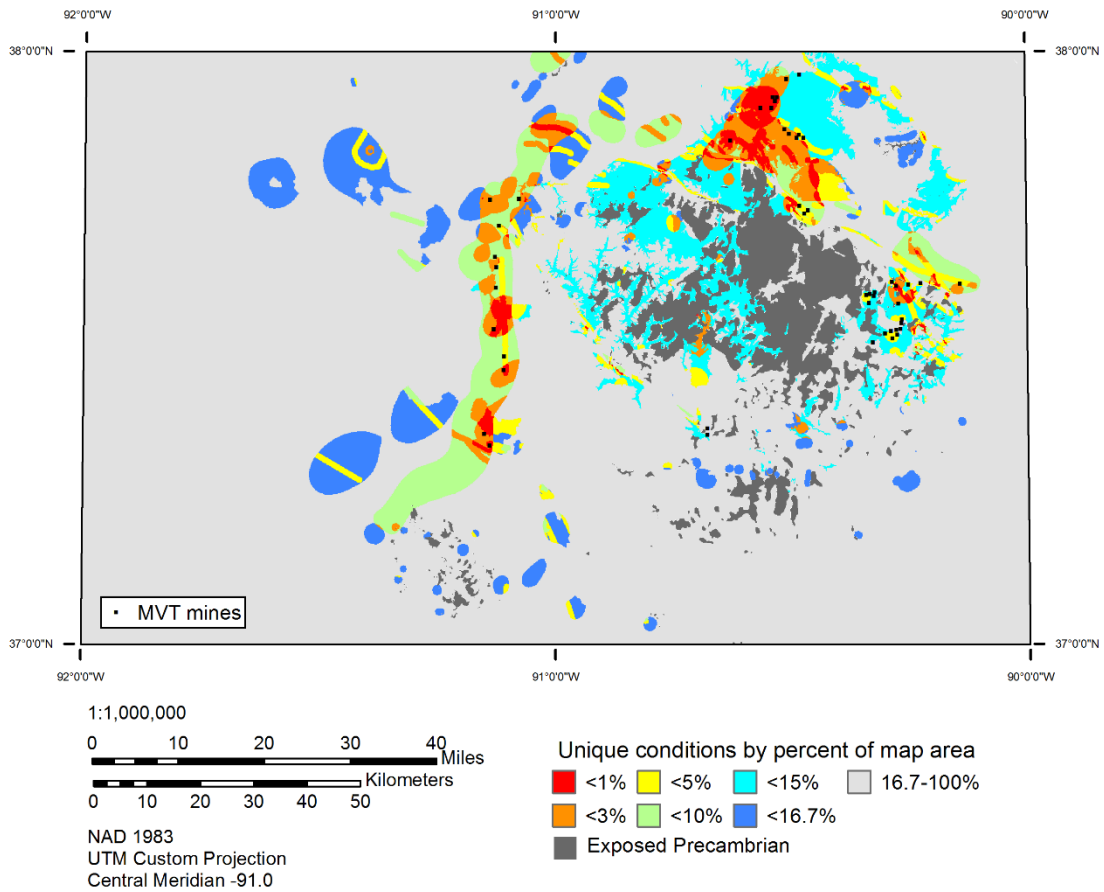
Figure 4.1:   Binary Model 101 for Southeast Missouri. The non-gray portion of the map occupies <16.7% of the map and represents areas where the posterior probability is higher than the prior probability. Validation deposits that fall within the light gray area are considered non-predicted deposits.
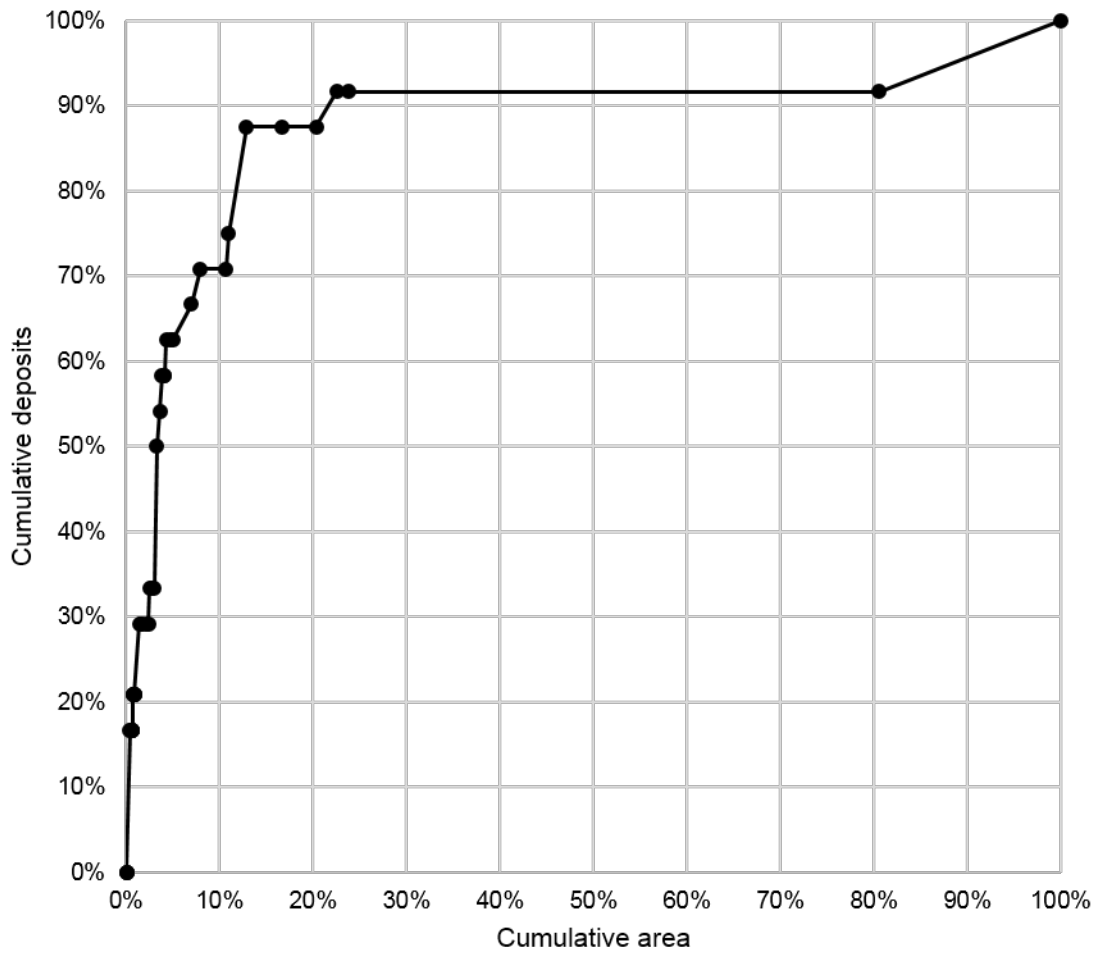
Figure 4.2:   Binary Model 101 prediction rate curve.

Additionally, 70.8% of the testing deposits occur within 8.0% of the study area with the highest posterior probabilities. The CI ratio for this model is 37.8%, which indicates a serious lack of conditional independence in the map inputs.

Fuzzy Model 101 (FM101) (Figures 4.3 and 4.4) is similar to BM101, but incorporates fuzzy classified inputs for proximity to NW-SE oriented faults, basement highs, and algal reef rocks. The use of these fuzzy layers increases the model efficiency by 4% to 91.9% and reduces the number of non-predicted validation deposits from 4 to 3. These improvements over BM101 are accompanied by a decrease in the CI ratio to 14.7%.

Binary Model 102 (BM102) (Figures 4.5 and 4.6) only differs from BM101 in the type of geochemical anomaly evidence considered. While BM101 considers areas containing geochemical residuals for Pb or Zn greater than the UIF, BM102 considers areas with Co residuals greater than the median plus two times the median of absolute deviations (2MAD). The primary reason Co is considered instead of the Pb or Zn layer is that the Central Texas has very few geochemically anomalous areas when an anomaly is defined as a residual greater than the UIF threshold. The result is that model BM102 has a similar efficiency score of 87.3% compared to BM101. The CI ratio is also similar at 40.7% and the number of nonpredicted deposits is identical at 4 (16.7%).

Likewise, Fuzzy Model 102 (FM102) (Figures 4.7 and 4.8) is nearly identical to FM101, with FM102 considering areas with Co anomalies rather than Pb or Zn. The efficiency score for FM102 (91.8%) is also very close to that of FM101 (91.9%), as is the CI ratio (15.5% vs. 14.7%) and number of non-predicted deposits (4 vs. 3).

The last category I model, Binary Model 103 (BM103) (Figures 4.9 and 4.10) is similar to BM102, but does not incorporate weights for surficial presence or absence of the Elvins Group and Bonneterre Dolomite. Surface geology is not considered in this model because it reflects an economic or practical association with known MVT deposits in

123

Figure 4.3: Fuzzy Model 101 for Southeast Missouri.

Figure 4.4:   Fuzzy Model 101 prediction rate curve.

Figure 4.5:   Binary Model 102 for Southeast Missouri.

Figure 4.6:   Binary Model 102 prediction rate curve.

Figure 4.7:   Fuzzy Model 102 for Southeast Missouri.

Figure 4.8: Fuzzy Model 102 prediction rate curve.

Figure 4.9:   Binary Model 103 for Southeast Missouri.
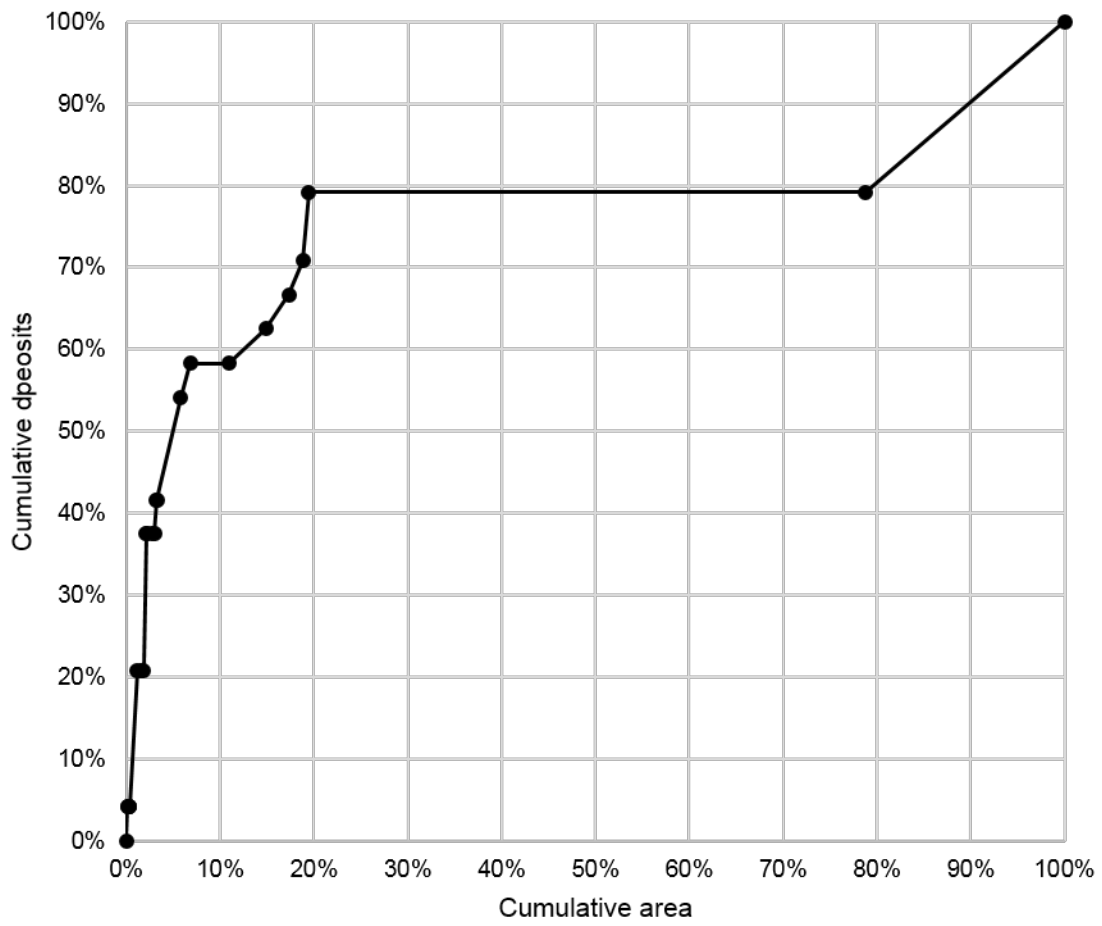
Figure 4.10: Binary Model 103 prediction rate curve.

Southeast Missouri rather than a geologic association. In the known deposits on both the east (Old Lead Belt and Fredericktown/Mine La Motte) and west (Viburnum Trend) of the St. Francois Mountains, the bulk of mineralization is hosted in the Bonneterre Formation. However, there are no surface exposures of the Bonneterre along the Viburnum Trend although it has produced more than twice as much metal as the Old Lead Belt (Ohle, 1990). Binary Model 103 seeks to identify areas with similar characteristics to known MVT deposits without considering surface geology. The resulting model has a substantially lower efficiency score (76.4%) than any of the other category I models. However, the CI ratio is substantially increased to 60.0%. While this CI ratio still indicates a lack of conditional independence because it fails to reach the threshold 85%, it is nearly 20% higher than the next best performing category I model (BM102).

CATEGORY II MODELS

Binary Model 111 (BM111) (Figures 4.11 and 4.12) combines weights from proximity to NW-SE oriented faults (within 500 m (1,600 ft)), presence of Elvins Group and Bonneterre Dolomite, presence of Pb or Zn stream-sediment anomalies as defined by residual values greater than the upper inner fence (UIF), and proximity to basement highs (within 500 m (1,600 ft)) evidence layers. This is nearly the same as the category I model BM101, but BM111 does not incorporate algal reef rock evidence. The model efficiency is more than 7% lower than BM101 at 80.6%, but the CI ratio is more than twice as high (81.3% vs. 37.8%). Both models fail to predict four of the twenty-four validation deposits (16.7%). Areas with higher posterior than prior probabilities occupy 20.9% of the map area and contain 20 of 24 (83.3%) of the testing deposits. The significant improvement of the CI ratio to over 80% indicates that there is a lack of CI between the algal reef rock and basement high evidence layers. While a CI ratio of 81.3% still indicates an overall lack of

132
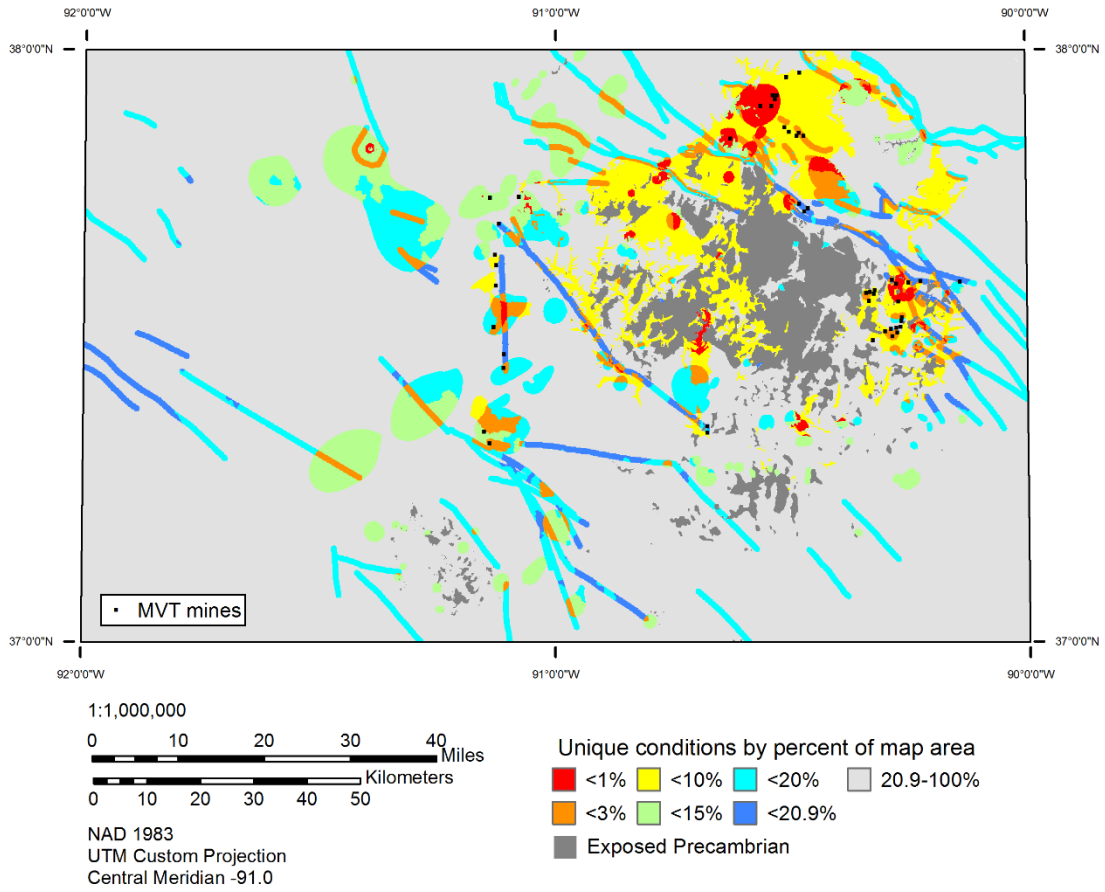
Figure 4.11: Binary Model 111 for Southeast Missouri.

133
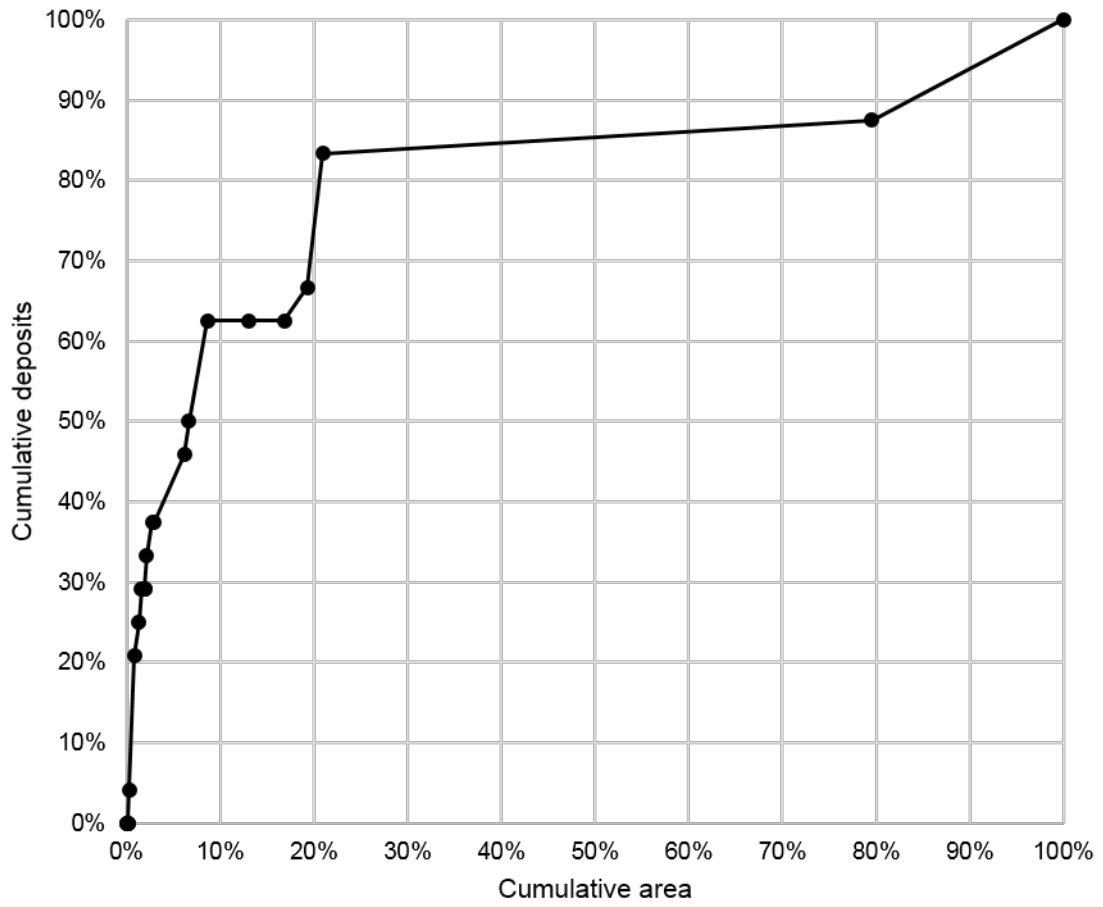
Figure 4.12: Binary Model 111 prediction rate curve.

CI between evidence layers in the model, it represents an improvement of over 20% compared to the best performing category I model.

Fuzzy Model 111 (FM111) (Figures 4.13 and 4.14) is identical to BM111 but uses fuzzy weights for the proximity to faults and basement-high data layers. The result is a nearly 10% increase in efficiency to 90.5%. However, this efficiency increase is accompanied by a decrease in the CI ratio to 60.9%, and an increase in the number of nonpredicted deposits to 5 (20.83%).

Binary Model 112 (BM112) (Figures 4.15 and 4.16) uses nearly the same data as BM111, but considers Co geochemical anomalies instead of Pb or Zn. The efficiency score for BM112 is slightly lower than for BM111 (80.0% vs. 80.6%) and the CI ratio is slightly higher (84.0% vs. 81.3%).

Fuzzy Model 112 (FM112) (Figures 4.17 and 4.18) using fuzzy values for fault proximity and basement highs results in an efficiency increase of 10.5% over BM112 from 80.0% to 90.5%. The CI ratio is lower at 61.7% and the number of nonpredicted deposits is increased from 4 to 5 out of 24.

Binary Model 113 (BM113) (Figures 4.19 and 4.20) is similar to BM112, but incorporates magnetics data instead of proximity to basement highs. This increases the efficiency to 88.8% compared to BM112 (80.0%), but also reduces the CI ratio to 77.9% and increases the number of nonpredicted deposits from 4 to 5. Interestingly, the corresponding fuzzy model (FM113) (Figures 4.21 and 4.22) has a 1% lower efficiency score of 87.8% as well as a lower CI ratio of 60.2%. However, FM113 predicts more of the validation deposits than any other model with 22 of 24 deposits occurring in areas where the posterior probability is higher than the prior probability.

Binary Model 114 (BM114) (Figures 4.23 and 4.24) and Fuzzy Model 114 (FM114) (Figures 4.25 and 4.26) incorporate fault proximity, Co anomalies, and magnetics
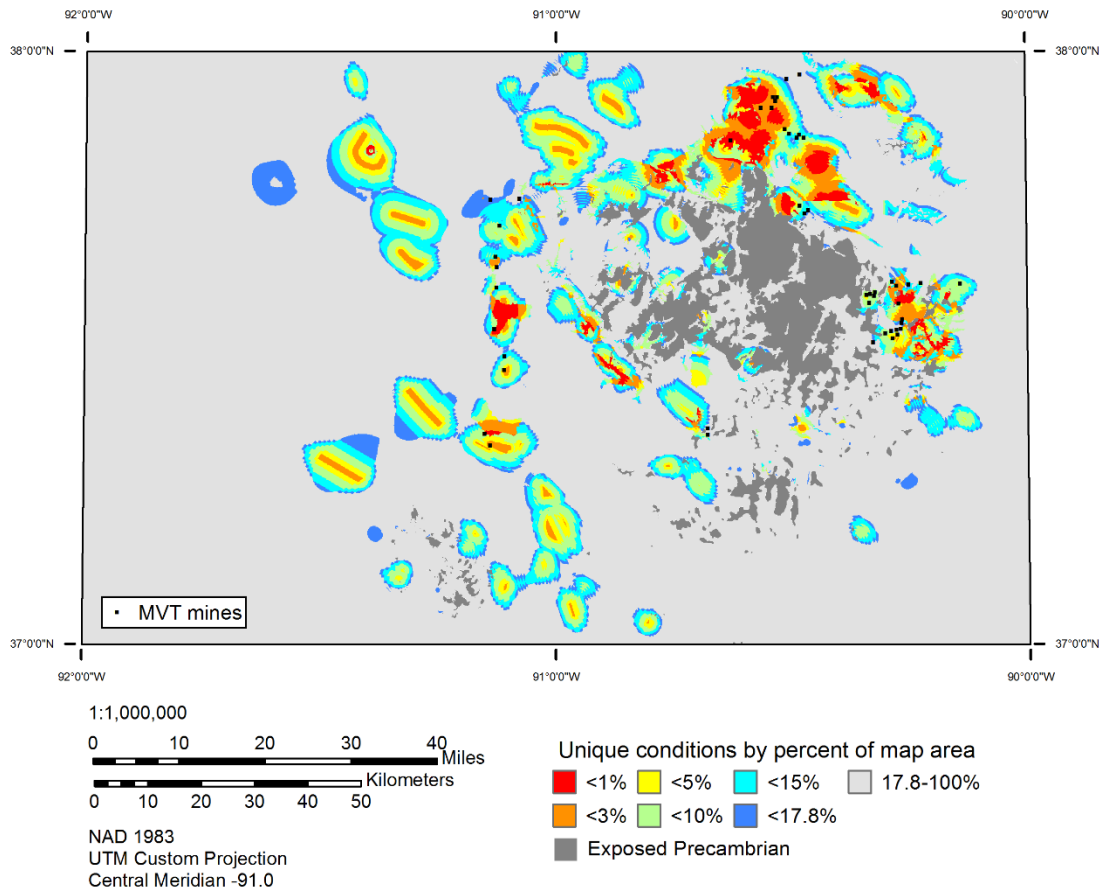
Figure 4.13: Fuzzy Model 111 for Southeast Missouri.
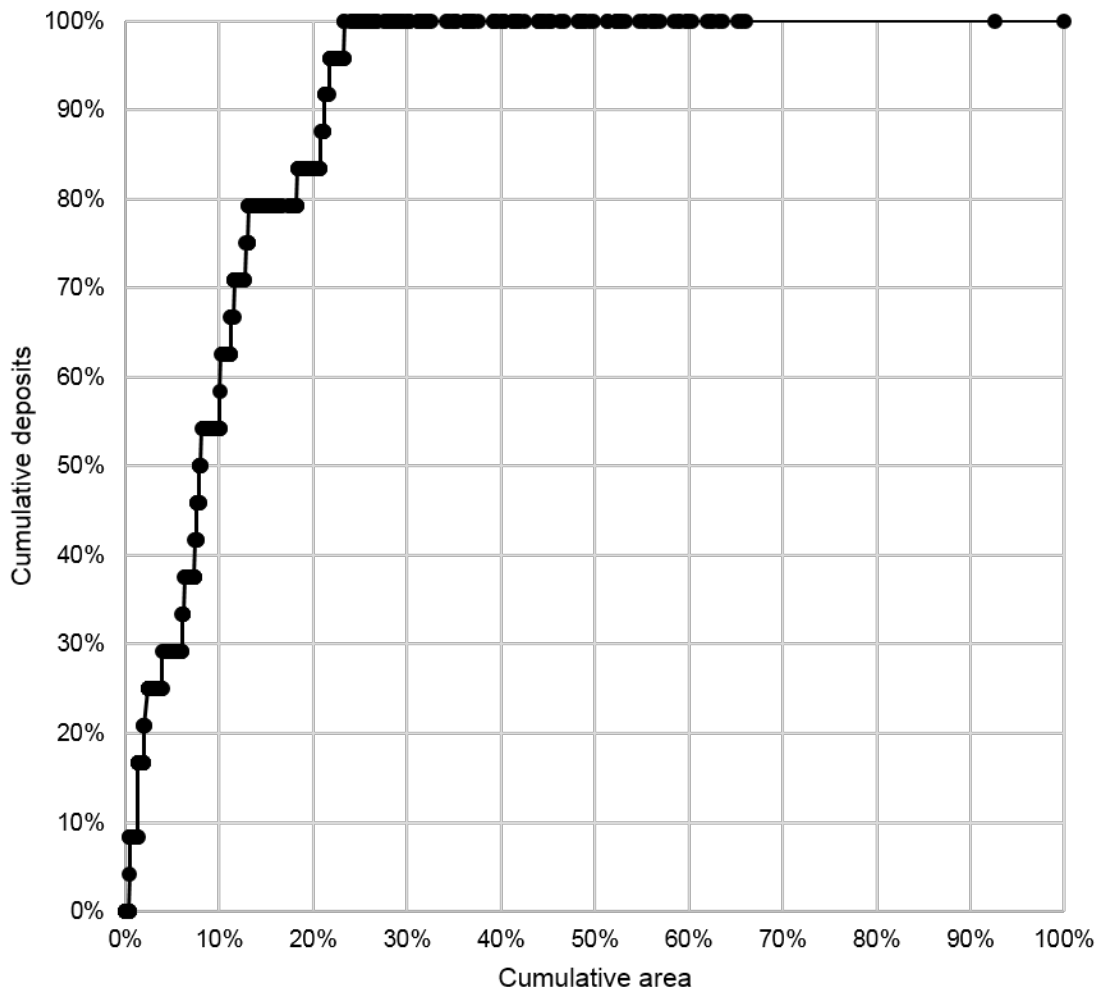
Figure 4.14: Fuzzy Model 111 prediction rate curve.
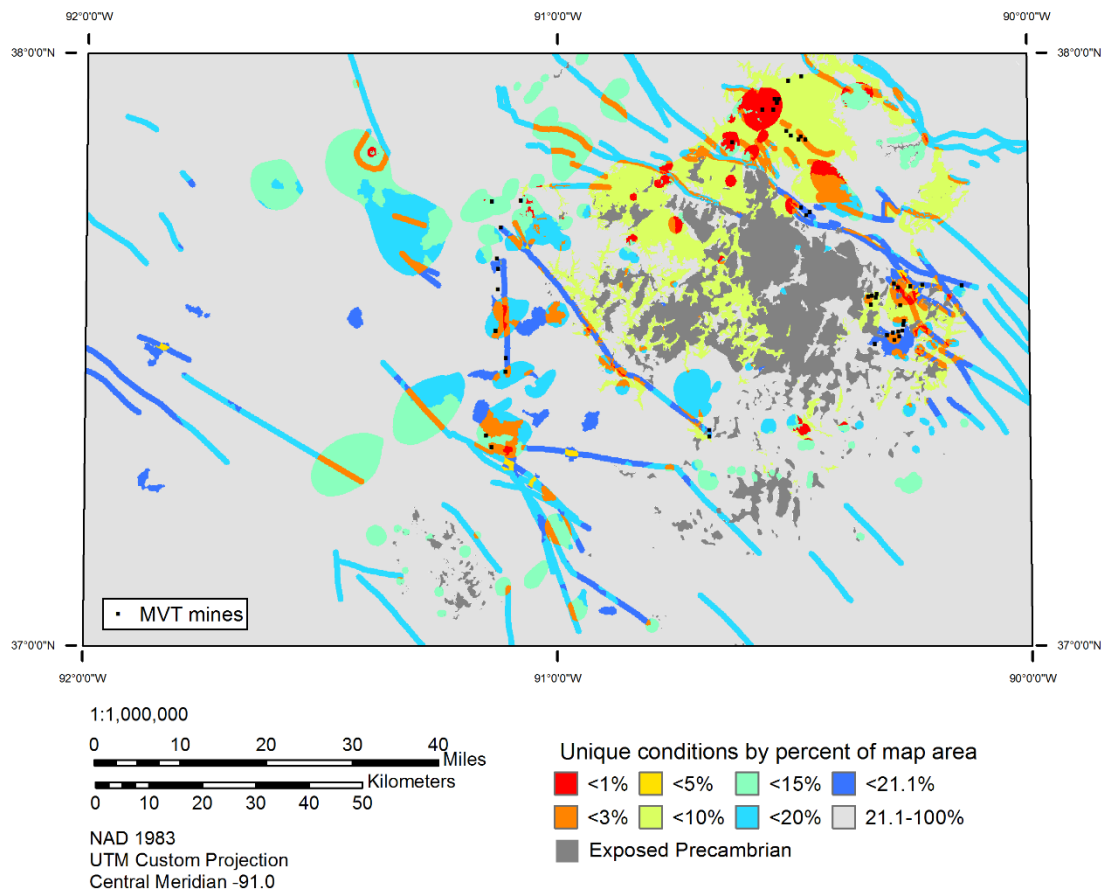
Figure 4.15: Binary Model 112 for Southeast Missouri.
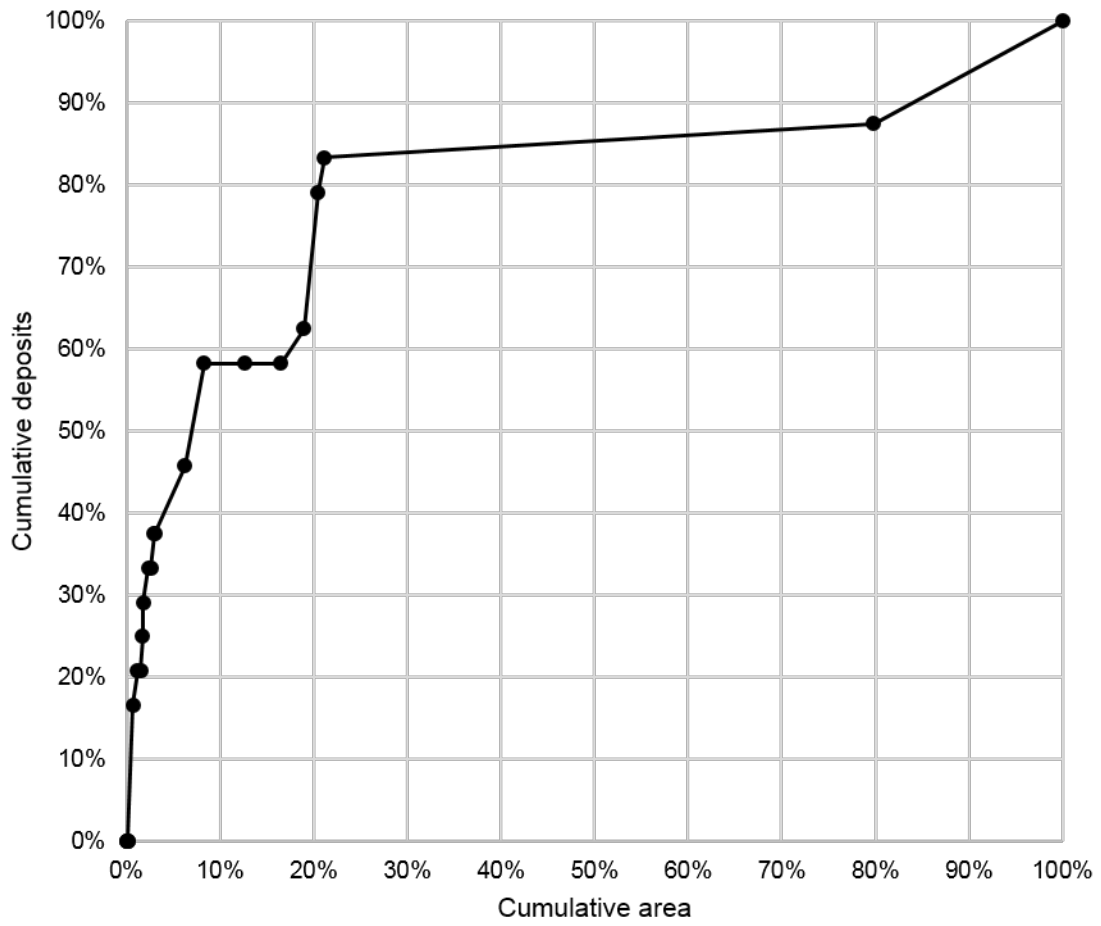
Figure 4.16: Binary Model 112 prediction rate curve.
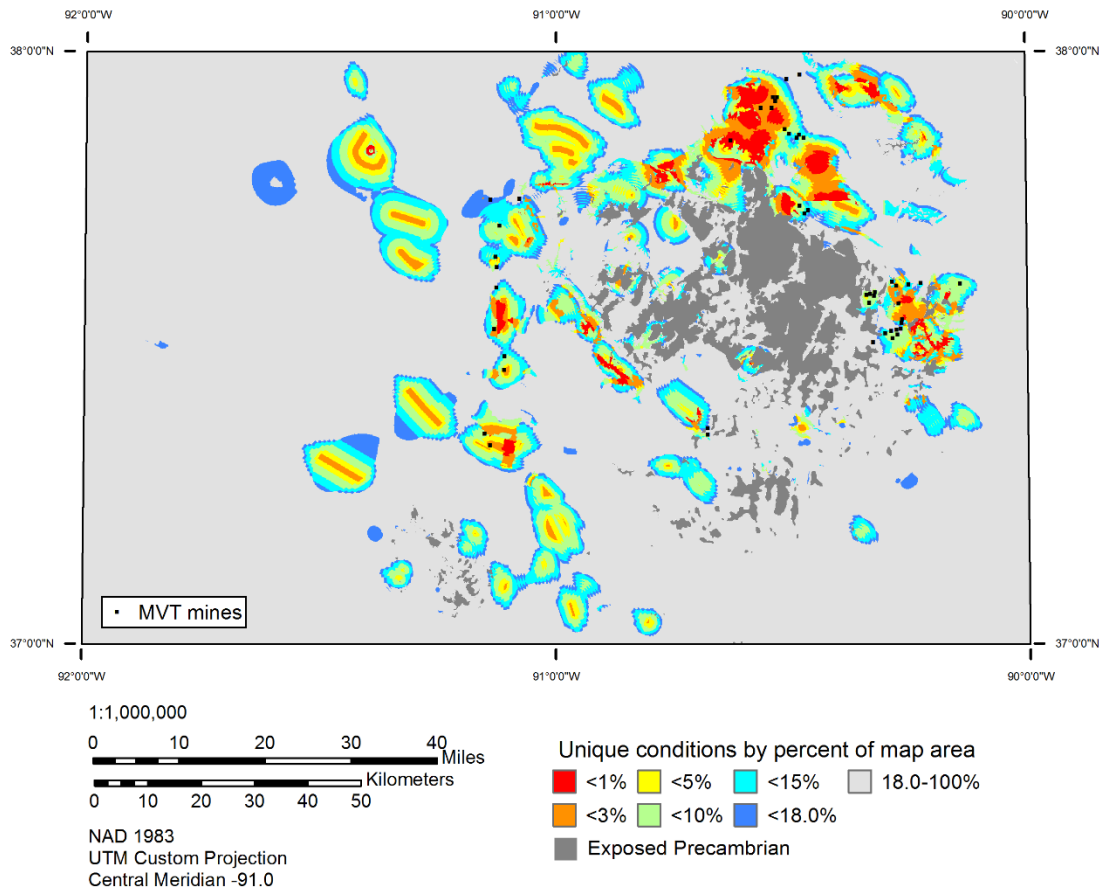
Figure 4.17: Fuzzy Model 112 for Southeast Missouri.
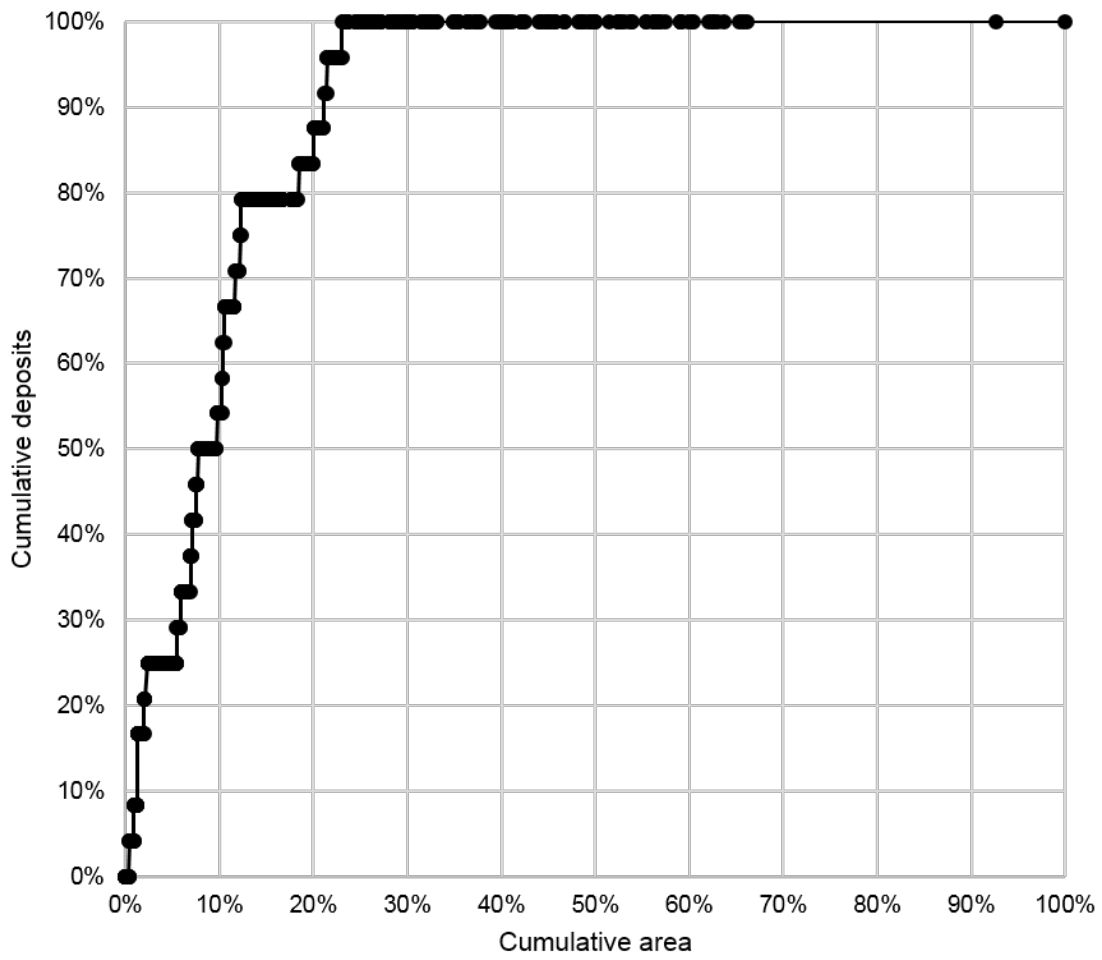
Figure 4.18: Fuzzy Model 112 prediction rate curve.
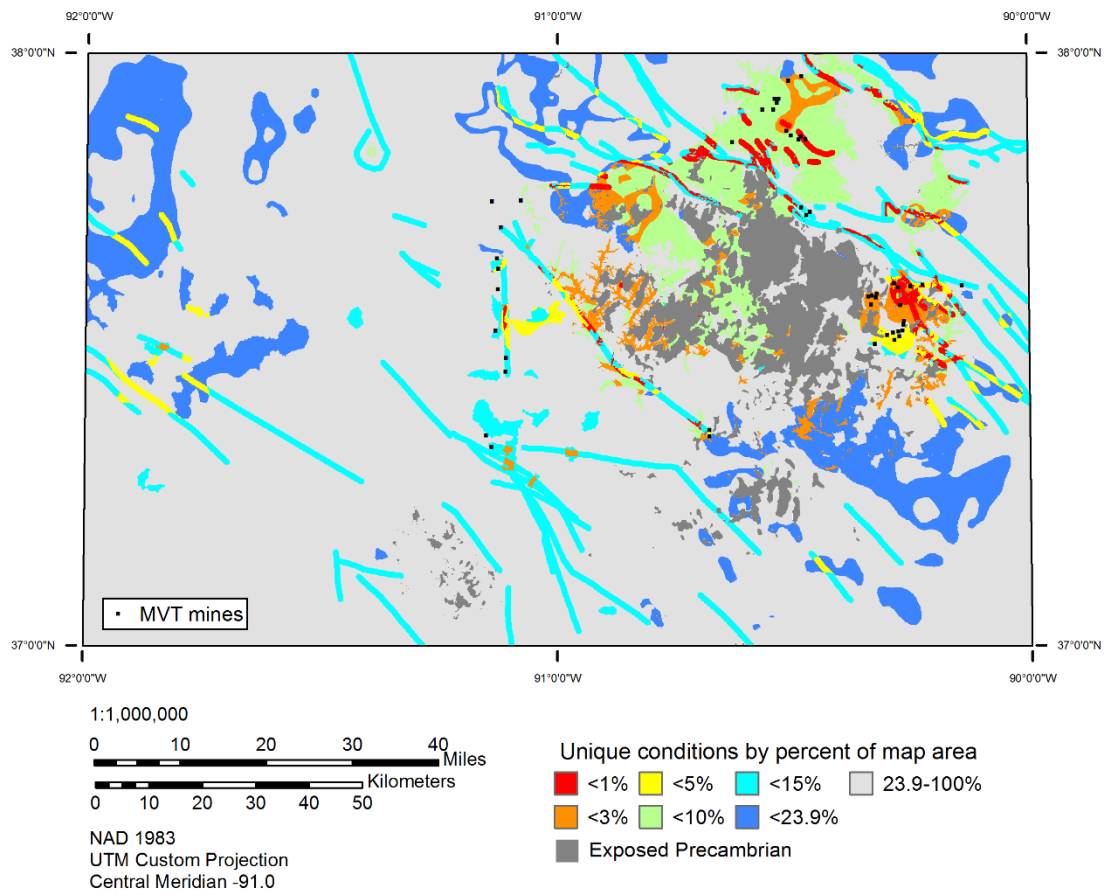
Figure 4.19: Binary Model 113 for Southeast Missouri.
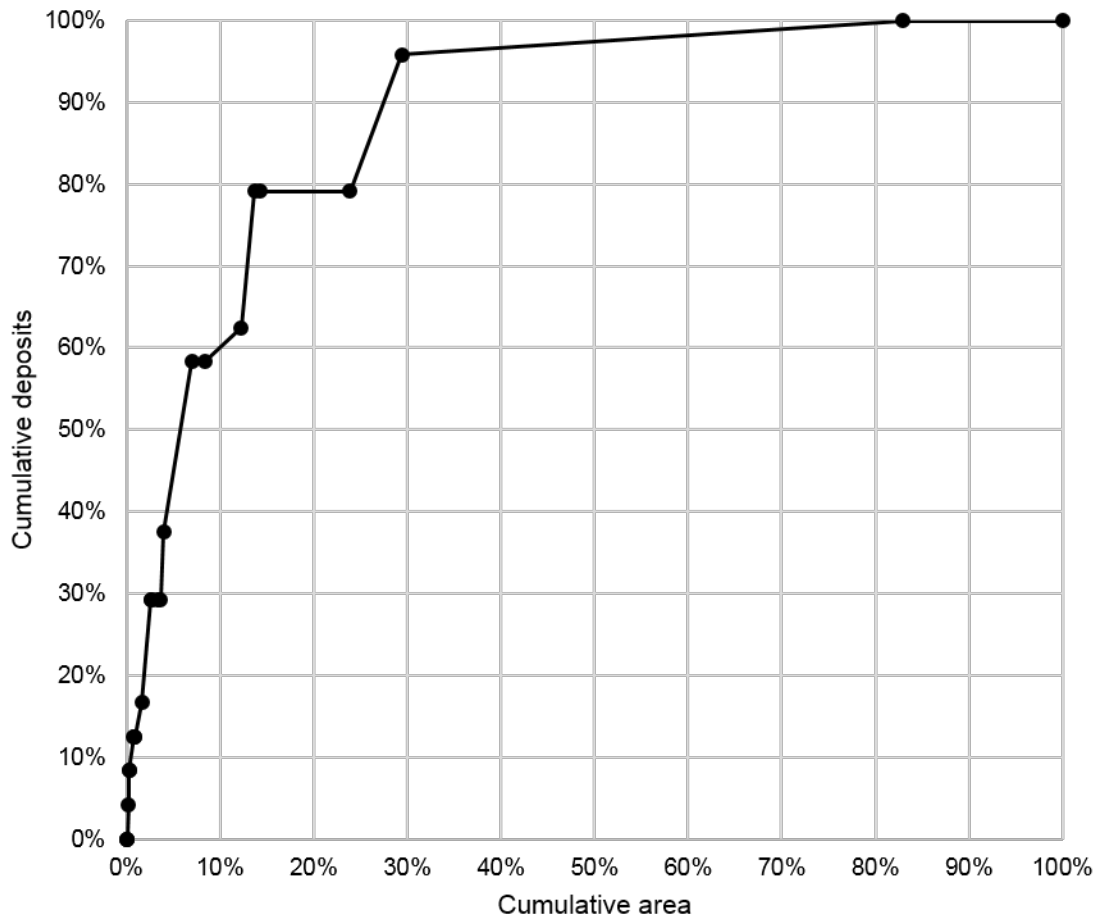
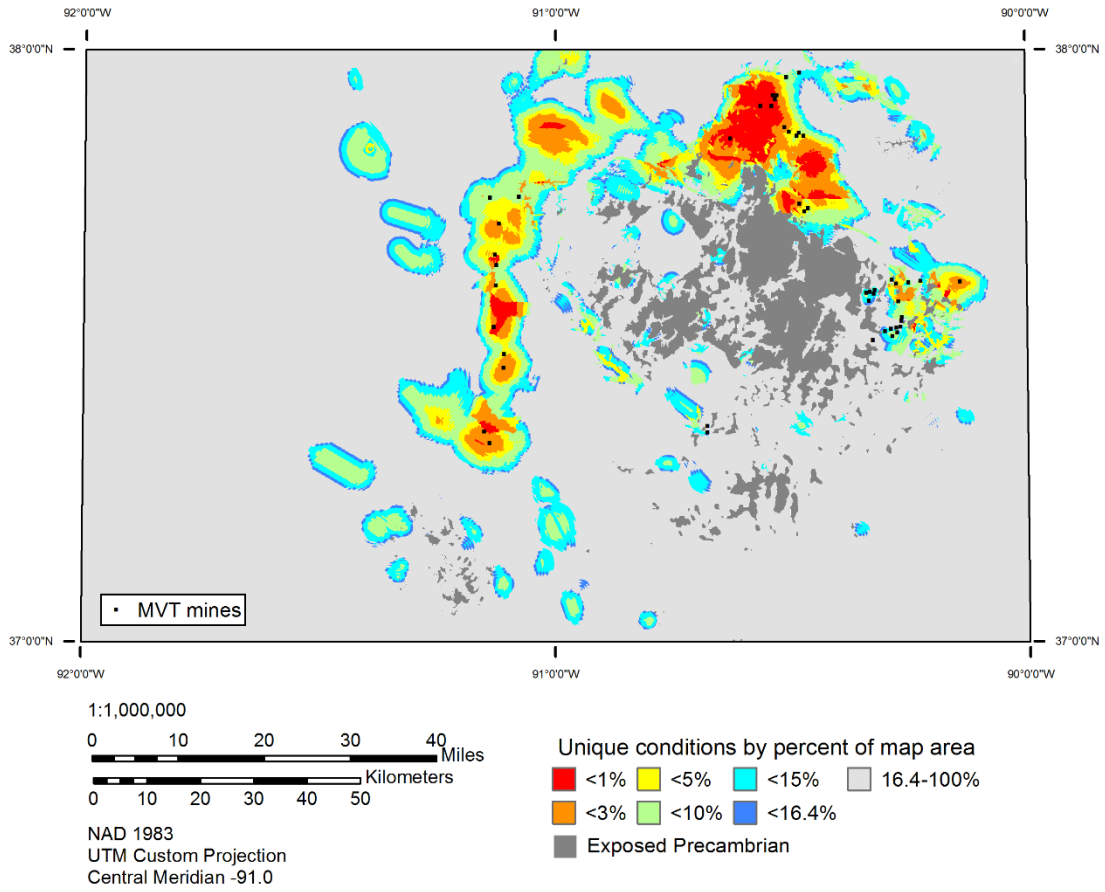Figure 4.20: Binary Model 113 prediction rate curve.

143
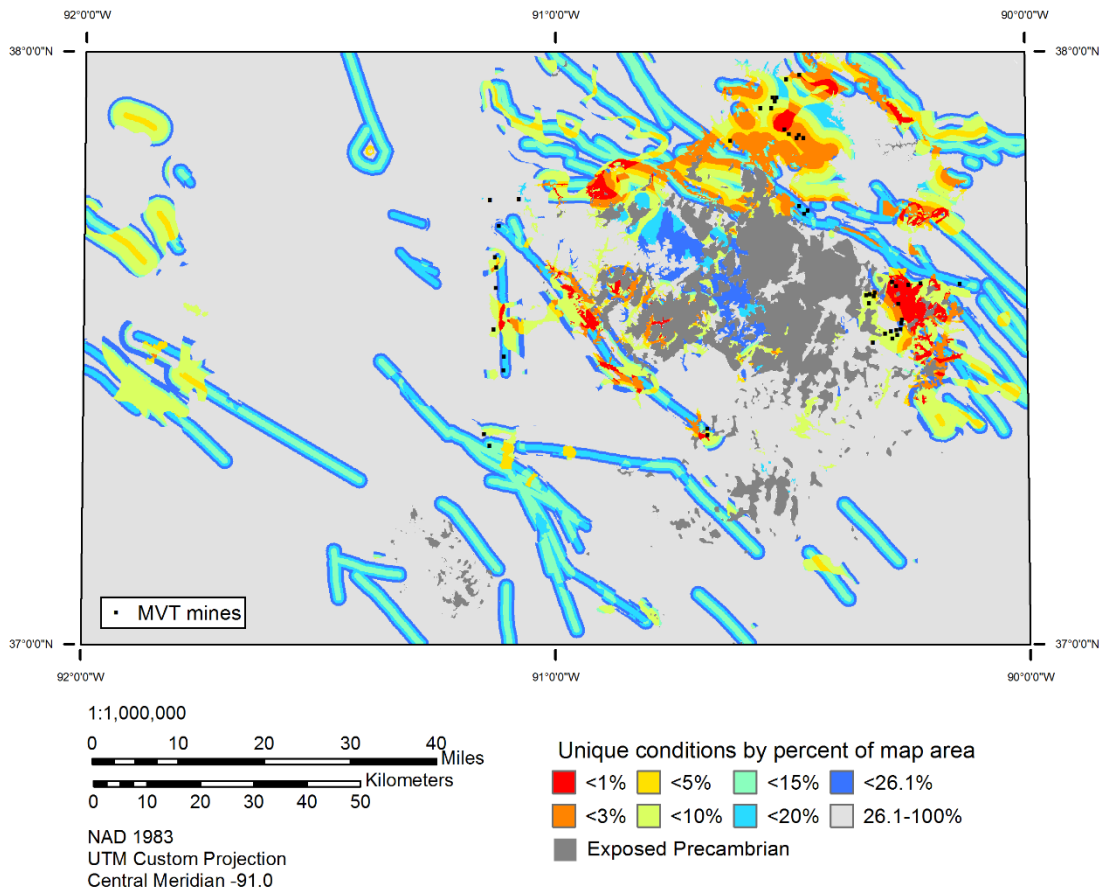
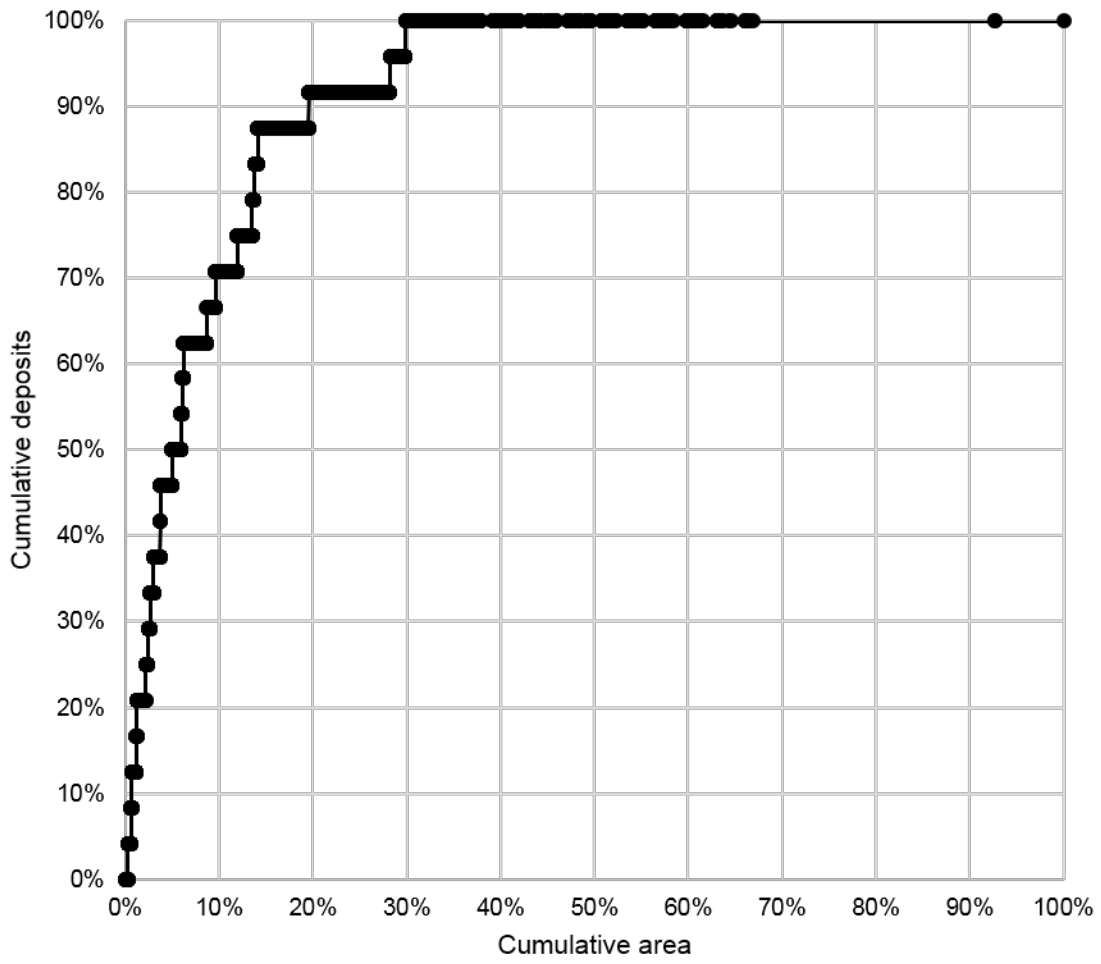Figure 4.21: Fuzzy Model 113 for Southeast Missouri.
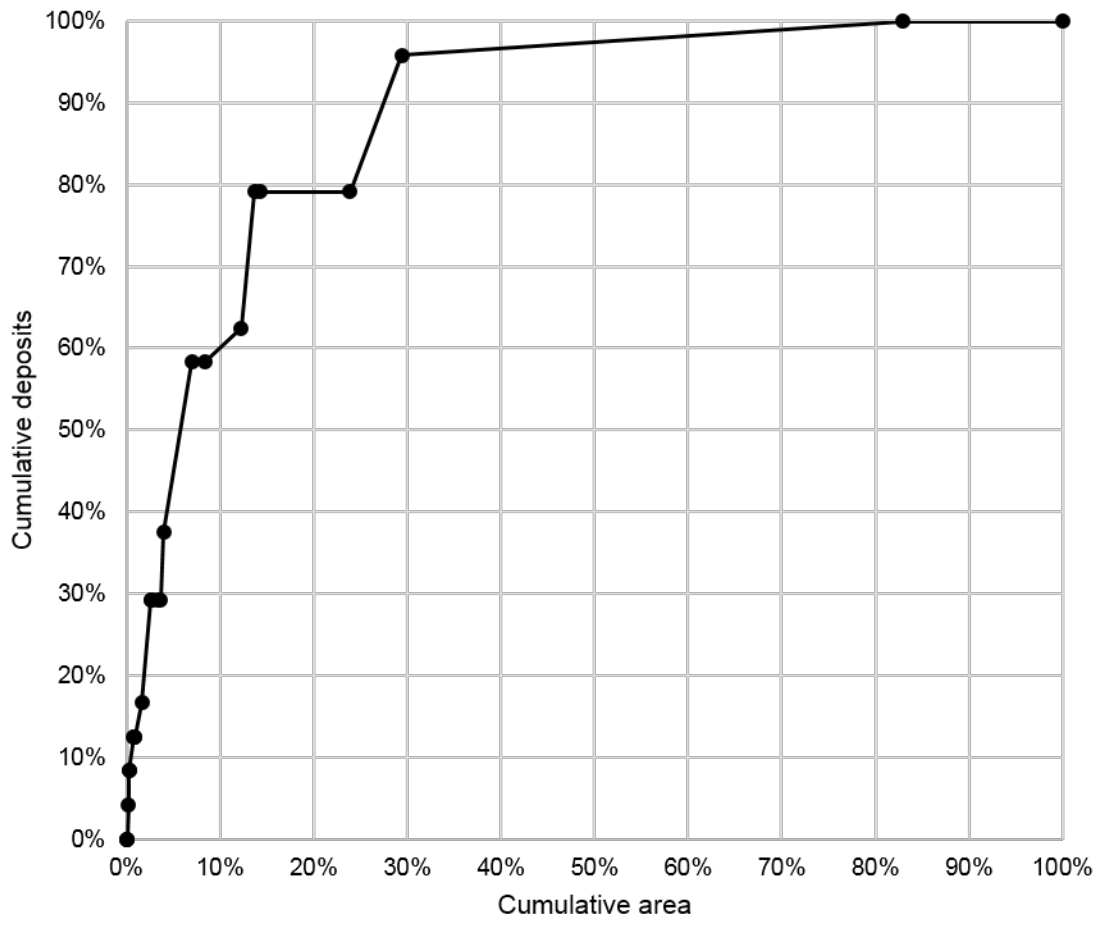
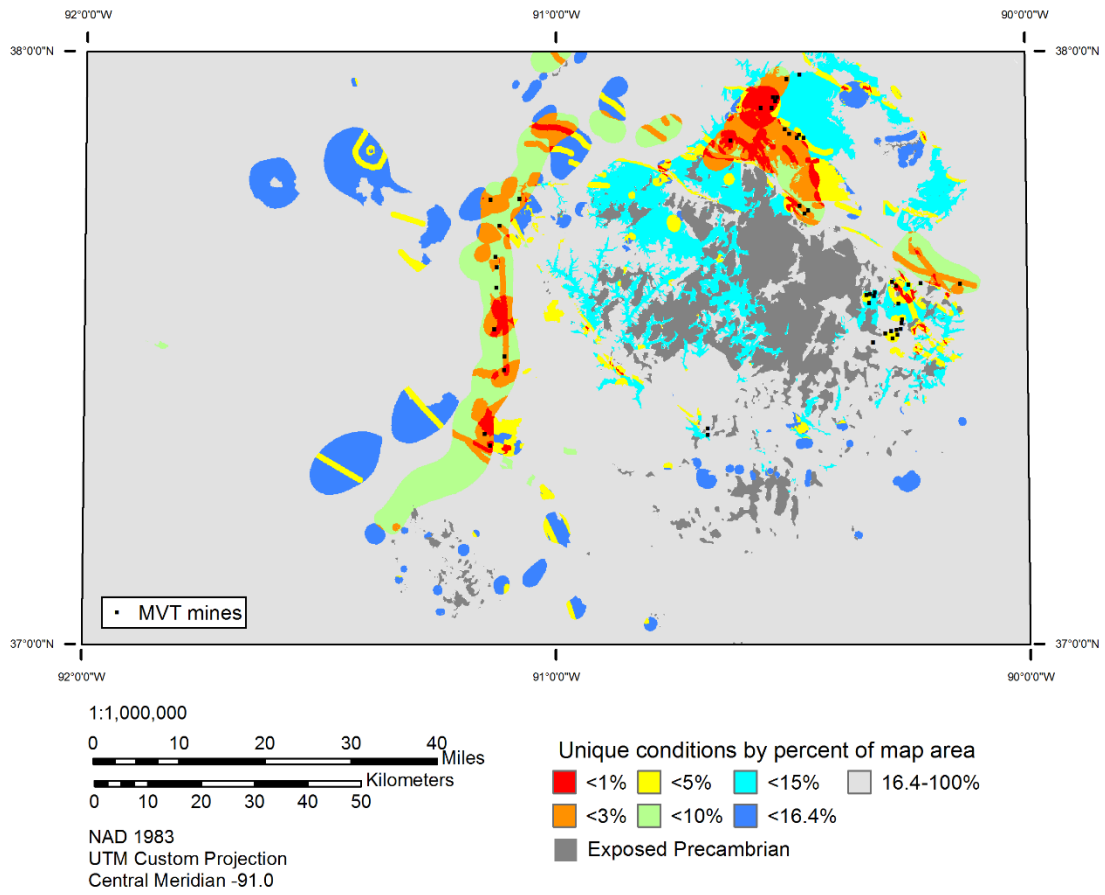Figure 4.22: Fuzzy Model 113 prediction rate curve.
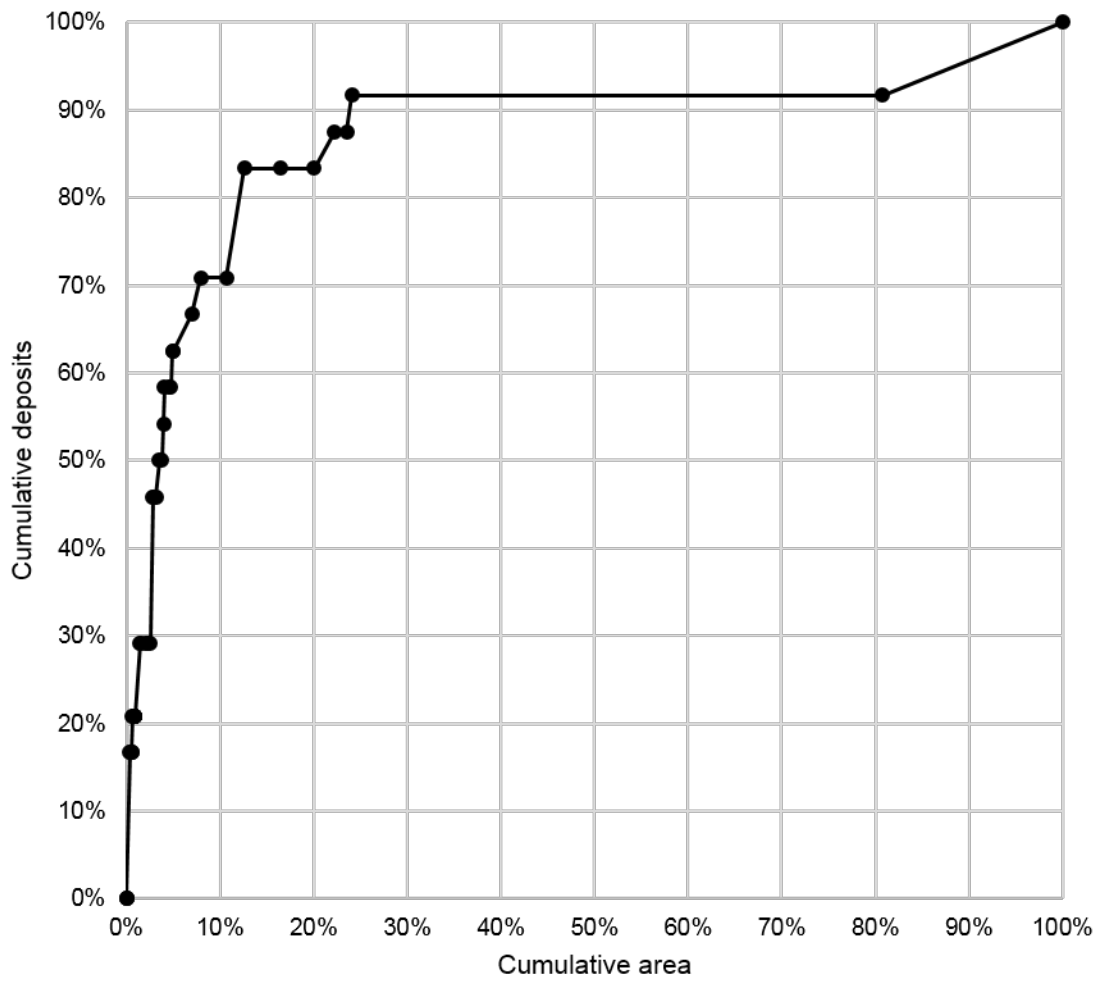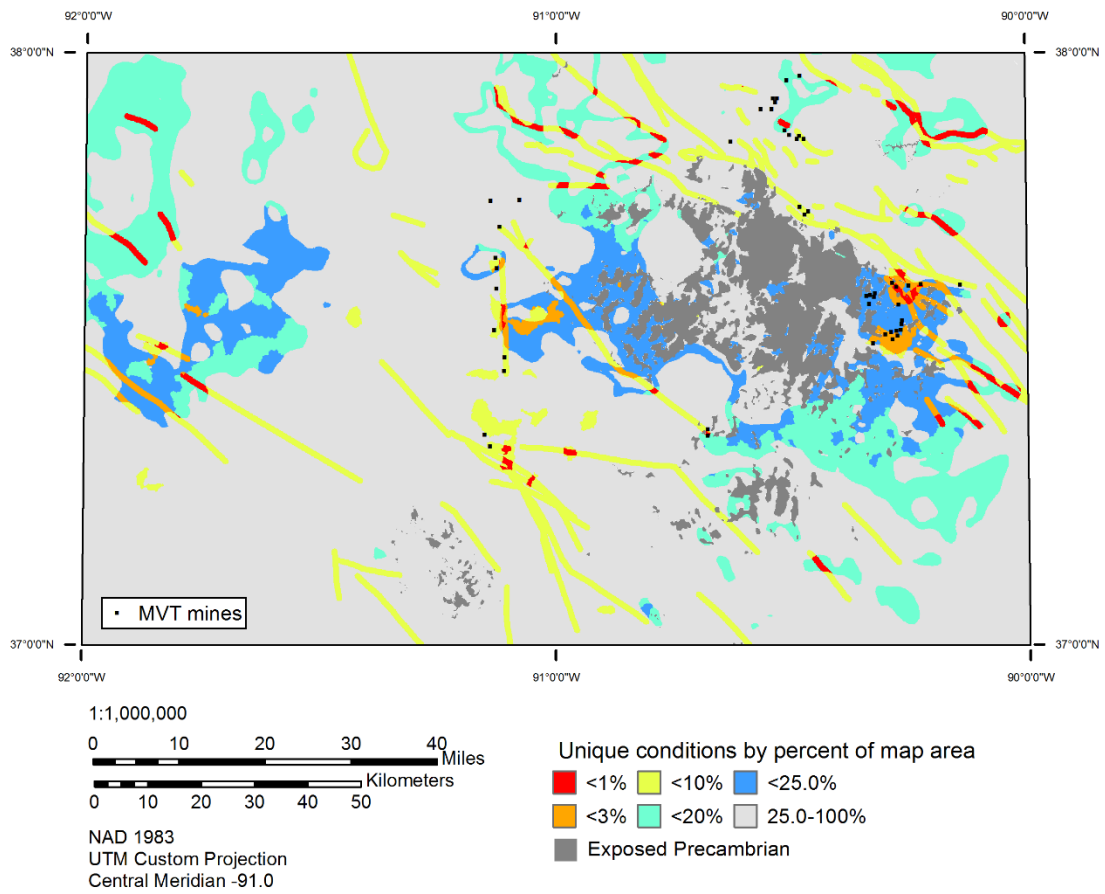
Figure 4.23: Binary Model 114 for Southeast Missouri.
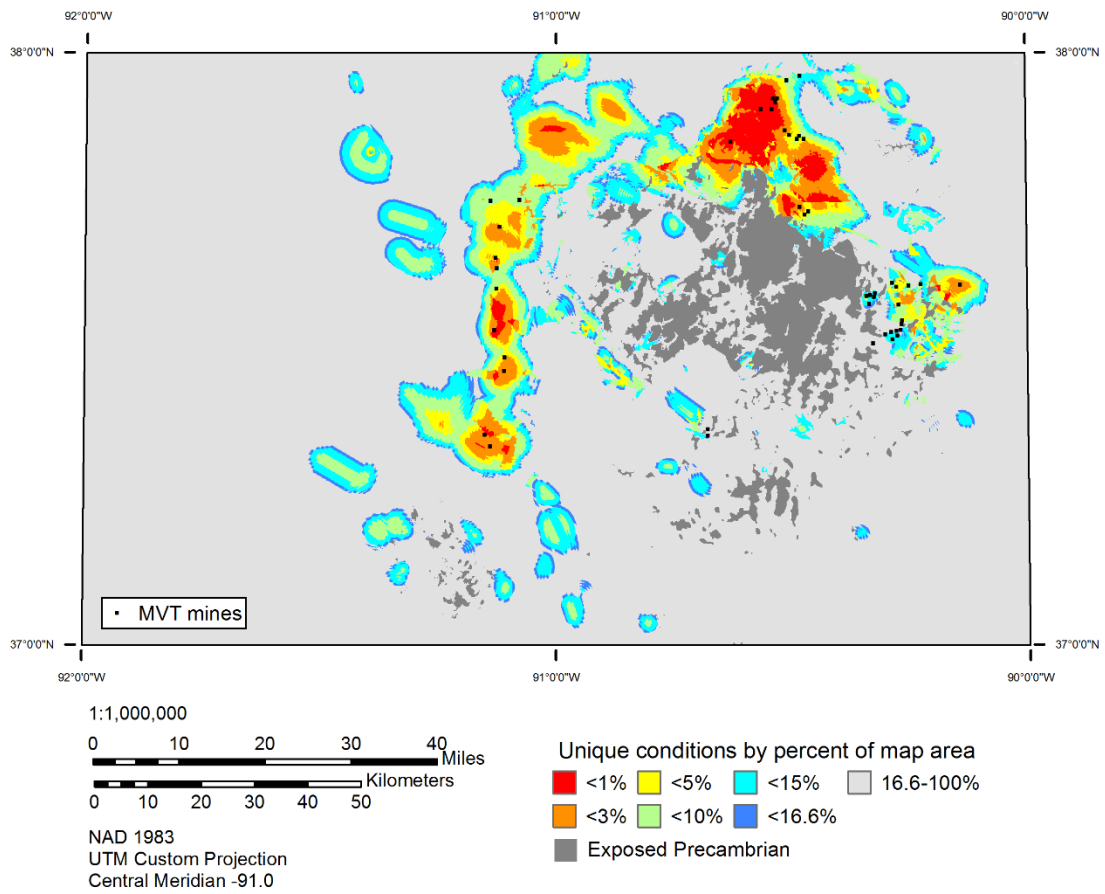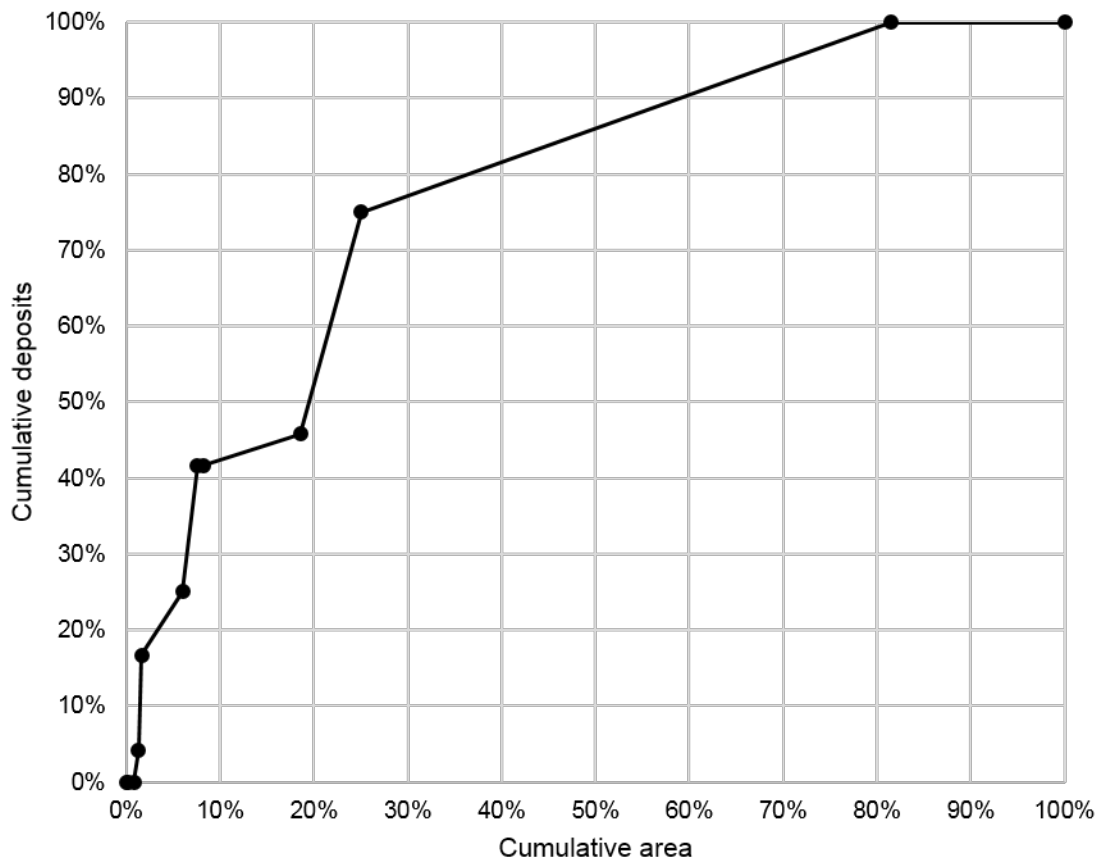
Figure 4.24: Binary Model 114 prediction rate curve.
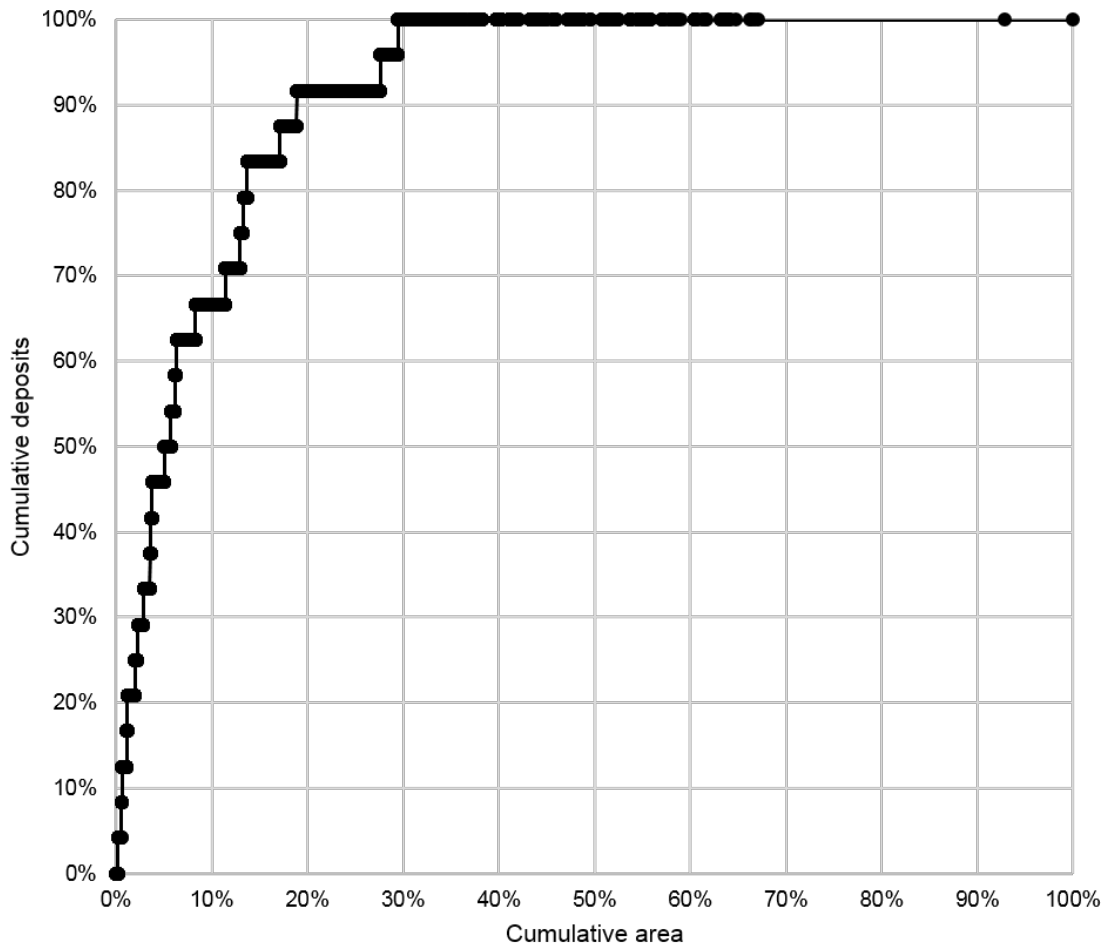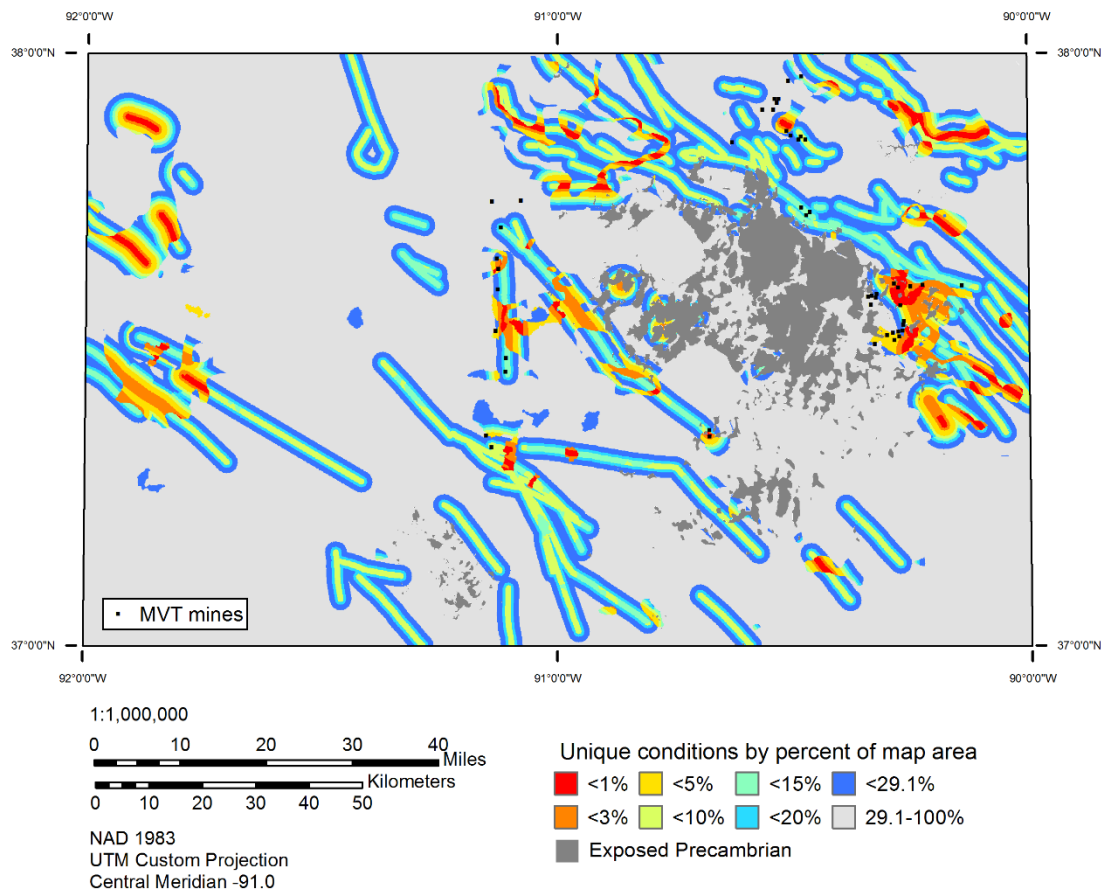
Figure 4.25: Fuzzy Model 114 for Southeast Missouri.
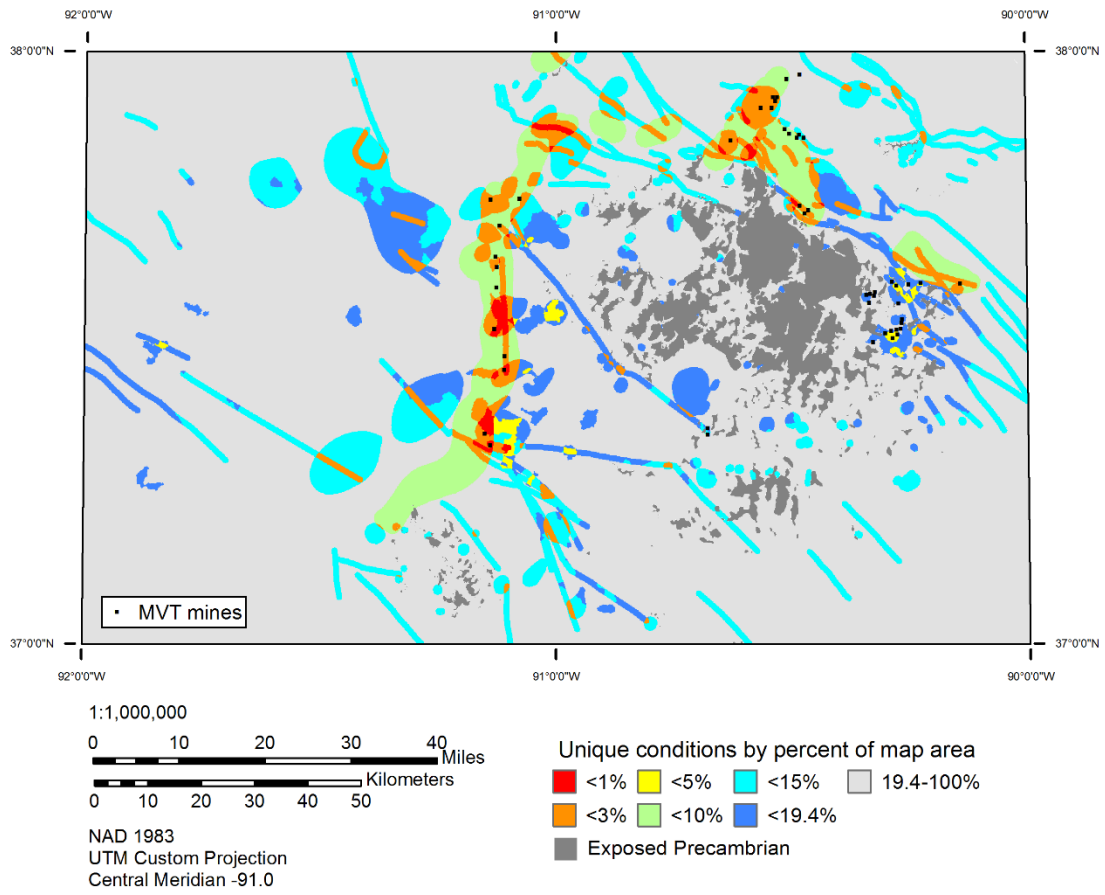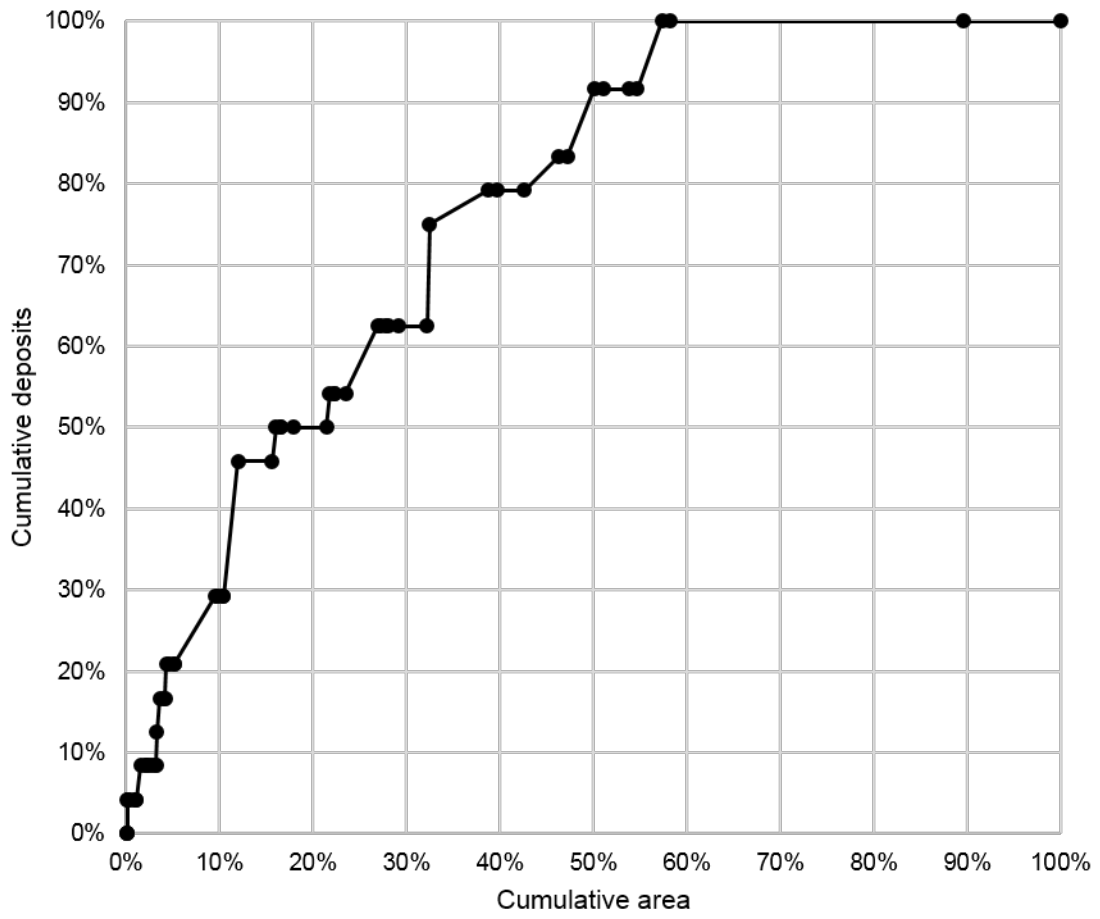
Figure 4.26: Fuzzy Model 114 prediction rate curve.

data while excluding surface geology for the reason discussed earlier. These models have efficiencies of 78.1% and 77.3% respectively. Additionally, BM114 has the highest CI ratio of all models considered at 93.6% and is the only model where CI is not violated. The downside is that these models failed to predict more validation deposits than any other with BM114 not predicting 6 of 24 and FM114 not predicting 9 of 24.

Binary Model 115 (BM115) (Figures 4.27 and 4.28) is the final category II model considered. This model incorporates weights for NW-SE fault proximity, presence of Elvins Group and Bonneterre Dolomite, Co anomalies, proximity to basement highs, and magnetics. Interestingly, this model has an efficiency score of 88.2%, which is only slightly lower than the similar model BM113 and moderately higher than BM112 which consider either proximity to basement highs, or magnetics, but not both. The CI ratio for BM115 is also lower than the ratios for these other two models, which suggests that there is only a slight advantage to including both proximity to basement highs and magnetics in the same model rather than magnetics alone.

CENTRAL TEXAS MODELS

The Central Texas models are generated using the same types of data as Southeast Missouri models FM112 and BM113. These two models had the highest efficiency scores among similar models that considered either proximity to basement highs or magnetics, although they also failed to predict 20.8% of the validation deposits. The results from binary and fuzzy model sets 101 to 102 and 111 to 112 indicate that there is a negligible difference in considering geochemical anomaly data from Pb or Zn anomalies above the UIF threshold, or Co anomalies defined as greater than the median + 2MAD in the Southeast Missouri study area. Co anomalies are used for all Central Texas models because there are more areas that meet the Co anomaly criteria than the Pb or Zn criteria.

150
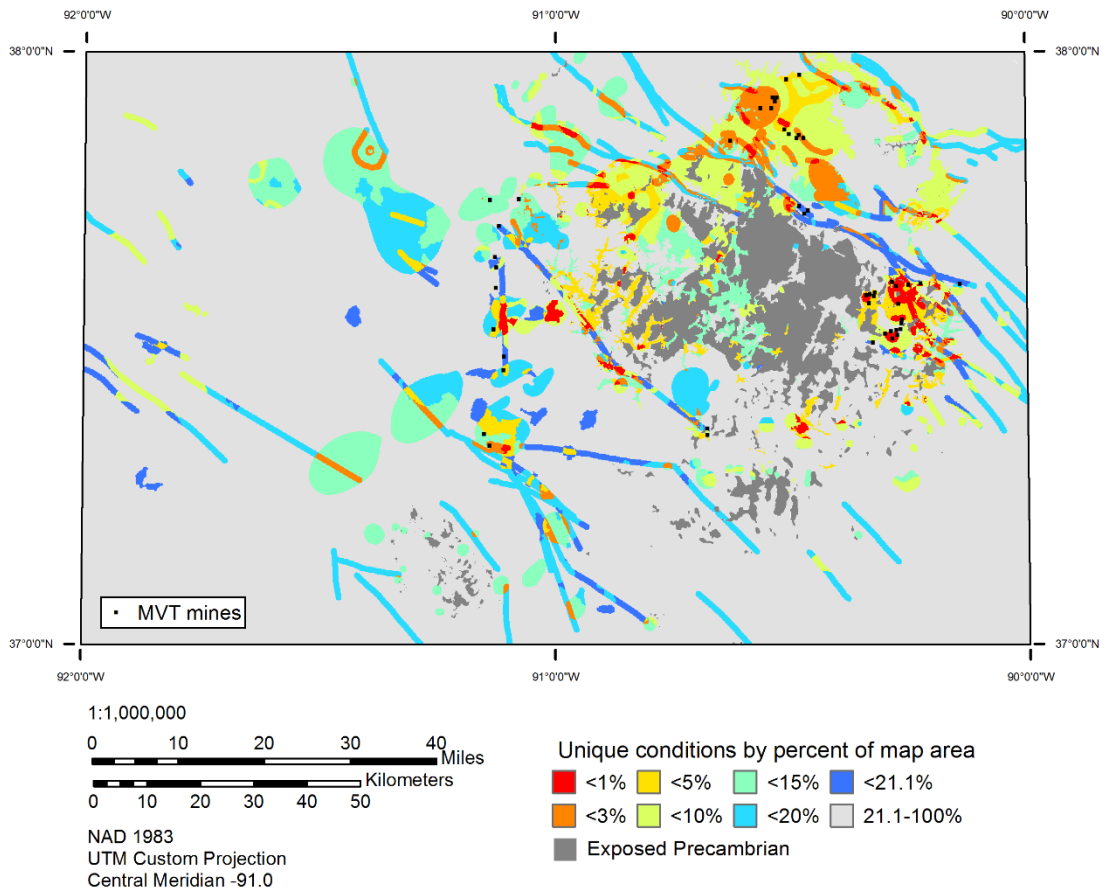
Figure 4.27: Binary Model 115 for Southeast Missouri.
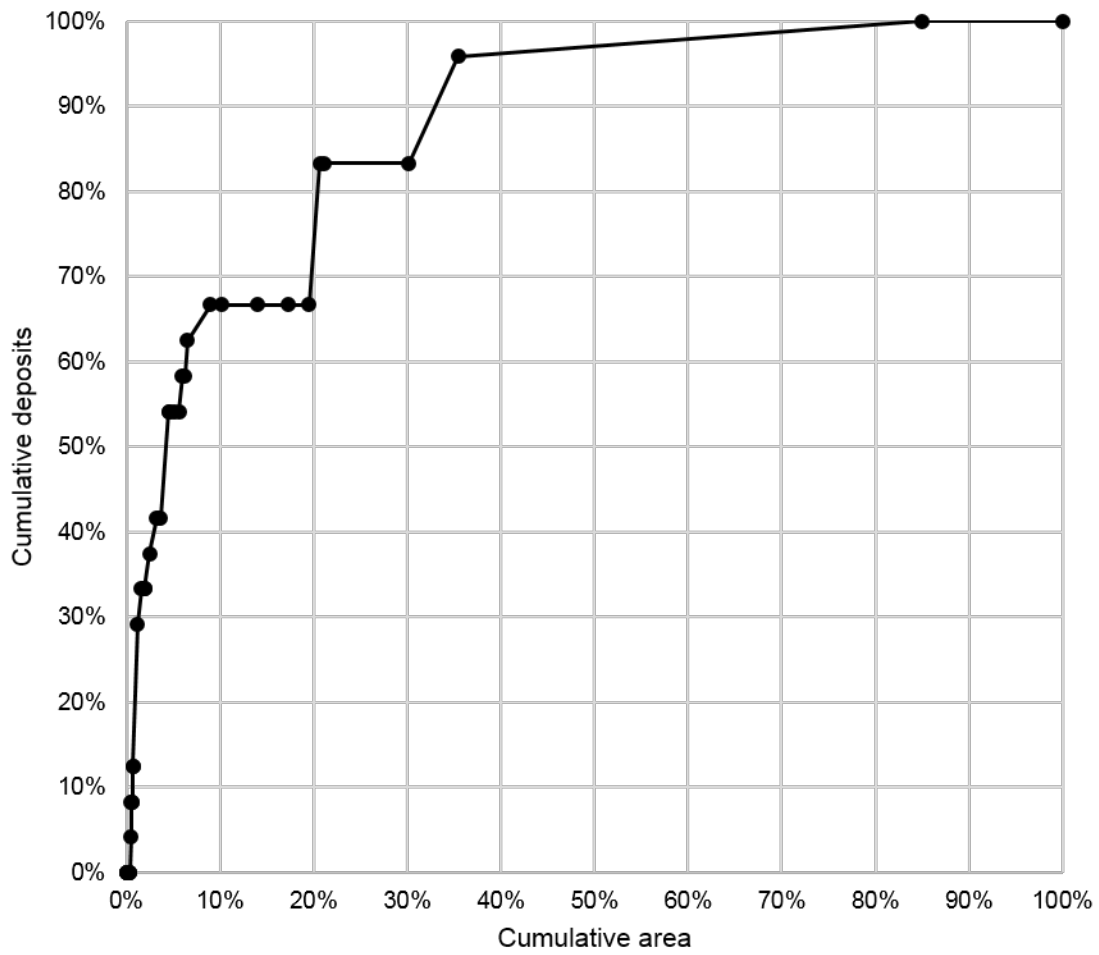
Figure 4.28: Binary Model 115 prediction rate curve.

The three Central Texas models include proximity to faults, presence of Co anomalies, and either proximity to basement highs (wherever available) or magnetics data (everywhere without basement-high information). The difference in each Texas model is the type of surficial geology. The eight near-surface MVT occurrences are used to calculate an efficiency score for each model. However, because the weights used in the Central Texas model are derived from Southeast Missouri, the resulting values for the mineral potential maps should be interpreted as "suitability scores" rather than as probabilities. Additionally, because the model output is not a posterior probability, the results can not be used to determine CI ratios or non-predicted deposits as was done for Southeast Missouri.

Texas Model 111 (TM111) (Figures 4.29 and 4.30) incorporates each of the data types mentioned above, and areas where any Paleozoic limestone unit is mapped at the surface on the Geologic Atlas of Texas 1:250,000 sheets. The efficiency score for TM111 is 90.27%, and all eight MVT occurrences fall within the upper 34.9% of the model area.

Texas Model 112 (TM112) (Figures 4.31 and 4.32) considers the presence of the Cap Mountain Limestone member of the Riley Formation instead of all Paleozoic limestones. The result is an increase in model efficiency to 94.5%. All eight MVT occurrences fall within the upper 25.3% of the model area.

The final Central Texas Model, Texas Model 113 (TM113) (Figures 4.33 and 4.34), does not consider any surficial geology information. The model has a lower efficiency score than either of the other two Central Texas models at 76.9%. The eight MVT occurrences are within the top 86.7% of the model area.

COMPARISON OF MODEL RESULTS WITH SEMI-QUANTITATIVE GEOCHEMISTRY DATA

Smith et al. (1981) reported geochemistry data measured from insoluble residues collected from 18 wells throughout the Llano region. These wells were matched to wells
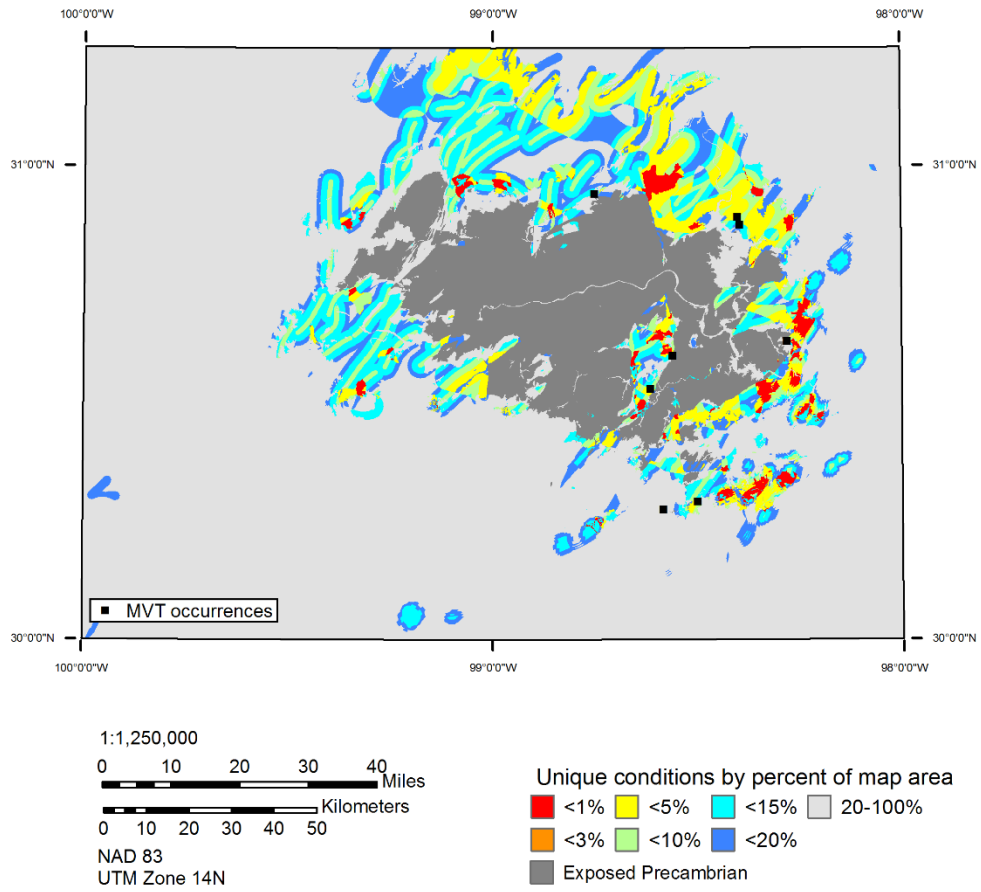
Figure 4.29: Texas Model 111. Note the high model values southwest of the exposed Precambrian core.
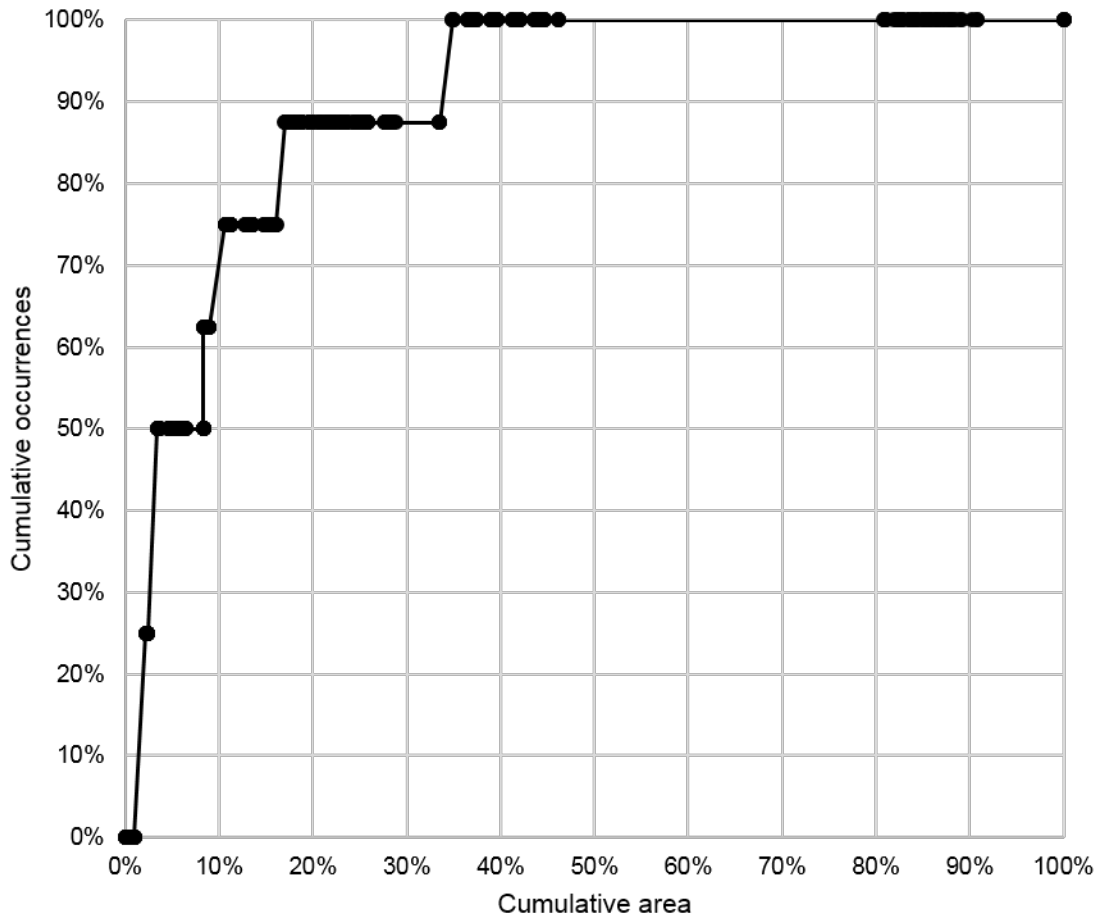
Figure 4.30: Texas Model 111 prediction rate curve.
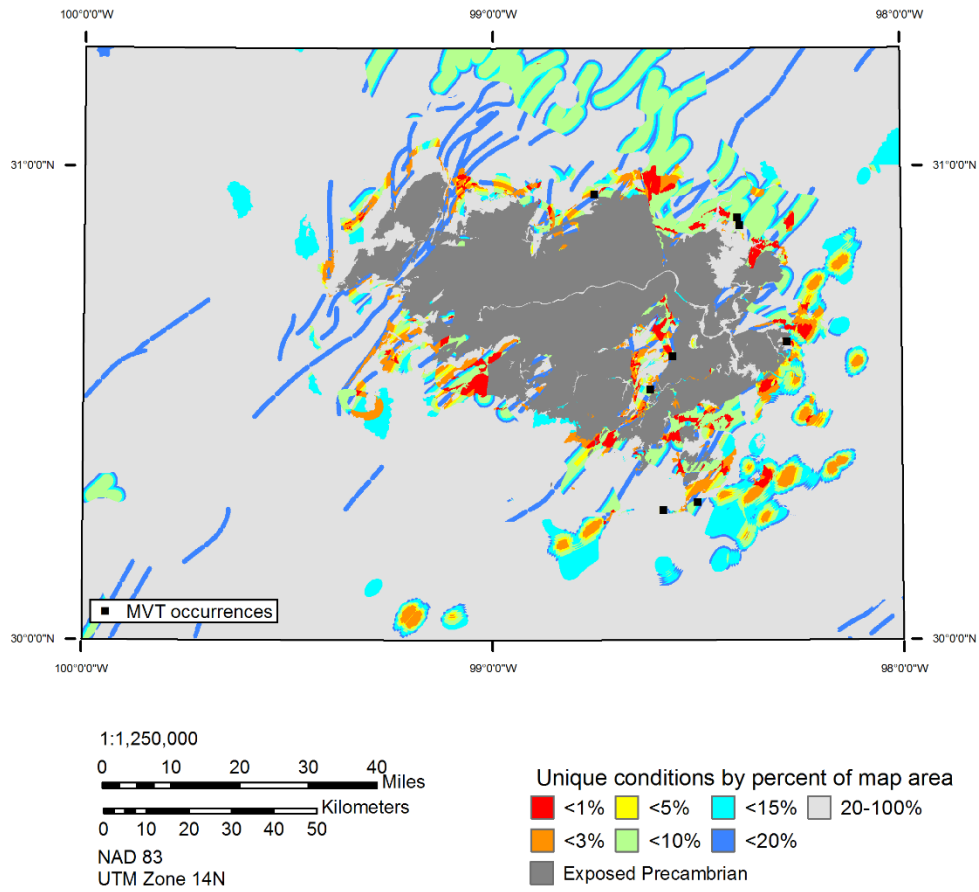
Figure 4.31: Texas Model 112. Note the high model values to the south and southwest of the exposed Precambrian core.
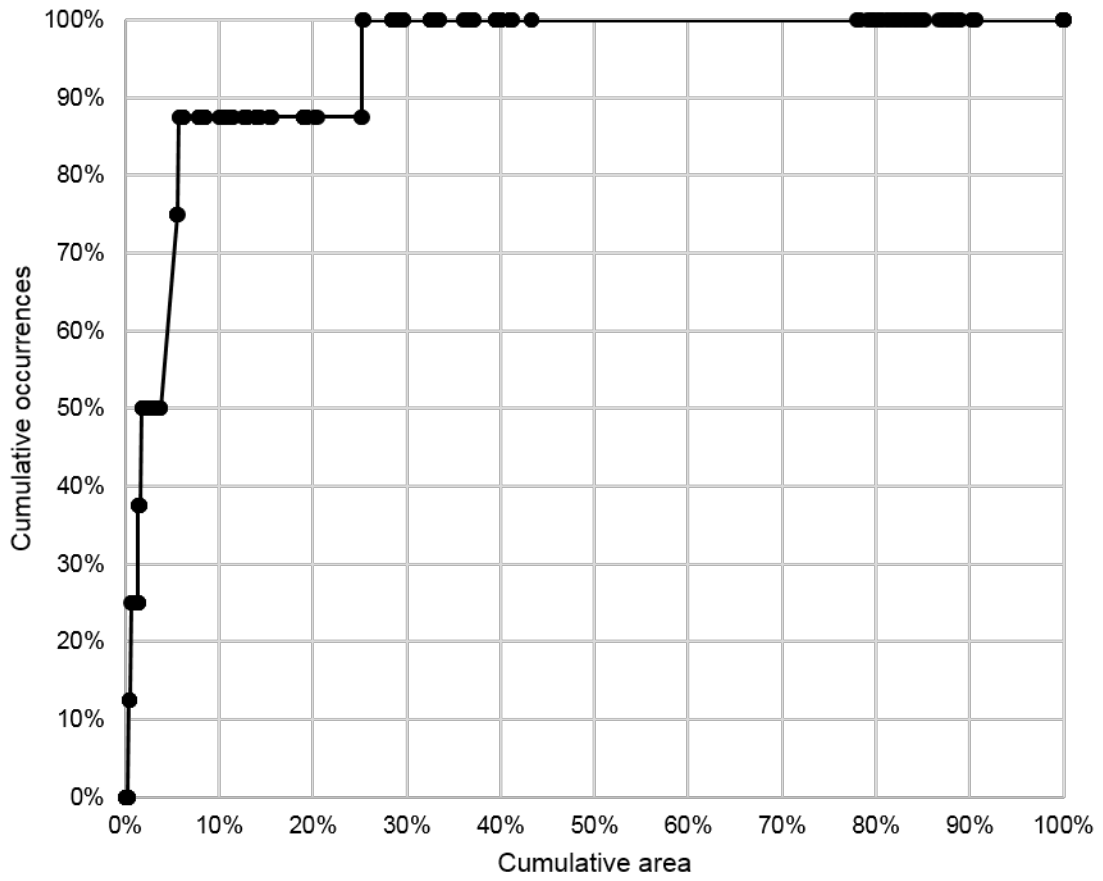
Figure 4.32: Texas Model 112 prediction rate curve.
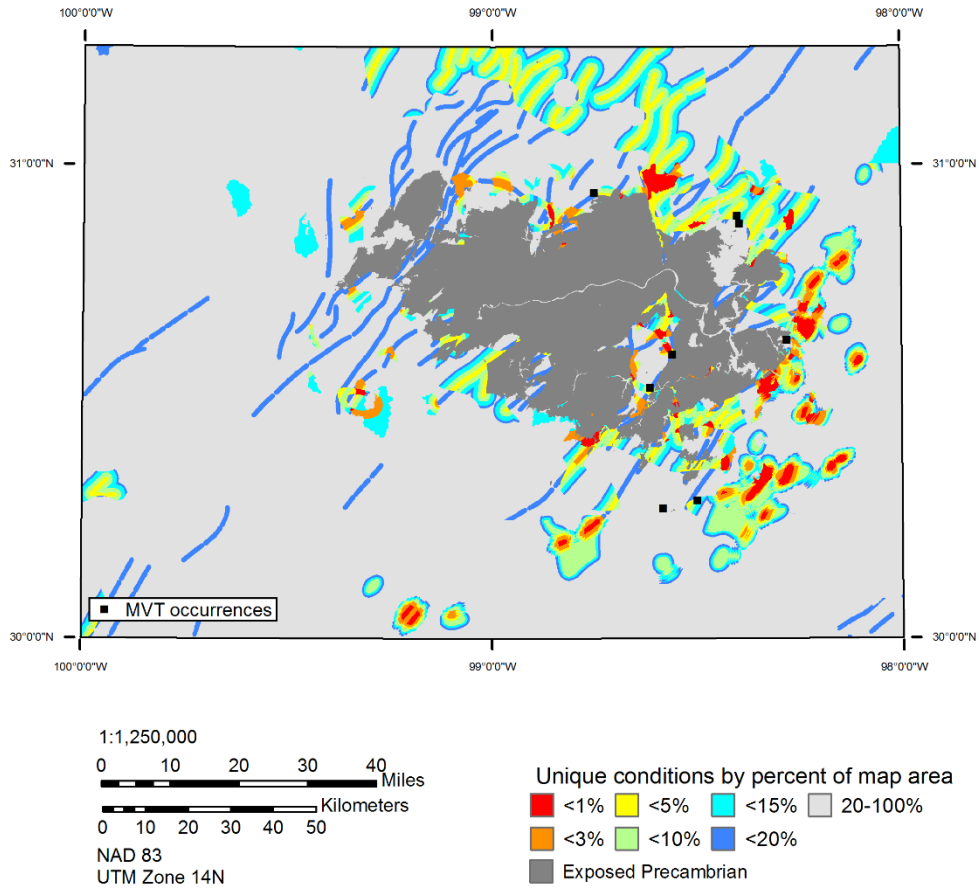
Figure 4.33: Texas Model 113. Note the high model values to the south and southwest of the exposed Precambrian core.
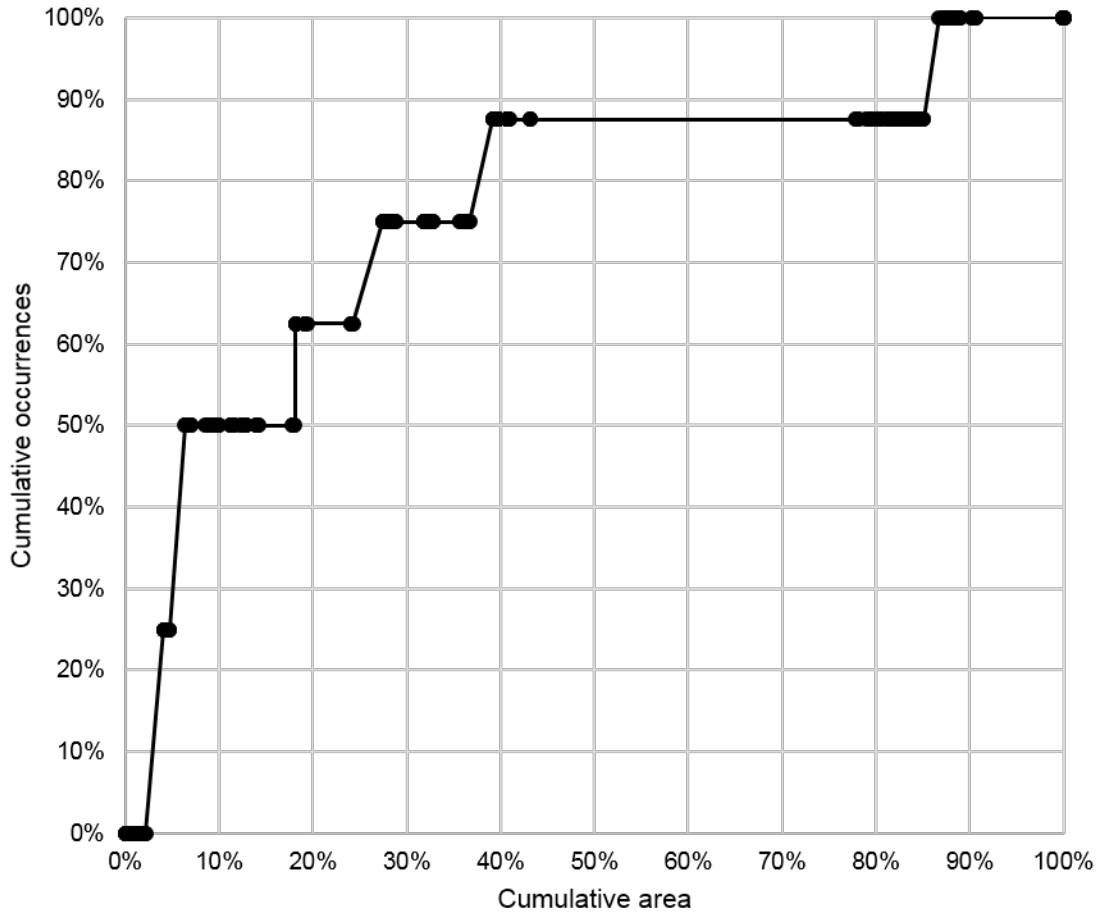
Figure 4.34: Texas Model 113 prediction rate curve.

in the Groundwater Database of Texas (GWDB) attribute table based on owner and driller information to determine the well locations. No match for the Fredericksburg Water Well #9 Wallendorf well was found in the GWDB, so this well was excluded. Additionally, the Magnolia #1, Below well is located in Kendall County south of the study area. The location of the remaining 16 wells are shown in Figure 4.35.

Smith et al. (1981) described the analytical method used to determine measurements from sulfide concentrates using a direct-current arc emission spectrographic technique and noted that the results are semiquantitative. Additionally, many wells contain samples that appear to be either above or below the detection limits for the analysis. These data were processed using a weighted average over the sample interval. Samples with values greater than the upper detection limit were given a value equal to the upper detection limit, and samples lower than the lower detection limit were eliminated because the value of the lower detection limit is not reported.

To account for known and unknown location errors for these wells, each well was assigned the highest model value within 300 m (980 ft) of its plotted location. The four wells with the highest weighted average values for Pb are: Rowntree #1 Knott (4015 ppm), Murchison Ranch Water Well (2321 ppm), Hog Thief Bend 77-5 (1467 ppm), and Montgomery #1 Yates (885 ppm). The Rowntree #1 Knott well in western Gillespie County is unexpectedly associated with low likelihood values for all models (Tables 4.5-4.7). However, the other three wells are located within the top 10% of the model areas for all models, and within the top 5% of the model area for the two best performing models (TM111 and TM112) (Figures 4.36-4.38).
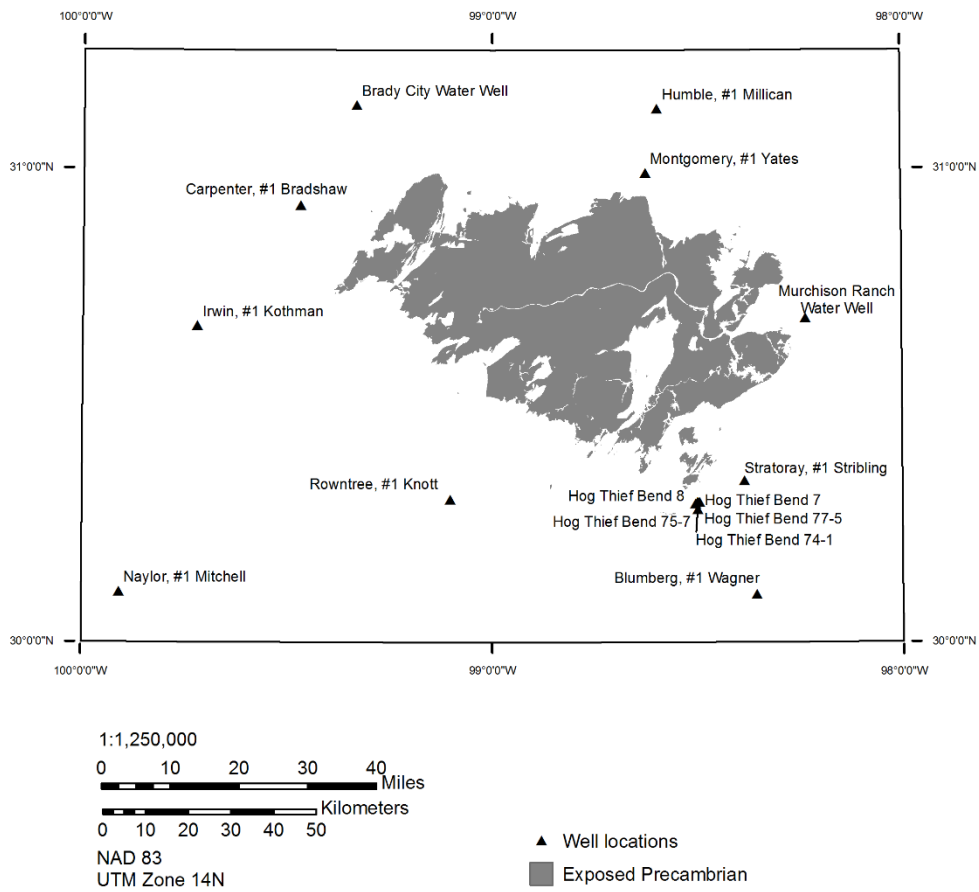
Figure 4.35: Location of wells from which geochemistry data were collected (Smith et al., 1981). These data were used to validate the performance of Central Texas models.

Well name	TM111	Pb	Zn	Co	Cu	Ni
Montgomery, #1 Yates	7.3414E-04	885	1647	49	507	
Humble, #1 Millican	1.6831E-04	63	1038	51	933	
Murchison Ranch Water Well	1.4550E-04	2321	2600	43	238	
Hog Thief Bend 75-7	1.2620E-04	266		17	63	47
Hog Thief Bend 7	1.2620E-04	99		44	28	142
Hog Thief Bend 8	1.2620E-04	78	9357	25	44	30
Hog Thief Bend 77-5	9.4615E-05	1467	1233	29	49	
Hog Thief Bend 74-1	7.0938E-05	65	2787	37	59	77
Brady City Water Well	8.1960E-06	216	3641	56	294	
Stratoray, #1 Stribling	8.0930E-06	281	3746	31	175	56
Naylor, #1 Mitchell	4.4380E-06	249	491	50	623	
Carpenter, #1 Bradshaw	3.4540E-06	237	770	83	371	
Irwin, #1 Kothman	1.0510E-06	75	1625	60	540	
Rowntree, #1 Knott	9.9600E-07	4015	3691	49	1465	
Blumberg, #1 Wagner	1.5700E-07	142	652	34	123	

Table 4.5: Comparison of TM111 values and geochemistry data. A comparison of TM111 values and semi-quantitative insoluble residue geochemistry from Smith et al. (1981). All concentrations are in ppm. The Rowntree #1 Knott well has the highest concentrations of Pb, but is associated with low values in all three Central Texas models. The Hog Thief Bend 75-7 and Hog Thief Bend 7 wells only contain one valid Zn measurement, so Zn values are not included for these wells.

Well name	TM112	Pb	Zn	Co	Cu	Ni
Hog Thief Bend 75-7	1.2620E-04	266		17	63	47
Hog Thief Bend 7	1.2620E-04	99		44	28	142
Hog Thief Bend 8	1.2620E-04	78	9357	25	44	30
Hog Thief Bend 77-5	9.4615E-05	1467	1233	29	49	
Montgomery, #1 Yates	7.0647E-05	885	1647	49	507	
Murchison Ranch Water Well	2.6481E-05	2321	2600	43	238	
Humble, #1 Millican	1.6188E-05	63	1038	51	933	
Stratoray, #1 Stribling	8.0930E-06	281	3746	31	175	56
Hog Thief Bend 74-1	6.8220E-06	65	2787	37	59	77
Naylor, #1 Mitchell	4.4380E-06	249	491	50	623	
Brady City Water Well	1.0510E-06	216	3641	56	294	
Irwin, #1 Kothman	1.0510E-06	75	1625	60	540	
Rowntree, #1 Knott	9.9600E-07	4015	3691	49	1465	
Carpenter, #1 Bradshaw	9.9600E-07	237	770	83	371	
Blumberg, #1 Wagner	1.5700E-07	142	652	34	123	

Table 4.6: Comparison of TM112 values and geochemistry data. A comparison of TM112 values and semi-quantitative insoluble residue geochemistry from Smith et al. (1981). All concentrations are in ppm. The Rowntree #1 Knott well has the highest concentrations of Pb, but is associated with low values in all three Central Texas models. The Hog Thief Bend 75-7 and Hog Thief Bend 7 wells only contain one valid Zn measurement, so Zn values are not included for these wells.

Well name	TM113	Pb	Zn	Co	Cu	Ni
Montgomery, #1 Yates	1.1729E-04	885	1647	49	507	
Murchison Ranch Water Well	4.3965E-05	2321	2600	43	238	
Humble, #1 Millican	2.6877E-05	63	1038	51	933	
Hog Thief Bend 75-7	2.0151E-05	266		17	63	47
Hog Thief Bend 7	2.0151E-05	99		44	28	142
Hog Thief Bend 8	2.0151E-05	78	9357	25	44	30
Hog Thief Bend 77-5	1.5107E-05	1467	1233	29	49	
Stratoray, #1 Stribling	1.3437E-05	281	3746	31	175	56
Hog Thief Bend 74-1	1.1326E-05	65	2787	37	59	77
Naylor, #1 Mitchell	7.3690E-06	249	491	50	623	
Brady City Water Well	1.7450E-06	216	3641	56	294	
Irwin, #1 Kothman	1.7450E-06	75	1625	60	540	
Rowntree, #1 Knott	1.6540E-06	4015	3691	49	1465	
Carpenter, #1 Bradshaw	1.6540E-06	237	770	83	371	
Blumberg, #1 Wagner	2.6000E-07	142	652	34	123	

Table 4.7: Comparison of TM113 values and geochemistry data. A comparison of TM113 values and semi-quantitative insoluble residue geochemistry from Smith et al. (1981). All concentrations are in ppm. The Rowntree #1 Knott well has the highest concentrations of Pb, but is associated with low values in all three Central Texas models. The Hog Thief Bend 75-7 and Hog Thief Bend 7 wells only contain one valid Zn measurement, so Zn values are not included for these wells.
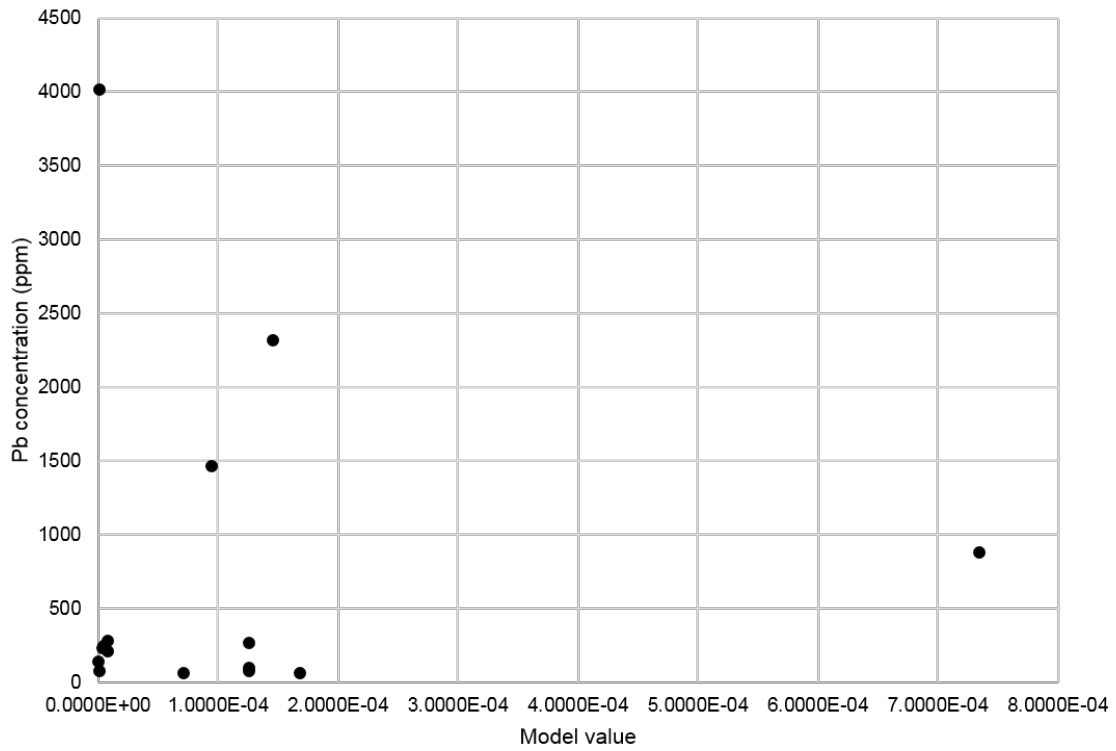
Figure 4.36: Plot of TM111 model values and corresponding insoluble residue geochemistry data from Smith et al. (1981). The Rowntree #1 Knott well is plotted in the upper left portion of the chart, corresponding to a low model value but high Pb concentration. The other three highest values are from wells that fall within the best performing 4.6% of the model area.
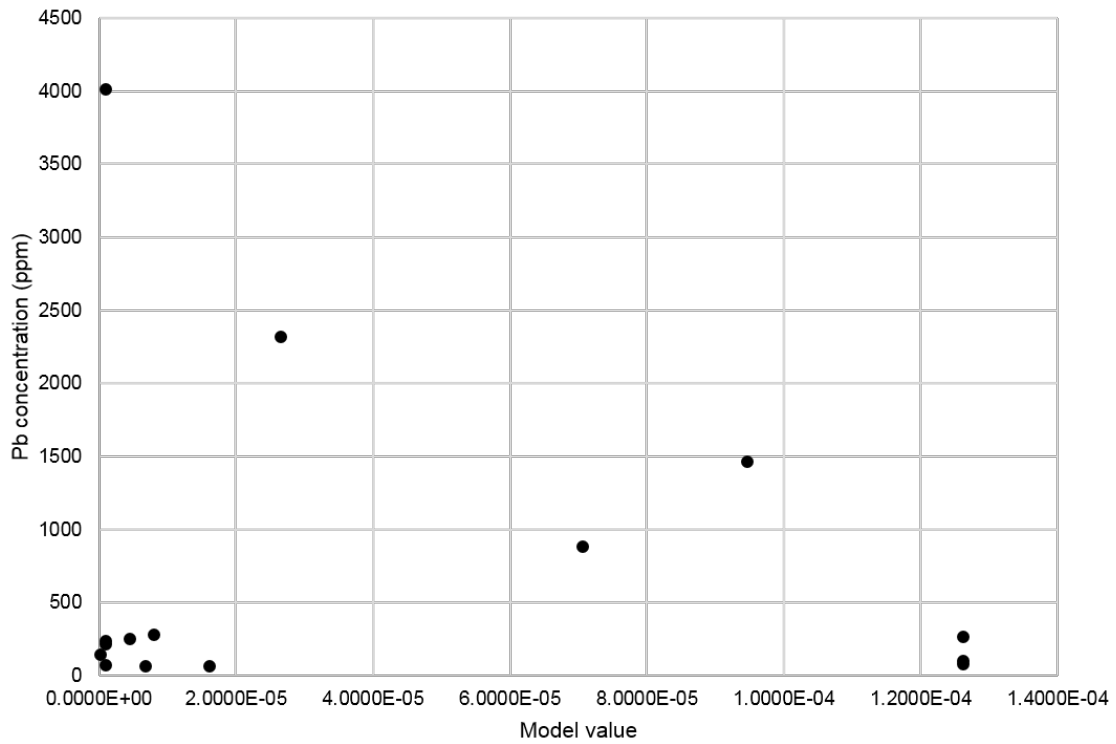
Figure 4.37: Plot of TM112 model values and corresponding insoluble residue geochemistry data from Smith et al. (1981). The Rowntree #1 Knott well is plotted in the upper left portion of the chart, corresponding to a low model value but high Pb concentration. The other three highest values are from wells that fall within the best performing 2.1% of the model area.
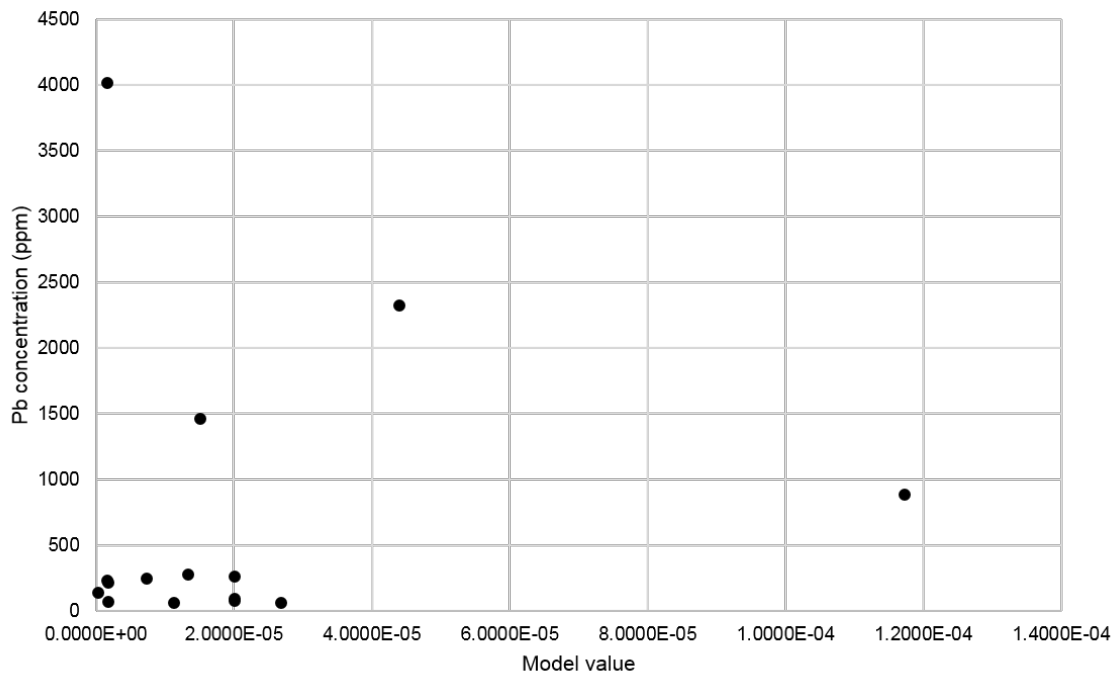
Figure 4.38: Plot of TM113 model values and corresponding insoluble residue geochemistry data from Smith et al. (1981). The Rowntree #1 Knott well is plotted in the upper left portion of the chart, corresponding to a low model value but high Pb concentration. The other three highest values are from wells that fall within the best performing 8.5% of the model area.

167

Chapter 5: Discussion, recommendations, and conclusions

This work demonstrates that evidence associated with MVT mineralization in Southeast Missouri may be directly applicable in mineral potential models for Central Texas. Exploration in Central Texas using mineral potential mapping techniques are primarily limited by the availability of data. As weight calculations for Southeast Missouri show, proximity to basement highs and proximity to faults are especially important forms of evidence related to MVT mineralization, but limited data are available to model these parameters for Central Texas. Additional processing of existing geophysical data and information from publicly available water-well databases may permit higher resolution basement structure maps for Central Texas and help identify regional faults that may be buried under Cretaceous cover. Detailed information on the facies distribution of Cambrian carbonates is also likely to be useful as demonstrated in Southeast Missouri. These pieces of information are likely key to discovering economic MVT deposits in the Central Texas region if they are present.

In addition to further work to directly identify primary and trace element MVT mineralization, there are numerous other ways to evaluate the performance of these models that were not conducted during this study, but that would constitute worthwhile future investigations. Each of these are potentially other lines of evidence to support MVT hot-fluid migration in Central Texas. Many of these focus on the basal Hickory Sandstone member of the Riley Formation that is a possible conduit for the fluids much like the Lamotte Sandstone in Southeast Missouri, although McBride et al. (2002) note a lack of evidence for this type of fluid in their extensive petrographic study. Some other evidence for MVT related processes are:

1. Presence of quartz cement in sandstones that have otherwise not been buried sufficiently deep to initiate precipitation may be related to MVT fluids.

2. Fluid inclusions in healed, postdepositional fractures in quartz grains as evidenced by fractures cutting multiple grains may contain elevated homogenization temperatures or presence of MVT related elements.

3. Extensive "postdiagenetic," or secondary, dolomite in otherwise unmineralized carbonate rocks may be the result of interaction with MVT fluids.

4. Bleaching of oxidized rocks bearing Fe minerals by conversion to sulfides may be caused by the interaction with H_2S-bearing MVT fluids.

Ultimately, as even early authors on Central Texas MVT potential noted, there may not be widespread, economic-grade mineralization in Central Texas (e.g., Comstock, 1891; Paige, 1911). It is possible that lack of a shale seal immediately over the Cap Mountain Limestone carbonates in Central Texas allowed most of the ore fluids to escape, or it was possible that the quantity of metals or sulfur in the Central Texas system was limited. However, the optimistic geologist should keep in mind that the Viburnum Trend was not discovered until nearly 250 years after Pb was initially discovered in the Old Lead Belt less than 75 km (50 miles) away, but has since produced well over twice as much metal (Ohle, 1990). As noted earlier, better subsurface data in the Central Texas area will be the key to future exploration success.

Appendix A

Class	Percent of Study Area	Percent of Deposits	W+	W-	Contrast (C)	σC	C/σC
500	11%	36%	1.22	-0.33	1.56	0.42	3.74
1000	19%	52%	1.00	-0.52	1.52	0.40	3.81
1500	27%	60%	0.81	-0.61	1.41	0.41	3.47
2000	33%	60%	0.58	-0.51	1.09	0.41	2.68
2500	40%	72%	0.60	-0.77	1.37	0.45	3.08
3000	45%	76%	0.52	-0.83	1.35	0.47	2.88
3500	50%	76%	0.41	-0.73	1.14	0.47	2.43
4000	55%	84%	0.42	-1.03	1.46	0.55	2.67
4500	59%	84%	0.35	-0.94	1.28	0.55	2.35
5000	63%	88%	0.33	-1.13	1.46	0.62	2.38
5500	66%	96%	0.37	-2.13	2.50	1.02	2.45
6000	69%	96%	0.33	-2.04	2.37	1.02	2.32
6500	72%	96%	0.29	-1.95	2.24	1.02	2.20
7000	74%	96%	0.26	-1.87	2.13	1.02	2.08
7500	76%	96%	0.23	-1.78	2.01	1.02	1.97
8000	78%	96%	0.21	-1.70	1.91	1.02	1.87
8500	80%	100%	0.23				

Table A.1: Weights and contrasts for all faults proximity classes. The class with the highest studentized contrast (C/σC) is highlighted as the best performing class.

Class	Percent of Study Area	Percent of Deposits	W+	W-	Contrast (C)	σC	C/σC
500	7%	32%	1.49	-0.31	1.81	0.43	4.21
1000	13%	44%	1.20	-0.44	1.64	0.40	4.07
1500	19%	52%	1.00	-0.52	1.53	0.40	3.82
2000	24%	52%	0.75	-0.45	1.21	0.40	3.02
2500	29%	68%	0.84	-0.79	1.63	0.43	3.80
3000	34%	72%	0.74	-0.85	1.60	0.45	3.58
3500	39%	72%	0.61	-0.78	1.39	0.45	3.12
4000	44%	80%	0.61	-1.04	1.65	0.50	3.29
4500	48%	80%	0.51	-0.96	1.47	0.50	2.94
5000	52%	84%	0.48	-1.10	1.58	0.55	2.89
5500	56%	96%	0.54	-2.40	2.94	1.02	2.88
6000	60%	96%	0.48	-2.31	2.79	1.02	2.73
6500	63%	96%	0.42	-2.23	2.65	1.02	2.59
7000	66%	96%	0.37	-2.14	2.51	1.02	2.46
7500	69%	96%	0.33	-2.05	2.38	1.02	2.33
8000	72%	96%	0.29	-1.96	2.25	1.02	2.20
8500	74%	100%	0.30				

Table A.2:   Weights and contrasts for NW-SE faults proximity classes.

Class	Percent of Study Area	Percent of Deposits	W+	W-	Contrast (C)	σC	C/σC
500	4%	4%	0.06	0.00	0.07	1.02	0.07
1000	7%	12%	0.52	-0.05	0.58	0.62	0.93
1500	11%	12%	0.13	-0.02	0.15	0.62	0.24
2000	14%	12%	-0.15	0.02	-0.17	0.62	-0.28
2500	17%	20%	0.14	-0.03	0.17	0.50	0.35
3000	21%	24%	0.14	-0.04	0.19	0.47	0.40
3500	24%	24%	-0.01	0.00	-0.01	0.47	-0.02
4000	28%	28%	0.02	-0.01	0.02	0.45	0.05
4500	31%	36%	0.16	-0.08	0.23	0.42	0.56
5000	34%	40%	0.16	-0.10	0.26	0.41	0.63
5500	37%	44%	0.17	-0.12	0.29	0.40	0.72
6000	40%	48%	0.19	-0.15	0.33	0.40	0.83
6500	43%	52%	0.20	-0.18	0.38	0.40	0.95
7000	45%	56%	0.22	-0.22	0.44	0.40	1.10
7500	47%	56%	0.17	-0.18	0.35	0.40	0.86
8000	50%	56%	0.12	-0.14	0.26	0.40	0.64
8500	52%	60%	0.15	-0.19	0.33	0.41	0.81

Table A.3:   Weights and contrasts for NE-SW faults proximity classes.

Class	Percent of Study Area	Percent of Deposits	W+	W-	Contrast (C)	σC	C/σC
500	2%	0%		0.02			
1000	4%	4%	0.02	0.00	0.02	1.02	0.02
1500	6%	8%	0.30	-0.02	0.32	0.74	0.44
2000	8%	8%	0.01	0.00	0.01	0.74	0.01
2500	10%	16%	0.48	-0.07	0.55	0.55	1.01
3000	12%	20%	0.52	-0.10	0.62	0.50	1.24
3500	14%	24%	0.55	-0.13	0.67	0.47	1.44
4000	16%	28%	0.57	-0.16	0.73	0.45	1.64
4500	18%	44%	0.91	-0.39	1.30	0.40	3.22
5000	19%	48%	0.90	-0.44	1.34	0.40	3.35
5500	21%	52%	0.90	-0.50	1.40	0.40	3.50
6000	23%	52%	0.83	-0.48	1.31	0.40	3.26
6500	24%	52%	0.76	-0.46	1.22	0.40	3.05
7000	26%	56%	0.78	-0.52	1.31	0.40	3.24
7500	27%	56%	0.73	-0.51	1.24	0.40	3.07
8000	28%	56%	0.69	-0.49	1.17	0.40	2.92
8500	29%	56%	0.65	-0.47	1.12	0.40	2.78
9000	30%	64%	0.74	-0.66	1.40	0.42	3.37
9500	31%	64%	0.71	-0.64	1.36	0.42	3.26
10000	32%	64%	0.68	-0.63	1.31	0.42	3.15
10500	33%	64%	0.66	-0.62	1.28	0.42	3.06
11000	34%	64%	0.64	-0.61	1.24	0.42	2.98
11500	35%	64%	0.62	-0.60	1.21	0.42	2.91
12000	35%	68%	0.66	-0.71	1.36	0.43	3.18
12500	36%	72%	0.70	-0.83	1.53	0.45	3.43
13000	36%	76%	0.74	-0.98	1.71	0.47	3.66
13500	37%	76%	0.72	-0.97	1.69	0.47	3.61
14000	37%	76%	0.71	-0.96	1.67	0.47	3.57
14500	38%	80%	0.75	-1.14	1.89	0.50	3.78
15000	38%	80%	0.75	-1.13	1.88	0.50	3.75

Table A.4:   Weights and contrasts for limestone-dolostone interface proximity classes.

Class	Percent of Study Area	Percent of Deposits	W+	W-	Contrast (C)	σC	C/σC
3000	27%	17%	-0.47	0.13	-0.59	1.10	-0.54
3500	31%	67%	0.76	-0.72	1.48	0.87	1.71
4000	36%	83%	0.84	-1.34	2.18	1.10	1.99
4500	41%	83%	0.71	-1.27	1.98	1.10	1.80
5000	46%	83%	0.60	-1.18	1.78	1.10	1.62
5500	51%	83%	0.49	-1.08	1.57	1.10	1.44

Table A.5:   Weights and contrasts for brown rock-white rock interface proximity classes. Note that the standard deviation of contrast (σC) is typically greater than 50% of the contrast values.

Class	Percent of Study Area	Percent of Deposits	W+	W-	Contrast (C)	σC	C/σC
0	3%	32%	2.46	-0.36	2.82	0.43	6.58
500	4%	32%	2.15	-0.35	2.50	0.43	5.83
1000	5%	40%	2.13	-0.46	2.60	0.41	6.36
1500	6%	48%	2.12	-0.59	2.71	0.40	6.78
2000	7%	48%	1.95	-0.58	2.54	0.40	6.33
2500	8%	56%	1.96	-0.74	2.70	0.40	6.70
3000	9%	56%	1.83	-0.73	2.55	0.40	6.34
3500	10%	60%	1.78	-0.81	2.59	0.41	6.34
4000	11%	64%	1.74	-0.90	2.64	0.42	6.34
4500	12%	64%	1.64	-0.89	2.53	0.42	6.08
5000	13%	64%	1.56	-0.88	2.43	0.42	5.84
5500	15%	68%	1.54	-0.98	2.52	0.43	5.88
6000	16%	68%	1.47	-0.97	2.43	0.43	5.68
6500	17%	68%	1.40	-0.96	2.35	0.43	5.49
7000	18%	68%	1.33	-0.94	2.28	0.43	5.31
7500	19%	68%	1.28	-0.93	2.20	0.43	5.14
8000	20%	68%	1.22	-0.92	2.14	0.43	4.98
8500	21%	68%	1.17	-0.90	2.07	0.43	4.83
9000	22%	72%	1.18	-1.02	2.20	0.45	4.94
9500	23%	72%	1.13	-1.01	2.14	0.45	4.81
10000	24%	80%	1.20	-1.33	2.53	0.50	5.06
10500	25%	80%	1.16	-1.32	2.48	0.50	4.95
11000	26%	80%	1.12	-1.31	2.42	0.50	4.85
11500	27%	80%	1.08	-1.29	2.37	0.50	4.75
12000	28%	80%	1.05	-1.28	2.33	0.50	4.66
12500	29%	80%	1.02	-1.27	2.28	0.50	4.56
13000	30%	84%	1.03	-1.48	2.51	0.55	4.60
13500	31%	84%	1.00	-1.46	2.47	0.55	4.52
14000	32%	88%	1.02	-1.74	2.76	0.62	4.48
14500	33%	88%	0.99	-1.73	2.72	0.62	4.42
15000	33%	88%	0.97	-1.71	2.68	0.62	4.35

Table A.6:   Weights and contrasts for algal reef rocks proximity classes.

Class	Percent of Study Area	Percent of Deposits	W+	W-	Contrast (C)	σC	C/σC
0	15%	16%	0.10	-0.02	0.11	0.55	0.21
500	16%	24%	0.41	-0.10	0.51	0.47	1.08
1000	18%	24%	0.31	-0.08	0.40	0.47	0.85
1500	19%	32%	0.52	-0.17	0.69	0.43	1.61
2000	21%	44%	0.75	-0.35	1.10	0.40	2.73
2500	22%	52%	0.84	-0.48	1.32	0.40	3.30
3000	24%	52%	0.77	-0.46	1.23	0.40	3.06
3500	26%	52%	0.70	-0.43	1.13	0.40	2.83
4000	28%	52%	0.63	-0.41	1.05	0.40	2.61
4500	29%	56%	0.65	-0.47	1.12	0.40	2.79
5000	31%	56%	0.59	-0.45	1.04	0.40	2.59
5500	33%	60%	0.61	-0.52	1.13	0.41	2.77
6000	34%	60%	0.56	-0.50	1.06	0.41	2.60
6500	36%	64%	0.58	-0.58	1.17	0.42	2.80
7000	37%	64%	0.54	-0.56	1.10	0.42	2.65
7500	39%	64%	0.51	-0.53	1.04	0.42	2.50
8000	40%	64%	0.47	-0.51	0.98	0.42	2.36
8500	41%	64%	0.44	-0.49	0.93	0.42	2.23
9000	43%	68%	0.47	-0.58	1.05	0.43	2.45
9500	44%	72%	0.49	-0.69	1.19	0.45	2.67
10000	45%	76%	0.52	-0.82	1.34	0.47	2.87
10500	47%	76%	0.49	-0.80	1.29	0.47	2.75
11000	48%	76%	0.46	-0.77	1.24	0.47	2.64
11500	49%	76%	0.43	-0.75	1.18	0.47	2.53
12000	51%	76%	0.41	-0.72	1.13	0.47	2.41

Table A.7:   Weights and contrasts for Lamotte Sandstone pinch-outs proximity classes.

Class	Percent of Study Area	Percent of Deposits	W+	W-	Contrast (C)	σC	C/σC
Elvins Group and Bonneterre Dolomite	7%	44%	1.83	-0.51	2.34	0.40	5.81
Eminence and Potosi Dolomites	28%	36%	0.26	-0.12	0.38	0.42	0.92
Gasconade Dolomite	25%	16%	-0.45	0.11	-0.56	0.55	-1.03
Roubidoux Formation	26%	4%	-1.85	0.25	-2.11	1.02	-2.06

Table A.8:   Weights and contrasts for host rock geology.

Class	Percent of Study Area	Percent of Deposits	W+	W-	Contrast (C)	σC	C/σC
0	6%	32%	1.66	-0.32	1.98	0.43	4.62
500	9%	40%	1.50	-0.42	1.92	0.41	4.70
1000	12%	44%	1.27	-0.45	1.72	0.40	4.26
1500	16%	52%	1.17	-0.56	1.73	0.40	4.31
2000	20%	52%	0.95	-0.51	1.46	0.40	3.65
2500	24%	56%	0.84	-0.54	1.39	0.40	3.44
3000	28%	68%	0.88	-0.81	1.68	0.43	3.92
3500	33%	72%	0.79	-0.88	1.67	0.45	3.76
4000	36%	72%	0.68	-0.82	1.50	0.45	3.37
4500	40%	76%	0.64	-0.91	1.55	0.47	3.31
5000	43%	76%	0.56	-0.86	1.41	0.47	3.02
5500	47%	84%	0.59	-1.21	1.80	0.55	3.30
6000	49%	96%	0.67	-2.54	3.21	1.02	3.14
6500	52%	100%	0.66				

Table A.9:   Weights and contrasts for Precambrian knob proximity classes.

Class	Percent of Study Area	Percent of Deposits	W+	W-	Contrast (C)	σC	C/σC
-200 - -100	17%	8%	-0.74	0.10	-0.84	0.74	-1.14
-100 - 0	21%	12%	-0.54	0.10	-0.64	0.62	-1.04
0 - 100	16%	20%	0.20	-0.04	0.24	0.50	0.48
100 - 200	12%	16%	0.25	-0.04	0.30	0.55	0.54
200 - 300	8%	20%	0.87	-0.14	1.01	0.50	2.01
300 - 400	5%	16%	1.18	-0.12	1.30	0.55	2.38
400 - 500	3%	4%	0.33	-0.01	0.34	1.02	0.34
500-1000	3%	4%	0.25	-0.01	0.26	1.02	0.26

Table A.10: Weights and contrasts for magnetic response classes.

Class	Percent of Study Area	Percent of Deposits	W+	W-	Contrast (C)	σC	C/σC
20-25	23%	12%	-0.64	0.13	-0.77	0.62	-1.25
25-30	24%	28%	0.17	-0.06	0.23	0.45	0.51
30-35	16%	16%	0.00	0.00	0.00	0.55	0.01
35-40	10%	20%	0.68	-0.12	0.79	0.50	1.58
40-45	5%	20%	1.33	-0.17	1.50	0.50	3.00
60-65	0%	4%	2.82	-0.04	2.85	1.02	2.80
35-45	15%	40%	0.95	-0.34	1.29	0.41	3.17

Table A.11: Weights and contrasts for percent magnetic response classes.

Class	Percent of Study Area	Percent of Deposits	W+	W-	Contrast (C)	σC	C/σC
0	17%	20%	0.18	-0.04	0.22	0.50	0.44
500	24%	28%	0.14	-0.05	0.19	0.45	0.43
1000	33%	36%	0.08	-0.04	0.13	0.42	0.31
1500	42%	56%	0.28	-0.27	0.55	0.40	1.36
2000	51%	68%	0.28	-0.42	0.70	0.43	1.62
2500	60%	76%	0.24	-0.51	0.75	0.47	1.61
3000	67%	76%	0.13	-0.32	0.44	0.47	0.95
3500	73%	76%	0.04	-0.11	0.15	0.47	0.33
4000	78%	76%	-0.03	0.09	-0.12	0.47	-0.26
4500	82%	92%	0.11	-0.79	0.90	0.74	1.22
5000	86%	92%	0.07	-0.58	0.65	0.74	0.88
5500	88%	96%	0.08	-1.06	1.14	1.02	1.12

Table A.12: Weights and contrasts for magnetic hills proximity classes.

Class	Percent of Study Area	Percent of Deposits	W+	W-	Contrast (C)	σC	C/σC
0-2.98	42%	8%	-1.65	0.46	-2.11	0.74	-2.86
6.82	31%	44%	0.35	-0.21	0.55	0.40	1.38
11.93	16%	32%	0.68	-0.21	0.89	0.43	2.08
18.32	7%	8%	0.20	-0.02	0.22	0.74	0.30
37.5	1%	8%	1.91	-0.07	1.98	0.74	2.68
6.82-37.5	58%	92%	0.47	-1.67	2.13	0.74	2.89

Table A.13: Weights and contrasts for magnetic slope classes. Magnetic slope in hundredths of nT/m.

Class	Percent of Study Area	Percent of Deposits	W+	W-	Contrast (C)	σC	C/σC
-50 - -45	13%	8%	-0.47	0.05	-0.52	0.74	-0.71
-45 - -40	12%	12%	0.02	0.00	0.03	0.62	0.05
-40 - -35	12%	12%	-0.02	0.00	-0.02	0.62	-0.03
-35 - -30	7%	0%		0.08			
-30 - -25	7%	0%		0.07			
-25 - -20	7%	12%	0.51	-0.05	0.56	0.62	0.91
-20 - -15	9%	8%	-0.08	0.01	-0.09	0.74	-0.12
-15 - -10	6%	40%	1.85	-0.45	2.30	0.41	5.63
-10 - -5	5%	8%	0.46	-0.03	0.49	0.74	0.67
-5 - 0	0%	0%		0.00			

Table A.14: Weights and contrasts for gravity anomaly classes. Gravity units are mGal. Gravity evidence maps were not included in any potential models due to the relatively coarse resolution of the data.

Class	Percent of Study Area	Percent of Deposits	W+	W-	Contrast (C)	σC	C/σC
0.5%	24%	32%	0.28	-0.11	0.39	0.43	0.91
11%	47%	60%	0.25	-0.29	0.54	0.41	1.32
17%	18%	8%	-0.80	0.11	-0.91	0.74	-1.24

Table A.15: Weights and contrasts for gravity slope classes. Gravity slope in hundredths of mGal/m. Gravity evidence maps were not included in any potential models due to the relatively coarse resolution of the data.

Class	Percent of Study Area	Percent of Deposits	W+	W-	Contrast (C)	σC	C/σC
0	13%	20%	0.40	-0.08	0.48	0.50	0.97
500	15%	20%	0.30	-0.06	0.37	0.50	0.73
1000	16%	20%	0.21	-0.05	0.26	0.50	0.52
1500	18%	20%	0.13	-0.03	0.16	0.50	0.32
2000	19%	20%	0.05	-0.01	0.06	0.50	0.12
2500	21%	24%	0.15	-0.04	0.20	0.47	0.42
3000	22%	24%	0.08	-0.02	0.10	0.47	0.22
3500	24%	28%	0.16	-0.06	0.22	0.45	0.49
4000	25%	28%	0.10	-0.03	0.13	0.45	0.29
4500	27%	28%	0.03	-0.01	0.04	0.45	0.10
5000	29%	28%	-0.03	0.01	-0.04	0.45	-0.08
5500	30%	28%	-0.08	0.03	-0.11	0.45	-0.26
6000	32%	32%	0.00	0.00	0.00	0.43	-0.01
6500	34%	32%	-0.05	0.03	-0.08	0.43	-0.19
7000	35%	32%	-0.10	0.05	-0.16	0.43	-0.36
7500	37%	32%	-0.15	0.08	-0.23	0.43	-0.53
8000	39%	32%	-0.19	0.11	-0.30	0.43	-0.70
8500	41%	36%	-0.12	0.07	-0.19	0.42	-0.46
9000	42%	36%	-0.16	0.10	-0.26	0.42	-0.62
9500	44%	36%	-0.19	0.13	-0.32	0.42	-0.77
10000	45%	40%	-0.12	0.09	-0.21	0.41	-0.52
10500	47%	44%	-0.06	0.05	-0.11	0.40	-0.26
11000	48%	44%	-0.09	0.08	-0.16	0.40	-0.41
11500	49%	44%	-0.12	0.10	-0.22	0.40	-0.55
12000	51%	44%	-0.14	0.13	-0.27	0.40	-0.67
12500	52%	48%	-0.08	0.08	-0.16	0.40	-0.40
13000	53%	56%	0.05	-0.06	0.12	0.40	0.29
13500	54%	56%	0.03	-0.04	0.07	0.40	0.18
14000	55%	56%	0.01	-0.02	0.03	0.40	0.08
14500	56%	56%	0.00	0.00	-0.01	0.40	-0.02
15000	57%	60%	0.05	-0.07	0.12	0.41	0.29

Table A.16: Weights and contrasts for tin granite plutons proximity classes.

Percent of Study Area	Percent of Deposits	W+	W-	Contrast (C)	σC	C/σC
14%	48%	1.25	-0.51	1.76	0.40	4.38

Table A.17: Weights and contrasts for presence or absence of base metal anomalies in insoluble residue of the Bonneterre Fm CUSMAP layer.

Class	Percent of Study Area	Percent of Deposits	W+	W-	Contrast (C)	σC	C/σC
Pb > UIF	3%	20%	1.87	-0.19	2.06	0.65	3.19
Zn > UIF	2%	20%	2.54	-0.21	2.75	0.65	4.26
Ba > UIF	0%	0%		0.00			
Fe > UIF	0%	0%		0.00			
Co > UIF	1%	7%	2.59	-0.06	2.65	1.04	2.56
Cu > UIF	2%	13%	1.98	-0.12	2.11	0.76	2.77
Ni > UIF	0%	7%	2.65	-0.06	2.71	1.04	2.62
Pb + other metal > UIF	2%	20%	2.39	-0.20	2.59	0.65	4.02
Pb Or Zn > UIF	3%	27%	2.09	-0.28	2.37	0.58	4.06
Pb > Median + 2MAD	13%	33%	0.97	-0.27	1.24	0.55	2.27
Zn > Median + 2MAD	13%	33%	0.95	-0.27	1.22	0.55	2.22
Ba > Median + 2MAD	5%	0%		0.05			
Co > Median + 2MAD	4%	20%	1.58	-0.18	1.76	0.65	2.73
Cu > Median + 2MAD	9%	20%	0.76	-0.12	0.88	0.65	1.37
Ni > Median + 2MAD	9%	20%	0.78	-0.13	0.91	0.65	1.41
Pb OR Zn > Median + 2MAD	15%	40%	0.98	-0.35	1.33	0.53	2.52

Table A.18: Weights and contrasts for NURE geochemistry layers.

Appendix B

NURE GIS Processing using ArcGIS 10.3 Hydrology Tools

1. Mosaiced 1 degree elevation tiles from National Elevation Dataset (2009). The elevation dataset must cover a larger extent than the study area.

2. Used "Fill" tool with a 30 m DEM as the input raster to prevent undefined flow directions in subsequent steps.

3. Used "Flow Direction" tool with DEM as input. Use the force edge cells out option.

4. Used "Flow Accumulation" tool with the flow direction raster created in step 3 as the input raster.

5. Used "Dissolve" tool on NURE points to remove duplicate values at the same point (potentially a result of samples being re-analyzed). Used lat and lon as dissolve fields. Used the MAX statistic to only retain the maximum value for Pb, Zn, Ba, Co, Cu, Ni, and Fe at the sample location.

6. Used "Snap Pour Points" tool with NURE points and flow accumulation raster as inputs. Allowed points to move 300 m to a cell of higher accumulation.

7. Used "Watershed" tool to calculate catchment basins for each NURE point using Object ID as the identity field.

8. Used "Raster to polygons" tool with the catchment basin raster as input with the simplify polygons option.

9. Used "Join" with NURE points and basins. NURE values below the detection limit (represented as negative numbers in the NURE dataset) were assigned a value equal to half of the detection limit. No values of 0 were kept due to apparently incomplete information.

10. Clipped geology using catchment basins.

11. Unioned bedrock geology and basins.

12. Joined stream sediment NURE attributes (elemental concentrations) to unioned geology and basins. All calculations performed on log transformed geochemistry data – used field calculator to transform NURE concentrations in ppm to log concentrations.

13. Multiplied area of each record with the corresponding log transformed stream sediment sample.

14. Used "Summary Statistics" tool to generate statistics for each "element x area" column and for the shape area column. Use rock unit name as the case field to produce summed log transformed geochemical data for each geologic formation.

15. Joined resulting table to unioned geology and basins layer with Unit Name as the key field.

16. Created a new column, divided summed element x area field by summed area field to return the average concentration for each map unit.

17. Created a new column, used EXP() to transform log average concentrations back to ppm.

18. In unioned geology and basins layer, created new columns for average log concentrations for each element.

19. Joined statistics table with the geology and basins layer based on rock unit name and used the field calculator to copy the average concentrations to the newly created columns.

20. Created new columns for average concentrations x area and filled with the field calculator.

21. Generated new summary statistics table with each of the new average concentrations x area columns with SUM as the method. Use gridcode as the case field. This produces summed values for each gridcode (which are unique to each basin).

22. Created new field for background values for each element. Divided the summed average elemental concentration by the summed areas using calculate field.

23. Added new field to attribute table of the basin feature class (not unioned basin and geology) for background elemental concentration. Used the gridcode as the join field, joined the statistics table to this attribute table, and copied the results into the new field.

References

Agterberg, F.P. and Bonham-Carter, G.F., 2005. Measuring the performance of mineral-potential maps. Natural Resources Research, v. 14, no. 1, p. 1-17.

Agterberg, F. P., and Cheng, Q., 2002 Conditional independence test for weights-of-evidence modeling: Natural Resources Research, v. 11, no. 4, p. 249-255.

Allie, A.D., 1981, Stratigraphic controls of carbonate-hosted sulfide mineralization, Iron Rock Creek Area, Blanco and Gillespie Counties, Texas: M.S. Thesis, The University of Texas at Austin, 101 p.

Allingham, J.W., 1976, Interpretation of aeromagnetic anomalies in Southeastern Missouri, US Geological Survey, Open File Report No. 76-868, 319p.

Anderson, G.M. and Macqueen, R.W., 1982, Ore deposit models-6, Mississippi Valley-type lead-zinc deposits: Geoscience Canada, v. 9, p. 107-117.

Baker, C.L., 1933, Disseminated Galena in the Upper Cambrian of the Central Mineral Region, Texas: Economic Geology v. 28, p. 163-170.

Baker, C.L., 1935, Lead minerals and ores, in The Geology of Texas, Vol. 11, Structural and Economic Geology: Univ. Texas Bull. 3401, Jan. 1, 1934, pp. 503-504.

Barnes, V. E., 1956, Lead Deposits in the Upper Cambrian of Central Texas: Bureau of Economic Geology Report of Investigations, no. 26, 69 p.

Barnes, V. E., and Bell, W. C., 1977, The Moore Hollow Group of Central Texas: University of Texas, Bureau of Economic Geology Report of Investigations, no. 88, 169 p.

Bastin, E.S. ed., 1939, Contributions to a knowledge of the lead and zinc deposits of the Mississippi Valley region, Geological Society of America Special Paper, No. 24.

Bickford, M.E. and Mose, D.G., 1975, Geochronology of Precambrian rocks in the St. Francois Mountains, Southeastern Missouri, Geological Society of America Special Papers, 165, p.1-48.

Blakey, R.C., 2003, Carboniferous–Permian palaeogeography of the assembly of Pangea, In: Wong, Th.E. (ed.), Proceedings of the XVth International Congress on Carboniferous and Permian stratigraphy. Utrecht, 10–16 August 2003, Royal Dutch Academy of Arts and Sciences, (Amsterdam), p. 443–456.

Bonham-Carter, G. F., 1994, Geographic information systems for geoscientists: modeling with GIS: Pergamon Press, Oxford, 398 p.

Carranza, E. J. M., 2009, Geochemical anomaly and mineral prospectivity mapping in GIS: Elsevier, 351 p.

Carranza, E.J.M. and Sadeghi, M., 2010, Predictive mapping of prospectivity and quantitative estimation of undiscovered VMS deposits in Skellefte district (Sweden). Ore Geology Reviews, v. 38, no. 3, p. 219-241.

Cheng, Q. and Agterberg, F.P., 1999, Fuzzy weights-of-evidence method and its application in mineral potential mapping, Natural resources research, v. 8, no. 1, p.27-35.

Comstock, T.B., 1890, A preliminary report on the geology of the Central Mineral region of Texas: Texas Geol. Surv., 1st Ann. Rept. 1889, p. 237-391.

Comstock, T.B., 1891, Report on the geology and mineral resources of the Central Mineral region of Texas: Texas Geol. Surv., 2nd Ann. Rept. 1890, p. 553-664.

Cordell, L. and Knepper, D.H., 1987, Aeromagnetic images: fresh insight to the buried basement, Rolla quadrangle, southeast Missouri, Geophysics, v. 52, no. 2, p.218-231.

Daneshfar, B., 1998, An evaluation of indicators of prospectivity and potential mapping of porphyry deposits in middle and southern British Columbia by a GIS study of regional geochemical and other geoscientific data, University of Ottawa, PhD thesis, 300 p.

Daneshfar, B., Desrochers, A., and Budkewitsch, P., 2006, Mineral-potential mapping for MVT deposits with limited data sets using Landsat data and geological evidence in the Borden Basin, Northern Baffin Island, Nunavut, Canada: Natural Resources Research, v. 15, no. 3, p. 129-149.

Daniels, V.B.A.C.D., Patricia, C.A.F.I.H., Mark, H.R.K.W.M., Victoria, P.C.R.W.R., Ronald, R.S.S.S.S., Phillips, S.J.V. and Ravat, J.D., 2002, Digital data grids for the magnetic anomaly map of North America, accessed from the Regional Geospatial Service Center of the University of Texas El Paso, <http://gis.utep.edu/subpages/GMData.html>

D'Ercole, C., Groves, D. I., and Knox-Robinson, C. M., 2000, Using fuzzy logic in a geographic information system environment to enhance conceptually based prospectivity analysis of Mississippi Valley-Type mineralisation: Australian Journal of Earth Sciences v. 47, p. 913-927.

ESRI, 2014, ArcGIS Desktop: Release 10.3, Redlands, CA: Environmental Systems Research Institute.

Ewing, T.E., Budnik, R.T., Ames, J.T., Ridner, D.M. and Dillon, R., 1990, Tectonic map of Texas: Bureau of Economic Geology, University of Texas at Austin, 1:750,000.

Fabbri, A.G. and Chung, C.J., 2008, On blind tests and spatial prediction models, Natural Resources Research, v. 17, no. 2, p. 107-118.

Farr, M. R. and Gose, W. A., 1991, Paleomagnetism of the Cambrian Moore Hollow Goup, Texas: Evidence for a primary magnetization carried by detrital magnetite: Journal of Geophysical Research, v. 96, no. B6, p. 9895-9907.

Feltrin, L., 2008, Predictive modelling of prospectivity for Pb–Zn deposits in the Lawn Hill Region, Queensland, Australia. Ore Geology Reviews, v. 34, no. 3, p.399-427.

Ford, A., Miller, J. M., Mol, A. G., 2015, A comparative analysis of weights-of-evidence, evidential belief functions, and fuzzy logic for mineral potential mapping using incomplete data at the scale of investigation: Natural Resources Research, p. 1-15.

Fullagar, P.K., Pears, G., Hutton, D. and Thompson, A., 2004, 3D gravity and aeromagnetic inversion for MVT lead-zinc exploration at Pillara, Western Australia. Exploration Geophysics, v. 35, no. 2, p.142-146.

Geologic Database of Texas [vector], accessed from the Texas Natural Resources Information System (TNRIS), <https://tnris.org/data-catalog/entry/geologic-database-of-texas/>

Groundwater Database of Texas [shapefile], Texas Water Development Board, <http://www.twdb.texas.gov/groundwater/data/gwdbrpt.asp>

Gutierrez, G.N., 1987, Controls on ore deposition in the Lamotte Sandstone. Goose Creek Mine, Indian Creek Subdistrict, southeast Missouri: M.S. Thesis, The University of Texas at Austin, 118 p.

Harris, D., Zurcher, L., Stanley, M., Marlow, J. and Pan, G., 2003, A comparative analysis of favorability mappings by weights-of-evidence, probabilistic neural networks, discriminant analysis, and logistic regression, Natural Resources Research, v. 12, no. 4, p. 241-255.

Hawkes, H.E., 1976, The downstream dilution of stream sediment anomalies, Journal of Geochemical Exploration, v. 6, p. 345-358.

Hengl, T., 2006, Finding the right pixel size: Computers and Geosciences, v. 32, no. 9, p. 1283-1298.

Hildenbrand, T.G., Briesacher, A., Flanagan, G., Hinze, W.J., Hittelman, A.M., Keller, G.R., Kucks, R.P., Plouff, D., Roest, W., Seeley, J. and Smith, D.A., 2002,

Rationale and operational plan to upgrade the US gravity database. US Geological Survey Open-File Report, 2-463, 12 p.

Horrall, K.B., Farr, M.R. and Hagni, R.D., 1996, Evidence for focusing of Mississippi Valley–type ore fluids along the Bloomfield Lineament Zone, Southeast Missouri, Carbonate-hosted lead-zinc deposits: Society of Economic Geologists Special Publication, no. 4, p. 400-412.

Kisvarsanyi, G., 1977, The role of the Precambrian igneous basement in the formation of the stratabound lead-zinc-copper deposits in Southeast Missouri, Economic Geology, v. 72, no. 3, p. 435-442.

Kisvarsanyi, E.B., 1979, Structure contour map of buried Precambrian basement-rock surface, Rolla 1 degree by 2 degrees Quadrangle and adjacent areas, Missouri (No. 1001-B).

Kolata, D.R., 2005, Bedrock geology of Illinois [vector digital data], 1:500,000, Illinois Map 14.

Krause, S. J., 1996, Stratigraphic framework, facies analysis, and depositional history of the Middle to Late Cambrian Riley Formation, Central Texas: The University of Texas at Austin, Master's thesis, 172 p.

Kyle, J. R., 2010, Exploration potential of Central Texas for Pb-dominant MVT deposits: Society of Economic Geologists 2010 Conference – The challenge of finding new mineral resources, program and extended abstracts, p. 38.

Kyle, J.R. and McBride, E.F., 2012. Geology of the Voca frac sand district, western Llano Uplift, Texas. In Proceedings, 48th Annual Forum on the Geology of Industrial Minerals: Arizona Geological Survey Special Paper, 15 p.

Leach, D. L., and Rowan, E. L., 1986, Genetic link between Ouachita foldbelt tectonism and the Mississippi Valley–type lead-zinc deposits of the Ozarks: Geology, v. 14, no. 11, p. 931-935.

Leach, D.L., Sangster, D.F., Kelley, K.D., Large, R.R., Garvin, Grant, Allen, C.R., Gutzmer, Jens, and Walters, S., 2005, Sediment-hosted lead-zinc deposits: a global perspective: Society of Economic Geologists, Economic Geology One Hundredth Anniversary Volume, 1905-2005, p. 561-607.

Leach, D. L., Taylor, R. D., Fey, D. L., Diehl, S. F., and Saltus, R. W., 2010, A deposit model for Mississippi ValleyType Lead-Zinc ores: USGS Scientific Investigations Report 2010–5070, 52 p.

Leach, D.L., Viets, J.B., Foley-Ayuso, N. and Klein, D.P., 1995, Mississippi Valley-type Pb-Zn deposits, Preliminary compilation of descriptive geoenvironmental mineral deposit models, US Geological Survey Open-File Report, p. 95-831.

Lindsay, M. D., Betts, P.G. and Ailleres, L., 2014, Data fusion and porphyry copper prospectivity models, southeastern Arizona, Ore Geology Reviews, 61, p. 120-140.

Lindsay, M., Aitken, A., Ford, A., Dentith, M., Hollis, J. and Tyler, I., 2016, Reducing subjectivity in multi-commodity mineral prospectivity analyses: Modelling the west Kimberley, Australia, Ore Geology Reviews, 76, p. 395-413.

McBride, E.F., Abdel-Wahab, A.A. and Milliken, K.L., 2002. Petrography and diagenesis of a half-billion-year-old cratonic sandstone (Hickory), Llano region, Texas (No. 264). Bureau of Economic Geology, University of Texas at Austin 74 p.

Missouri Department of Natural Resources, Lead information, (n.d.), retrieved May 11, 2016, http://dnr.mo.gov/env/lead.htm

Missouri Department of Natural Resources, Missouri lead mining history by county, (n.d.), retrieved November 10, 2016, https://dnr.mo.gov/env/hwp/sfund/lead-mo-history-more.htm

MO 2011 Bedrock 500K [vector digital data], 1:500,000, 2011, Missouri Department of Natural Resources (DNR), Division of Geology and Land Survey (DGLS), Geological Survey Program (GSP), <ftp://msdis.missouri.edu/pub/Geological_Geophysical/MO_2011_Bedrock_500 K_shp.zip>

Moon, C.J., 1999, Towards a quantitative model of downstream dilution of point source geochemical anomalies, Journal of Geochemical Exploration, v. 65, no. 2, p.111-132.

Mosher, S., Levine, J.S.F., and Carlson, W.D., 2008, Mesoproterozoic plate tectonics: A collisional model for the Grenville-aged orogenic belt in the Llano uplift, Central Texas: Geological Society of America Bulletin, v. 36, p. 55-58.

National Elevation Dataset [raster digital data], Sioux Falls, SD: U.S. Geological Survey, 2009. <http://nationalmap.gov>

Nykänen, V., Groves, D.I., Ojala, V.J., Eilu, P. and Gardoll, S.J., 2008, Reconnaissance-scale conceptual fuzzy-logic prospectivity modelling for iron oxide copper–gold deposits in the northern Fennoscandian Shield, Finland. Australian Journal of Earth Sciences, v. 55, no. 1, p. 25-38.

Nykänen, V. and Ojala, V.J., 2007, Spatial analysis techniques as successful mineral-potential mapping tools for orogenic gold deposits in the northern Fennoscandian Shield, Finland, Natural Resources Research, v. 16, no. 2, p. 85-92.

Ohle, E.L. and Brown, J.S., 1954, Geologic problems in the Southeast Missouri lead district: Geological Society of America Bulletin, v. 65, no. 3, p. 201-222.

Ohle, E.L., 1990, A comparison of the Old Lead Belt and the New Lead Belt in Southeast Missouri. Economic Geology, v. 85, no. 8, p.1894-1895.

Paige, S., 1911, Mineral resources of the Llano-Burnet region, Texas with an account of the pre-Cambrian geology: U.S. Geol. Survey Bull. 450, 103 p.

Paterson Grant and Watson Limited, 1981a, Magnetic depth calculations Kerr Basin – Ouachita Trend area [map], 1:100,000, Numbers 1-5.

Paterson Grant and Watson Limited, 1981b, Magnetic susceptibility and interpretation map Kerr Basin – Ouachita Trend area [map], 1:96,000, Numbers 1-5.

Pratt, W.P., Erickson, R.L., Mosier, E.L., Odland, S.K., Erickson, M.S., Viets, J.G., Miller, M.H., Heyl, A.V., Anderson, K.H., Martin, J.A., Satterfield, I.R., Wharton, H.M., and Middendorf, M.A., 1981, Mississippi Valley-Type base-metal deposits in the Bonneterre Formation and Lamotte Sandstone, in Pratt, W.P. ed., Metallic mineral-resource potential of the Rolla 1 x 2 quadrangle, Missouri, as appraised in September 1980, US Geological Survey Open File Report 81-518, 77 p.

Pratt, W.P., Erickson, R.L., Jenson, S.K. and Hastings, D.A., 1986, The Rolla and Springfield, Missouri, CUSMAP resource assessments, in Cargill, S.M., and Green, S.B., eds., Prospects for mineral resource assessments on public lands: proceedings of the Leesburg workshop, US Geological Survey Circular 980, 330 p.

Raines, G. L., 2006, Resource materials for a GIS spatial analysis course: revision of lectures: USGS Open File Report 01-221, version 1.1., 122 p.

Sangster, D.F. ed., 1996, Cabonate-hosted lead-zinc deposits: Society of Economic Geologists, Special Publication no. 4, 664 p.

Schmitt, E., 2010, Weights-of-evidence mineral prospectivity modelling with ArcGIS: EOSC 448 Directed Studies, Department of Earth, Ocean & Atmospheric Studies, University of British Columbia, Vancouver, 65 p.

Seeger, C. M., 2008, History of mining in the Southeast Missouri Lead District and description of mine processes, regulatory controls, environmental effects, and mine facilities in the Viburnum Trend Subdistrict: USGS Scientific Investigations Report 2008-5140, p. 5-33.

196

Singer, D.A. and Kouda, R., 1999, A comparison of the weights-of-evidence method and probabilistic neural networks, Natural Resources Research, v. 8, no. 4, p. 287-298.

Smith, G. E., Jackson, M., and Ingram, J., 1981, Regional recognition of subsurface base-metal resources in the Llano region of central Texas: Bureau of Economic Geology, University of Texas at Austin, open file report, 225 p.

Smith, S.M., 2006, Reformatted data from the National Uranium Resource Evaluation (NURE) hydrogeochemical and stream sediment reconnaissance (HSSR) program, version 1.40, US Geological Survey Open-File Report 97-492.

Snyder, F.G. and Gerdemann, P.E., 1968, Geology of the Southeast Missouri lead district, in Ridge, J.D., ed., Ore deposits of the United States, 1933–1967, Graton-Sales Volume: New York, American Institute of Mining, Metallurgical, and Petroleum Engineers, p. 327–358.

Stensgaard, B.M., Chung, C.J., Rasmussen, T.M. and Stendal, H., 2006, Assessment of mineral potential using cross-validation techniques and statistical analysis: a case study from the Paleoproterozoic of West Greenland. Economic Geology, v. 101, no. 7, p. 1397-1413.

Sibson, R., 1981, A brief description of natural neighbour interpolation, Interpreting multivariate data, 21, p. 21-36.

Symons, D.T., Lewchuk, M.T. and Leach, D.L., 1998, Age and duration of the Mississippi Valley-type mineralizing fluid flow event in the Viburnum Trend, Southeast Missouri, USA, determined from palaeomagnetism, Geological Society, London, Special Publications, no. 144, p.27-39.

Tarr, W.A., 1933, Disseminated galena, Upper Cambrian of Central Mineral region, Texas: Economic Geology, v. 28, p. 607.

Tarr, W.A., 1936, Origin of the Southeastern Missouri lead deposits, Part 1: Economic Geology, v. 31, no. 7, p.712-754.

Thacker, J.L. and Anderson, K.H., 1977, The geologic setting of the Southeast Missouri lead district; regional geologic history, structure and stratigraphy, Economic Geology, v. 72 no. 3, p. 339-348.

U.S. Geological Survey, 2004, National Uranium Resource Evaluation (NURE) Hydrogeochemical and Stream Sediment Reconnaissance data: U.S. Geological Survey, Denver, Co, <https://mrdata.usgs.gov/nure/sediment/>

Wharton, H. M., 1975, Introduction to the Southeast Missouri Lead District: Missouri Geological Survey, Report of Investigations no. 58, p. 2-14.

Wisniowiecki, M.J., Van der Voo, R., McCabe, C. and Kelly, W.C., 1983, A Pennsylvanian paleomagnetic pole from the mineralized Late Cambrian Bonneterre Formation, Southeast Missouri, Journal of Geophysical Research: Solid Earth, v. 88, no. B8, p. 6540-6548.

Wu, Y. and Beales, F., 1981, A reconnaissance study by paleomagnetic methods of the age of mineralization along the Viburnum Trend, southeast Missouri, Economic Geology, v. 76, no. 7, p. 1879-1894.

Young, L.M., and Jackson, D.H., 1981, Fluid-inclusion temperature study of Paleozoic carbonates, Llano Uplift, Texas: Gulf Coast Association of Geological Societies Transactions, v. 31, p. 421-425.